



CENTER FOR INFRASTRUCTURE ENGINEERING STUDIES

Strengthening of Masonry: Opportunities and Challenges in the Use of Composites

By

**Marco Casareto
Alessandro Oliveri
Alessandro Romelli**

University of Missouri-Rolla

**CIES
03-40**

UNIVERSITA' DEGLI STUDI DI GENOVA
FACOLTA' DI INGEGNERIA
Dipartimento di Ingegneria Strutturale e Geotecnica
D.I.S.E.G.



U.M.R. - University of Missouri - Rolla, U.S.A.
FACULTY OF ENGINEERING
Center for Infrastructure Engineering Studies
C.I.E.S.



TESI DI LAUREA

*Strengthening of Masonry: Opportunities and Challenges
in the Use of Composites*

*Rinforzo della Muratura: Campi di Applicazione e Prospettive
nell'Utilizzo dei Materiali Compositi*

Relatori: Chiar.mo Prof. Ing. Sergio Lagomarsino
Chiar.mo Prof. Ing. Antonio Nanni

Correlatore: Ph.D. Gustavo Jaime Tumialan

Candidati: Marco Casareto
Alessandro Oliveri
Alessandro Romelli

Aprile 2002

Disclaimer

The contents of this report reflect the views of the author(s), who are responsible for the facts and the accuracy of information presented herein. This document is disseminated under the sponsorship of the Center for Infrastructure Engineering Studies (CIES), University of Missouri -Rolla, in the interest of information exchange. CIES assumes no liability for the contents or use thereof.

The mission of CIES is to provide leadership in research and education for solving society's problems affecting the nation's infrastructure systems. CIES is the primary conduit for communication among those on the UMR campus interested in infrastructure studies and provides coordination for collaborative efforts. CIES activities include interdisciplinary research and development with projects tailored to address needs of federal agencies, state agencies, and private industry as well as technology transfer and continuing/distance education to the engineering community and industry.

Center for Infrastructure Engineering Studies (CIES)
University of Missouri-Rolla
223 Engineering Research Lab
1870 Miner Circle
Rolla, MO 65409-0710
Tel: (573) 341-6223; fax -6215
E-mail: cies@umr.edu
www.cies.umr.edu

TABLE OF CONTENTS

<i>SOMMARIO</i> _____	1
<i>ABSTRACT</i> _____	5
1. INTRODUCTION _____	7
1.1. General _____	7
1.2. Problem Statement: Out-of-Plane and In-Plane Behavior of URM Walls	11
1.3. Problem Statement: Post Tensioning of Masonry _____	18
1.4. Conventional Retrofit Techniques _____	20
1.5. Scope and Objectives _____	23
1.6. Thesis Layout _____	24
2. THE FRP MATERIALS _____	25
2.1. Composite Materials _____	25
2.2. FRP Composites _____	28
2.3. FRP Reinforcement Forms _____	35
2.4. FRP Physical and Mechanical Properties _____	40
2.5. Durability of FRP Materials _____	47
3. FRP INSTALLATION TECHNIQUE _____	53
3.1. The Wet-lay-up System _____	53
3.2. Near-surface Mounted FRP Rod System _____	59
4. MATERIALS AND BOND CHARACTERIZATION _____	65
4.1. Materials Characterization _____	65
4.1.1. Introduction _____	65
4.1.2. Concrete blocks (arching test) _____	65
4.1.3. Dark clay bricks (arching test) _____	67
4.1.4. Light clay bricks (in-plane test) _____	69
4.1.5. Mortar _____	73
4.1.6. AFRP and GFRP laminates _____	74
4.1.7. CFRP Strips _____	78
4.1.8. GFRP Rods _____	80
4.1.9. Primer and Saturant _____	81

4.1.10. GFRP G1 Rods _____	81
4.2. Bond Characterization _____	82
4.2.1. Test Specimens _____	82
4.2.2. Test Setup _____	87
4.2.3. Test Results _____	89
4.2.4. Strain Data _____	92
4.2.5. Analytical Work _____	98
4.2.6. Conclusions _____	107
4.2.7. Design _____	107
4.3. Durability of Putty and Its Characterization With and Without Fillers _____	109
4.3.1. Background _____	109
4.3.2. Test Specimens _____	109
4.3.3. Durability _____	119
4.3.4. Conclusions _____	130
4.4. Bond Test Controlling the Thickness of Putty _____	131
4.4.1. Test Specimens _____	132
4.4.2. Test Setup _____	134
4.4.3. Test Results _____	135
4.4.4. Conclusions _____	136
5. INFLUENCE OF ARCHING MECHANISM IN MASONRY WALLS STRENGTHENED WITH FRP LAMINATES _____	137
5.1. Previous Results _____	137
5.2. Experimental Program _____	148
5.3. Test Setup _____	154
5.4. Test Results _____	157
5.5. Analytical Study _____	168
6. IN-PLANE BEHAVIOR OF MASONRY WALLS STRENGTHENED WITH FRP LAMINATES AND RODS _____	176
6.1. Previous Results _____	177
6.2. Test Specimens _____	184
6.3. Test Setup _____	189
6.4. Test Results _____	191
6.5. Mechanism of Failure _____	198
6.6. Conclusions _____	202

7. POST - TENSIONING	205
7.1. Background	205
7.2. Tensioning and Anchor Devices	215
7.3. Test Setup	224
7.4. Test Results	225
7.5. Validation of the System	226
7.5.1. Test Setup	227
7.5.2. Test Results	229
7.6. Conclusions	233
8. CONCLUSIONS AND FUTURE WORKS	235
8.1. Conclusions	235
8.2. Future works	235
8.3. New frontiers for FRP composites (Blast upgrading)	237
APPENDIX A: ARCHING EFFECT	239
Appendix A.1: Beams design	240
Appendix A.2: Strengthening scheme	247
Appendix A.3: Test Setup	250
Appendix A.4: Test results	251
Appendix A.5: Analytical study	264
APPENDIX B: IN - PLANE	277
APPENDIX B.1: Test Specimens	278
APPENDIX B.2: Test Setup	280
APPENDIX B.3: Test Results	281
APPENDIX B.4: Mechanism of Failure	290
APPENDIX C: POST -TENSIONING	293
APPENDIX C.1: Tensioning and Anchor Devices	294
APPENDIX C.2: Tensile Tests	299
APPENDIX C.3: Long Term Tests	300
APPENDIX C.4: Validation of the System	302

APPENDIX C.5: Patent Disclosure	305
<i>APPENDIX D: MATERIALS AND BOND CHARACTERIZATION</i>	307
APPENDIX D.1: Specimens Preparation (Bond Tests)	308
APPENDIX D.2: Test Setup (Bond Tests)	309
APPENDIX D.3: Test Results (Bond Tests)	311
APPENDIX D.4: Photographs (Bond Tests)	317
APPENDIX D.5: Specimens Preparation (Putty Tensile Tests)	319
APPENDIX D.6: Test Setup (Putty Tensile Tests)	320
APPENDIX D.7: Test Results (Putty Tensile Tests)	321
APPENDIX D.8: Durability Tests (Putty)	327
APPENDIX D.9: Test Specimens (Controlling the Putty)	336
APPENDIX D.10: Test Setup (Controlling the Putty)	337
APPENDIX D.11: Test Results (Controlling the Putty)	338
<i>BIBLIOGRAPHY</i>	341

SOMMARIO

L'elaborato di tesi dal titolo: *“Strengthening of masonry: opportunities and challenges in the use of composites / Rinforzo della muratura: campi di applicazione e prospettive nell'utilizzo dei materiali compositi”* è stato svolto nell'ambito di un programma a carattere sperimentale dell'Università del Missouri – Rolla (USA), utilizzando i laboratori del dipartimento di Ingegneria Civile C.I.E.S. (Center for Infrastructure Engineering Studies) diretti dal Prof. Ing. Antonio Nanni. Per questo motivo esso è presentato interamente in lingua inglese.

Con i test sperimentali svolti non ci si è limitati allo studio di una sola problematica riguardante il rinforzo delle murature, ma si è cercato di sviluppare più argomenti al fine di fornire una metodologia di progettazione e di realizzazione del rinforzo nel campo del recupero e del mantenimento delle opere in muratura. Tutto questo è stato possibile grazie alle enormi potenzialità dell'Università Americana che ha permesso di disporre appieno di attrezzature, laboratori, materiali e mano d'opera, ma soprattutto grazie all'appoggio di una organizzazione pressoché perfetta.

La tesi ha avuto quindi un carattere prettamente sperimentale con lo sviluppo di modelli teorici di interpretazione per i risultati ottenuti. Questo sommario vuole essere un breve riepilogo del lavoro presentato nei seguenti capitoli.

Sono state affrontate le seguenti problematiche:

- Sperimentazione su murature rinforzate con FRP soggette a forze agenti nel piano
- Sperimentazione su murature rinforzate con FRP soggette a forze agenti fuori dal piano
- Invenzione di un nuovo metodo di post-tensione per barre termoplastiche in fibra di vetro al fine di sostituire, nel campo del rinforzo, le catene in acciaio
- Studio dell'aderenza sviluppata tra gli FRP e la muratura
- Prove di durabilità inerenti i materiali utilizzati per l'applicazione dei materiali compositi

La comunità internazionale degli ingegneri ha individuato nel collasso di murature non rinforzate una delle maggiori cause di danni materiali e perdite di vite umane in occasione di eventi sismici. Le convenzionali tecniche di rinforzo sono generalmente invasive ed apportano un notevole incremento delle masse, aumentando così le forze sismiche ed il peso complessivo della struttura. Inoltre, queste tecniche, richiedono tempi di installazione lunghi che non permettono l'immediata messa in sicurezza dell'edificio. E' quindi necessario sviluppare metodologie di rinforzo strutturale affidabili, durabili e di veloce installazione.

Gli *FRP* appartengono alla vasta famiglia dei "compositi strutturali", ossia, di quei materiali costituiti da due o più fasi di cui almeno una - il *rinforzo* - è presente in forma discontinua ed è caratterizzata da elevate prestazioni meccaniche, mentre l'altra - la *matrice* - è identificabile come un elemento continuo e meccanicamente più debole (capitolo 2). Nel settore delle costruzioni si è assistito, nell'ultima decade, ad un notevole incremento dell'utilizzo di compositi strutturali a matrice polimerica. In Giappone, paese che per primo ha eseguito sperimentazioni e realizzato applicazioni pratiche di materiali *FRP* in edilizia, il consumo delle fibre per uso strutturale è passato dalle 6 tonnellate del 1993 alle 250 tonnellate del 1997. Analogo andamento è stato registrato negli ultimi anni negli Stati Uniti, altro paese trainante nell'utilizzo degli *FRP* nel campo delle costruzioni. Il maggiore utilizzo degli *FRP* nell'edilizia, come si è accennato precedentemente, riguarda essenzialmente il settore del restauro statico delle strutture degradate o danneggiate e, in particolare, quello dell'adeguamento sismico. Le fibre più adatte ad essere utilizzate nel restauro delle strutture in cemento armato sono quelle in carbonio a media-alta resistenza e medio-alto modulo elastico. Le fibre di aramide e, ancor di più quelle in vetro, trovano un utilizzo più limitato nelle strutture in cemento armato a causa del loro più basso modulo elastico e alla conseguente minore capacità di assumere carichi, a parità di deformazioni impresse. Il loro impiego risulta essere più estensivo ed appropriato nel campo della riqualificazione degli edifici in muratura dove un modulo elastico particolarmente elevato non costituisce un'esigenza primaria e può, invece, rappresentare, in alcuni casi, una problematica. Inoltre, un aspetto non trascurabile, è che le fibre di aramide e di vetro hanno costi notevolmente inferiori rispetto a quelle

in carbonio e sperimentazioni sui muri rinforzati con questo tipo di compositi hanno mostrato notevoli incrementi in resistenza e duttilità.

I principali vantaggi degli *FRP* rispetto ai materiali tradizionali si possono riassumere in: leggerezza, alto rapporto resistenza/peso specifico, durabilità in ambienti umidi ed aggressivi, velocità di installazione, possibilità di adattarsi a superfici curve (capitolo 2). I compositi strutturali vengono utilizzati nel restauro delle costruzioni sotto forma di tessuti unidirezionali o pluridirezionali che vengono impregnati direttamente in opera (*wet-lay-up*, capitolo 3), oppure sotto forma di elementi rigidi già impregnati con la resina, ottenuti per mezzo di un processo industriale di estrusione che prende il nome di *pultrusione* (capitolo 3). I pultrusi vengono utilizzati sottoforma di piastre o di barre cilindriche che vengono inserite nella struttura da restaurare mediante metodi come quello delle *Near Surface Mounted Rods* (capitolo 3).

Per quanto la letteratura tecnica abbondi di ricerche eseguite in laboratorio e sul campo, non esiste ancora una conoscenza sufficientemente attendibile sui modelli di comportamento di elementi compressi o inflessi rinforzati con fasce o barre di *FRP*, soprattutto nel campo delle murature. Conoscenza che deve tenere conto di diversi fattori che possono influenzare gli *FRP* quali, ad esempio, quelli trattati nel presente elaborato, ovvero: la *delaminazione* dei laminati prima della rottura delle fibre stesse (capitolo 4), l'influenza delle condizioni di vincolo e della snellezza (rapporto altezza/spessore) delle murature soggette a carichi fuori dal piano (capitoli 1 e 5), le percentuali di rinforzo in grado di fornire un comportamento duttile ed un contemporaneo aumento di resistenza alle murature soggette a carichi nel piano (capitoli 1 e 6), la durabilità degli elementi costituenti la preparazione della superficie per l'installazione dei laminati (capitolo 4).

L'utilizzo degli *FRP* può inoltre essere esteso anche ad altri interventi, quali per esempio la sostituzione di catene in acciaio per operazioni di post-tensione. Il materiale tradizionalmente usato in questo tipo di applicazioni è appunto l'acciaio, al cui utilizzo sono connessi problemi legati a fenomeni quali: creep, rilassamento, invecchiamento e corrosione. La post-tensione richiede la creazione di ancoraggi alle estremità delle barre per trasmettere lo stato di tensione e nel caso delle barre in *FRP* quest'aspetto costituisce il problema principale.

La tecnica di post-tensione proposta nella tesi (capitolo 7), utilizza barre termoplastiche in fibra di vetro (*GFRP*) mediante particolari dispositivi di ancoraggio in grado di ridurre i problemi connessi alla durabilità e all'invecchiamento e di garantire un miglior comportamento strutturale d'insieme grazie al basso modulo di elasticità, molto più vicino a quello delle murature. L'efficacia di questa tecnica è stata dimostrata mediante prove sperimentali di laboratorio.

Per ogni argomento affrontato all'interno del seguente elaborato sono fornite conclusioni e raccomandazioni per lavori futuri.

Nota: Il lavoro esposto nell'elaborato di tesi ha già ottenuto i seguenti riconoscimenti scientifici:

- 8-11 Giugno 2001: “National Science Foundation Industry meeting”, University of Missouri Rolla. Esposizione dei lavori svolti e riportati nei capitoli 4-5 e 7.
- 29-31 Maggio 2002: “Durability of fiber reinforced polymer (FRP) composites for construction”, Hotel Delta Centre Ville, Montréal Québec (Canada), esposizione dell'articolo intitolato “Tensile Characterization and Durability of Putty Used for Externally Bonded FRP Strengthening”.
- 10-12 Giugno 2002: “Third international conference on composites in infrastructure , ICCI 2002”, San Francisco (California), esposizione dell'articolo intitolato “Influence of Arching Mechanism in Masonry Walls Strengthened with FRP Laminates”.
- Il giornale “L'edilizia” ha chiesto di pubblicare l'articolo dal titolo: “L'Utilizzo di Barre Termoplastiche in FRP negli Interventi di Riabilitazione Strutturale” in uno dei suoi prossimi numeri.
- Per il metodo di ancoraggio proposto nel capitolo 7 è stata inoltrata domanda di brevetto internazionale.

ABSTRACT

The worldwide engineering community has identified failures of Unreinforced masonry (URM) walls as one of the major causes of material damage and loss of human life due to seismic events. Therefore, the development of effective and affordable retrofitting techniques for masonry members is an urgent need. To date, previous works on URM and reinforced masonry walls strengthened with fiber reinforced polymeric (FRP) materials have shown notable increases in capacity and ductility. Unfortunately, field applications involving the use of FRP laminate on masonry members may be carried out even if not supported by rigorous experimental background. The cause of that is the implicit assumption that the high performances of FRP should always benefit a compromised structural situation. Part of the present experimental programs (i.e. bond tests, out-of-plane behavior with arching effect, in-plane behavior) shows the detrimental effects produced by inaccurate design. Conclusions and recommendations are provided for all the studied issues.

Use of FRP materials is not limited to strengthen walls subjected to out-of-plane and in-plane loads, but can be in the form of tendons in pre-stressing applications. This could be a new frontier for the FRP materials because of advantages over steel tendons such as light weight, resistance to corrosion, lower or higher elastic modulus etc. A major problem facing the use of FRP in pre-stressing applications is the anchorage. The new anchor system showed in section 7 demonstrated that FRP can be successfully used for the postensioning of masonry in substitution of steel.

A technical obstacle preventing the extended use of FRP materials in construction is a lack of long-term and durability performance data comparable to the body of knowledge available for traditional construction materials. A durability test was conducted as part of this thesis on a type of putty (used to prepare the surface) to demonstrate the implications of this concern.

1. INTRODUCTION

1.1. General

Masonry is one of the oldest construction materials. For thousand years masonry was the predominant building material until modern materials such as concrete, steel and wood appeared in the nineteenth century. Masonry constitutes approximately 70% of the existing building inventory in the United States. Most of these buildings possess unreinforced masonry (URM) walls. URM buildings have features that can threaten human integrity. Structural weakness, overloading, dynamic vibrations, settlement, in-plane and out-of-plane overstresses can cause failure of masonry structures. Organizations such as the Federal Emergency Management Agency (FEMA) and The Masonry Society (TMS) in the United States have identified that failure of URM walls results in most of the material damage and loss of human life. Figure 1.1 illustrates the collapse of URM walls due to out-of-plane and in-plane loads after the earthquake in Izmit, Turkey in 1999. These kinds of failure are a potential threat to bystanders.



(a) *Out-of-plane failure*



(b) *In-plane failure*

Fig. 1.1. Failure of URM walls

In 1986 a building evaluation carried out in the state of California, U.S.ci on URM buildings showed that 96% of these needed to be retrofitted, which would result in approximately \$4 billion in retrofit expenditures. To date, it has been estimated that only half of the owners have taken remedial actions, which may be attributed to high

retrofitting costs. Thereby, the development of an effective and affordable retrofitting technique for masonry elements is an urgent need.

In the United States there are three typical masonry walls:

- Panel walls
- Curtain walls
- Bearing walls

Panel walls

Panel walls are single-story walls and are common façade elements in buildings conformed by frames or steel or reinforced concrete. These kinds of walls consist of two wythes separated by at least 50.8 mm (2 inches) air space, commonly referred to as cavity walls. The air space in the cavity improves the thermal performance of the wall, which can be enhanced by inserting insulation in the cavity. In most applications the inner wythe supports the weight of floors and the outer is non load bearing. These walls may also consist of single wythe or multiple wythes in contact with each other (composite walls).

When built in reinforced concrete (RC) or steel frames, these walls are called infill walls and they protect the interior from the external environment. Infill walls can be subjected to in-plane loads caused by their interaction with the surrounding frame. Due to vertical spans of 3.3 m (11 feet) or less, panel walls can satisfactorily resist out-of-plane loading and are generally unreinforced. However, during a seismic event, excessive damage due to in-plane seismic loading can lead to significant stiffness reduction in the lateral direction making, therefore, these walls susceptible to out-of-plane collapse.

Curtain walls

Curtain walls are multi-story walls that also resist out-of-plane loads due to earthquake or wind. If a single wythe is used, horizontal steel, in the form of welded reinforcement, is placed in the mortar joints to increase the resistance. This kind of construction is commonly referred to as “partially reinforced”.

Bearing walls

Bearing walls are arranged at fairly uniform spacing to resist out-of-plane loads, in-plane loads and vertical loads from self-weight and upper derived from floor areas. Cavity and composite walls can also lie on this category. Depending on the load solicitations, bearing walls can be unreinforced or reinforced.

Masonry in backup walls

Commonly two different masonry units are found in backup or inner walls; clay tiles and concrete units. A clay tile is a hollow unit, which is characterized by possessing parallel cores and thin webs and faceshells. Clay materials were mixed with water to create a homogeneous mass and then formed into brick units by pressing into a mold. Structural clay tiles have been first manufactured in the United States approximately since 1875.

In the beginning, structural tile was used in building floors and as fireproofing material for steel frame constructions. Due to its lightweight, large unit size and ease of handling during constructions, the use of clay tiles was extended to load-bearing walls, wall facings, silos, columns, etc.

In the early 1900's, structural clay tiles were used in infill walls throughout the United States.

Some notable structures where it is possible to observe this kind of construction are the New York Chrysler building (New York) and the Los Angeles City Hall Building (California).



Fig. 1.2. Los Angeles City Hall Building (California)

Today, the whole brickmaking process (mining, forming, drying, firing, cooling and delivery) is highly mechanized and can be completed in less than a week.

Can be observed that the production of clay tiles decreased during the 1960's, when concrete units began to be widely used. It is important to point out that the use of concrete units was not new in the United States. Concrete blocks were first manufactured in the United States at about the turn of the 20th century in small one-at-a-time machine that could be operated by hand. Using this kind of machine, the production was limited to 10 blocks per man-hour. Concrete blocks were not widely used until the 1920's when the manufacturing process was improved; however due to the recession many plants had close or merge. It was not until the 1960's that the market started to change. This change is attributed to the automation of plant equipment, which increased the production capability of concrete blocks. The manufacturing process of concrete units allowed a better quality control of the products and also concrete units showed more uniformity since they were not fired during their fabrication. Also, the brittle characteristics of clay tiles when being handled and transported increased the demand of concrete units. Modern concrete blocks are generally manufactured by vibrating a mixture of Portland cement, sand and aggregate in a mold under pressure, curing with low-pressure or high-pressure steam and then, in some cases, exposing them to carbon dioxide in the curing chamber to reduce subsequent shrinkage of the units. To date there is a large use of concrete blocks inside the USA, for different kinds of buildings.

1.2. Problem Statement: Out-of-Plane and In-Plane Behavior of URM Walls

Out-of-plane behavior

Masonry walls may be subjected to out-of-plane loads. These walls are referred to as flexural walls since the mode of deformation is primarily flexure with little or no externally applied load. The load can be permanent, such as earth pressure against a retaining wall or basement wall or they can be transient, such as wind or earthquake. Walls must be also sufficiently robust to not cause disproportionate amounts of damage or failure. In ancient masonry buildings walls were generally thick enough that flexural stresses from the lateral load were much lower than axial compressive stresses from self-weight and other gravity loads. To date, the tensile strength of masonry has become upon to provide flexural resistance to out-of-plane loads.

The load-resisting mechanisms for the unreinforced masonry walls depend on the tensile strength of masonry, in-plane compressive strength, boundary conditions and slenderness ratio (height/thickness).

Walls that are *simply supported* and span in only the vertical direction must resist lateral action by bending action. The bending capacity is directly related to the axial compression and the moment capacity is different if the flexural tensile strength of masonry is taken in account or no. If the tensile strength is neglected (figure 1.3a), the bending capacity is directly related to the axial compression and the moment capacity is:

$$M = f_a S$$

Where:

f_a = axial compressive stress = P/A_n

A_n = effective mortar bedded area

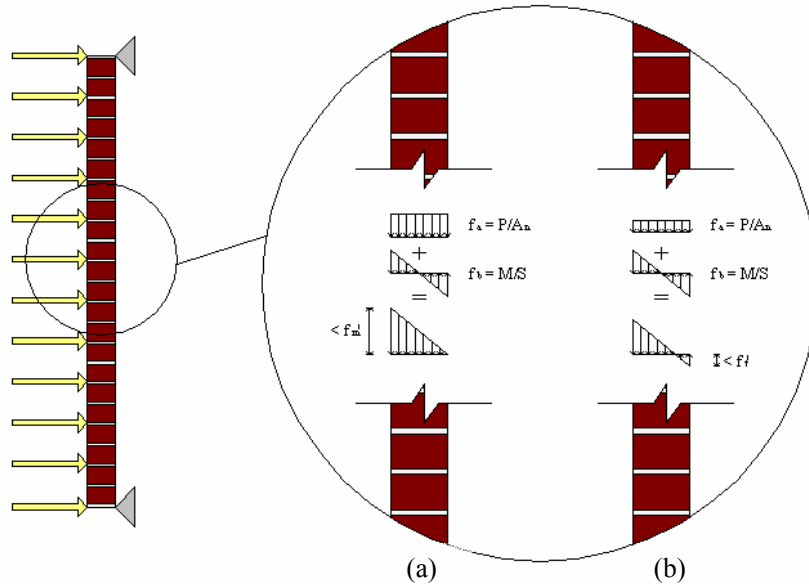
S = section modulus for out-of-plane bending

If the tensile strength of masonry can be taken in account (figure 1.3b) the moment capacity becomes:

$$M = (f_a + f_t')S$$

Where:

f_t' = flexural tensile strength normal to bed joints.



Note: f_m' = maximum compressive strength of the masonry

Fig. 1.3. Flexural behavior of unreinforced section (linear elastic material)

When the tensile stress reaches the limiting tensile strength, this is usually defined as the flexural tensile capacity. However, if cracking is allowed additional lateral load can be applied.

When a wall is built between supports that restrain the outward movement, axial compressive forces accompanied by the shear forces (F_v and F_h in figure 1.4) are induced as the wall bends. The in-plane compression forces can delay cracking. After cracking the so-called *arching action* can be observed, which in many cases increases several times the capacity of the wall. Analysis (L.R. Baker, 1978; A.W. Hendry, 1981) have shown that the induced forces can increase the cracking load by a factor of about 2.5 if the end supports are completely rigid.

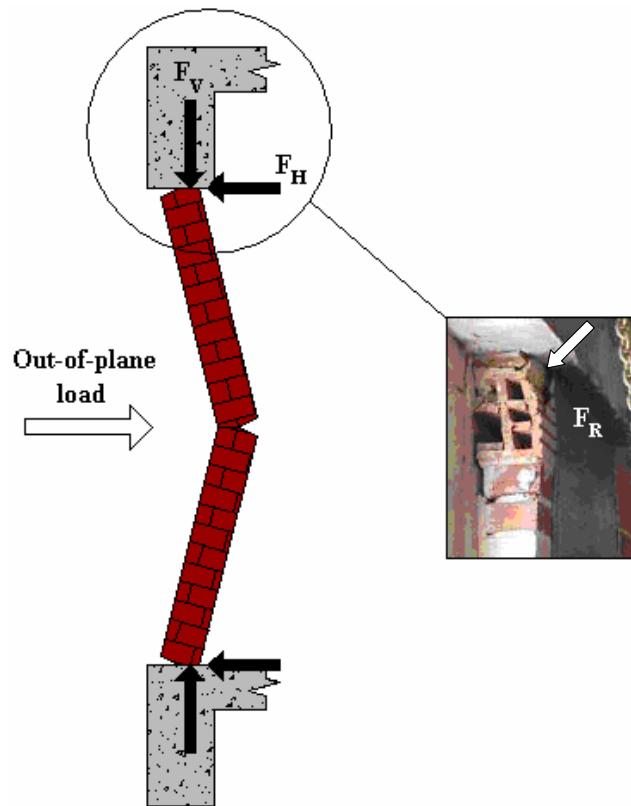


Fig. 1.4. Wall subjected to Arching Effect (Scheme)

Investigations have shown that the resultant force between F_v and F_h (F_r in figure 1.4) could cause the fracture of the corner. It has been reported also that for slenderness ratio (h/t) larger than 20, the arching action is small (Angel et al., 1994).

Once that the wall has been cracked at mid-height, it can be assumed that the two resulting segments can rotate as rigid bodies like shown in figure 1.4, forming a three hinged arch.

Analyzing the top segment of the wall, the following consideration can be derived: Being BC equal to $B'C'$ for simple geometric considerations (figure 1.5) the arm for the resistance moment (figure 1.6) can be assumed, for very small angle θ , equal to:

$$a - \Delta_0$$

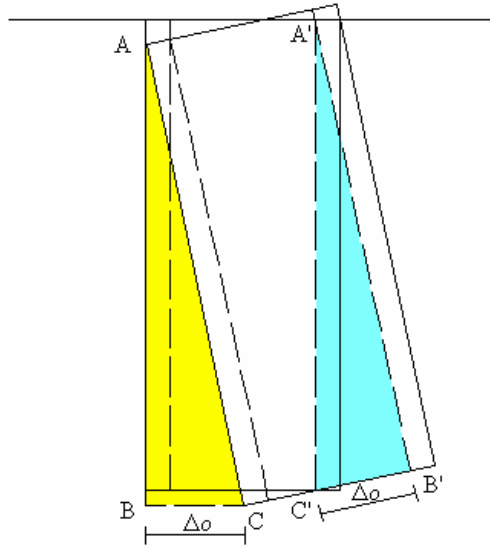


Fig. 1.5. Geometric considerations for the top segment of the wall

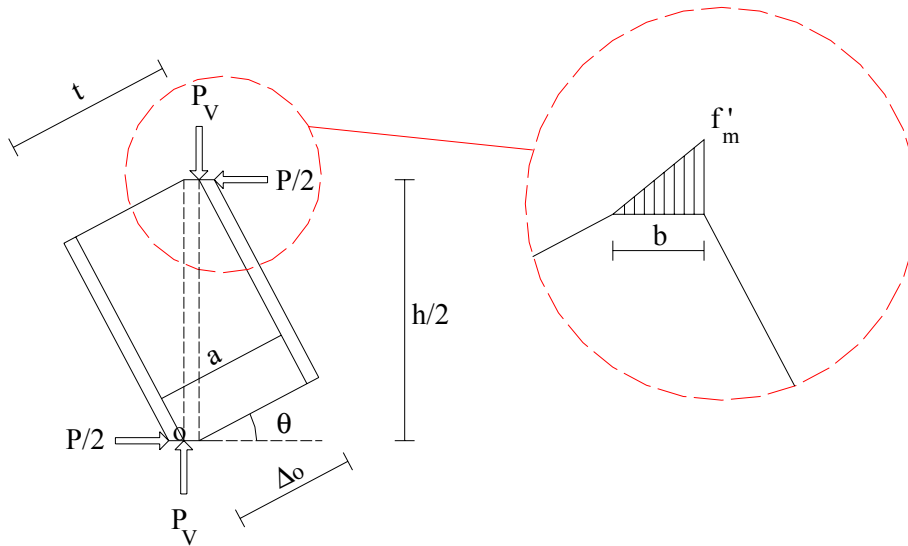


Fig. 1.6. Free body diagram of upper part of the wall

Where:

P = out-of-plane-load

P_v = clamping force

h = height of the wall

t = thickness of the wall

a = arm distance between clamping forces

b = bearing width

Δ_0 = wall deflection

f_m' = compressive strength of masonry

Taking moment about “O” can be calculated the equilibrium that is:

$$\frac{P}{2} \cdot \frac{h}{2} = P_v \cdot (a - \Delta_0)$$

So, the out-of-plane force allows on the wall is:

$$P = \frac{4 \cdot P_v (a - \Delta_0)}{h}$$

In general the wall behavior can be controlled by crushing of the mortar joints in the boundary regions. However, in the case of walls built with masonry units with brittle characteristics such as clay tiles, the wall behavior can be controlled by fracture of the units (Tumialan, 2001).

If a masonry wall is separated from the top by a small gap due to poor construction, wall shrinkage etc., arching can still develop, but to a lesser extent.

In-Plane Behavior of Infill Walls

Masonry walls are widely used as interior partitions within steel and RC frame structures as exterior walls to form part of the building envelope. For the latter case, depending on design considerations, the infill walls may or not may resist to lateral and vertical loads. In order to simplify the design, the potential interaction between the infill walls and the structural frame has been ordinarily ignored. Ignoring the contribution of the masonry infill walls does not always represent a conservative design. Their presence can lead to stiffening their frames (Sabnis, 1976) and thereby cause a redistribution of the lateral loads in the building plan.

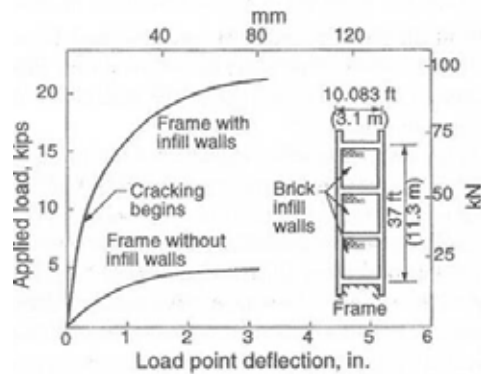


Fig. 1.7. Load deflection curves of frames with and without infill walls (Sabnis)

Infill walls can be totally enclosed in a surrounding frame of beams and columns, as typical in a multi story building. These walls can be subjected to high in-plane loads during exceptional events such as high wind or earthquake. These loads are due to the interaction between the infill walls and the surrounding structural frames. Previous investigations (Sabnis, 1976) have demonstrated that the composite action between the masonry infill and the surrounding frame is depending on the level of the in-plane load, degree of bond or anchorage at the interfaces and geometric and stiffness characteristics of the two components. At very low levels of lateral load, a full composite action between the infill wall and the frame is observed (Figure 1.8).

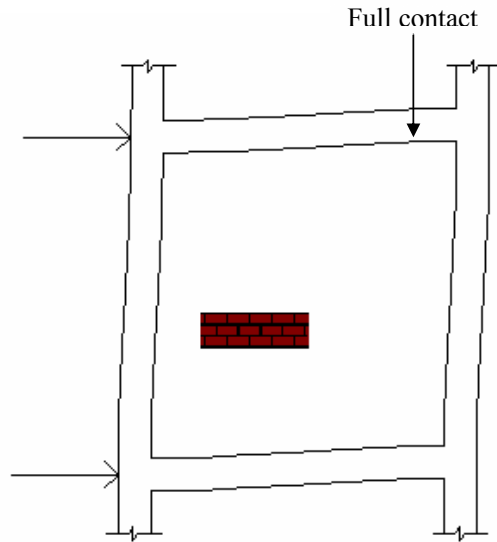


Fig. 1.8. Full composite action between frame and infill panel

As the load increases, deformations increase and separation between the wall and the frame takes place except in the vicinity of the two corners where compression forces are transmitted through the wall. This leads the formation of a diagonal compression strut (Figure 1.9).

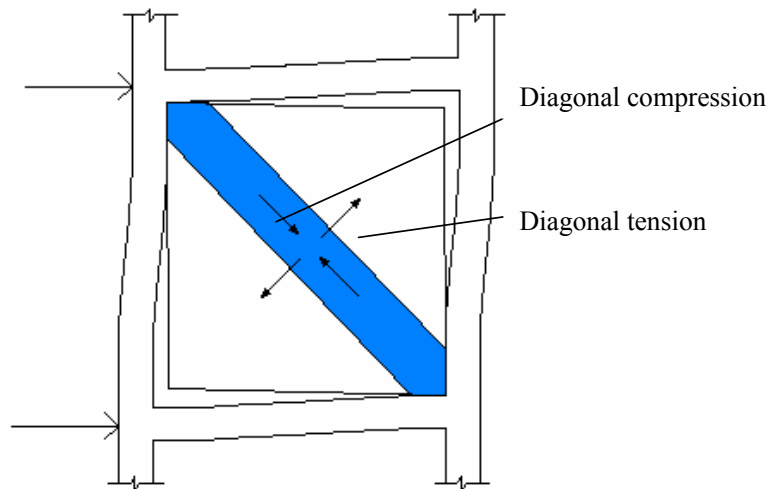


Fig. 1.9. Diagonal compression strut

This resulting structural system is usually analyzed as a truss. The stiffness of the infill starts decreasing once cracking is developed.

Alternatively, the wall may fail in shear along a bed joint rather than by diagonal compression. This could happen at a lower load level as compared to the load causing the latter mentioned failure. The formation of the shear crack separates the panel into two parts and the behavior in this case is controlled by either the flexural or shear capacity of the columns. This failure mechanism is commonly known as Knee Brace or Joint Slip (Figure 1.10).

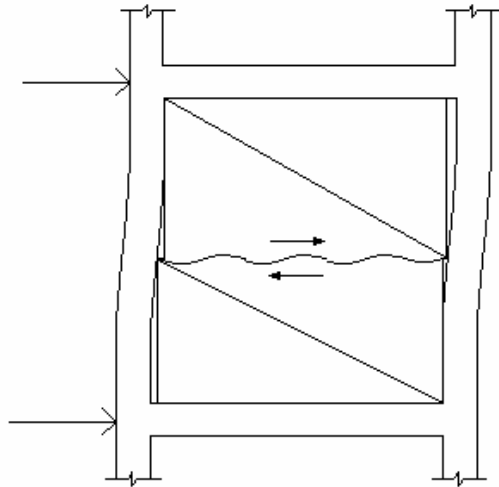


Fig. 1.10. Joint-Slip failure

1.3. Problem Statement: Post Tensioning of Masonry

During their life walls could show cracks due to past seismic events or differential settlement that compromise the building stability and aesthetic sense. Pre-stressing forces are used in masonry to reduce or eliminate tensile stresses due to externally applied loads or to close the cracks caused by passed events by using controlled

precompression. The precompression is generated by prestressing tendons, either bars, wires, or strands, that are contained in openings in the masonry, which may be grouted. The prestressing tendons can be pre-tensioned (stresses against external abutments prior to placing the masonry), or post-tensioned (stresses against the masonry after it has been placed). Internal pre tensioning has been used successfully to increase strength and provide ductility to existing URM masonry structures. In situations where internal pre-tensioning is not feasible, post-tensioning of URM masonry is often a viable option. Most construction application to date have involved post-tensioned. The prestressing bars or strands can be installed in pairs on opposite sides of a wall so that out-of-plane bending is not introduced. Figure 1.11 illustrates an example of the use of external horizontal post-tensioning to improve the structural integrity and resistance to lateral loads in a masonry building.

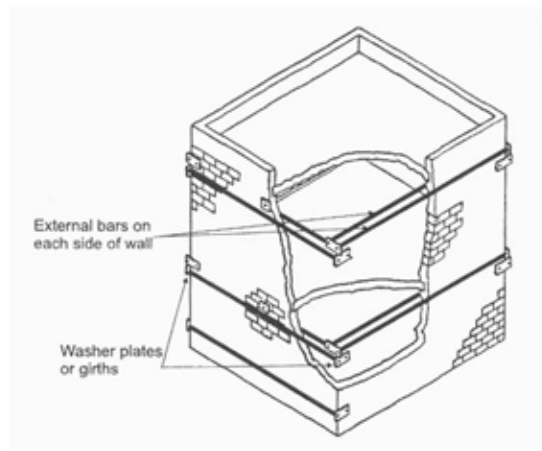


Fig. 1.11. Use of external prestressing for strengthening masonry buildings

Effective prestress is not a fixed quantity over time. Research had shown that the the loss and the gain of prestress in masonry is extensive and it is due to phenomena such as creep, shrinkage, moisture expansion, deformations of the masonry, and prestressing-tendon stress relaxation.

1.4. Conventional Retrofit Techniques

Common retrofitting techniques with conventional methods can include internal reinforcement, external reinforcement overlay, internal steel reinforcing, external steel plate reinforcing and grout filling of hollow and cavity walls.

Internal Reinforcement

In hollow masonry and cavity walls, it is sometimes possible to improve the flexural strength of walls for both in-plane and out-of-plane vertical bending by cutting openings in the wall and threading reinforcing bars vertically (up and down). Grouting can then be completed the technique. Figure 1.12 shows the aforementioned technique.

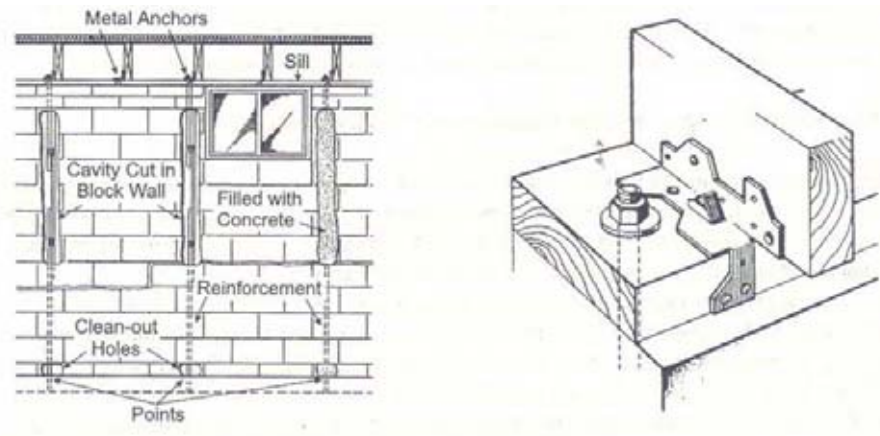


Fig. 1.12. Internal reinforcement technique

External Reinforcement Overlay

Where the aesthetic sense is not a controlling concern, the external reinforcement overlay can be used. Ferrocement is the most common overlay producing an orthotropic material consisting of high-strength cement mortar and layers of fine steel wires configured in the form of a mesh. The overall thickness is usually varies

between 12 to 25 mm (1 to 2 in.). These overlays are used to increase in-plane and out-of-plane resistance.

Internal Steel Reinforcing

This technique consists to repair the URM walls subjected to in-plane loads by horizontal and vertical steel reinforcement. The installation procedure includes grooving of the bed joints followed by placement of the steel and sealing with the mortar.

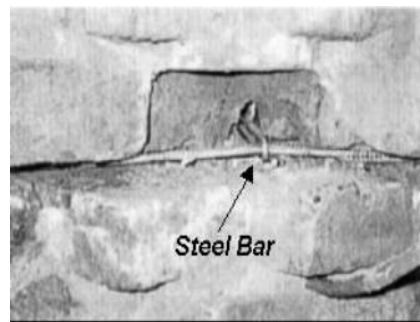


Fig. 1.13. Internal steel reinforcing

External Steel Plate Reinforcing

Steel plates and angles can be used to strengthen walls subjected to in-plane and out-of-plane loads. Figure 1.14 shows a strengthening method proposed by Taghdi et al. (2000), used for in-plane loads. This method could be also effective for out-of-plane loads.

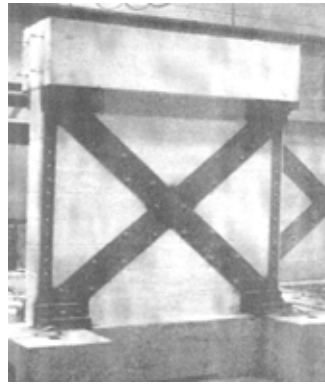


Fig. 1.14. External steel plate reinforcing

Grout Filling of Hollow and Cavity Walls

Filling the cells of hollow units with grout increases the compressive capacity and, because of the greater tensile strength of grout compared to mortar bond, also produces a significant improvement in flexural and in-plane shear capacities. Filling voids with grout can also improve the resistance to water penetration, particularly for single-wythe construction. Except for very large cells or cavity widths, gravity placement of grout is typically not reliable due to obstructions from mortar fins and droppings and because of the difficulty of providing vibration for consolidation. Therefore, pressure grouting from the bottom up is usually the most reliable method for achieving complete filling. The vertical spacing is limited by the ability of the masonry to withstand internal pressure., by the capacity of the pump, and by the desire to limit the height of lifts to allow for some consolidation due to water absorption and compaction of the grout. Fine grout, often incorporating a plasticizer, is typically used and commercially available products that also recommended to avoid shrink-back of the grout and creation of voids in the grout or between the grout and the masonry.

The FRP Materials

Although the concept of fiber reinforced materials can be traced back to the use of straw as reinforcement in bricks manufactured by the Israelites in 800 B.C., and in more recent times to the use of short glass fiber reinforcement in cement in United

States in the early 1930's, fiber reinforced resin matrix materials (or *fiber reinforced composites* as we know them today) were not developed until the early 1940's.

After World War II, US manufacturers began producing *fiberglass* and *polyester resin* composite boat hulls and radomes (radar cover). The automotive industry first introduced composites into vehicle bodies in the early 1950s. Because of the highly desirable light weight, corrosion resistance, and high strength characteristics in composites; research emphasis went into improving the material science and manufacturing process. That effort led to the development of two new manufacturing techniques known as *filament winding* and *pultrusion*, which helped advance the composite technology into new markets. There was a great demand by the recreation industry for composite fishing rods, tennis rackets, ski equipment and golf clubs. The aerospace industry began to use composites in pressure vessels, containers, and non-structural aircraft components. The US Navy applied composites in mine sweeping vessels, crew boats and submarine parts. The domestic consumers began installing composite bath tubs, covers, railings, ladders and electrical equipment. The first civil application in composites was a dome structure built in Benghazi in 1968, and other structures followed slowly.

1.5. Scope and Objectives

To date, previous works on URM and reinforced masonry walls strengthened with fiber reinforced polymeric (FRP) materials have shown notable increases in capacity and ductility (Hamilton et al., Tumialan, Morbin, Velazquez). During a seismic event URM walls located at upper building stories can collapse due to higher seismic accelerations, walls located at the bottom story could be overstressed because the shear forces at that level could be larger than any other story.

During their life walls could show cracks due to past seismic events or differential settlement that compromise the building stability and aesthetic sense.

The main objectives of this research are to evaluate the effectiveness of different kinds of commercially available and experimental forms of FRP composite materials to illustrate the ability of FRP to increase the flexural and shear capacity of the walls,

to demonstrate that FRP can be used for the posttensioning in substitution of steel, and to provide design guidelines and recommendations.

1.6. Thesis Layout

Section One introduces several issues that could be encountered in the masonry buildings and the significance of the strengthening of masonry elements.

In *Section Two*, material properties of different FRP materials are presented. *Section Three* shows the installation process of FRP composites on the masonry walls. Since debonding of FRP laminates from masonry has been identified as the predominant mode of failure, *Section Four* deals with bond between FRP laminates and masonry. The influence of putty on the bond between FRP laminates and masonry is also discussed in this section.

The experimental program on flexural strengthening due to out-of-plane loads is discussed in the *Section Five*. The experimental program on shear strengthening due to in-plane loads is shown in *Section Six*.

Section Seven, introduces a new anchor system for post-tensioning Glass FRP (GFRP) bars. Due to anchorage limitations, the use of GFRP bars in post-tensioning applications has been limited.

Finally, *Section Eight* provides conclusions and recommendations for future works in the area of masonry strengthening with FRP composites.

2. THE FRP MATERIALS

2.1. Composite Materials

Composite materials are a unique class of materials made by combining two or more materials to obtain a new material that has properties from both components.

These materials offer some significant advantages to metals in many structural applications due to the ability to select various combinations of fiber reinforcement and resin material. A composite material can be selected from this spectrum to provide the optimal choice to meet application requirements.

Composite materials are composed of a **matrix** material reinforced with any of a variety of fibers (**reinforcing phase**) made from ceramics, metals, or polymers. The reinforcing fibers are the primary load carriers of the material, with the matrix component transferring the load from fiber to fiber. Reinforcement of the matrix material may be achieved in a variety of ways: fibers may be either continuous or discontinuous, and the reinforcement may also be in the form of particles (Figure 2.1).

Selection of the optimal reinforcement form and material is dependent on the property requirements of the finished part.

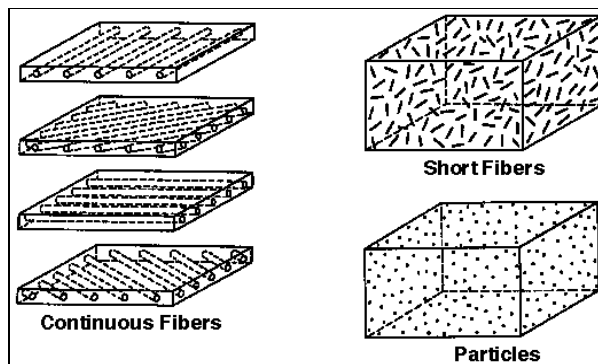


Fig. 2.1. Reinforcement of matrix material

The advantages of composite materials over metals are:

- Light weight
- Can tailor the fiber/resin mix to meet
- Meet stiffness/strength/manufacturing requirements
- Reduced machining
- Resistance to corrosion
- Resistance to fatigue damage
- Good damping characteristics
- Low coefficient of thermal expansion

Weight: A weight savings of 27% is attainable in most structures. This is due to the lower density of composites, which range (depending on material form) from 1246 kg/m³ (0.045 lb/in³) to 1800 kg/m³ (0.065 lb/in³) as compared to 2768 kg/m³ (0.10 lb/in³) for aluminum. Some applications may require thicker composite sections to meet strength/stiffness requirements, however, a weight savings will still result.

Part consolidation: Consolidating many parts in an assembly into one part is a major benefit gained by using composite materials. It enables the designer to go beyond mere material substitution and produce true composite parts. Complex shapes can be produced. Part consolidation reduces part count, fasteners and assembly time. The attachment areas of parts are where the majority of failures occur, due to high point loads and stress concentrations; elimination of these interfaces improves the reliability of the structure.

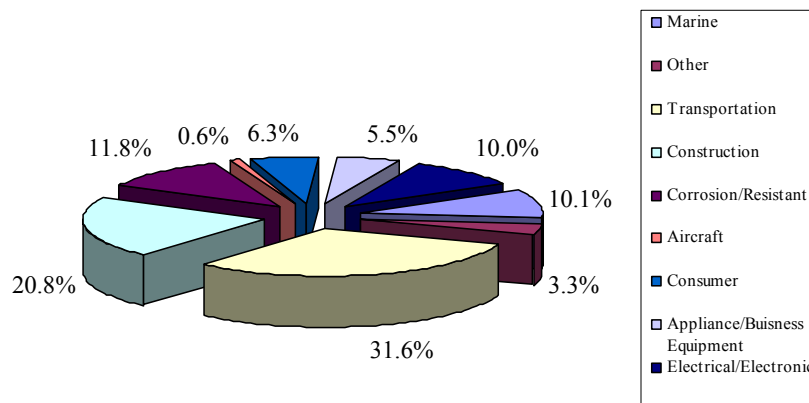
Cost: Low cost, high volume manufacturing methods are used to make composites cost competitive with metals: tooling costs for high volume production of metals and composites parts are similar and also the production labor time is similar, so the higher cost of composite parts is mostly due to high raw material costs; a judicious selection of the optimal material for the part (not the best material) and of the suppliers will control these costs and can minimize the cost penalty.

Composite performance: Composites have inherent properties that provide performance benefits over metals. A wide range of fibers and resins are available to

select the optimal material combination to meet the structural requirements. The strength-to-weight and stiffness-to-weight ratios are the primary reasons composites are used. The fiber reinforcements provide good damping characteristics and high resistance to fatigue and most resins provide very good resistance to chemicals and corrosion. The fracture toughness of composites is better than aluminum castings; by their nature, castings basically have built-in notches that can catastrophically fracture under impact. The fiber reinforcement of composites alter this failure sequence; resulting in an increased resistance to impact. The impact toughness of composites can be maximized by fiber selection, length of fiber and use of tougher resin such as thermoplastics.

Composite materials will provide structure that saves weight and has better performance over the competing metallic structure. The structure will be more durable and tougher. Composites will enable the consolidation of parts thus improving the reliability of the structure and keeping the costs competitive with metallic structure. In the passed thirty years, new composite materials appeared in the market: the fiber reinforced polymeric (FRP) materials.

The composite industry associations and materials producers track the FRP composites shipments in eight primary markets like shown in figure 2.2.



Note: Includes shipments of reinforced thermoset and thermoplastic resin composites, reinforcements and fillers.

Fig. 2.2. SPI Composites Institute, May 1999

The composites industry has shown growth over the past ten years and is projected to increase as FRP composites are accepted in new markets. Figure 1.3 shows the growth of FRP composites during these years.

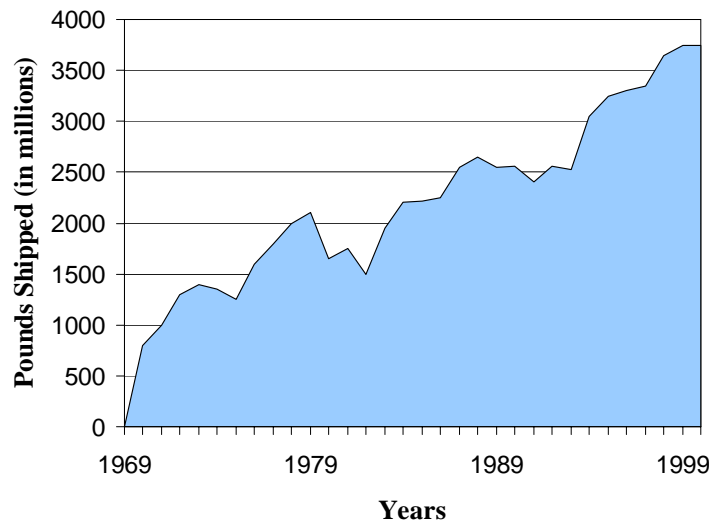


Fig. 2.3. Growth of FRP composites from 1970 to 2000

2.2. FRP Composites

Fiber reinforced polymers (**FRP**) are a particular typology of composite materials, made of high resistance fibers impregnated with polymeric resins. The mixing result is a material with tensile properties between fiber's and resin's one (Figure 2.4).

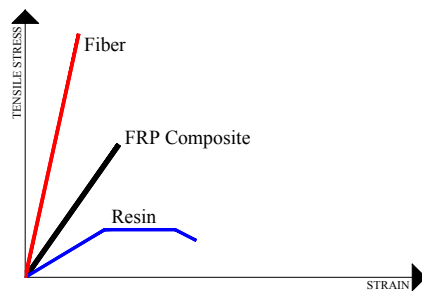


Fig. 2.4. Comparison among fiber's, resin's and composite's tensile properties

They are characterized by excellent tensile strength in the direction of the fibers and by negligible strength in the direction transverse to the fibers; this illustrates the anisotropic nature of these materials. FRP composites do not exhibit yielding, but instead are elastic up to failure and they are also characterized by relatively low modulus of elasticity in tension and low compressive properties.

Their function usually consists in adsorbing tensile stress due to shear and flexural actions. Often, among the reachable advantages, are also the increase of the overall stiffness and ductility.

FRP's properties make these materials particularly suitable for structural applications, especially in support or substitution of steel.

The general advantages of FRP reinforcement compared to steel are:

- Durability in aggressive environments
- High strength-to-density ratio
- Magnetic and electric neutrality
- Low specific weight
- Low axial coefficient of thermal expansion

Without underlining the importance of a lower installation cost, the use of FRP composites possesses some advantages compared to traditional retrofitting methods; as an example, the disturbance of the occupants is minimal and there is no loss of valuable space. In addition, from the structural point of view, the dynamic properties of the structure remain unchanging because there is no addition of weight that would lead to increases in seismic forces.

FRP products are commercialized in different shapes: rods, tendons, laminates and three-dimensional components.

FRP reinforcement comes in the shape of rods of circular cross-sections, strips of rectangular cross-sections, strands, and laminates, which enable different types of applications. Figure 2.5 shows different kinds of FRP.

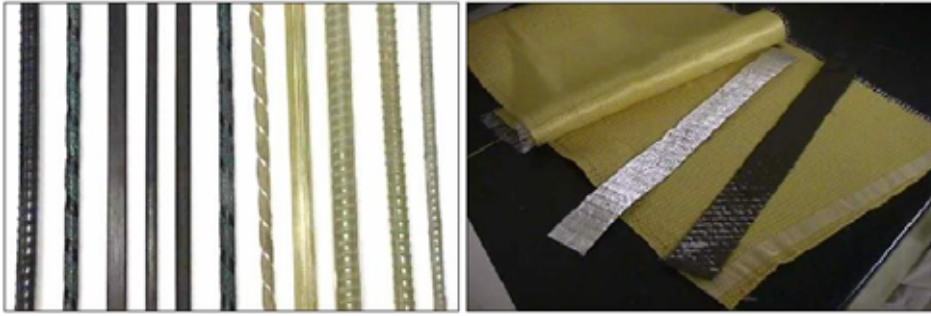


Fig. 2.5. Different kinds of FRP

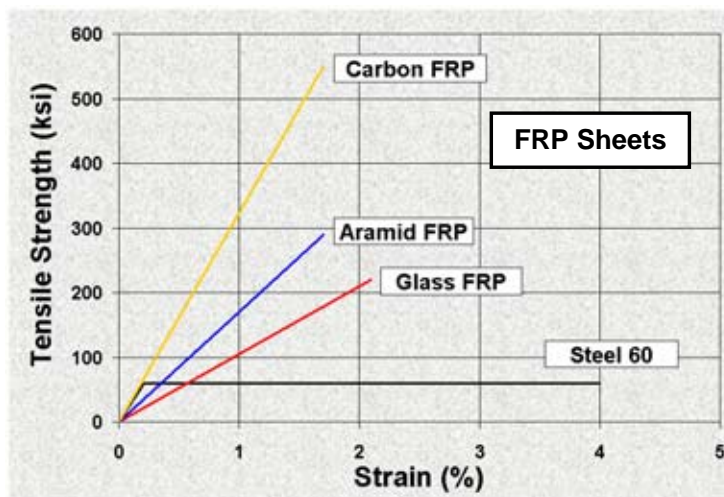
The Fibers

The three most common types of FRP used in construction are made of carbon, aramid or glass fibers.

- **Carbon Fibers:** Fiber produced by heating organic precursor materials containing a substantial amount of carbon (93÷95%), such as rayon, polyacrylonitrile (PAN), or pitch (a black residue from the distillation of petroleum) in an inert environment. This kind of fibers is the strongest, stiffest, and most durable; they are more expensive than glass fibers but offer an excellent combination of strength, low weight, high modulus and fatigue properties.
- **Aramid Fibers (ex. Kevlar):** Highly oriented organic fiber derived from polyamide incorporating into aromatic ring structure. This kind of fibers offers excellent impact resistance, a good electric and temperature insulating properties and they are also resistant to organic solvents, fuels and lubricants. They have a medium modulus and a very low density as compared to glass and carbon.
It is available in tows, yarns and various woven cloth products.
- **Glass Fibers:** Fiber drawn from an inorganic product of fusion that has cooled without crystallizing. **E-Glass** fibers are considered the predominant reinforcement for polymer matrix composites, due to their high electrical

insulating properties and low susceptibility to moisture. Other commercial composition includes **S-Glass**, with higher strength, heat resistance and modulus, as well as some specialized glass reinforcements with improved chemical resistance, such as AR Glass (alkali resistant). On the other hand, these products are very expensive. Glass produces a common, low-cost reinforcing fiber, but they weight more than carbon or aramid and the lower modulus requires special design treatment where stiffness is critical. Glass has been the predominant fiber for many civil engineering applications because of an economical balance of cost and specific strength properties.

A comparison based on fiber area only among sheets made of carbon (CFRP), aramid (AFRP), glass (GFRP) and reinforcing steel in terms of stress-strain relationship is illustrated figure 2.6.



Note: 1 ksi = 6.89 MPa

Fig. 2.6. Comparison among AFRP, CFRP, GFRP and Steel

The matrix

The FRP matrix consists of a polymer, or resin, used as a binder for the reinforcing fibers, and it has two main functions: it enables the load to be transferred among fibers and protects the fibers from environmental effects.

The resin is fundamental for interlaminar and in-plane shear strength: the interlaminar strength is important for the structures inflection and the in-plane strength is important for the torsion. Furthermore, FRP workability and defects depend of some physical-thermal resin's properties like viscosity, vulcanization temp and melting point.

Polymeric resins are subdivided in two big categories, thermosetting and thermoplastic:

- The **thermosetting polymers** after the vulcanization (with energy under appearances of heat energy or with catalysts) are insoluble and not melt also with high temperature.
- The **thermoplastic polymers** are instead soluble, because they have a low molecular bond; so, these resins can be weak, melted and mold infinite times.

The glass transition temperature (T_g) is used to measure the softening of cured resin. Generally the resins are isotropic and they have an elastic-brittle behavior.

Also if the thermoplastic resins had a large development as for thermosetting polymers, there are still many problems to soak the fibers. Thus, in the field, there are three types of commonly available thermo-setting resins: epoxy, vinyl ester and phenolic.

- **Epoxy** resins are the most common and have excellent structural properties as well as excellent adhesion characteristics; a major benefit of epoxy resins is their lower shrinkage. Epoxy can also be formulated with different materials or blended with other epoxy resins to achieve specific performance features. Epoxies are used primarily for fabricating high performance composites with

superior mechanical properties and good performance at elevated temperatures; this kind of resin has particularly good UV resistance and their maximum use temperature is on the order of 93° C (200° F). Epoxy resins are available in a range of viscosities, and will work with a number of curing agents or hardeners.

- **Vinyl ester** resins are a lower cost matrix material with good durability characteristics, excellent corrosion resistance and very good mechanical toughness, but they have lower structural performance and low resistance to heat. Vinyl esters were developed to combine the advantages of epoxy resin with the better handling/faster cure, which are typical for unsaturated polyester resins.
- **Phenolic** are a class of resins commonly based on phenol and formaldehyde. Phenolic composites have many desirable performance qualities include high temperature resistance, creep resistance, excellent thermal insulation and sound damping properties, corrosion resistance and excellent fire/smoke toxicity properties.

Phenolic appears the most important resin, but epoxy and vinyl ester are the most commonly used because of durability and adhesion properties.

For example, table 2.1 reports the main mechanical properties of a common epoxy resin.

Tab. 2.1. Typical properties of the epoxy resin

Properties	Values
Density	1200 kg/m ³
Elastic modulus	3.4 GPa
Shear modulus	1.308 GPa
Tensile strength	72 MPa

Note: 1000 kg/m³ = 0.036 lb/in³; 1 MPa = 145 psi

Thermosetting resins are generally heat activated, or cured, from an initial liquid state. Resins are often combined with additives and fillers for environmental

resistance, flame resistance, appearance, and cost reduction.

Fillers

The use of inorganic fillers in composites is increasing; they not only reduce the cost of composites, but also frequently impart performance that might not otherwise be achieved by the reinforcement and resin ingredients alone.

These materials improve the following performance:

- They reduce the shrinkage of the composites part
- They influence the fire resistance
- They can influence the mechanical strengths of composites
- Crack resistance and crack prevention properties are improved with filled resin systems
- Uniformity of the laminates can be enhanced by use of fillers

There are a lot of inorganic filler materials that can be used with composites including Calcium Carbonate (the most used), Kaolin, Alumina trihydrate, Calcium sulfate etc...

Additives

A wide of additives are used in composites to modify materials properties and tailor the FRP performance. Additive used in thermosetting composites include the following:

- Fire resistance (in place of fillers)
- Viscosity control
- Toughness
- Heat stabilizers
- Ultraviolet stabilizers

2.3. FRP Reinforcement Forms

Reinforcements are available in forms to serve a wide range of processes and end-product requirements and they can be obtained using multi-end or single-end roving. Multi-end roving consists of many individual strands or bundles of filaments, which are then chopped and randomly deposited into the resin matrix; these products can be used in pultrusion application.

The single-end roving consists of many individual filaments wound into a single strand. The product is generally used in processes that utilize a unidirectional reinforcement.

Materials supplied as reinforcement include:

- Mats
- Woven, stitched, braided & 3D fabrics
- Unidirectional
- Bars
- Laminates

Mats

Reinforcing mats are usually described by weight-per-unit-of-area; the type and amount of binder that is used to hold the mat together dictate differences between mat products.

Woven, stitched, braided & 3D fabrics

There are many types of fabrics that can be used to reinforce resin in a composite. Multidirectional reinforcements are produced by weaving, knitting, stitched or braiding continuous fibers into a fabric form twisted and plied yarn.

Fabrics allow the precise placement of the reinforcement.

- **Woven** fabrics are fabricated on looms in a variety of weights, weaves and widths. In a plain weave, each fill yarn or roving is alternately crosses over and under each

warp fiber. This work allows the fabric to be more drapeable and conform to curved surface.

- **Stitched** fabrics have optimized strength properties because of the fiber architecture. Stitched fabrics are produced by assembling successive layers of aligned fibers. Typically, the available fiber orientations include the 0° direction (warp), 90° direction (weft) and 45° direction (bias). This type of construction allows for load sharing between fibers so that a higher modulus, both tensile and flexural, is typically observed. Multiple orientations provide a quasi-isotropic reinforcement. Figure 2.7 shows the typical fiber's orientation.

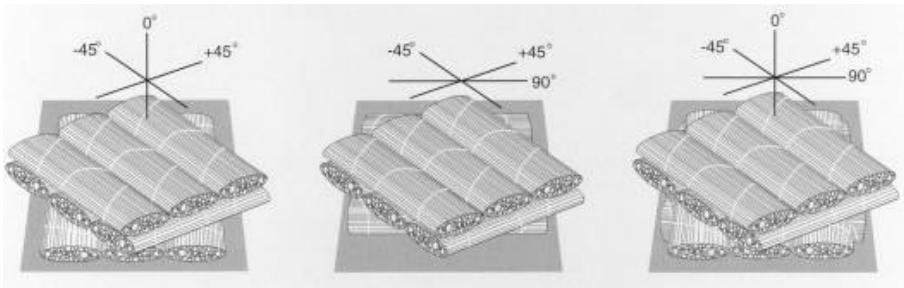


Fig. 2.7. Diagram of stitched triaxial and quadriaxial fabrics

- **Braided** fabrics are engineered with a system of two or more yarns intertwined in such a way that all of the yarns are interlocked for optimum load distribution. Biaxial braids provide reinforcement in the bias direction only with fiber angles ranging from $\pm 15^\circ$ to $\pm 95^\circ$; triaxial braids provide reinforcement in the bias direction with fiber angles ranging from $\pm 10^\circ$ to $\pm 80^\circ$ and axial (0°) direction.



Fig. 2.8. Biaxial and triaxial braided fabric

- A **3-D** fabrics use a special weaving process that ties multiple layers and multiaxial fibers together with “Z-yarns”. This Z improves the integrity of the fabric. This technology is capable to make forms for panels and structural profiles.

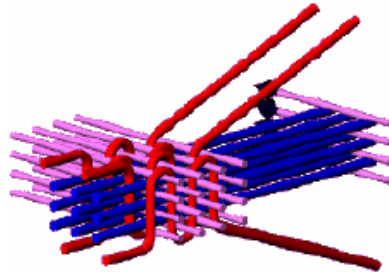


Fig. 2.9. 3-D fabric weaving process

Unidirectional

Unidirectional reinforcements include tapes, tows and roving. Fibers in this form are all aligned parallel in one direction and the composites that use this method have high strength in the fiber direction. Unidirectional sheets are thin and multiple layers are required for most structural application.

Bars

FRP bars are anisotropic, with the longitudinal axis being the major axis. Their mechanical properties can vary significantly from one manufacturer to another and within the same product. They are made for braiding, weaving or pultrusion that is a continuous molding process that combines fiber reinforcements and thermosetting resin. Figure 2.10 illustrates the pultrusion process that is used in the fabrication of composite parts that have a constant cross-section profile.

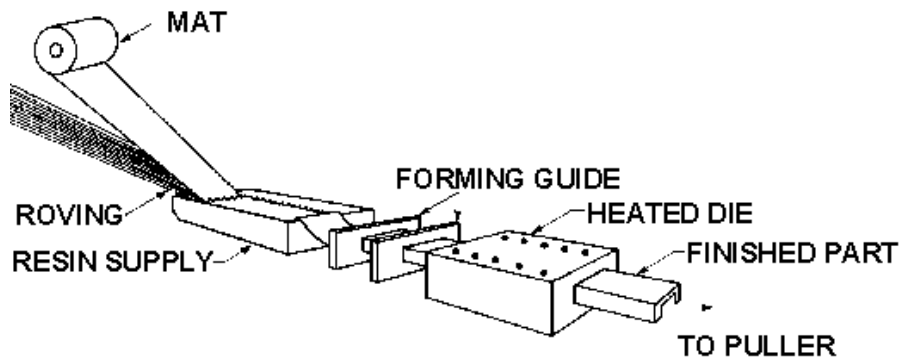


Fig. 2.10. Manufacturing process: pultrusion

The pultrusion process is normally continuous and highly automated: reinforcement materials are positioned in a specific location using preforming shapers or guides to form the profile. The reinforcements are drawn through a resin bath or wet-out where the material is thoroughly coated or impregnated with a liquid thermosetting resin; then the resin-saturated reinforcements enter a heated metal pultrusion die; the dimensions and shape of the die will define the finished part being fabricated. Inside the metal die, heat is transferred initiated by precise temperature control to the reinforcements and liquid resin. The heat energy activates the curing or polymerization of the thermoset resin changing it from a liquid to a solid; the solid laminate emerges from the pultrusion die to the exact shape of the die cavity. The laminate solidifies when cooled and it is continuously pulled through the pultrusion machine and cut to the desired length.

The process is driven by a system of caterpillar or tandem pullers located between the die exit and the cut-off mechanism.

In order to improve the bond performance through mechanical interlock, the rods are produced by manufacturers in various types and with different deformation systems, including exterior wound fibers, sand coating and separately formed deformations.

Figure 2.11 shows different kinds of FRP bars.

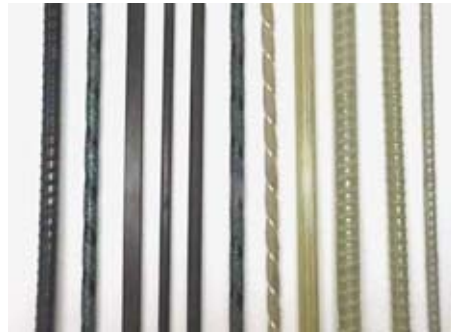


Fig. 2.11. Different kinds of FRP bars

Laminates

Lamination technology is based on the joining or bonding of two or more laminae to form a laminate. The materials can vary in type and mechanical properties in addition to property specific orientation; there are three types of laminated construction, these include sandwich lamination consisting of at least two high stiffness and strength outer layers connected by a core.

All laminate constructions utilize relatively high strength/stiffness materials.

Figure 2.12 illustrates an example of multi-ply construction. The figure shows the different orientation of the layers.

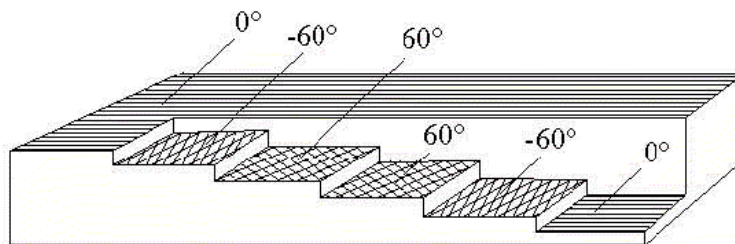


Fig. 2.12. Multi-ply Construction

2.4. FRP Physical and Mechanical Properties

In the following paragraphs a brief description of the main mechanical and physical properties for some kinds of FRP is presented.

FRP Bars

FRP bars offer advantages over steel reinforcement because FRP bars are non-corrosive and non conductive; the available FRP bars are made of aramid, carbon or glass.

Factors, such as fiber volume, type of fiber, type of resin, fiber orientation, dimensional effects and manufacturing methods play a major role in establishing product characteristics.

The relative volume of fibers and resin in the product affects the properties of FRP rods; a usual fiber volume is between 0.5 and 0.7. Furthermore, the mechanical properties of FRP bars, like all structural materials, are affected by factors such as loading history and duration, temperature and moisture.

FRP bars have a density ranging from four to six times smaller than that of steel; the reduced weight leads to lower transportation costs and decreased handling and installation time per bar on the job site.

Coefficient of thermal expansion and effects of high temperatures

The coefficients of thermal expansion of FRP bars vary in the longitudinal and transverse directions depending on the types of fiber, resin and volume fraction fiber. Table 2.2 lists the longitudinal and transverse coefficients of thermal expansion for typical FRP bars and steel bars: note that a negative coefficient of thermal expansion indicates that the material contracts with increased temperature and expands with decreased temperature.

Tab. 2.2. Typical coefficients of thermal expansion for reinforcing bars

Direction	Steel	GFRP	CFRP	AFRP
Long, α_L	11.7x10 ⁻⁶ /°C (6.5x10 ⁻⁶ /°F)	6 to 10x10 ⁻⁶ /°C (3.3 to 5.6 x10 ⁻⁶ /°F)	-2 to 0x10 ⁻⁶ /°C (-4 to 0 x10 ⁻⁶ /°F)	-6 to 2x10 ⁻⁶ /°C (-3.3 to -1.1x10 ⁻⁶ /°F)
Trans, α_T	11.7x10 ⁻⁶ /°C (6.5x10 ⁻⁶ /°F)	21 to 23x10 ⁻⁶ /°C (11.7 to 12.8x10 ⁻⁶ /°F)	23 to 32x10 ⁻⁶ /°C (41 to 58 x10 ⁻⁶ /°F)	60 to 80x10 ⁻⁶ /°C (33.3 to 44.4x10 ⁻⁶ /°F)

The use of FRP reinforcement is not recommended for structures in which fire resistance is essential to maintain structural integrity, because the polymers will soften due to the excessive heat. Beyond the glass-transition temperature, the elastic modulus of a polymer is significantly reduced due to changes in its molecular structure; however, the tensile properties of the overall composite are reduced due to a reduction in force transfer between fibers through bond to the resin.

Other properties more directly affected by the shear transfer through the resin, such as shear and bending strength, are reduced significantly at temperatures above the T_g .

Structural collapse can be avoided if high temperatures are not reached at the end regions of FRP bars allowing anchorage to be maintained.

Mechanical properties and behavior

- ***Tensile behavior***

Ultimate tensile strength of FRP bars is reached without exhibiting any plastic yielding; the tensile behavior is characterized by a linearly elastic stress-strain relationship until failure.

Unlike steel bars, some FRP bars exhibit a substantial size effect: the fibers located near the center of the bar cross section are subjected at less stress as for the fibers that are near the outer surface. This phenomenon results in reduced strength and efficiency in large diameter bars; for example, in a study GFRP bars from three different manufacturers show tensile strength reductions of up to 40% as the diameter increases proportionally from 9.5 to 22.2 mm (0.375-0.875 in.).

Table 2.3 illustrates the tensile properties of some commonly used FRP bars.

Tab. 2.3. Usual tensile properties of reinforcing bars

	Steel	GFRP	CFRP	AFRP
Tensile strength, (MPa)	483-690	483-1600	600-3690	1720-2540
Elastic modulus (GPa)	200	35-51	120-580	41-125
Yield strain, %	0.14-0.25	N/A	N/A	N/A
Rupture strain, %	0.6-0.12	1.2-3.1	0.5-1.7	1.9-4.4

Note: 1 MPa = 145 psi.

Strength and stiffness variations will occur in bars with various fiber-volume fractions, even in bars with the same diameter, appearance, and constituents.

- Compressive behavior

Compressive strengths of 55%, 78%, and 20% of the tensile strength have been reported for GFRP, CFRP, and AFRP, respectively.

The compressive modulus of elasticity of FRP reinforcing bars appears to be smaller than its tensile modulus of elasticity; according to reports, the compressive modulus of elasticity is approximately 80% for GFRP, 85% for CFRP, and 100% for AFRP of the tensile modulus of elasticity for the same product.

Standard test methods are not yet established to characterize the compressive behavior of FRP bars; if the compressive properties of a particular FRP bar are needed, these should be obtained from the bar manufacturer.

However it is not recommended to rely on FRP bars to resist compressive stresses.

- Shear behavior

Most FRP bar composites are relatively weak in interlaminar shear where layers of unreinforced resin lie between layers of fibers, because there is usually no reinforcement across layers, and the interlaminar shear strength is governed by the

relatively weak polymer matrix. This shortcoming can be overcome by orienting the FRP bars so that they resist the applied loads through axial tension.

Standard test methods are not yet established to characterize the shear behavior of FRP bars.

- Bond behavior

Bond performance of an FRP bar is dependent on the design, manufacturing process, mechanical properties of the bar itself, and the environmental conditions.

The bond force of an embedded bar can be transferred by:

- Adhesion resistance of the interface, also known as chemical bond
- Frictional resistance of the interface against slip
- Mechanical interlock due to interface irregularity.

Handling of FRP bars

FRP reinforcing bars are susceptible to surface damage and the puncturing their surface can significantly reduce the strength capacity; in the case of glass FRP bars, the surface damage can cause a loss of durability due to infiltration of alkalis. The following handling guidelines are recommended to minimize damage to both the bars and the bar handlers:

- FRP-reinforcing bars should be handled with work gloves to avoid personal injuries from either exposed fibers or sharp edges
- FRP bars should not be stored on the ground, pallets should be placed under the bars to keep them clean and to provide easy handling
- High temperatures, ultraviolet rays, and chemical substances should be avoided
- When necessary, cutting should be performed with a high-speed grinding cutter or a fine blade saw. FRP bars should never be sheared. Dust masks, gloves, and glasses for eye protection are recommended when cutting because there is insufficient research available to make any recommendation on treatment of saw-cut bar ends.

FRP laminates, sheets and fabrics

One of the best quality of these materials is the thickness because this property is often requested for rehabilitate or restore the strength of a weakened structural element, or retrofit or strengthen a sound structural element to resist increased loads due to changes in use of the structure.

Coefficient of thermal expansion and effects of high temperatures

The coefficients of thermal expansion of unidirectional FRP materials differ in the longitudinal and transverse directions, depending on the types of fiber, resin, and volume fraction of fiber. Table 2.4 illustrates the typical coefficients of thermal expansion for unidirectional materials.

Tab. 2.4. Typical coeff. of thermal expansion for unidirectional FRP materials

Direction	Steel	GFRP	CFRP	AFRP
Long, α_L	$11.7 \times 10^{-6} / ^\circ\text{C}$ ($6.5 \times 10^{-6} / ^\circ\text{F}$)	6 to $10 \times 10^{-6} / ^\circ\text{C}$ (3.3 to $5.6 \times 10^{-6} / ^\circ\text{F}$)	-1 to $0 \times 10^{-6} / ^\circ\text{C}$ (0.6 to $0 \times 10^{-6} / ^\circ\text{F}$)	-6 to $2 \times 10^{-6} / ^\circ\text{C}$ (-3.3 to $-1.1 \times 10^{-6} / ^\circ\text{F}$)
Trans, α_T	$11.7 \times 10^{-6} / ^\circ\text{C}$ ($6.5 \times 10^{-6} / ^\circ\text{F}$)	19 to $23 \times 10^{-6} / ^\circ\text{C}$ (10.4 to $12.6 \times 10^{-6} / ^\circ\text{F}$)	22 to $50 \times 10^{-6} / ^\circ\text{C}$ (12 to $27 \times 10^{-6} / ^\circ\text{F}$)	60 to $80 \times 10^{-6} / ^\circ\text{C}$ (33 to $44 \times 10^{-6} / ^\circ\text{F}$)

When there is high temperature, beyond the T_g , the elastic modulus of a polymer is significantly reduced due to changes in its molecular structure; due to a reduction in force transfer between fibers through bond to the resin, the tensile properties of the overall composite are reduced. Test results have indicated that temperatures of 250°C (480°F), much higher than the resin T_g , will reduce the tensile strength of GFRP and CFRP materials in excess of 20%.

Other properties affected by the shear transfer through the resin, such as bending strength, are reduced significantly at lower temperatures.

Mechanical properties and behavior

- *Tensile behavior*

The properties of an FRP system should be characterized as a composite, recognizing not just the material properties of the individual fibers but also the efficiency of the fiber-resin system and fabric architecture.

The tensile properties of some commercially available FRP-strengthening systems are summarized in table 2.5.

Tab. 2.5. Properties of some commercially available FRP systems

FRP-system description (fiber type/saturating resin/fabric type)	Fabric weight g/m ²	Ultimate strength ⁽¹⁾ kN/m
General purpose carbon/epoxy/ unidirectional sheet	200	500
	400	625
High-strength carbon/epoxy/ unidirectional sheet	230	315
	300	700
	620	960
High-modulus carbon/epoxy/ unidirectional sheet	300	600
General-purpose carbon/epoxy/ balanced fabric	300	175
E-glass/epoxy/ unidirectional sheet	900	720
	350	230
E-glass/epoxy/ balanced fabric	300	120
Aramid/epoxy/ unidirectional sheet	415	700
High-strength carbon/epoxy/ precurd, unidirectional laminate	2385	3300
E-glass/vinyl ester/ precurd, unidirectional shell	1695	1575

⁽¹⁾ Ultimate tensile strength per unit of sheet or fabric

Note: 1000 g/m² = 0.023 oz/in² ; 1 kN/m = 5.7 Pd/in

Table 2.6 shows the typical tensile properties of FRP laminates with fiber volumes between 40% to 60%.

Tab. 2.6. Tensile properties of FRP laminates with fiber volumes of 40% to 60%

(zero degrees represent unidirectional fiber orientation, zero/ninety degrees [or ± 45 degrees] represents fiber balanced in two orthogonal directions, where zero degrees is the direction of the load)

FRP-system description (fiber orientation)	Young's modulus		Ultimate tensile strength		Rupture strain at 0 degrees
	Property at 0 degrees	Property at 90 degrees	Property at 0 degrees	Property at 90 degrees	
	(GPa)	(MPa)	(MPa)	(MPa)	(%)
High-strength carbon/epoxy, degrees					
0	100-145	2-7	1025-2075	35-70	1.0-1.5
0/90	55-76	55-75	700-1025	525-1025	1.0-1.5
+45/-45	14-28	14-28	175-275	175-275	1.5-2.5
E-glass/epoxy, degrees					
0	20-40	2-7	525-1400	35-70	1.5-3.0
0/90	14-34	14-35	525-1025	525-1025	2.0-3.0
+45/-45	14-21	14-20	175-275	175-275	2.5-3.5
High-perform. aramid/ epoxy, degrees					
0	48-68	2-7	700-1725	35-70	2.0-3.0
0/90	28-34	28-35	275-550	275-550	2.0-3.0
+45/-45	7-14	7-14	140-205	(140-200)	2.0-3.0

Note: 1 MPa = 145 psi.

- Compressive behavior

Generally, compressive strength are higher for materials with higher tensile strengths except in the case of AFRP where the fibers exhibit nonlinear behavior in compression at relatively low level of stress. For all others compressive behaviors, see the paragraph on FRP bars.

Handling of FRP laminates, sheets and fabrics

Each FRP-system-constituent material has different handling and storage requirements to prevent damage, so, the better way is the consults with the material manufacturer for guidance.

There are precautions that should be observed when handling thermosetting resins and their component materials. The workforce has to wear suits and gloves; disposable rubber or plastic gloves are recommended and should be discarded after each use. Gloves should be resistant to resins and solvents. Respiratory protection, such as dust masks or respirators, should be used when fiber fly, dust, or organic vapors are present.

2.5. Durability of FRP Materials

The most significant technical obstacle preventing the extended use of FRP is a lack of long-term and durability performance data comparable to the data available for more traditional construction materials. Although there have been numerous studies on creep, stress corrosion, fatigue, environmental fatigue, chemical and physical ageing and natural weathering of composites, most of these are not related for civil engineering application. Therefore the lack of durability data generate, at the moment, a big obstacle: a majority of civil engineers are not familiar with composites and are skeptical about using of FRP to replace conventional materials in the structures.

It was already mentioned that corrosion problems of steel reinforcement and the good mechanical properties of FRP materials opened a large field for the use of composite in new constructions and for repairing purposes, but the determination of the durability is one of the most important issues.

Durability of material can be defined as its ability to resist cracking, oxidation, chemical degradation, delamination, wear and the effects of foreign object damage for a specified period of time under specified environmental conditions.

Damage tolerance is defined as the ability of a material or structure to resist failure and continue performing at prescribed levels of performance in the presence of damage for a specified period of time under specified environmental conditions.

The overall concept is illustrated schematically in the figure 2.13.

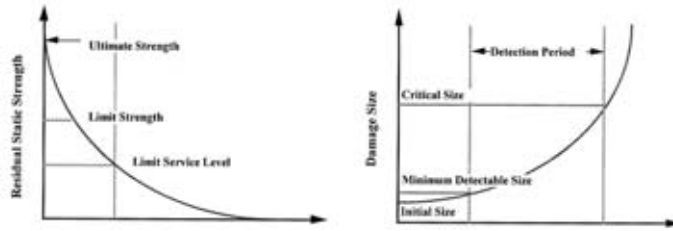


Fig. 2.13. Concepts of durability and damage tolerance design

The performance of FRP composites is given on the interactions between the selected constituent materials (fibers, resin, fillers and additives), determination of microstructure/architecture and geometrical configuration and influences of the appropriate manufacturing process.

Moisture (water) absorption

All resins adsorb moisture with the percentage of moisture absorption depending on the resin structure, degree of cure and water temperature. In general moisture effects over the short-term cause degradation in strength rather than stiffness levels in a composite.

Moisture absorption in FRP composite depends on type of resins, laminate composition, thickness, laminate quality, curing condition, fiber/resin interface and manufacturing process. In some applications, performance is improved with the use of corrosion barrier.

Alkaline solutions

Alkaline solutions, such as the pore water of concrete, have a high pH and high concentration of alkali ions. This combination has no relevant effect on carbon reinforcement but may lead to degradation at the resin matrix and/or interface levels (strength and stiffness have been reported to each decrease between 0-20%).

Tensile strength reductions in GFRP bars ranging from zero to 75% of initial values have been reported in literature, while tensile stiffness reductions in GFRP bars range between zero and 20%.

Tensile strength and stiffness of AFRP rods in elevated temperature alkaline solutions either with and without tensile stress applied has been reported to decrease between 10-50% and 0-20% of initial values, respectively.

Resin damage via alkali is generally more severe than that due to moisture.

Aggressive chemical solutions

FRP composites generally exhibit a variable performance when exposed to solution such as acids or corrosives; the resin type primarily influences this performance.

In the case of CFRP immersed in hydrochloric acid at the temperature of 80°C, the tensile strength reduced about 20% after 120 days.

Reports have reported that the tensile stress of glass fiber reduced rapidly with time when immersed in any of the solution (NaOH, HCl, H₂O) at the temperature of 80°C and when immersed in sodium hydroxide (Uomoto et al., 1999). For the AFRP (Technora fiber), has been reported that after immersing for 90 days, strength reduced about 80% in hydrochloric acid and about 45% in sodium hydroxide solution. However no particular sign of degradation were observed when the AFRP were immersed in distilled water at temperatures of 20, 40 and 80°C (Uomoto et al., 1999).

Sub-zero and freeze-thaw exposure

Composites display excellent freeze-thaw resistance and are expected to withstand years of sub-zero conditions and hundreds of freeze-thaw cycles, with minimal loss of properties.

In general, freeze-thaw exposure does not affect fibers although it can affect the resin and the fiber/resin interface.

Temperature and thermal cycling (above zero)

The primary effects of temperature are on viscoelastic response of the resin and hence of the composites. If the temperature exceeds the glass transition temperature (T_g), FRP composite performance can be expected to drop.

Thermal cycling in general does not cause deleterious effects, although extended cycles of brittle resin systems can result in microcrack formation.

Creep and relaxation

FRP subjected to a constant load over time can suddenly fail after a time period called the endurance time. This phenomenon is known as creep rupture (or static fatigue).

Creep rupture is not an issue with steel bars in reinforced concrete except in extremely high temperatures such as those encountered in a fire.

The creep rupture endurance time can also irreversibly decrease under sufficiently adverse environmental conditions, such as high temperature, ultraviolet radiation exposure, high alkalinity, wet and dry cycles, or freezing-thawing cycles.

In general, carbon fibers are the least susceptible to creep rupture. Aramid fibers are moderately susceptible, and glass fibers are most susceptible to creep rupture.

Results indicated that a linear relationship exists between creep rupture strength and the logarithm of time for times up to nearly 100 hr. The ratios of stress level at creep rupture to the initial strength of the GFRP, AFRP, and CFRP bars after 500,000 hours (more than 50 years) were linearly extrapolated to be 0.29, 0.47, and 0.93, respectively.

Creep will not be a significant factor if the load to the structure is kept within manufacturer recommended stress levels.

For a typical civil infrastructure composite application, the creep-stress relaxation properties are dominated by the resin-dependent properties, rather than on the fiber or interfacial properties.

Traditionally glass-fiber reinforced composites have been designed to ensure that stress levels under sustained do not exceed 25-30% of ultimate to avoid premature failure due to stress rupture.

Fatigue

FRP composites show significantly enhanced fatigue resistance over metallic materials. However, FRP composites structures are still susceptible to failure at joints and connections under fatigue loading and must be designed to reduce stress concentrations and geometrical discontinuities, which decrease overall fatigue resistance. Fatigue failure in FRP composites is usually initiated through fiber/matrix debonding and matrix microcracking.

Although the data on fatigue in large structural application is limited, the data that is available indicates that fatigue failure is unlikely to occur at the lower stress levels used in design except at the joints and connection details.

Of all types of current FRP composites for infrastructure application, CFRP is generally thought to be the least prone to fatigue failure like E-glass and S-glass, but, for the last two types, environmental factors play an important role in the fatigue behavior due to their susceptibility to moisture, alkaline and acidic solutions.

Aramid fibers, for which substantial durability data are available, appear to behave similarly to carbon and glass fibers in fatigue.

Ultraviolet (UV) radiation

In general, effects are rarely severe in terms of mechanical performance, although some resins can show significant embrittlement and surface erosion.

The most deleterious effect of UV exposure is probably not the UV-related damage, but the potential for increased penetration of moisture and other agents via the damaged region.

FRP composites can be protected from UV-related degradation through the use of appropriate additives in the resin and/or use of appropriate coatings.

Fire and high thermal exposure

All polymeric systems degrade in the presence of extreme heat over prolonged periods. The primary effect in most fires is that of resin degradation and softening followed by charring of surface layers, which often causes the FRP composites to self-extinguish.

In critical applications, the FRP may be fireproofed with the use of special fire-resistant additives, intumescent coatings and the addition of inorganic fillers, but these increases the costs and however depending on the application (may not be possible). The usual method to achieve the necessary structural fire rating is to use the FRP reinforcement as supplemental reinforcement: with this concept, the existing structure will not be able of total collapse without FRP reinforcement.

In FRP reinforced concrete the concrete itself acts as a thermal barrier reducing effects of thermal load.

3. FRP INSTALLATION TECHNIQUE

3.1. The Wet-lay-up System

The use of Fiber Reinforced Polymer (FRP) materials for external strengthening of RC, PC, and masonry structures has emerged as one of the most exciting and promising technologies in materials and structural engineering.

As a result, their use in repair/rehabilitation can present many significant advantages with respect to the conventional methods.

Externally bonded FRP laminates have been successfully used to increase the flexural and/or shear capacity (sometimes also the stiffness) of RC beams, to provide confinement to RC columns, and to strengthen masonry walls subjected to out-of-plane as well as in-plane loading. A notable amount of experimental research has been carried out and is currently ongoing towards the characterization of RC and masonry structures strengthened with this technique (De Lorenzis, 1999).

With wet-lay-up, the strengthening system can easily be installed in a series of few steps; the fiber materials (like fabrics, sheets etc.) are placed on the surface dry and then impregnated with epoxy resins to form an FRP laminate.

The integrity of the system depends on the quality and strength of the masonry as well as the bond between the FRP and the masonry. The following list provides general guidelines for the FRP reinforcement, because many bond-related failures may be avoided with few recommendations:

- Fibers cannot turn inside corners
- Provides a minimum of $\cong 13$ mm ($\frac{1}{2}$ inch) radius when the sheets turn outside the corners
- Inject all cracks prior to FRP installation
- Avoid surface irregularities

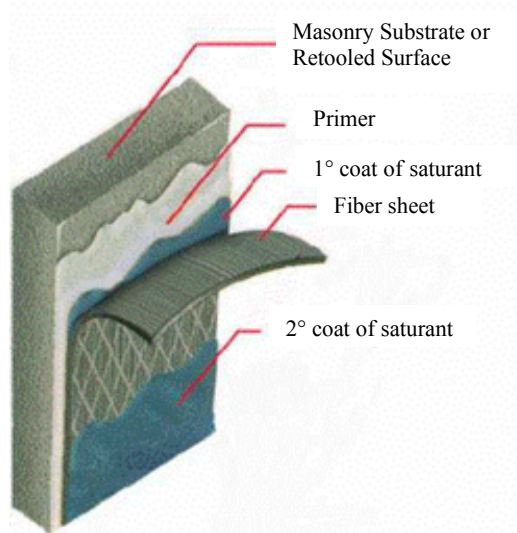


Fig. 3.1. FRP Laminates

The procedure can be summarized as follows:

- Preparation of the substrate
- Application of primer
- Application of putty
- Application of the first coat of saturant
- Application of reinforcement
- Application of the second coat of saturant
- Application of additional reinforcement plies

Preparation of the substrate

First of all, the substrate must be prepared to accept the system, so, the surface of the masonry should be free of unsound materials; dust, dirt, oil etc. should be removed. Masonry generally does not need to be roughened with sandblasting or something similar because it is a porous structure (not like concrete). However, if the FRP is applied directly on the plaster, the surface needs to become roughened using sandblasting or a grinder.

Application of primer

After surface preparation, the primer is applied on the surface using a short nap roller.



Fig. 3.2. Application of the primer

The primer is a 100% solid epoxy and is applied to provide adequate bond to the base masonry (it is formulated to penetrate the pores).

Application of putty

The putty is applied, when required, on a surface using a trowel. It should be used to fill any surface defects so complete coverage is not necessary. When surface defects are not present, putty is not required.



Fig. 3.3. Application of the putty

The putty can also be used for leveling and patching small holes and it has to be applied on a freshly primed surface without waiting for the primer to cure.

Application of the first coat of saturant

The saturant is applied to the primed and puttied surface with a medium nap roller.



Fig. 3.4. Application of the first coat of saturant

It is used to impregnate the dry fibers and it maintains the fibers in their intended orientation, distributes the stress and protects them from abrasion and environmental effects. The saturant is formulated to quickly wet the fibers and hold the sheet in place while the system cures. The volume of saturant depends on the FRP sheets used.

Application of reinforcement

Reinforce is prepared before, using a scissors, in sheets and is placed on the masonry surface, dry of saturant, with a delicate pressure into the saturant.

The reinforcement should be cut to the appropriate length and width prior to application. The dry sheets are then placed into the saturant in the proper orientation by delicately pressing them into place.



(a) (b)
 Fig. 3.5. FRP sheets and placement of the sheet

After placement, a ribbed roller must be used to remove any air bubbles and to facilitate impregnation of the saturant by separating fibers.



(a) (b)

Fig. 3.6. Pressing of the FRP into the saturant and removing air bubbles

The ribbed roller should never be used in a direction transverse to the fibers since the fibers could be damaged. Streaks of saturant should be visible on the fiber sheet after rolling.

Application of the second coat of saturant

A second coat of saturant must be applied 30 minutes after placing and rolling the fibers. This period of time allows the first coat of saturant to be completely absorbed by the fibers.



Fig. 3.7. Application of the second coat of saturant

Application of additional reinforcement plies

If required, re-saturate the surface 30 minutes after the second saturant coat is applied and repeat the last two steps until the required number of plies is applied.



Fig. 3.8. Final removing of the air bubbles

3.2. Near-surface Mounted FRP Rod System

A new FRP-based strengthening technique is emerging as a valid alternative to externally bonded FRP laminates. From this point forward, it will be referred to as Near-Surface Mounted (NSM) FRP rods. Although the use of FRP rods for this application is very recent, NSM steel rods have been used in Europe for strengthening of RC structures since the early 50's. In 1948, an RC bridge in Sweden experienced excessive settlement of the negative moment reinforcement during construction, so that the negative moment capacity needed to be increased. This was accomplished by grooving the surface, filling the grooves with cement mortar and embedding steel rebars in them. To date, FRP rods can be used in place of steel and epoxy paste can replace the cement mortar. The advantage is primarily the resistance of FRP to corrosion. This property is particularly important in this case due to the position of the rods being very close to the surface, which exposes them to the environmental attacks (De Lorenzis, 1999).

The use of NSM FRP rods is an attractive method for increasing the flexural and shear strength of deficient RC members and masonry walls and, in certain cases, can be more convenient than using FRP laminates. Application of NSM FRP rods does not require surface preparation work (other than grooving) and minimal installation time compared to FRP laminates is required.

Another advantage is the feasibility of anchoring these rods into members adjacent to the one to be strengthened.

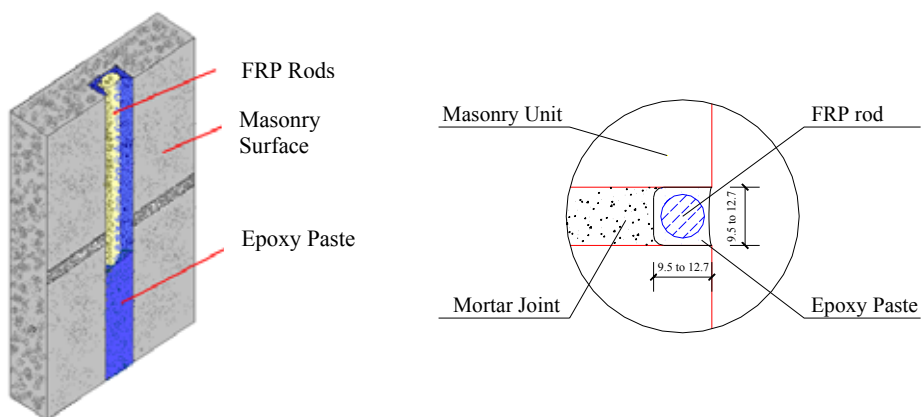


Fig. 3.9. NSM rods explanation with section (measure in mm)

The use of NSM rods can also be more attractive since the removal of plaster is not required.

When the FRP rods are installed in either the horizontal or vertical (only for stack bond patterns) masonry joints, the aforementioned technique receives the name of FRP Structural Repointing. Repointing is a traditional retrofitting technique, commonly used in the masonry industry, which consists in replacing missing mortar in the joints.

The term “structural” is added to describe a strengthening method aimed at restoring the integrity and/or upgrading the capacity of the walls. This is achieved by placing into the joints FRP rods, which are bonded to the masonry wall by the paste. Structural repointing offers advantages compared to the use of FRP laminates.

The method itself is simpler since the surface preparation is reduced; sandblasting and puttying are not required. In addition, the aesthetics of the masonry are preserved (Tumialan, 2001).

For the walls where NSM rods can be installed, the procedure can be summarized as follows:

- Grinding and cleaning of groove
- Application of paste
- Installation of FRP rod

Grinding and cleaning of the groove

Using a grinder with a diamond blade make a groove with dimensions close to the diameter of the FRP rods used. Plaster and masonry materials should be removed using a chisel and hammer to complete the slots. The groove is then cleaned (e.g., pressured air) to remove all loose particles and dust.



(a)



(b)

Fig. 3.10. Preparation of the grooves and cleaning of the wall

Application of paste

An epoxy-based paste is used to provide bond between the masonry and the rods.

Using a mason gun, a layer of paste is placed into the groove. Masking of the masonry surface will avoid staining when the aesthetics are a concern.



Fig. 3.11. Placing the epoxy-based paste into the slot

Installation of FRP rod

Once the groove is filled half-way with epoxy paste, then the FRP rod is placed in the groove and lightly pressed, forcing the paste to flow around the bar and fill completely the space between the bar and the sides of the groove.



Fig. 3.12. Drawn of the bar into the epoxy-based paste

Then, the groove is filled with more of the same paste and the surface is leveled.

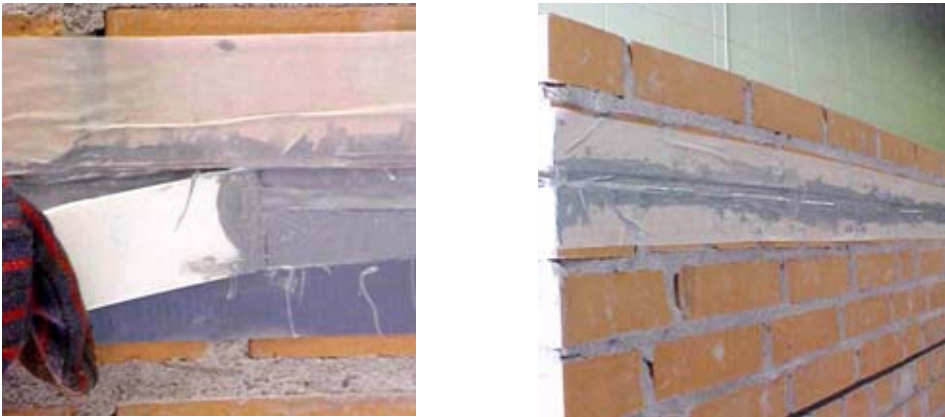


Fig. 3.13. Filling and leveling of the surface

After approximately 30 minutes, remove the masking around the groove.

The following figure illustrates the final product, detailing both the overall and cross-sectional views.



Fig. 3.14. Final product

4. MATERIALS AND BOND CHARACTERIZATION

4.1. Materials Characterization

4.1.1. Introduction

This section presents the properties of the materials used in the experimental program. These materials included concrete blocks, clay bricks, mortar, GFRP rods, AFRP and GFRP laminates, carbon strips, epoxy paste, primer, putty and saturant.

Standard tests were performed to determine the compressive strength of mortar cubes and concrete and clay prisms. Tests on concrete unit and clay unit triplets were performed for the purpose of measuring the shear strength along mortar bed joints.

4.1.2. Concrete blocks (arching test)

Compression tests following ASTM C1314 standard protocol were performed. The concrete masonry units involved in this investigation are commonly employed in a particular masonry typology called infill panels, utilised as exterior walls in reinforced concrete frame structures to form part of the building envelope. A Tinius Olsen Universal Testing Machine was used to apply the compression load.

The nominal dimensions of the concrete units are 102x203x305 mm (4x8x12 in), see figure 4.1. The specified block dimensions are 3/8 in. (10 mm) less than the nominal values to allow for a standard mortar joint thickness.



Fig. 4.1. Concrete block unit

Five prisms consisting of two units incorporating one full mortar bedding in 10mm (3/8 in) flush joint were constructed and tested. In order to create a uniform distribution of compression stresses on the edges of the specimens one plywood strips and two steel plates were cut and inserted between the edges and the two cross-heads of the machine, Figure 4.2 illustrates the test setup; in this manner undesirable crushing failures at the borders were also prevented.



Fig. 4.2. Test preparation

An LVDT was also fixed to the steel plate on the top and the movement was measurement relativity the bottom fixed cross-heads of the machine in order to calculate the average vertical strain of the masonry sample. Applied load and strain, values were recorded by a data acquisition system, consisting of Data general Conditioner Rack and LABTECH (Laboratory Technologies Corp.) data acquisition software. The sampling rate was set to 1 Hz. Table 4.1 gathers concrete unit geometrical data and the table 4.2 summarizes the test results.

Tab. 4.1. Concrete unit specifications

Designation	Concrete hollow two-cells unit
Nominal dimensions [mm]	102x203x305
Gross Area [mm ²]	31110
Net Area [mm ²]	21058
Percentage of solid [%]	68

Note: 1 mm = 0.03937 in

Tab. 4.2. Test results

Prism #	Compressive Strength f'_m [MPa]
1	11.4
2	18.7
3	16.8
4	15.2
5	10.9
Average	14.6

Concrete blocks	[MPa]
Compressive Strength	14.6
Standard Deviation	3.4
Modulus of elasticity	13140

Note: 1 MPa = 145 psi

The Modulus of elasticity was calculated in according with the MSJC Code (1999) like $900 \cdot f'_m$.

4.1.3. Dark clay bricks (arching test)

Compression tests were performed on five prisms made of dark molded bricks. Modern clay units often have compressive strengths much higher than required to satisfy product specifications and generally exceed by large margins the requirements for member design strengths. However, in order to calculate the experimental plastic-moment in the midspan of the walls subjected to out-of-plane loading, this type of tests was required by the experimental program.

Tab. 4.3. Specifications for clay bricks

Designation	Clay solid unit
Nominal dimensions [mm]	102x203x64
Gross Area [mm ²]	20706
Net Area [mm ²]	15231
Percentage of solid [%]	74

Note: 1 mm = 0.03937 in



Fig. 4.3. Dark clay brick unit

ASTM C1314 standard protocol was followed. Similarly to compression tests on concrete coupons a Tinius Olsen machine was used. Applied load and vertical strain of the masonry specimens were recorded with the same instrumentation. The tests were performed in displacement control mode.



(a)



(b)

Fig. 4.4. Dark clay prism before (a) and after failure (b)

Test results are illustrated in table 4.4.

Tab. 4.4. Test results

Prism #	Compressive Strength f'_m [MPa]
1	25.6
2	24.0
3	18.0
4	16.4
5	16.8
Average	20.2

Dark clay bricks	[MPa]
Compressive Strength	20.2
Standard Deviation	4.3
Modulus of elasticity	14140

Note: 1 MPa = 145 psi

The Modulus of elasticity was calculated in according with the MSJC Code (1999) like $700 \cdot f'_m$.

4.1.4. Light clay bricks (in-plane test)

Compression tests were also performed on seven prisms made of light extruded bricks. This type of tests was required by the experimental program in order to calculate the correct amount of FRP reinforcement for walls subjected to in-plane loading. Nominal dimensions, gross area, net are and percentage of solid are similar to dark brick specifications. The difference are the manufacturing process and the type of clay. No differences were applied in the test procedure.

Tab. 4.5. Specifications for clay bricks

Designation	Clay solid unit
Nominal dimensions [mm]	102x203x64
Gross Area [mm ²]	20706
Net Area [mm ²]	14215
Percentage of solid [%]	69

Note: 1 mm = 0.03937 in;

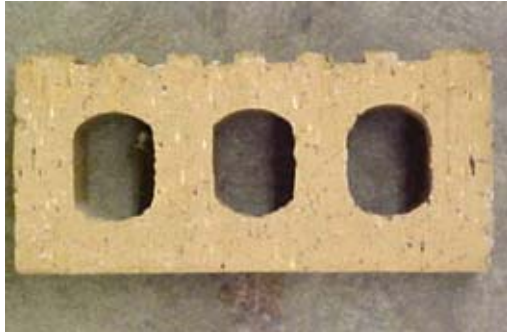


Fig. 4.5. Light clay brick unit

Applied load and vertical strain of the masonry specimens were recorded with the same apparatus utilized for the dark clay brick tests.



(a)

(b)

Fig. 4.6. Light clay prism before (a) and after failure (b)

Test results are presented in table 4.6.

Tab. 4.6. Test results

Prism #	Compressive Strength f'_m [MPa]
1	16.4
2	18.7
3	26.8
4	12.9
5	15.0
6	14.9
7	21.8
Average	18.1

Dark clay bricks	[MPa]
Compressive Strength	18.1
Standard Deviation	4.8
Modulus of elasticity	12670

Note: 1 MPa = 145 psi

The Modulus of elasticity was calculated in according with the MSJC Code (1999) like $700 \cdot f'_m$.

Nineteen triplets were also constructed in order to estimate the shear stresses along the bed mortar joints. They were tested and constructed as shown in figure 4.7.

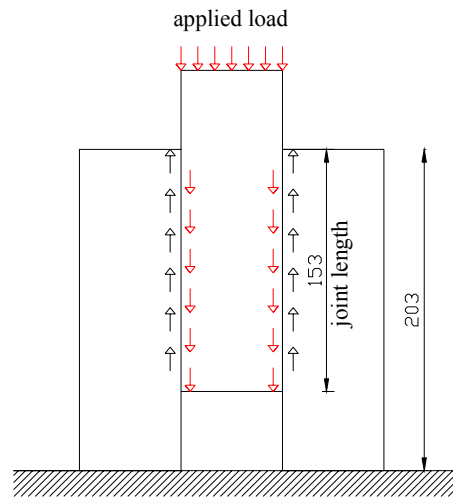


Fig. 4.7. Scheme of bed joint shear test (measure in mm)

Four confinement stresses were chosen: 0.05, 0.1, 0.3, 0.5 MPa (7, 14, 42, 70 psi). Cohesion and coefficient of friction according to Coulomb criterion expression $\tau = \tau_o + \mu \sigma_n$ were calculated by means of linear interpolation of the data provided by the tests. Test results are showed in figure 4.8.

According to Coulomb criterion $\tau = 824.42 + 1.35\sigma_n$ [kPa] for $\sigma_n < 483$ kPa

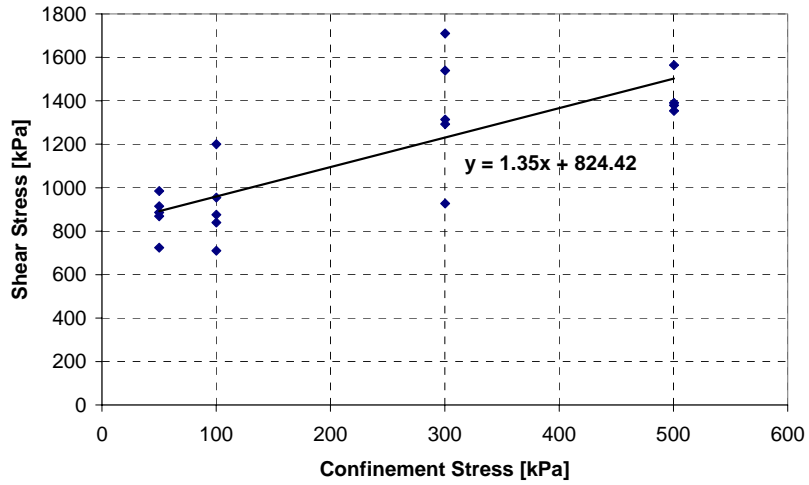


Fig. 4.8. Test results from clay triplets



Fig. 4.9. Clay triplet under loading

4.1.5. Mortar

The mortar used for the walls was available in bags in a dry premixed composition of cement and sand, and was classified as Type N according to the standard ASTM C270. Table 4.7 illustrates property specifications requirements for Type N masonry mortar.

Tab. 4.7. Specifications for Type N masonry mortar

Mortar	Type	Average compressive strength at 28 days [MPa]	Water Retention [%]	Air Content [%]
Masonry cement	N	5.2	75	20

Note: 1 MPa = 145 psi

According to ASTM C1019 six cubes of dimensions 51x51x51 mm (2x2x2 in) were built using a special plastic grid. This mortar was used for the construction of the walls used in the arching tests with dark clay bricks and concrete blocks and the construction, with light clay bricks, of clay panels for in-plane experimental program. The load was applied by means of a Tinius Olsen Machine. The test setup is showed in the figure 4.10 and in figure 4.11 is shown the cubes after tested.



Fig. 4.10. Mortar cube under loading



(a)



(b)

Fig. 4.11. Cubes after failure

Test results are illustrated in table 4.8.

Tab. 4.8. Mortar: test results

Prism #	Compressive Strength f'_m [MPa]
A1	10.2
A2	12.3
A3	11.3
A4	11.1
A5	8.2
A6	9.1
Average	10.4

Mortar	[MPa]
Compressive Strength	10.4
Standard Deviation	1.4

Note: 1 MPa = 145 psi

4.1.6. AFRP and GFRP laminates

Mechanical properties of AFRP (Aramid) and GFRP (Glass) fabrics used at the beginning of the experimental program are presented in table 4.9; the manufacturers provided all the data.

Tab. 4.9. Mechanical properties for Aramid and E-Glass Fabrics

Designation	Fiber Type	Guaranteed Ultimate Strength, [MPa]	Load per Sheet width, [kN/mm]	Thickness [mm]	Tensile Modulus, [MPa]	Guaranteed Ultimate Strain [%]
AK60	Aramid	1998	0.56	0.28	117130	1.7
EG 900	E-Glass	1516	0.53	0.35	72345	2.1

Note: 1 MPa = 145 psi, 1 mm = 0.03937 in

In order to verify the mechanical properties provided by the manufacturers of AFRP and GFRP laminates, tensile tests on thin flat strip of material having a constant rectangular cross section were performed in laboratory environment, following specifications provided by ASTM D3039.

Laminate panels were fabricated by the well-known wet lay-up technique and coupons were cut from the panels after complete cure. A 610x460x13 mm (24x18x1/2 in) plywood sheet was set as the base of the mold which was a rectangular plastic plate covered with a thin polyethylene film as the release agent. After the mold was prepared, a thin layer of saturant was placed on it with a roller. Then the aramid and glass fiber plies were spread on the saturant layer and a plastic roller was used to remove air entrapped between fiber plies and saturant.



Fig. 4.12. Final impregnation of laminate plies

After approximately 30 minutes, a second layer of saturant was applied and the plastic roller was used again to work the resin into the fibers. The wet laminates were left to cure for seven days and then released from the mold. The laminate panels were then ready to be cut into coupons along predetermined lines in order to obtain equal widths of 38 mm (1.5 in). All the specimens had a length of 381 mm (15 in) as shown in figure 4.13.

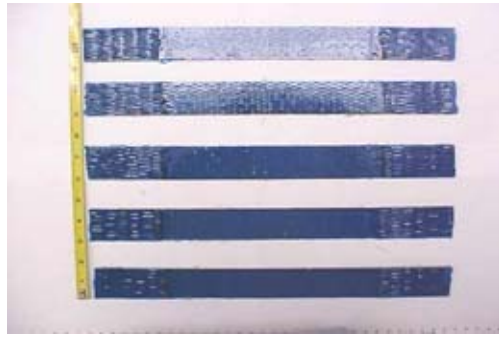


Fig. 4.13. Coupons to be tested

An extensometer with a gauge length of 25.4 mm (1 in) was attached to the mold-side surface of each specimens in the longitudinal direction. A built-in hydraulic pressure transducer of the Universal Testing Machine INSTRON 4485 under displacement control acquired the load. The testing frame is shown in figure 4.14, the loading head is rotationally self-aligning, which eliminates the potential of bending and twisting the specimen.



Fig. 4.14. Test apparatus

The wedge grips are self-tightening, to keep a constant pressure, so the clamping conditions do not change due to laminate contraction. All specimens were tested under displacement control with a constant loading speed of 2mm/min. The same mode of building and testing the specimens was used for GFRP and AFRP. In the

following figures are showed the laminates before and after failure for both type of tests.



(a)



(b)

Fig. 4.15. Test setup and coupon failure of GFRP



(a)



(b)

Fig. 4.16. Test setup and coupon failure of AFRP

In table 4.10 test results for AFRP and GFRP laminates respectively are presented.

Tab. 4.10. AFRP laminates: test results

Designation	Maximum Strain [%]	Maximum Stress [MPa]	Modulus of Elasticity [MPa]
A1	1.48	1670	117700
A2	1.64	1940	141000
A3	1.52	1760	120200
A4	1.74	2070	118000
A5	1.76	1980	115900
A6	1.66	1860	114060
Average	1.63	1880	121140
Standard deviation	0.11	140	9940

Note: 1 MPa = 145 psi

Tab. 4.11. GFRP laminates: test results

Designation	Maximum Strain [%]	Maximum Stress [MPa]	Modulus of Elasticity [MPa]
G1	2.14	1750	78750
G2	1.63	1700	82370
G3	2.16	1710	85480
G4	1.59	1680	85460
G5	1.80	1500	83700
G6	1.60	1760	83000
Average	1.82	1690	83130
Standard deviation	0.26	97	2496

Note: 1 MPa = 145 psi

4.1.7. CFRP Strips

In order to calculate the mechanical properties of CFRP (Carbon) strips, used in two walls tested with in-plane load, tensile tests on thin flat strip of material having a constant rectangular cross section, were performed in laboratory environment, following specifications provided by ASTM D3039. The mechanical properties from manufactures were not available because of the newly of the material.

The tests were conducted with the same apparatus that tested the AFRP and the GFRP. Since the lack of the data relative the mechanical properties, eight strips were prepared and tested, an electronic extensometer with 25.4 mm (1 in) gauge length and 1/10000 accuracy was clamped at mid-length of the test region to measure strain. All

the specimens had a total length of 381 mm (15 in) and the nominal dimensions of the strips were 15.24x2.11 mm (0.6x0.083 in) and they were cut from a coil 30000 mm (1181 in) long.

Figure 4.17 illustrates the strips ready to be tested.

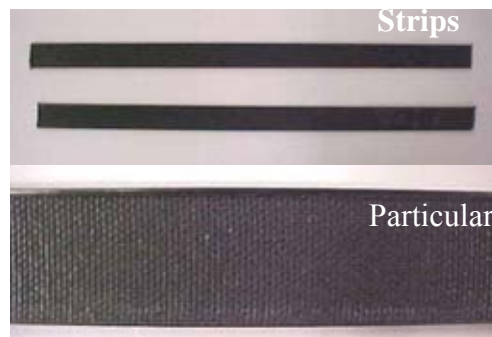
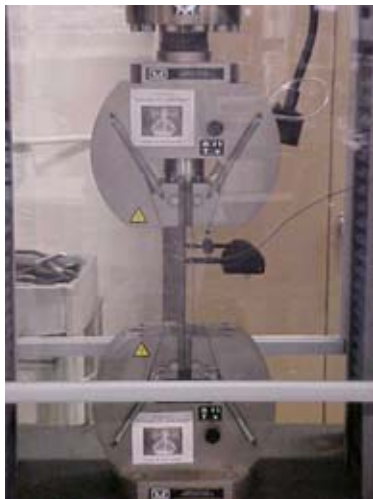


Fig. 4.17. Strips

In the following figures are shown the strips before and after failure.



(a)



(b)

Fig. 4.18. Test setup and coupon failure of CFRP strips



Fig. 4.19. Failure of the specimens

In table 4.12 the test results for the CFRP strips are presented.

Tab. 4.12. CFRP strips: test results

Designation	Maximum Strain [%]	Maximum Stress [MPa]	Modulus of Elasticity [MPa]
A1	1.18	1370	133804
A2	0.86	1470	147968
A3	1.47	1370	142160
A4	0.88	1450	149401
A5	0.78	1270	144975
A6	0.91	1370	141293
A7	0.87	1420	141088
A8	0.87	1410	141194
Average	0.98	1390	142735
Standard deviation	0.23	6.1	4842

Note: 1 MPa = 145 psi

4.1.8. GFRP Rods

In table 4.13 the experimental mechanical properties of GFRP rods utilized as Near Surface Mounted rods (see Section 3.2) are illustrated (Micelli, 2001).

Tab. 4.13. Mechanical properties of GFRP rod #2

Bar diameter [mm]	Cross-Sectional Area [mm ²]	Nominal Diameter [mm]	Tensile Strength, [MPa]	Tensile Modulus of Elasticity [MPa]
6	33.23	6.35	760	40789

4.1.9. Primer and Saturant

In table 4.14 the mechanical properties of primer and saturant are exposed. The manufacturers provided all the data.

Tab. 4.14. Mechanical properties for primer, putty and saturant

Material	Tensile Strength [MPa]	Tensile Elastic Modulus [MPa]	Tensile Strain [%]	Compressive Strength [kPa]	Compressive Modulus [MPa]
Primer	12.41	723.9	3	24.13	655.00
Saturant	54.46	3033.0	2.5	86.10	26.20

Note: 1 Mpa = 145 psi

4.1.10. GFRP G1 Rods

In table 4.15 the experimental mechanical properties of GFRP rods are illustrated (Micelli, 2001).

Tab. 4.15. Material properties for GFRP G1 Rods

Bar diameter [mm]	Cross-Sectional Area [mm²]	T_g [°C]	Tensile Strength, [MPa]	Tensile Strain [%]	Tensile Modulus of Elasticity [MPa]
12.7	127	138	924	2.17	42574

Note: 1 Mpa = 145 psi

4.2. Bond Characterization

FRP laminates are successfully used for strengthening of existing RC and PC structures. Bond of the external FRP reinforcement to the concrete substrate is of critical importance for the effectiveness of this technique. Bond mechanism consists of shear transfer mechanism and local region tension at the interface between the concrete and FRP. Delamination before ultimate FRP strain may be encountered.

In the case of masonry, have shown that debonding of FRP laminates is the predominant mode of failure (Tumialan, 2001; Morbin, 2001 etc.). Therefore, the issue of bond is also one of the ultimate states to consider in the design of strengthening with externally bonded FRP laminates. To date there has been few bond research conducted on masonry elements (Roko et al., 1999); the objective of this section is to develop an analytical model to determine the proper bonded length for FRP laminates. Debonding has a direct relationship with the porosity of the masonry, the type of masonry, the umidity, the type of fiber, the quantity of saturant used etc..

4.2.1. Test Specimens

Standard hollow concrete blocks and clay bricks (see also description in sections 4.1.2 and 4.1.3) specimens were tested, to investigate the bond behavior of AFRP sheets on different types of masonry surface.

The FRP sheets used were AK60 Master builders technologies with the following properties from the material characterization (section 4.1.6):

Tab. 4.15. Properties of AK60 Master builders technologies sheet

Rupture [MPa]	1880
Tensile Elastic Modulus [GPa]	121
Tensile strain [%]	1.63
Thickness [mm]	0.28*

Note: 1 MPa = 145 psi; 1 mm = 0.03937 in; * = value from manufacturer

According with the manufacturer the tensile properties of primer, putty and saturant are reported in table 4.16. The resin was allowed to cure for at least 4 days prior to testing the specimens.

Tab. 4.16. Properties of MBrace primer, putty and saturant

Material	Tensile strength [MPa]	Tensile elastic modulus [MPa]	Tensile strain [%]	Compressive strength [MPa]	Compressive Modulus [MPa]
Primer	12.41	723.9	3	24.13	655
Putty	12.41	1792	1.5	24.13	1068
Saturant	54.46	3033	2.5	86.18	2620

Note: 1 MPa = 145 psi

To determine the effective bonded length several lengths were investigated; different widths of AFRP sheets were employed to evaluate the different behavior and size effect. Depending on these variables, the configurations of the blocks were different, as shown in figure 4.20.

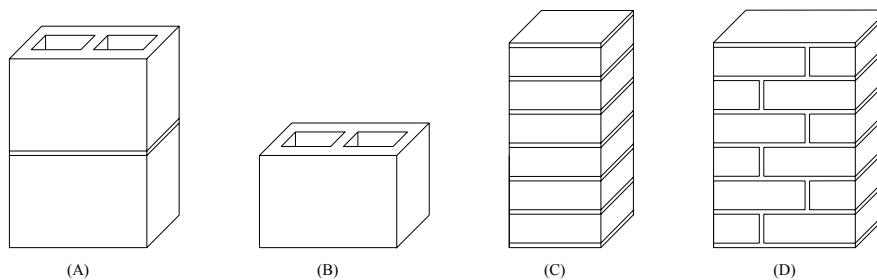


Fig. 4.20. Specimens configuration

Two prisms were used for each test; figure 4.21 shows the configuration utilized for the tests explaining in what way the generic blocks (X and Y) were positioned:

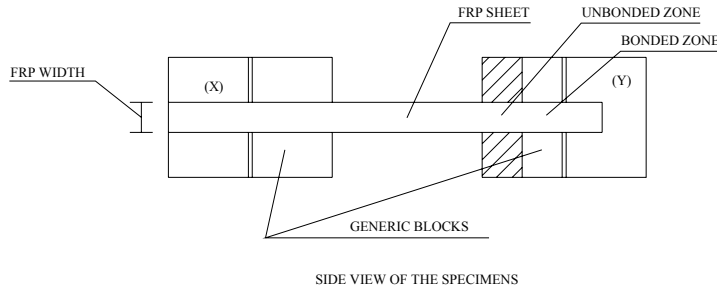


Fig. 4.21. Generic test configuration

Tables 4.17 and 4.18 summarize the test configurations:

Tab. 4.17. Test configuration for concrete blocks

Test name	FRP width [mm]	Bonded length [mm]	Unbonded length [mm]	Blocks used (X - Y)
CA3-4	76.2	101.6	101.6	A - B
CA3-8	76.2	203.2	101.6	A - A
CA3-12	76.2	304.8	101.6	A - A
CA6-4	152.4	101.6	101.6	A - B
CA6-8	152.4	203.2	101.6	A - A
CA6-12	152.4	304.8	101.6	A - A

Note: 1 mm = 0.03937 in

Tab. 4.18. Test configuration for clay bricks

Test name	FRP width [mm]	Bonded length [mm]	Unbonded length [mm]	Blocks used (X - Y)
BA3-4	76.2	101.6	101.6	C - C
BA3-8	76.2	203.2	101.6	C - C
BA3-12	76.2	304.8	101.6	C - C
BA6-4	152.4	101.6	101.6	D - D
BA6-8	152.4	203.2	101.6	D - D
BA6-12	152.4	304.8	101.6	D - D

Note: 1 mm = 0.03937 in

The dimensions of the blocks were described in sections 4.1.2 and 4.1.3. One FRP sheet was applied to each face of the blocks in the longitudinal direction, connecting

the two blocks together. Only one block was instrumented, this area called test region had the AFRP laminate with a limited bonded length and being unbonded the remaining part (using adhesive tape) to force the delamination in the test region. Length and position of the bonded part were the same on both faces of the test block. However, to avoid failure in the non-instrumental regions, transversal sheets were applied as can be seen in figure 4.22 where there are illustrated the two side views of the specimens.

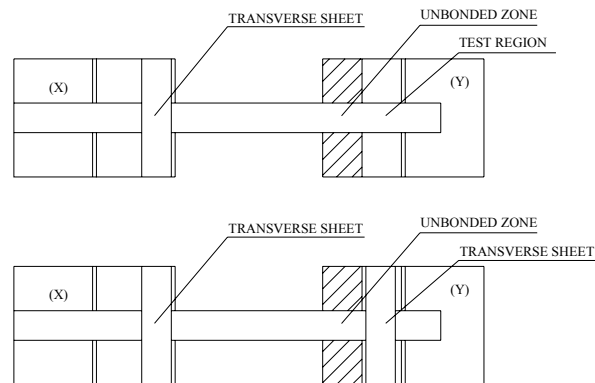


Fig. 4.22. Side views of the specimens

The test specimens were laid on the floor, after they were aligned along the major axis (figure 4.23).



Fig. 4.23. Specimens aligned

Then, the specimens were prepared following the wet-lay-up technique (see section 3.1).

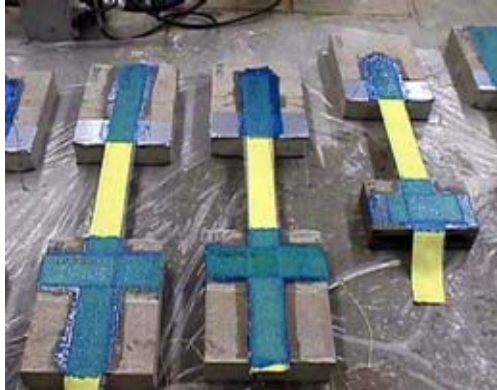


Fig. 4.24. Specimens ready

The only difference between concrete blocks and bricks were the application of putty on the bricks surfaces, but in the test region it was applied only to cover the surfaces irregularities, to not influence significantly the bond behavior.

Strain gages were applied on the AFRP laminates to monitor the strain distribution along the laminate during the tests. All the strain gages had a gage length of 12.7 mm (1/2 inch) to ensure localized strain measurement. The surface of laminate was smoothed and conditioned to assure a perfect bond between strain gage and sheet.

Two strain gages were applied on the unbonded region at 25.4 mm (1 in) from the beginning of the unbonded region; their spacing was 50.8 mm (2 in). The unbonded regions were taken 101.6 mm (4 in) for all the specimens.

The others strain gages in the bonded region were applied from 25.4 mm (1 in) from the beginning of this region, their distance were 50.8 mm (2 in) except for the bond length of 101.6 mm (4 in) where the distance was only 25.4 mm (1 in).

Figure 4.25 indicates the typical location of the strain gages on the AFRP laminates.

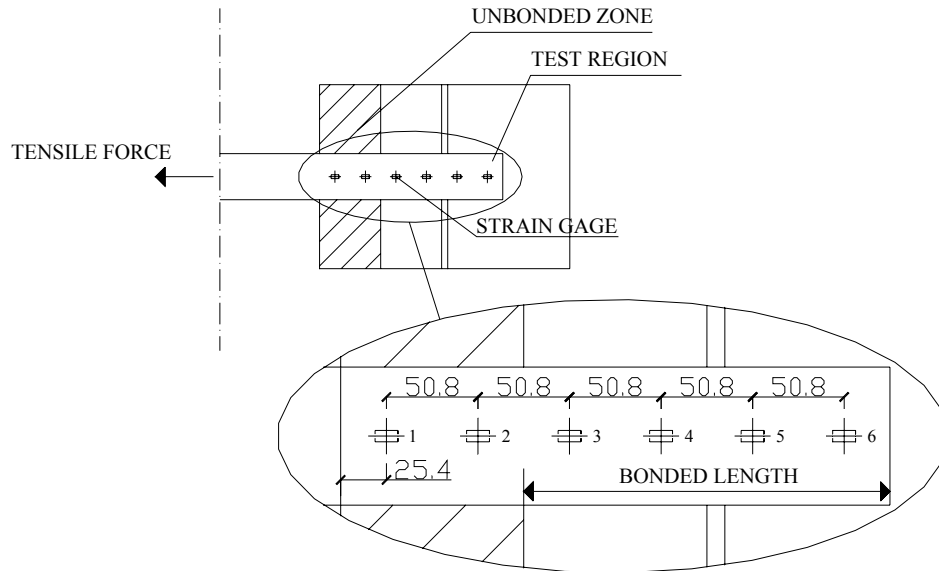


Fig. 4.25. Typical location of the strain gages

4.2.2. Test Setup

The test bed consisted of a steel plate with dimensions 1524 mm (5 ft.) by 609.6 mm (2 ft.) and thickness of 3.175 mm (1/8 in.). Five steel angles were bolted on the plate to delimitate the position where the blocks had to be placed. The purpose of the plate was to ensure the proper positioning of the specimens during preparation and testing. Grease was placed between the plate and the bottom surface of the blocks, in order to minimize the friction between the two surfaces during testing.

Load was applied by means of a 12-ton hydraulic jack connected to a hydraulic pump. The jack was placed horizontally between the two blocks.

A Sensotek pressure transducer connected to the hydraulic jack recorded the load. Load and strains were all recorded with a one-Hertz sampling rate by a LABTECH data acquisition system. Figures 4.26 and 4.27 illustrate the test setup.

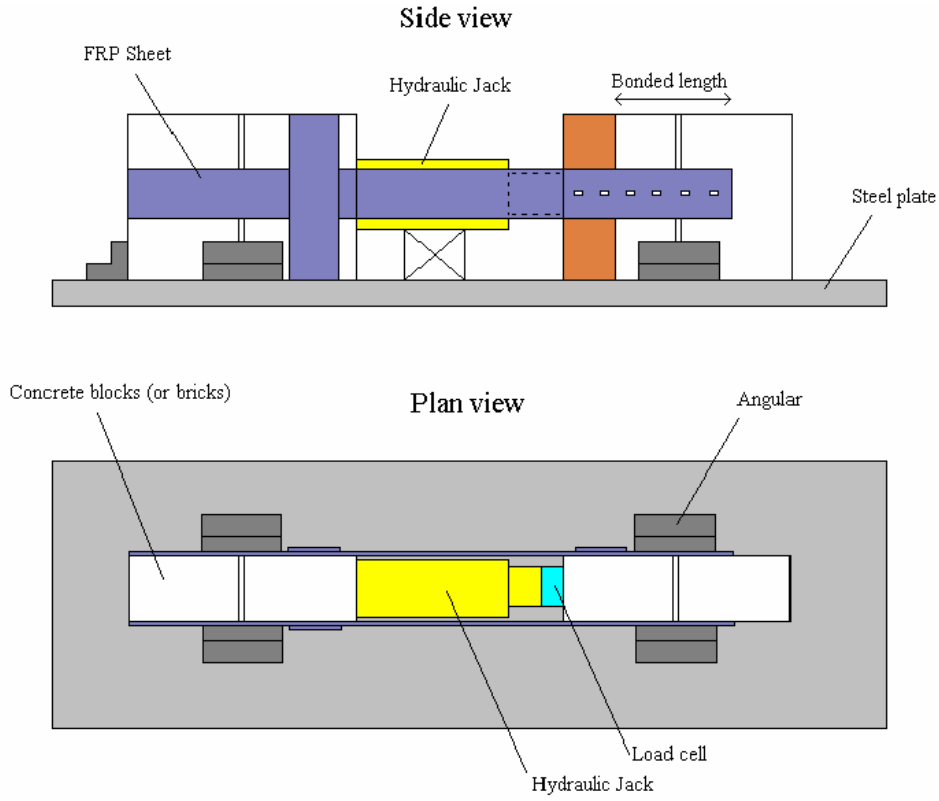


Fig. 4.26. Test setup scheme

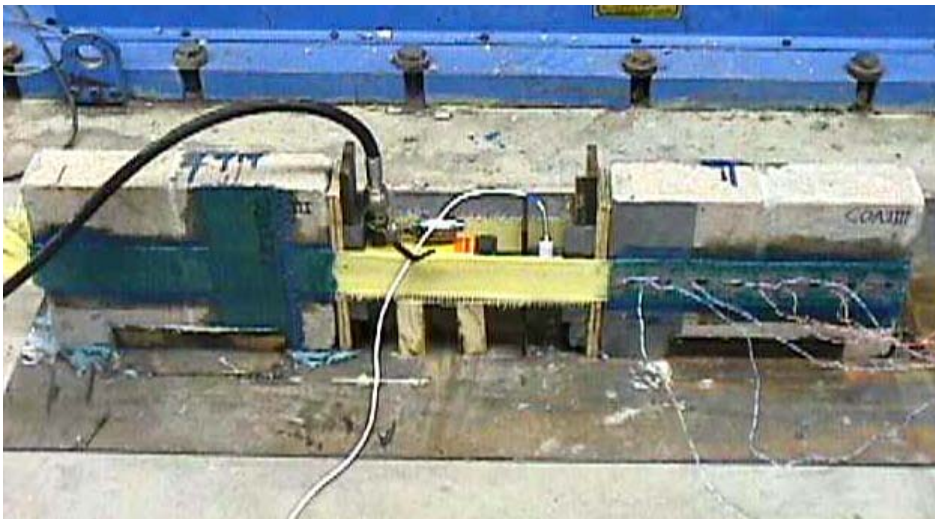


Fig. 4.27. Test setup



Fig. 4.28. Detail of hydraulic jack and pressure transducer

4.2.3. Test Results

General Results. Test results in terms of ultimate load and failure mode are summarized in table 4.19 and 4.20. The value of the ultimate load was obtained dividing by two the maximum load registered by the load cell.

Tab. 4.19. Test results for Concrete Masonry

Test name	Sheet width [mm]	Bonded length [mm]	Ultim. load [KN]	Failure mode
CA3-4	76.2	101.6	23.7	D
CA3-8	76.2	203.2	26.5	D
CA3-12	76.2	304.8	24.6	R+D
CA6-4	152.4	101.6	37.5	D
CA6-8	152.4	203.2	48.2	D
CA6-12	152.4	304.8	48.9	D

Legend: D = Delamination; R = Fiber rupture Note: 1 mm = 0.03937 in; 1 KN = 0.2248 Kip

Tab. 4.20. Test results for Clay Masonry

Test name	Sheet width [mm]	Bonded length [mm]	Ultim. load [KN]	Failure mode
BA3-4	76.2	101.6	29.0	D
BA3-8	76.2	203.2	27.9	D
BA3-12	76.2	304.8	24.0	R+D
BA6-4	152.4	101.6	46.4	D
BA6-8	152.4	203.2	31.3	D
BA6-12	152.4	304.8	46.6	D

Legend: D = Delamination ; R = Fiber rupture Note: 1 mm = 0.03937 in ; 1 KN = 0.2248 Kip

As indicated in tables 4.19 and 4.20, two different failure modes were observed. In the specimens CA3-12 and BA3-12 with 304.8 mm (12 in.) of bonded length, failure occurred by fiber delamination (not complete, the fiber did not detach completely from the specimens) in the test region followed by fiber rupture on the other side. This can be explained as follows: during delamination process, load switched in the backside of the specimens because of eccentricity causing suddenly the fiber rupture.

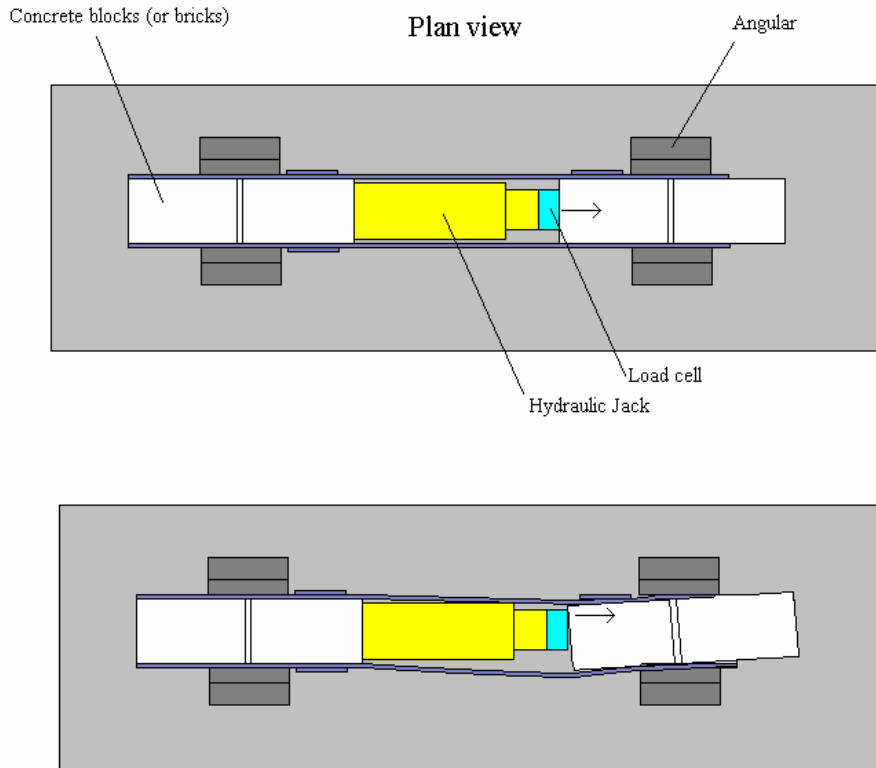


Fig. 4.29. Cause of failure in tests CA3-12 and BA3-12

In the remaining specimens failure occurred only for delamination. Due to geometrical imperfections, the tensile force was not perfectly centered. These imperfections were evident when the specimens were not perfectly aligned. This eccentric force introduced an additional bending moment. Previous study on this phenomenon (Van Gemert D. et al., 2001) had shown that no significant differences were recorded. Due to the eccentricity, a premature peeling off of the FRP laminates could be observed, which can explain the mode of failure observed in specimens CA6-4 and BA6-8.

In figure 4.30 can be seen the debonding for several specimens and can be seen also that some concrete blocks and masonry bricks surrounding the fiber were damaged, meaning that a good engagement was created between FRP laminates and masonry surface.



(a) Test CA3-8



(b) Test CA6-4



(c) Test BA6-12



(d) Test BA6-8



(e) Damage in the masonry bricks



(f) Damage in the concrete blocks

Fig. 4.30. Failure of specimens

4.2.4. Strain Data

Strain gages were placed at various locations to monitor the strain distribution along the laminate during the test. The strain gages were numbered starting from one in the unbonded region towards the sheet free end.

The two strain gages in the unbonded region were used to determine the tensile modulus of elasticity of the FRP laminate. Assuming the strain the average between the two strain gages in the unbonded region and building the load-strain diagram the axial stiffness EA can be found (figure 4.31).

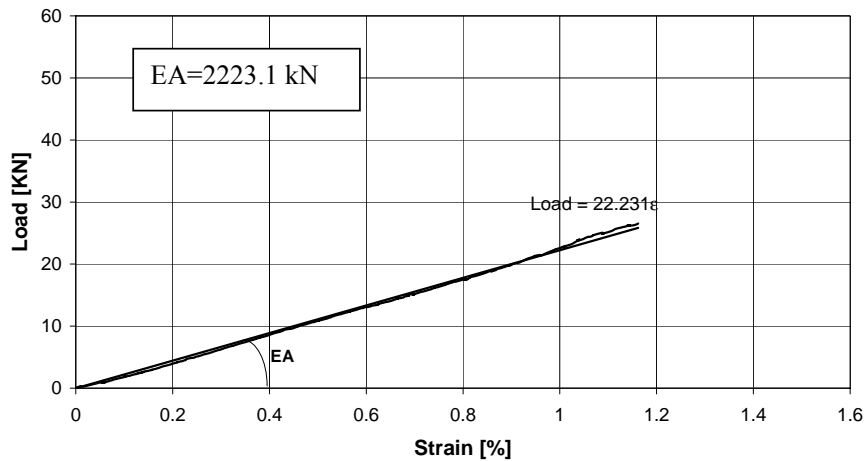


Fig. 4.31. Axial stiffness for CA3-8

Then, can be calculated the FRP tensile modulus simply dividing the axial stiffness by the FRP area relating to that test.

Tables 4.21 and 4.22 show the values of the AFRP tensile elastic modulus calculated for all the specimens.

Tab. 4.21. Exp. tensile modulus of elasticity for AFRP on concrete blocks

Specimen	Width [mm]	Bond Length [mm]	Thickness* [mm]	Axial Stiffness EA [KN]	E [GPa]
CA3-4	76.2	101.6	0.28	2263.1	106.1
CA3-8	76.2	203.2	0.28	2223.1	104.2
CA3-12	76.2	304.8	0.28	2236.9	104.8
CA6-4	152.4	101.6	0.28	3826.5	89.7
CA6-8	152.4	203.2	0.28	4701.8	110.2
CA6-12	152.4	304.8	0.28	3985.9	93.4

Note: 1 mm = 0.03937 in; 1 KN = 0.2248 Kip; 1 MPa = 145 Psi * = Values from manufacturer

Tab. 4.22. Exp. tensile modulus of elasticity for AFRP on masonry bricks

Specimen	Width [mm]	Bond Length [mm]	Thickness* [mm]	Axial Stiffness [KN]	E [GPa]
BA3-4	76.2	101.6	0.28	N/A	N/A
BA3-8	76.2	203.2	0.28	2381.4	111.6
BA3-12	76.2	304.8	0.28	1855.7	87.0
BA6-4	152.4	101.6	0.28	4081.4	95.6
BA6-8	152.4	203.2	0.28	N/A	N/A
BA6-12	152.4	304.8	0.28	4518.4	105.9

Note: 1 mm = 0.03937 in; 1 KN = 0.2248 Kip; 1 MPa = 145 Psi * = Values from manufacturer
N/A = Not available

The experimental tensile modulus of elasticity is computed as by the average of all these values and it is equal to 100.8 GPa (14616 ksi).

This value is lower that provided by manufacturer value that is 117.2 GPa (17000 ksi). The strain gages in the bonded region were used to determine the bond behavior for the FRP sheet.

Assuming that the strain at the beginning of the bonded region at determinate values of load is:

$$\varepsilon_b = \frac{N}{E_t A}$$

Where:

N = load

E_t = experimental modulus of elasticity (average)

A = AFRP area

The strain-location graphics can be found.

Figure 4.32 and figure 4.33 shown the strain-location graphics for two specimens; from the experimental results, it can be observed that the strain vs. location graphics for concrete blocks and masonry bricks have similar behavior. From table 4.19 and 4.20 can be observed that the bonded length does not significantly influence the ultimate load.

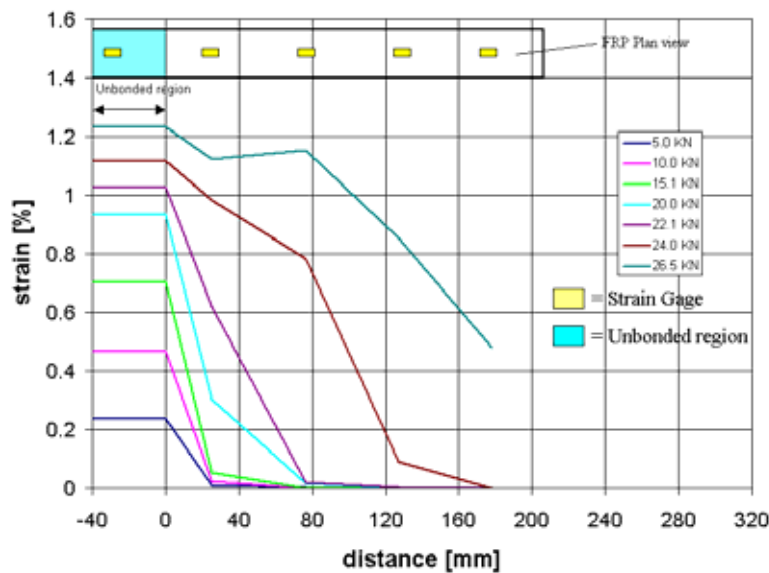


Fig. 4.32. Typical strain vs. location graph for concrete blocks (specimen CA3-8)

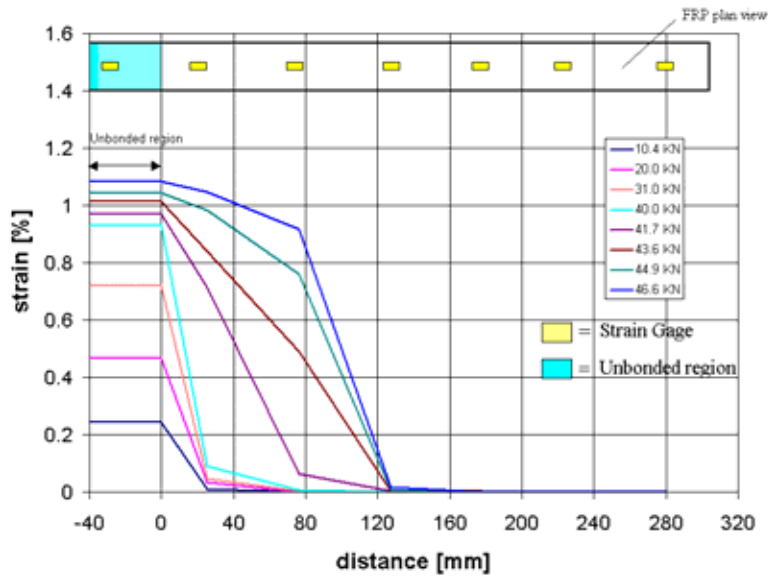


Fig. 4.33. Typical strain-location graph for masonry bricks (specimen BA6-12)

In order to determine the effective bond length, the ultimate load is not very significant because FRP is already detached at this value of load. Peeling load is the load when the fiber starts the delamination. It is identified as the load level at which the strain distribution becomes linear. Figure 4.34 shows different theoretical stages. It can be observed that after the peeling load the effective bond length slip towards the end of the fiber, but has always the same length.

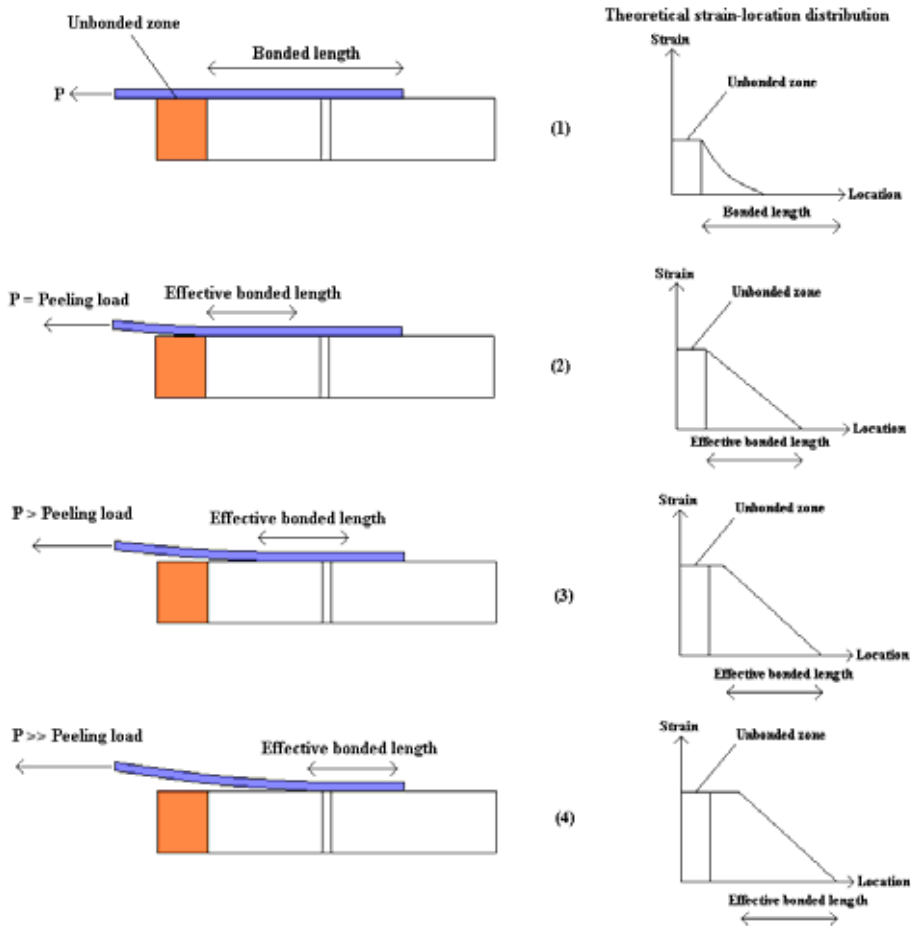


Fig. 4.34. Theoretical peeling load

Figure 4.35 illustrates how the load corresponding to imminent peeling was determined. To that effect specimen CA3-8 was used. From the figure 4.34 the theoretical behavior after the peeling load can be assumed parallel to the straight line that characterize the peeling load. The theoretical behavior after the peeling load can be found following the experimental behavior. Figure 4.35 shows that the fiber is already detached, like the theoretical behavior explains. Tracking the parallel lines the

peeling load can be found and also the imminent peeling load that is the closest experimental behavior.

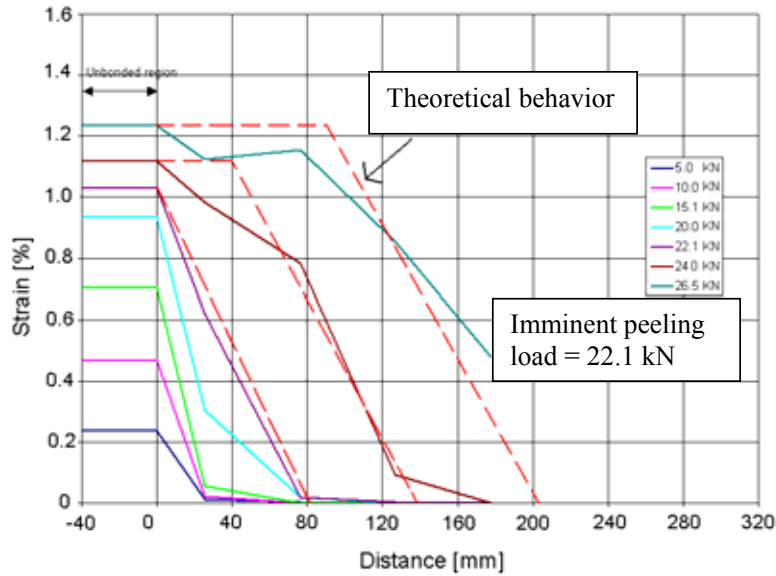


Fig. 4.35. Determination of imminent peeling load for specimen CA3-8

Table 4.23 shows the imminent peeling load values estimated for the test specimens

Tab. 4.23. Imminent peeling load estimated for the specimens

Specimen	Imm. peeling [kN]	Specimen	Imm. peeling [kN]
CA3-4	22.1	BA3-4	N/A
CA3-8	22.1	BA3-8	24.2
CA3-12	24.0	BA3-12	N/A
CA6-4	37.4	BA6-4	N/A
CA6-8	44.0	BA6-8	41.7
CA6-12	46.4	BA6-12	N/A

Note: 1 kN = 0.2248 kip

Because of imperfections in the clay masonry specimens (such as misalignment of the laminate), it was not possible to clearly determine the strain distribution over the bonded length of the FRP laminate. Also, it was not possible to determine the peeling load for several specimens. As a consequence, the analytical model proposed in the

next paragraph could not be validated in this case. However, the overall test trends indicated the following:

- The bonded length does not significantly influence the ultimate load
- The bonded length could be about 100 mm (4 in.)
- In some specimens, the strain versus location behavior is similar to that specimens made with concrete blocks

4.2.5. Analytical Work

The bond issue is an important limit stated to consider in the strengthening design of externally bonded FRP laminates. When failure is bond-controlled, the maximum stress in the FRP cannot be considered equal to the tensile strength of the FRP material. To reach a possible design, the ACI committee 440 seems to indicate a reduced ultimate strain level in the FRP reinforcement:

$$\varepsilon_{ub} = k_r \cdot \varepsilon_u \quad (4.1)$$

Where:

ε_u = ultimate strain of the FRP laminate

k_r = reduction factor

In order to determine the k_r coefficient and then the bonded length, a model developed by De Lorenzis et al. (2000) can also be used for masonry, since the hypotheses are fundamentally the same:

- Linear elastic behavior of materials
- Flexural stiffness of sheets negligible
- The masonry strain is negligible if compared to that of FRP

The bond failure load can be found using non-linear fracture mechanics approach (Taljsten, 1994). It has been observed that with an energy approach, the same results of classical Volkersen's theory can be found. This theory was used like starting point for the bond.

$$P_{ub} = b_f \sqrt{2 \cdot E_f \cdot t_f \cdot G_f} \quad (4.2)$$

Where:

b_f , E_f , t_f = width, tensile elastic modulus and thickness of FRP sheet

G_f = fracture energy per unit area of the joint

The energy needed to bring a connection with a certain area to failure is called fracture energy and it is determined building the τ -slip curve. The fracture energy is the area underneath this graphic ($G_f = \int \tau ds$).

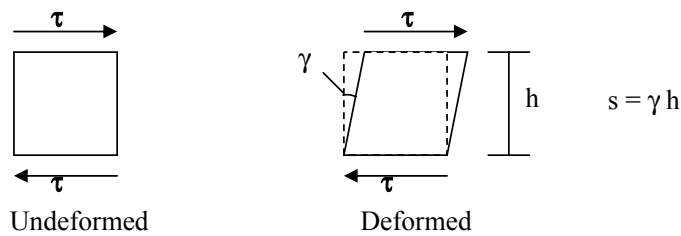
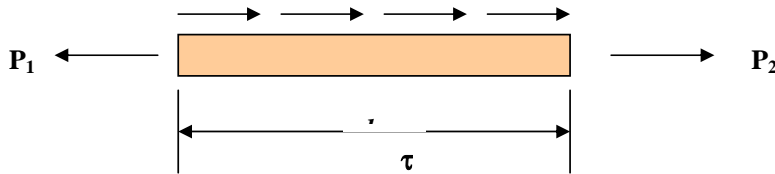


Fig. 4.36. Infinitesimal part of adhesive layer subjected to angular distortion

Because the slip “s” value is more used in civil engineering than the “ γ ” value, it was decided to use the τ -slip relationship rather than the τ - γ relationship, also because the slip value is much easier to record experimentally, and the thickness of the glue layer “h” is in most cases unknown or it is difficult to determine.

The local τ -slip curve can be obtained from the experimental data. The bond stress (τ) can be found by equilibrium of forces:



Being the generic force P equal to:

$$P = \sigma_f \cdot t_f \cdot b_f \quad (4.3)$$

The follow equation can be obtained:

$$P_1 - P_2 = \tau(x) \cdot b_f \cdot dx \quad (4.4)$$

The force P can be expressed in terms of strain (elastic-linear behavior):

$$P = \varepsilon_f \cdot E_f \cdot t_f \cdot b_f \quad (4.5)$$

So the equation (4.4) becomes:

$$(\varepsilon_1 - \varepsilon_2) \cdot E_f \cdot t_f \cdot b_f = \tau(x) \cdot b_f \cdot dx \quad (4.6)$$

Substituting $(\varepsilon_1 - \varepsilon_2)$ with $d\varepsilon_f(x)$ and solving for $\tau(x)$ the average bond stress can be obtained:

$$\tau(x) = t_f \cdot E_f \cdot \frac{d\varepsilon_f(x)}{dx} \quad (4.7)$$

Where ε_f is the strain in the FRP laminate. Therefore, the τ - location can be obtained from equation of the strain-location multiplied by the elastic modulus E_f and the thickness t_f of FRP sheet. To calculate the $\varepsilon_f(x)$ is used a cubic approximation for the experimental results with the hypothesis that the strain to the end of the fiber is zero ($\varepsilon_f(L) = 0$).

Figure 4.37 shows a typical approximation for $\varepsilon_f(x)$ obtained with Maple 6.0.

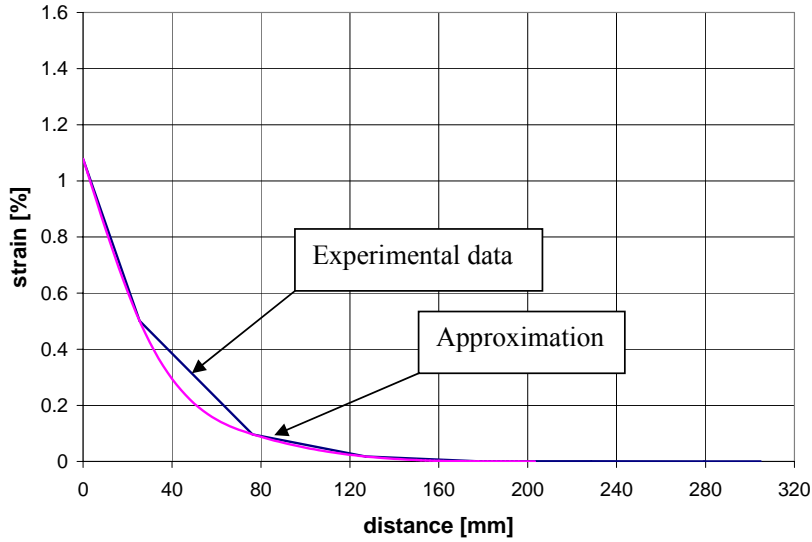


Fig. 4.37. Approximation of $\varepsilon(x)$ for the specimen CA6-12

The graphics were developed at imminent peeling load level, because after this load the G_f is not significant since the first part of fiber is already detached. As an example shown the τ versus location behavior for specimen CA3-8 is shown in figure 4.38:

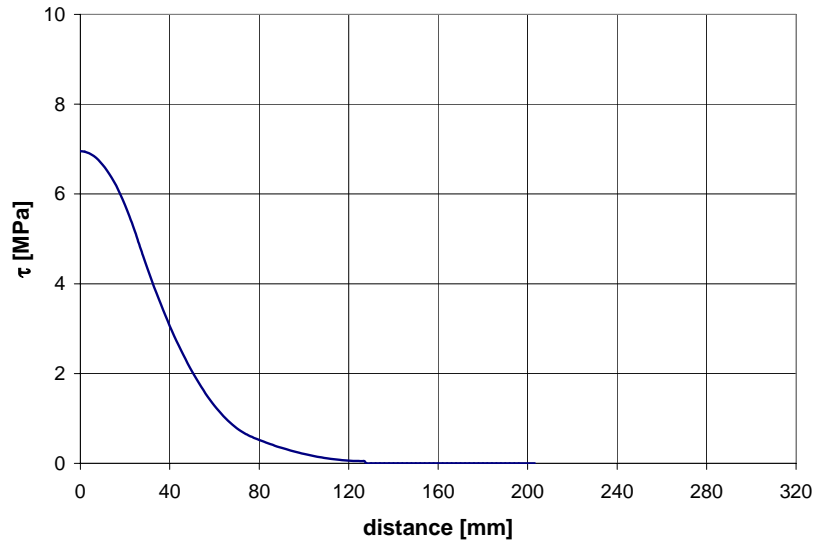


Fig. 4.38. τ vs. location at peeling load for the specimen CA6-8

For the slip “s” it can be assumed that the strain in masonry is negligible compared to the FRP strain, so the follow equation can be used to measure the slip:

$$\frac{ds}{dx} = \epsilon_f \quad (4.8)$$

from which:

$$s(x) = s(0) + \int_0^x \epsilon_f(x) dx \quad (4.9)$$

Assuming $s(0)$ the slip at the end of the laminate equal to zero (can be consider negligible prior to delamination), the slip-location diagram can be obtained only from the integration of the strain-location curve. Figure 4.39 shows the behavior for specimen CA3-8:

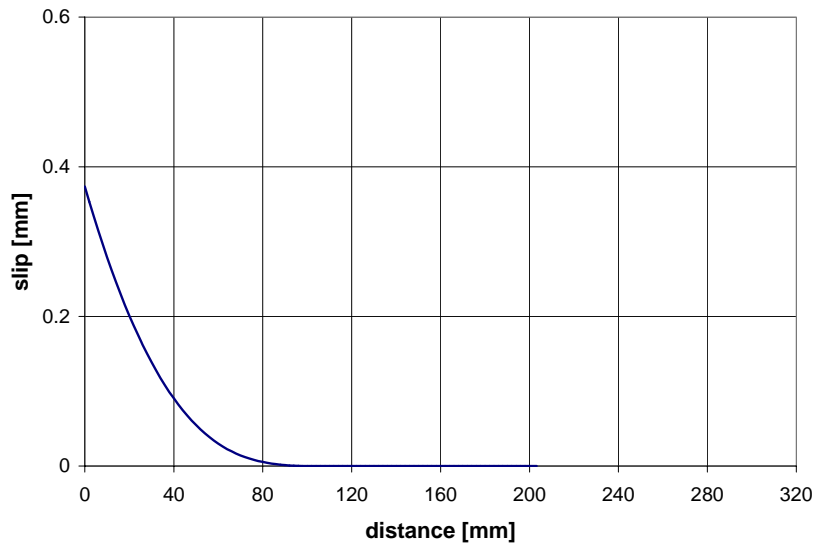


Fig. 4.39. Slip vs. s location behavior for specimen CA3-8

To the end, the local τ -slip relationship can be achieved by combining the two curves $\tau(x)$ and $s(x)$. This diagram can be done for all the loads; figure 4.40 shows the τ -slip curves of a tested specimens at a load level corresponding to imminent peeling.

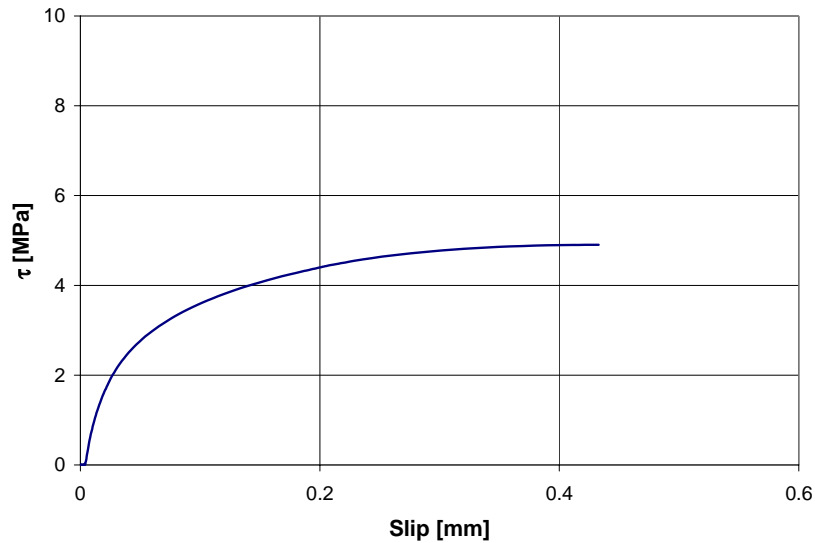


Fig. 4.40. τ vs. slip behavior for the specimen CA3-12

Following this procedure the experimental graphics for all the specimens can be found. Figure 4.41 and following show the comparison from the experimental data.

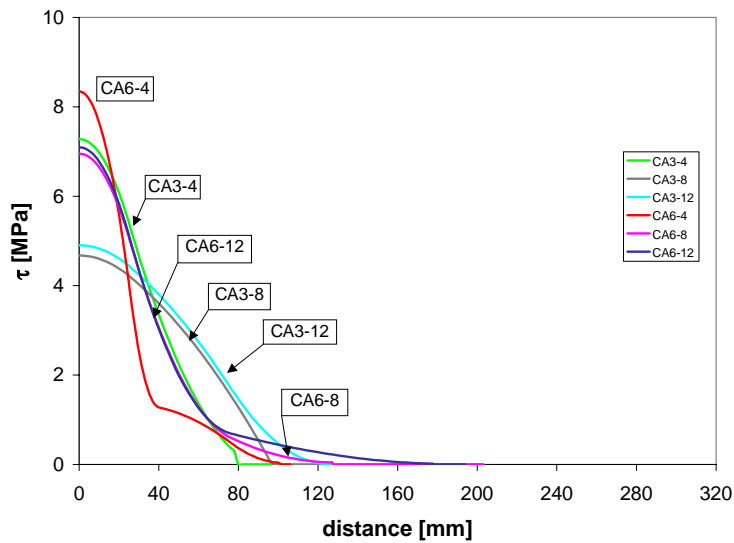


Fig. 4.41. Experimental results in terms of τ vs. location for the concrete blocks

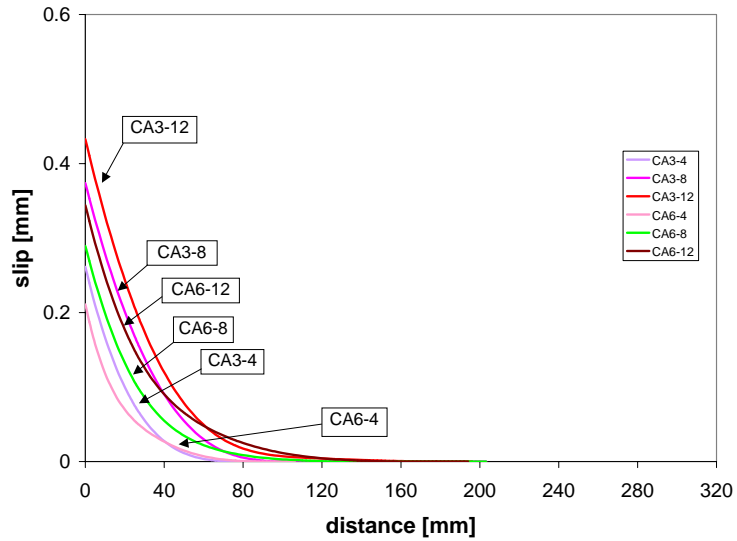


Fig. 4.42. Experimental results in terms of slip vs. location for concrete blocks

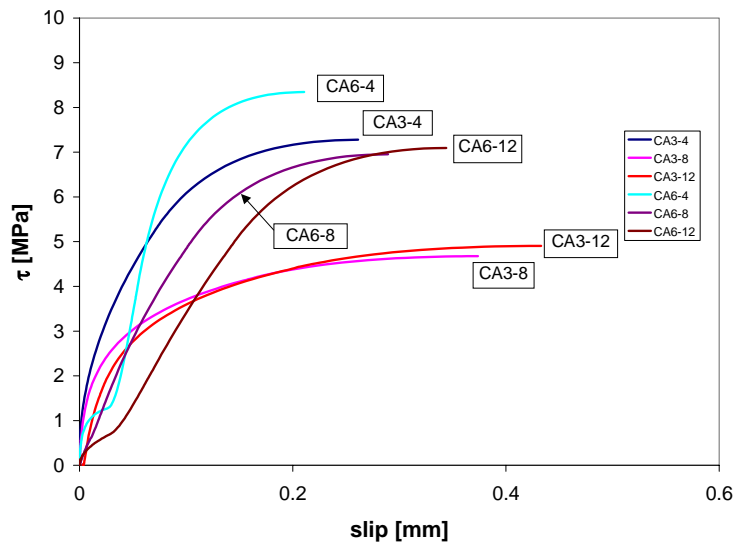


Fig. 4.43. Experimental results in terms of τ vs. slip for concrete blocks

Fig. 4.43 illustrates the τ -slip curves obtained for the specimens at load level corresponding to imminent peeling. An ascending branch is followed by a second region characterized by plastic or softening behavior, until an ultimate value of slip is

reached. The plastic branch of the curve explains the attainment of a linear strain distribution close to peeling. The limited value of ultimate slip suggests a brittle behavior of the joint, that is, the localization of load transfer within a short effective area even for long bonded lengths.

The fracture energy per unit area of the bonded joint “ G_f ”, its corresponding slip “ S_m ” and the value of “ τ_m ” (i.e. the maximum value of τ in the τ -slip curve) can be found.

Tab. 4.24. Values of G_f , S_m , and τ_m for the concrete blocks

Specimen	G_f [N·mm/mm ²]	S_m [mm]	τ_m [MPa]
CA3-4	1.500	0.261	7.278
CA3-8	1.486	0.374	4.674
CA3-12	1.757	0.433	4.905
CA6-4	1.252	0.211	8.346
CA6-8	1.477	0.289	6.954
CA6-12	1.642	0.344	7.095

Note: 1 Nmm/mm² = 5.71 lbs in./in²; 1 mm = 0.03937 in; 1 MPa = 145 psi

It can be noted that the fracture energies are almost the same for all the specimens. To determine the FRP ultimate strain (see equation 4.1) the follow procedure can be used:

Being $\sigma_{ub} = E_f \cdot \varepsilon_{ub}$ (assuming a elastic-linear behavior) the ultimate peeling strength, combining the last equations and the 4.2 the equation for ultimate strain of FRP laminate before peeling ε_{ub} can be found:

$$\varepsilon_{ub} = \sqrt{\frac{2 \cdot G_f}{E_f \cdot t_f}} \quad (4.10)$$

Using the G_f average “ G_{fm} ” for the concrete block specimens, the ultimate strain before peeling can be found. Being $G_{fm} = 1.519 \text{ N}\cdot\text{mm}/\text{mm}^2$ (8.67 lbs·in/in²) ε_{ub} becomes:

$$\varepsilon_{ub} = \sqrt{\frac{2 \cdot 1.519}{100800 \cdot 0.28}} = 0.0104 = 1.04 \%$$

So, the experimental reduction factors can be found with the equation shown below:

$$k_r = \frac{\varepsilon_{ub}}{\varepsilon_u} = \frac{1.04}{1.7} = 0.61 \quad (4.11)$$

Previous works on reinforced concrete (Chajes et al., 1999; Maeda et al., 1997; Talijsten, 1994; and De Lorenzis, 2000) have shown that the reduction factor k_r becomes very low if the stiffness of the laminate increases. From this, is evident that further research on this area needs to be considered. Anyway, the value of k_r found at $E_t = 28224 \text{ N/mm}$ (160.7 kips/in) is in according with the previous researches.

Effective bond length

The effective bond length can be expressed as follows:

$$l_{eff} = \frac{\varepsilon_{ub}}{\left. \frac{d\varepsilon}{dx} \right|_{peel}} \quad (4.12)$$

The τ -slip curve can be modeled having an initial ascending branch followed by a perfectly plastic behavior at value τ_m then:

$$\left. \frac{d\varepsilon}{dx} \right|_{peel} = \frac{\tau_m}{E_f \cdot t_f} \quad (4.13)$$

Using the equations 4.10, 4.12 and 4.13, the equation 4.10 can be modified:

$$l_{eff} = \frac{\sqrt{2 \cdot E_t \cdot G_{fm}}}{\tau_m} \quad (4.14)$$

Using the average of τ_m (τ_{ma}) the effective bonded length can be found. Taking τ_{ma} equal to 6.54 MPa (948 psi) the effective bond length is:

$$l_{\text{eff}} = \frac{\sqrt{2 \cdot 100800 \cdot 1.533}}{6.54} = 85 \text{ mm (3.35 in.)}$$

4.2.6. Conclusions

Several specimens were prepared to study bond between masonry and FRP sheets. Failure occurred in the masonry-adhesive interface, sometimes with signs of damage into the masonry. The experimental bonded length did not affect the ultimate load, as shown in previous works on concrete specimens (i.e. De Lorenzis et al., 2000). This confirms the existence of an effective bonded length beyond which no stress is transferred after peeling occurs. No significance increase in resistance to peeling is attainable.

4.2.7. Design

To date, there are few investigations conducted on the bond between FRP sheets and masonry; the reported work represents intends to establish a limit for the FRP strain and for determination of an effective development length. The extent of the experimental work is not sufficient for the calibration of the model but allows for its validation.

It can be seen from the experimental results that the τ values are included in a range of values between 8.346 MPa (1210 psi) and 4.674 MPa (678 psi) (see figure 4.44).

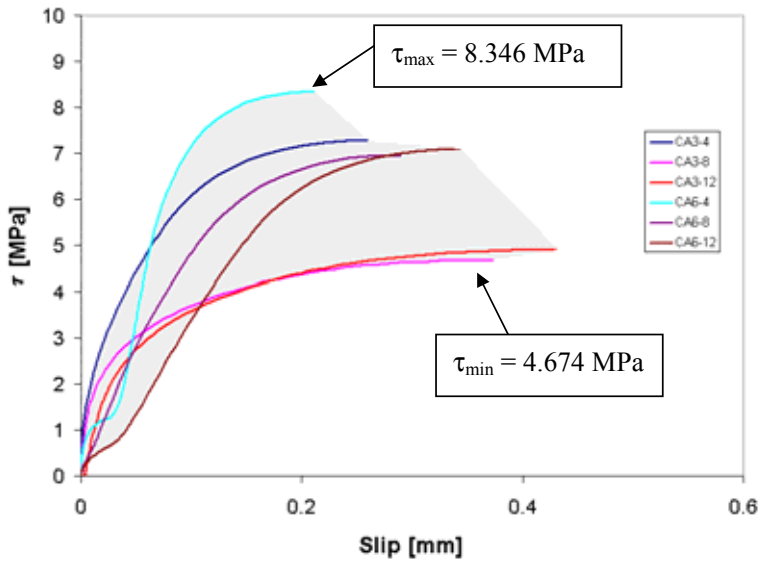


Fig. 4.44. τ vs. slip fuse

For a conservative design, the τ values corresponding to the lower boundary of the experimental results can be adopted. Considering a safety factor equal to 2 it is suggested a maximum value of:

$$\tau = \frac{4.674}{2} \cong 2.2 \text{ MPa (319 Psi)}$$

Correspondingly, based on average fracture energy value G_{fm} the minimum development length becomes:

$$l_{\min} = \frac{\sqrt{2 \cdot 100800 \cdot 1.533}}{2.2} = 253 \text{ mm (10 in.)}$$

Furthermore, being the ultimate strain before peeling equal to $\epsilon_{ub} = 1.04$ %, to avoid debonding from the masonry surface it is recommended that the ultimate design strain should not exceeded $\epsilon_{ub} = 0.8$ %, because of the presence of the normal component of stress due to flexural behavior. This recommendation is similar to the strain limit

adopted by a previous work on flexural strengthening of masonry elements (Tumialan, 2001).

4.3. Durability of Putty and Its Characterization With and Without Fillers

4.3.1. Background

FRP laminates are bonded on concrete and masonry surfaces for strengthening purposes. A typical installation procedure for manual lay-up includes the following phases: surface cleaning (e.g., sand blasting), primer application, putty application, first layer of saturant, fiber application and second layer of saturant (see section 3). The putty applied by trowel is used to prepare the surface filling any defect before applying the FRP laminate. It can also be used for leveling and patching small holes. So, putty may have a primary influence on bond behavior between FRP and surfaces. In particular, the thickness and the mechanical properties of the putty might influence the bond behavior. For this purpose, tensile tests were conducted on one type of putty currently used with one of the commercially available FRP strengthening systems. Specimens were fabricated with glass beads and sand as fillers. The function of the filler is to change the workability of the putty and to allow the installer to control its thickness when single-size particles are used. Virgin and pre-conditioned tensile specimens were tested for a preliminary investigation on durability. In addition, gravimetric measurements were conducted to determine a correlation between tensile properties changes and sorption for conditioned samples.

4.3.2. Test Specimens

In order to control the thickness of the putty on the masonry surface, glass beads with diameters of 0.8, 1, 1.25, 1.75, 2.25 mm (0.0315, 0.0394, 0.0492, 0.0689, 0.0886 in) were included in the mixture. To determine the best workability, percentages in weight of 1, 2, 3, 4, 5, 8, and 10 of beads were considered and tensile tests were conducted to measure the losses of mechanical properties, compared to the putty

without fillers. The dimensions of the specimens were 6.35 mm ($\frac{1}{4}$ in) deep by 12.7 mm ($\frac{1}{2}$ in) wide by 76.2 mm (3 in) long. Figure 4.45 shows a typical specimen.

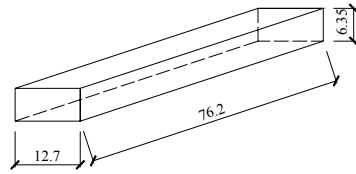


Fig. 4.45. Specimen configuration

Specimens with sand were also prepared because various amounts of sand (from 10% to 20% in weight) are used in the field to increase the viscosity of the putty. So, a loss of mechanical and bond properties could be expected.

The beads used were E-glass, with the properties as provided by the manufacturer illustrates in table 4.25.

Tab. 4.25. Mechanical properties for the beads

Vickers hardness [MPa]	Abrasion index [%]	Compressive strength [MPa]
6600	1	390



(a)



(b)

Fig. 4.46. Packing and beads with different diameters

The sand used was siliceous sand passing through sieve number 40 (0.425 mm).

Table 4.26 Illustrates the mechanical properties of the putty obtained from the manufacturer.

Tab. 4.26. Mechanical properties for the putty

Material	Tensile strength [MPa]	Elastic modulus [MPa]	Tensile strain [%]	Compressive strength [MPa]	Compressive modulus [MPa]
Putty	12.41	1792	1.5	24.13	1068

Note: 1MPa = 145 psi

To calculate the percentage in weight for the beads and the sand, a precision scale (± 0.1 g) was used. Also five specimens were prepared with no filler. For the preparation of the specimens a wooden gang mold with 42 openings was built. Each opening was about 76 by 76 mm (3 by 3 in). A trowel was used to level the surface and to make it smooth.

Figure 4.47 shows the preparation of the specimens.



Fig. 4.47. Preparation of the specimens

After curing each specimen was cut into five strips using a saw. Figure 4.48 illustrates the frame and several specimens ready to be tested.

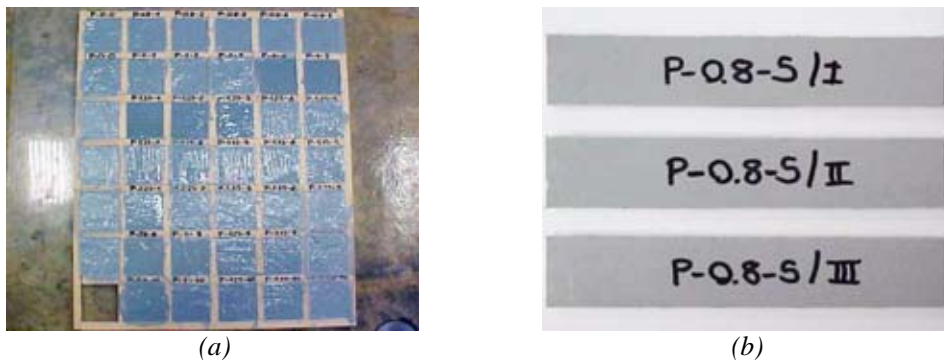


Fig. 4.48. Specimens ready

Five samples for each kind of combination were prepared. Three samples were used to perform a tensile test without chemical conditioning and two of them were used to conduct a durability test (section 4.3.3). Specimens were tested using a Universal Testing Machine INSTRON 4469 under displacement control. The rate of loading crosshead motion was 2.6 mm/min (0.1 in/min) according to ASTM 638-00. The data were recorded automatically by a SATEC TCS 1200 data acquisition system.

Figure 4.49 illustrates a picture of the tensile testing apparatus.



Fig. 4.49. Test apparatus

An electronic extensometer with 25.4 mm (1 in) gauge length and 1/10000 accuracy was clamped at mid-length of the test region to measure strain. Figure 4.50 shows a generic specimen with the extensometer.



Fig. 4.50. Tensile test configuration

Temperature and humidity were taken into account for each test. The testing machine had a passive grip interfaces. Generally this type of grip has the load applied by the test machine to the test specimen through a direct mechanical link. In this case the link was manual. The self-aligning grip was attached to the movable member of the testing machine in such a manner that it could move freely into alignment as soon as any load was applied. The specimens had to be aligned as perfectly as possible with the direction of pull, so that no rotary motion, that might induce slippage, occurred in the grips. Almost all specimens failed at mid-length. The rupture of the specimens had to occur in the uniformly stressed gage length. Tests where rupture occurred outside the gage length were reject and interpreted as failed tests due to stress concentration close to the gripping.

Figure 4.51 Illustrates several specimens after failure.



Fig. 4.51. Failure of the specimens

At the completion of every test, the grips were controlled to evaluate possible slipping. No slip was encountered for all the specimens tested.

In two cases, failure was due to voids inside the specimens, due to poor consolidation. Those specimens were rejected. Figure 4.52 illustrates the specimens after their removal from the testing machine.

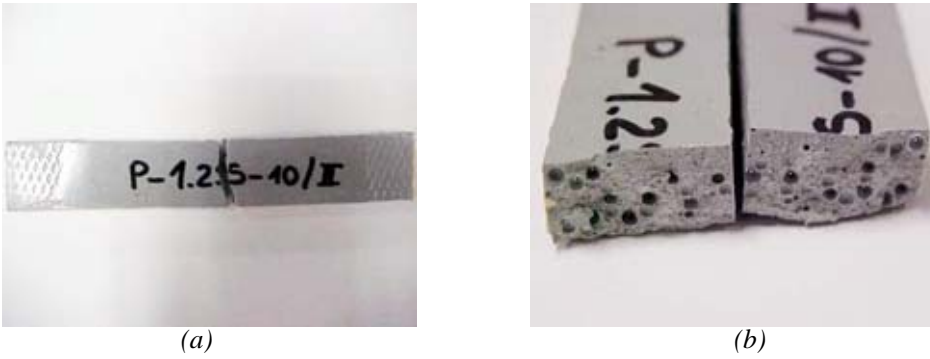


Fig. 4.52. Specimen after the test

Test results showed an elasto-plastic behavior for all the specimens. As an example, figure 4.53 shows a typical behavior for one specimen.

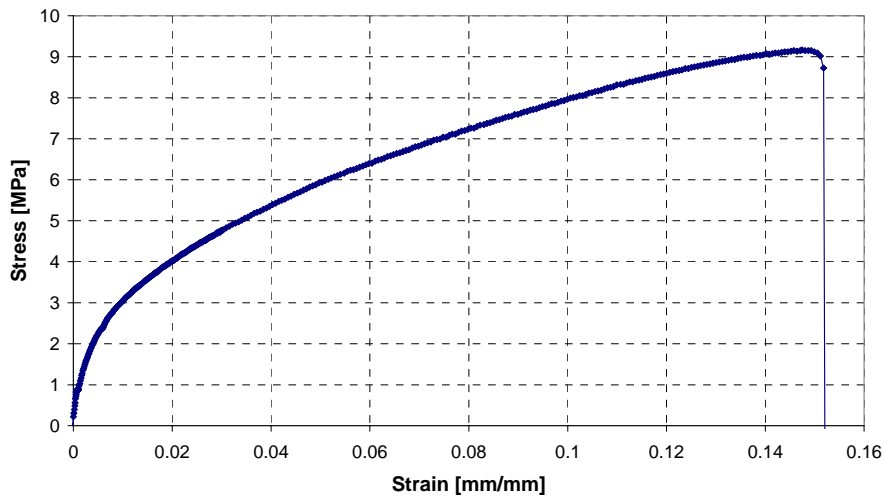


Fig. 4.53. Example of experimental behavior of the specimens

The modulus of elasticity was calculated following the ASTM E111-97 (Standard test Method for Young's Modulus, Tangent Modulus, and Chord Modulus) that uses a mathematical implementation. It allows to have an estimation of the precision of the Young's modulus value, based on the summation of the precision of the respective value.

The stress is defined as:

$$\sigma = \frac{P}{A}$$

Where:

P = Uniaxial tensile load [N]

A = Cross-section area [mm²]

The strain is defined as:

$$\varepsilon = \frac{(l - l_o)}{l_o}$$

Where:

l = Gage length at any time [mm]

l_o = Original gage length [mm]

All valid specimens, 123 in total, were analyzed with this method. The results are summarized in tables 4.27, 4.28, 4.29, where the average for each combination is presented.

Tab. 4.27. Young's Modulus values [MPa]

Beads %								
Beads diameters	0	1	2	3	4	5	8	10
0.8 mm	1319	1352	1250	1191	1214	1203	1312	1309
1 mm		1237	1376	1251	1167	1256	1413	1299
1.25 mm		1078	1134	1053	1249	1218	1437	1286
1.75 mm		1275	1200	1352	1256	1180	1375	1228
2.25 mm		1239	1350	1373	1433	1050	1233	1070

Note: 1 MPa = 145 psi; 1 mm = 0.03937 in

Tab. 4.28. Stress values [MPa]

Beads %								
Beads diameters	0	1	2	3	4	5	8	10
0.8 mm	10.398	9.595	9.485	9.368	9.407	9.464	9.835	9.896
1 mm		10.650	9.817	9.675	8.295	7.960	9.585	9.272
1.25 mm		9.037	8.610	8.041	9.441	9.284	9.369	9.551
1.75 mm		9.004	9.626	9.160	9.473	9.429	9.467	9.378
2.25 mm		10.070	8.188	8.079	8.422	7.608	6.999	7.485

Note: 1 MPa = 145 psi; 1 mm = 0.03937 in

Tab. 4.29. Strain values [mm/mm]

Beads %		0	1	2	3	4	5	8	10
Beads diameters									
0.8 mm	0.190		0.202	0.199	0.200	0.194	0.189	0.138	0.143
1 mm			0.174	0.178	0.180	0.223	0.221	0.162	0.153
1.25 mm			0.225	0.232	0.232	0.182	0.149	0.147	0.116
1.75 mm			0.177	0.172	0.173	0.165	0.149	0.175	0.172
2.25 mm			0.196	0.145	0.136	0.136	0.121	0.107	0.135

Note: 1 MPa = 145 psi; 1 mm = 0.03937 in

With regard to accuracy, the coefficients of variation have ranges of 14-23%, 5-7%, and 12-18% for the Young's Modulus, strength, and strain, respectively. Figure 4.54, 4.55 and 4.56 illustrate the graphs of the mechanical properties for all the specimens tested, with and without glass bead filler.

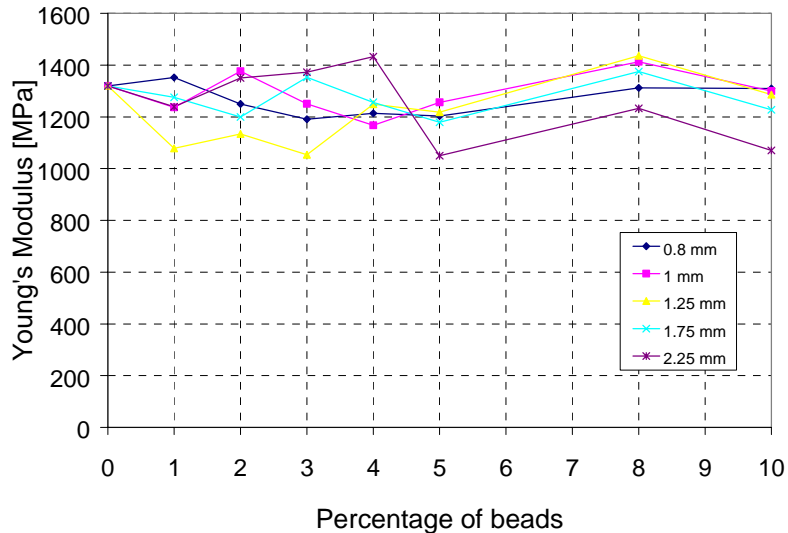


Fig. 4.54. Young's Modulus as a function of beads percentage

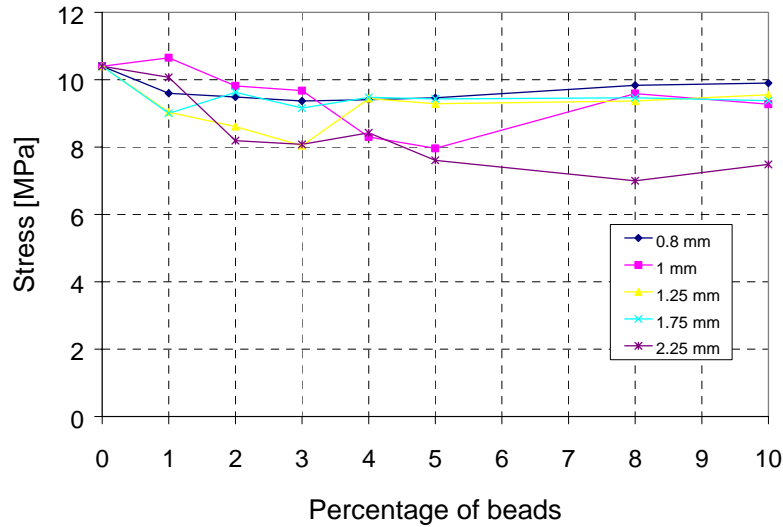


Fig. 4.55. Strength as a function of beads percentage

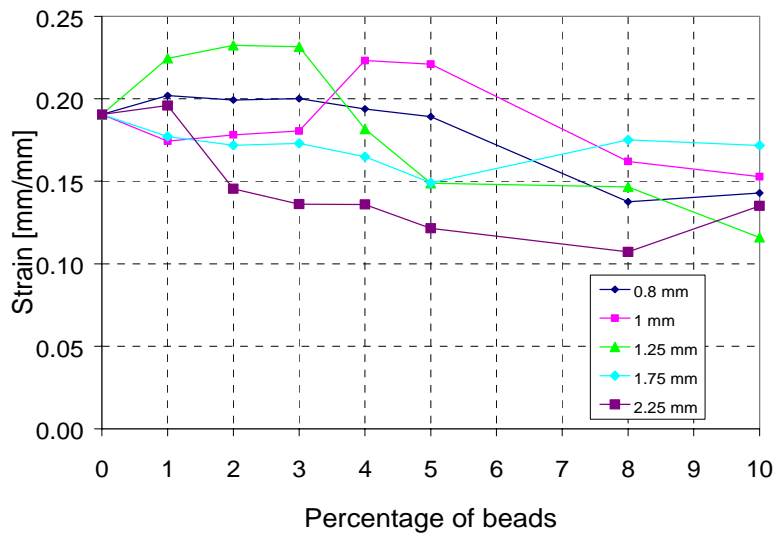


Fig. 4.56. Strain as a function of beads percentage

The experimental values show that there is not a significant decreasing trend in mechanical properties for specimens with increasing percentages of glass beads. An exception can be seen for the specimens with beads of 2.25 mm in diameter. For these

kinds of specimens a loss of mechanical properties bigger than in the other specimens is noted. It is reasonable to think that the loss was due to the dimensions of the beads. The data of the specimens with different percentages of sand are summarized in table 4.30.

Tab. 4.30. Values for the specimens with the sand

	0%	5%	10%	15%	20%
Young's Modulus [MPa]	1319	1226	1248	1227	1096
Stress [MPa]	10.40	8.88	8.71	8.94	8.52
Strain [mm/mm]	0.190	0.163	0.126	0.118	0.126

Note: 1 MPa = 145 psi; 1 mm = 0.03937 in

Figure 4.57 illustrates the graphs of the normalized mechanical properties for all the specimens with and without sand.

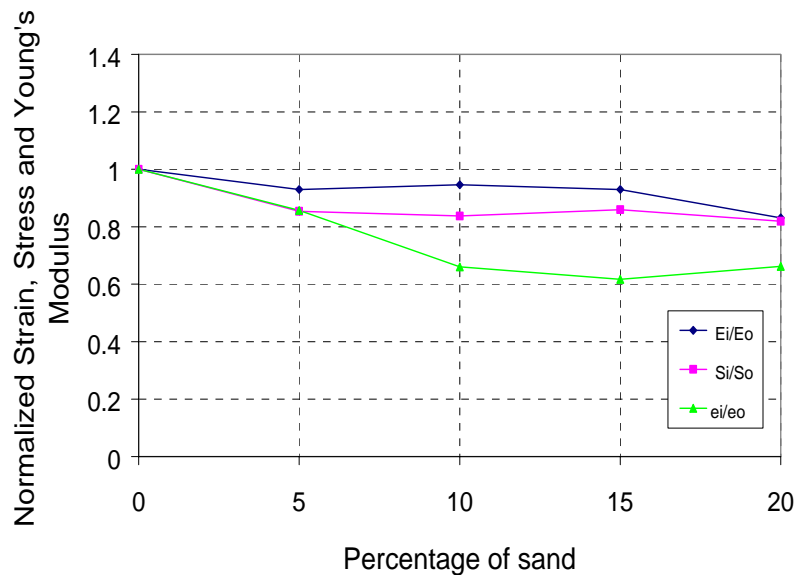


Fig. 4.57. Young's Modulus, strength and strain as a function of sand percentage

A slight decrease of tensile mechanical properties can be seen comparing the specimen with and without sand. For example, the loss of mechanical properties for the data obtained from specimens with 20% of sand, is shown in the following table.

Tab. 4.31. Losses of mechanical properties

	Virgin Specimen	20% Sand	Loss (%)
Young's Modulus [MPa]	1319	1096	17
Stress [MPa]	10.40	8.52	18
Strain [mm/mm]	0.190	0.126	34

4.3.3. Durability

Beyond the cost issues, the most significant technical obstacle preventing the extended use of FRP materials in construction is a lack of long-term and durability performance data comparable to the data available for traditional construction materials.

In general durability of a structure or a material can be defined as the ability to resist cracking, oxidation, chemical degradation, delamination, wear, and/or the effects of foreign object damage for a specific period of time, under the specified load and environmental conditions.

The effect of moisture or alkaline solutions sorption in the materials varies and may produce in general, a loss in strength and stiffness (Micelli et al., 2001). The study of the alkaline attack has particular importance in construction applications. Usually putty is necessary when the laminates are used. So, its durability may have an influence on bond behavior between FRP laminates and surface.

The alkaline solutions in general produce an embrittlement of the materials and a damage at the fiber resin interface level by chemical attack and growth of hydration products. These effects lead to a loss in tensile strength and interlaminar properties (Devalapura, 1997; Franke et al., 1987). Previous studies (Litherland et al., 1981; Vijay et al., 1999; Ganga Rao et al., 1997) showed how temperature influences the sorption and diffusive properties of alkaline solutions in FRP composites, comparing natural aging and accelerated test results. Therefore, it may be possible to conduct accelerated tests in which the long-term behavior can be simulated with satisfactory

accuracy. The following equation is used to relate the temperature and time used for conditioning to real conditions:

$$\frac{N}{C} = 0.098 \cdot e^{0.0558(T+32)\frac{9}{5}} \quad (4.15)$$

Where:

N = age in natural days

T = conditioning temperature in °C

C = days of accelerated exposure at temperature T

The diagram in figure 4.58 represents the relationship.

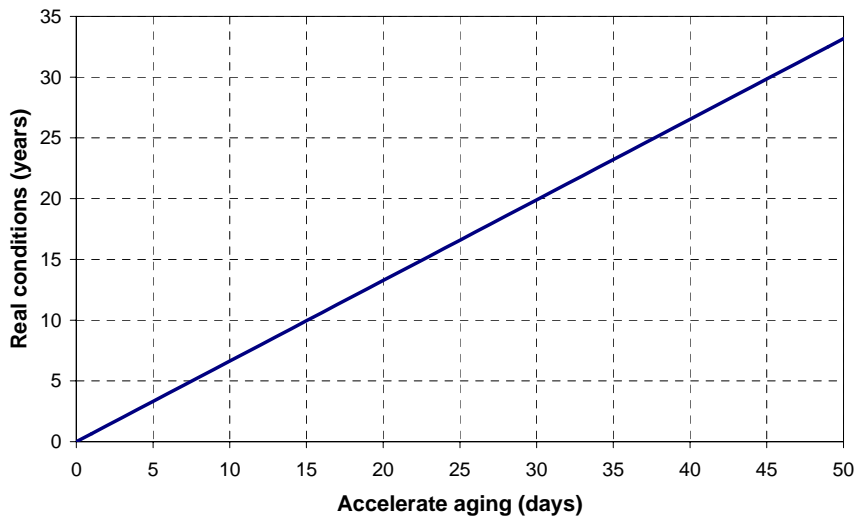


Fig. 4.58. Accelerated aging in alkaline solutions for $T = 60\text{ }^{\circ}\text{C}$ ($140\text{ }^{\circ}\text{F}$)

Infrastructure systems are exposed to external agents during their life cycle, so the mechanical behavior under natural weathering needs to be understood.

Alkaline Solution Exposure

An attempt has been made in this study to reproduce the alkaline pore water in or from the concrete, rather than a solution with high pH.

The solution used was the following:

$$0.012\% \text{Ca(OH)}_2 + 0.073\% \text{Na(OH)} + 0.103\% \text{K(OH)} \quad (4.16)$$

Where:

Ca(OH)_2 = calcium hydroxide

Na(OH) = sodium hydroxide

K(OH) = potassium hydroxide

The selected amounts represent the percentages in weight that were solved in distilled water. The pH measurements showed that a pH = 12.6 was the constant value, before and after the conditioning.

To replicate the exposure of putty to an alkaline environment, 84 specimens were immersed in the alkaline solution with pH 12.6 at temperature of 60 °C (140 °F). Specimens were tested in direct tension after 21 and 42 days of exposure, which correspond to real times of 14 and 28 years respectively.

Young's modulus, strength and strain behavior were measured and compared with the properties of the control specimens. Problems occurred during the tests of the specimens at 42 days and the data can not be utilized.

Test results of the specimens after 21 days

The 42 specimens were analyzed with the same method used for the unconditioned specimens. The results are summarized in tables 4.32, 4.33 and 4.34 where the average for each diameter and percentage of beads is represented.

Tab. 4.32. Young's Modulus values [MPa]

Beads %								
Beads diameters	0	1	2	3	4	5	8	10
0.8 mm	687	561	552	581	587	547	687	581
1 mm		676	685	631	594	587	576	606
1.25 mm		569	596	554	698	658	616	685
1.75 mm		629	608	692	564	552	495	522
2.25 mm		656	658	641	621	601	565	502

Note: 1 MPa = 145 psi; 1 mm = 0.03937 in

Tab. 4.33. Stress values [MPa]

Beads %								
Beads diameters	0	1	2	3	4	5	8	10
0.8 mm	4.497	4.742	4.492	4.663	4.655	4.337	4.113	4.058
1 mm		4.960	4.775	4.764	3.822	4.224	4.150	4.384
1.25 mm		3.731	3.835	4.150	4.303	4.442	4.415	3.571
1.75 mm		4.122	3.644	3.463	3.879	3.489	3.378	3.252
2.25 mm		3.307	3.152	2.901	3.408	3.066	3.313	2.672

Note: 1 MPa = 145 psi; 1 mm = 0.03937 in

Tab. 4.34. Strain values [mm/mm]

Beads %								
Beads diameters	0	1	2	3	4	5	8	10
0.8 mm	0.098	0.122	0.117	0.123	0.106	0.116	0.087	0.075
1 mm		0.121	0.121	0.118	0.123	0.140	0.103	0.112
1.25 mm		0.128	0.132	0.127	0.102	0.098	0.103	0.095
1.75 mm		0.106	0.092	0.090	0.105	0.107	0.124	0.118
2.25 mm		0.121	0.101	0.069	0.092	0.082	0.089	0.086

Note: 1 MPa = 145 psi; 1 mm = 0.03937 in

Figure 4.59, 4.60 and 4.61 illustrate the graphs of the mechanical properties for all the specimens compared with those specimens without filler at same days of cure in the alkaline bath.

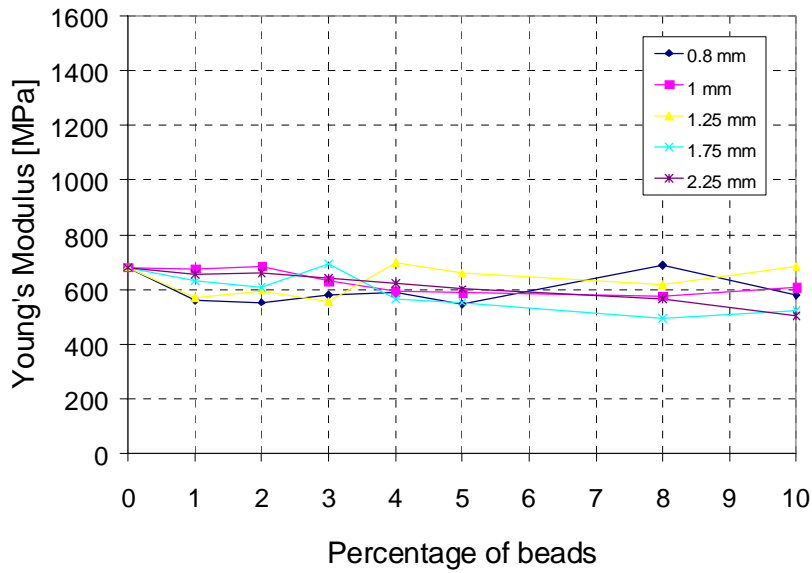


Fig. 4.59. Young's Modulus for specimens with and without beads

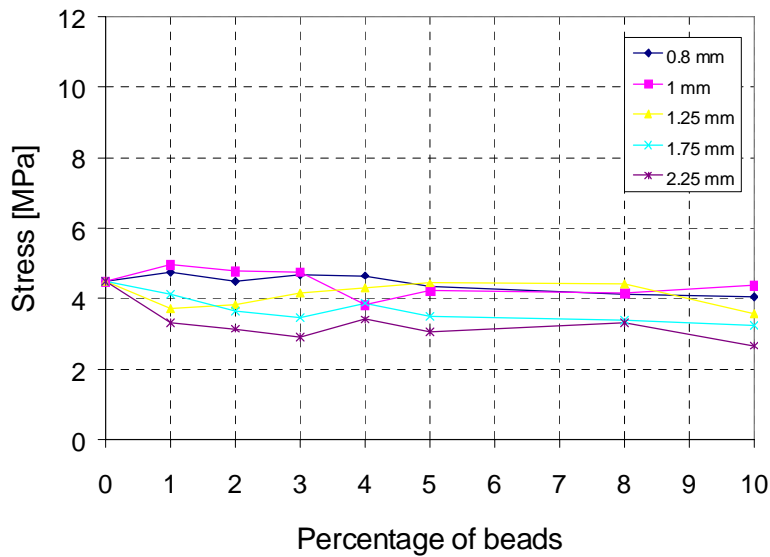


Fig. 4.60. Stresses for specimens with and without beads

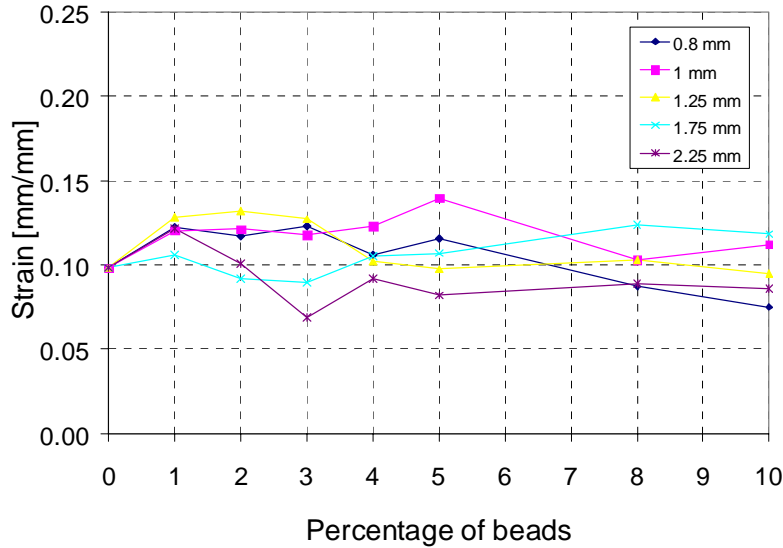


Fig. 4.61. Strains for specimens with and without beads

Specimens containing glass beads and left for 21 days in the alkaline solution experienced a significant loss in mechanical properties in comparison with specimens without filler. Behavior similar to that obtained from the unconditioned specimens can be observed in the specimen with different percentages of glass beads. An exception was observed for the specimens with beads of 2.25 mm where their relatively large diameter causes a relevant decrease of mechanical properties.

As an example the percentile difference between the values of the specimens without filler at 0 days and 21 days is summarized in table 4.35.

Tab. 4.35. Losses of mechanical properties between the results at 21 and 0 days

	Variation
Young's Modulus [MPa]	48 %
Stress [MPa]	57 %
Strain [mm/mm]	48 %

These values could be also assumed for the other specimens, seeing that the mechanical properties obtained from the tests are almost equal.

From the experiments an embrittlement of the material was also observed.

Figure 4.62 shows a different behavior as for the specimens at 0 days (figure 4.52) and can be noted that the specimen showed a stretching along the free gage length but not a clearly failure of the cross section like the specimens at 0 days (see also figure 4.52)

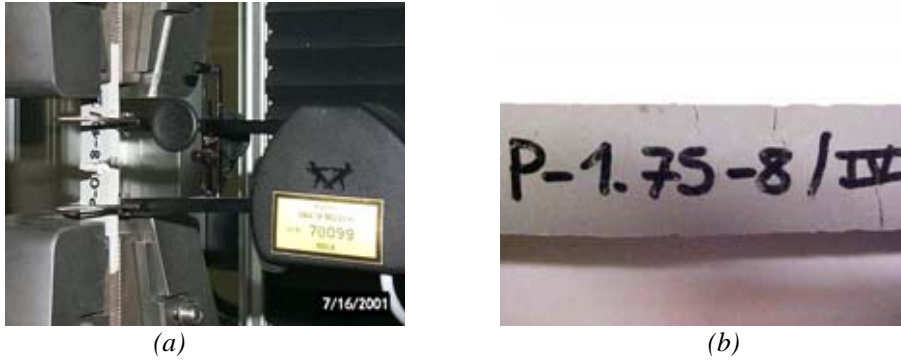


Fig. 4.62. Failure of the specimens

As an example, figure 4.63 shows the experimental behavior of a specimen at 0 and 21 days of exposure.

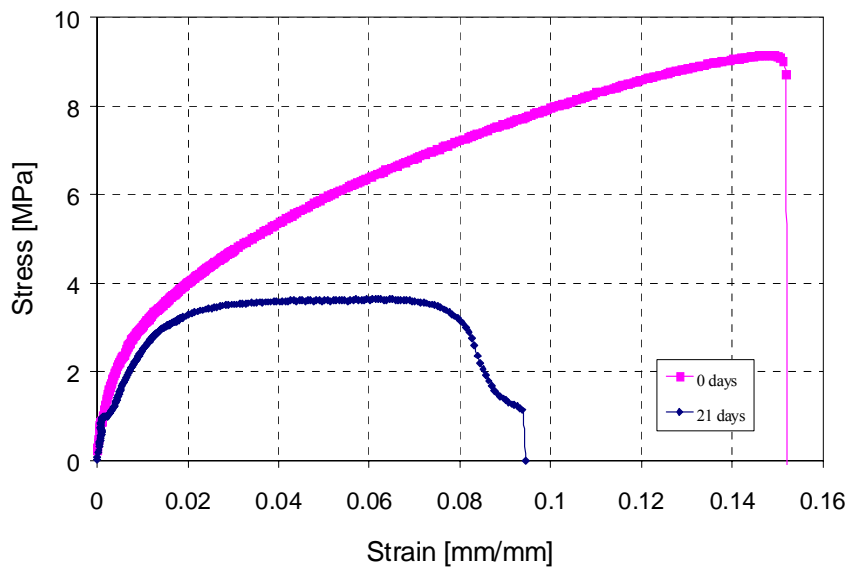


Fig. 4.63. Example of experimental behavior of a specimen at 0 and 21 days

Data for specimens with different percentage of sand are summarized in table 4.36.

Tab. 4.36. Values for the specimens with the sand

	0%	5%	10%	15%	20%
Young's Modulus [MPa]	680.6	687.0	677.4	760.8	876.8
Stress [MPa]	4.497	3.786	3.584	3.631	3.433
Strain [mm/mm]	0.098	0.113	0.078	0.073	0.081

Note: 1 MPa = 145 psi; 1 mm = 0.03937 in

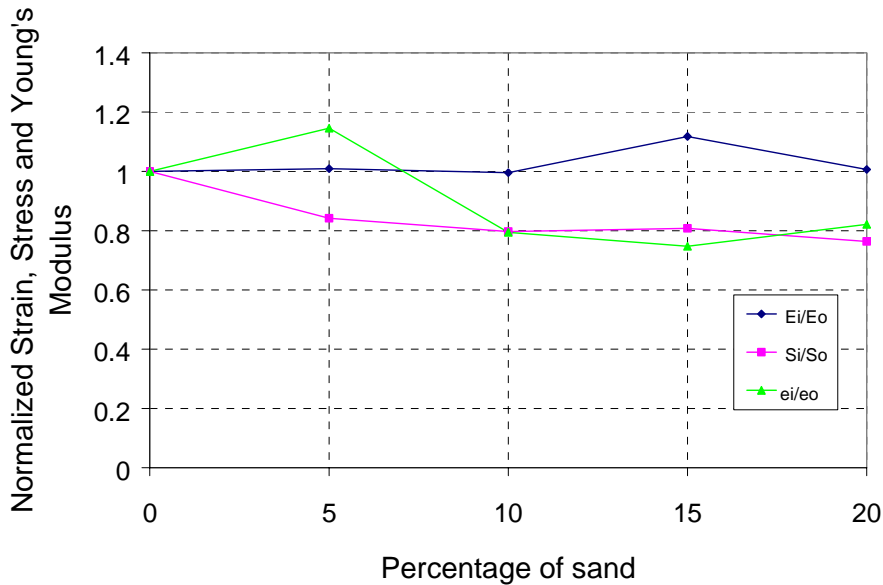


Fig. 4.64. Mechanical properties for specimens with and without sand

A decrease in mechanical properties can be also seen for the specimens with sand comparing unconditioned specimens and those exposed for 21 days. To have an order of magnitude of the losses of mechanical properties, in the table 4.37 the data

obtained from the specimens were compared with those obtained from unconditioned specimens.

Tab. 4.37. Losses of mechanical properties

	Virgin Specimen
Young's Modulus [MPa]	41 %
Stress [MPa]	57 %
Strain [mm/mm]	36 %

The experimental data show that after the conditioning not substantial difference of mechanical properties between the 0% sand specimen and the specimen with the sand were encountered. This could mean that the long term behavior is governed by the putty itself.

Problems occurred during the tests of the specimens at 42 days and the data can not be utilized, however the results of these tests are sufficient to say that there would be some durability problems and a thorough investigation utilizing more than one material is necessary since the putty occupy an important place on the bond behavior between FRP and surfaces.

Gravimetric Measurements

Putty specimens were also used for gravimetric measurements; 84 specimens were immersed in the alkaline solution at temperature of $T = 60\text{ }^{\circ}\text{C}$ ($140\text{ }^{\circ}\text{F}$) for 21 and 42 days and weighted every seven days. The weight change investigation presents important information. In fact, absorption properties such as diffusivity of the putty can be easily computed once the weight increase is known. The fluid content was measured as follows:

$$M_t(\%) = \frac{W - W_d}{W_d} \cdot 100 \quad (4.17)$$

Where:

$M_t(\%)$ = percentage of fluid content at time t

W_d = weight of the dry specimen at time $t = 0$

W = weight of the moist specimen at time t

If the absorption is linear, as usually happens in the first part of the exposure, the diffusivity δ can be computed using the following equation with reference to figure 4.65, in which the typical absorption of FRP composites is shown:

$$\delta = \frac{\pi \cdot R^2}{16} \left(\frac{M_2 - M_1}{M_m} \right)^2 \cdot \left(\frac{1}{\sqrt{t_2} - \sqrt{t_1}} \right)^2 \quad (4.18)$$

Where:

δ = diffusivity [mm²/min] (in²/min)

R = radius of the rod [mm] (in)

M₁ = percentage of fluid content at time t₁

M₂ = percentage of fluid content at time t₂

M_m = percentage of fluid content at the end of the linear behavior

t₁ = starting time of observation (min)

t₂ = end time of observation (min)

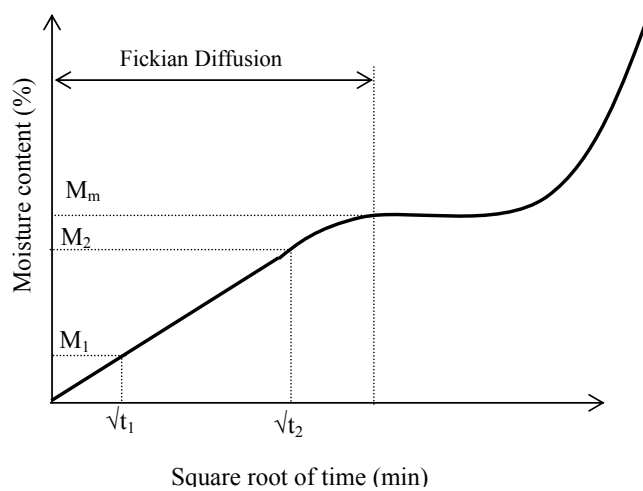


Fig. 4.65. Typical absorption behavior of FRP composites

Since the specimen cross section is rectangular, an equivalent radius was used imposing an equal perimeter length between the specimen and the “equivalent cylinder”.

In correspondence of M_m , the slope of the curve changes dramatically because a particular phenomena occurs: the fluid penetration after a time t_m causes a macroscopic mechanical degradation of the system. This means that cracks open and allow a fast fluid penetration that is represented by the second curve with increased slope. Therefore, after the fickian diffusion region the absorption behavior is controlled by the fluid penetration in the open cracks developed from the surface to the inner part of the sample. The behavior of the putty has been different. In particular, test results showed that after the first fast penetration of the fluid occurred in the first 14 days with an increase of the weight, the slope of the curve changed dramatically in opposite direction finishing after 42 days close to the starting weight or, in many cases, to a lower one. This means that the fluid penetration causes a macroscopic mechanical degradation of putty and beads with a dispersion of material in the solution. Some beads used to make the specimens were also weighted at $t = 0$ days and at $t = 42$ days; the result was that in a sample of about 4 g. the percentage of glass lost was 2.19% in weight. Thereby is also presumable that after the 42 days of the test, the weight could still be descendent, because of the increment of degradation of putty and beads.

In figure 4.66 an example of the behavior observed in the tests is shown.

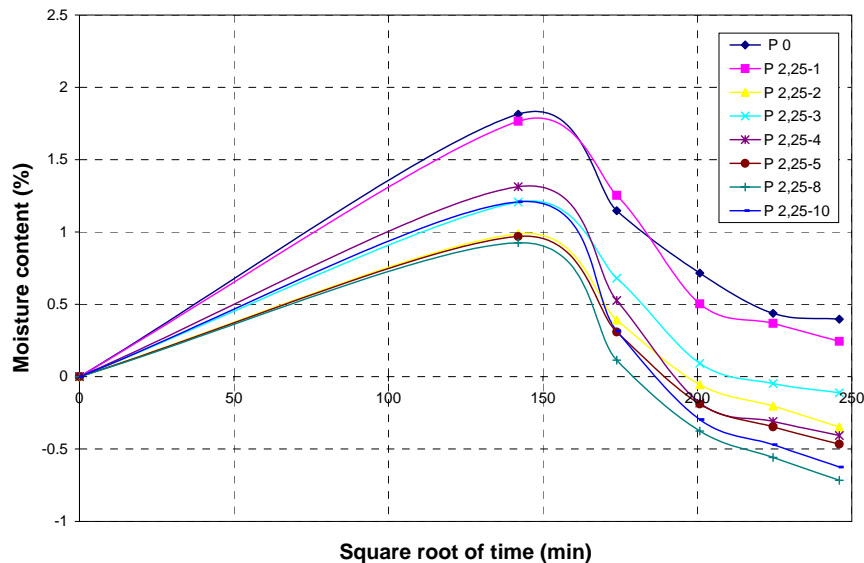


Fig. 4.66. Example of typical absorption behavior of putty with beads

From the graphs, it is possible to see that the specimens with higher percent of beads lost more weight than the others. It is also possible to see that the weight loss for the specimens without beads was lower than the one of all the other specimens. In general, this behavior is common to all the other tests apart from some cases, probably caused by the imperfection of the specimens that can determine an infiltration of more solution.

The figure 4.67 shows the state of moisture for the specimens with various percentage of sand.

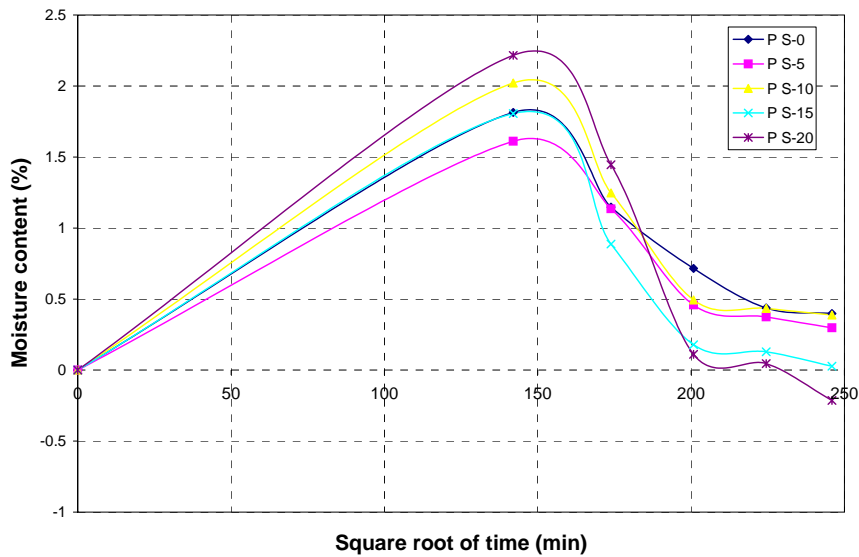


Fig. 4.67. Typical absorption behavior of putty with sand

4.3.4. Conclusions

Experimental values from this research show that there is not a significant decreasing trend for each kind of unconditioned specimens with different percentages of glass beads. This means that the beads do not significantly affect the tensile mechanical properties. A trend can be seen for the specimens with beads of 2.25 mm (0.0886 in) in diameter. For these specimens, a loss of mechanical properties greater than in the other specimens was noted. For the specimens with sand as filler, a slight decrease of

tensile mechanical properties could be seen as a function of sand content. For the pre-conditioned specimens left for 21 days in the alkaline solution, a significant loss of mechanical properties and an embrittlement of the material were noted as compared to a specimen without fillers. From the experimental values, it can be observed that the specimens with beads have a behavior similar to the one obtained from the unconditioned specimens, which means that there is not significant influence of the beads. Beads of 2.25 mm (0.0886 in) diameter may be a threshold size as they caused a relevant decrease of mechanical properties. A decrease of mechanical properties due to alkaline exposure can also be seen for the specimens with sand. From the experimental data recorded at 21 days, there was no effect due to sand content and this could mean that the long term behavior is governed by the putty itself. The results of these tests are a warning with respect to durability. An in-depth investigation of this and other types of putty may be warranted. The gravimetric test results showed that after the initial rapid sorption of the fluid that occurred in the first 14 days with an increase of weight, the slope of the curve (\sqrt{t} vs. moisture) changed dramatically in the opposite direction, finishing after 42 days close to or lower than the starting weight. This may mean that the fluid penetration causes a macroscopic mechanical degradation of putty and glass beads with a dispersion of material in the solution. From the graphs it is possible to see that the specimens with higher percent of beads lost more weight than the ones without fillers.

4.4. Bond Test Controlling the Thickness of Putty

Putty may have a primary influence on bond behavior between FRP and surfaces; the scope of this investigation is verifying it. Glass beads with different diameters were included into the mixture to control the thickness of the putty on the masonry surface. In particular, after the previous results, the glass beads with diameter 2.25 mm (0.0886 in) were discarded because of consistent loss of mechanical properties of the material founded. Because of this, the beads with diameter 0.8 mm (0.0315 in) were chosen, and to have a significant difference between the thickness of putty applied on the surface of the specimens, the beads with diameter 1.75 mm (0.0689 in) were also used in the tests.

4.4.1. Test Specimens

Standard hollow clay bricks and AFRP sheets were used to investigate the bond behavior in order to understand it as function of the thickness of putty. Nine specimens were built, three control specimens without beads inside the putty and the others specimens with beads diameters 0.8 and 1.75 mm (0.0315, 0.0689 in). A percentile of beads of 5% in weight was chosen because it was the best compromise between work-ability of the mixture and the creation a unique layer without imperfections like holes or hollows.

Table 4.38 illustrates the configuration of the specimens.

Tab. 4.38. Thickness of the putty for each specimen

Specimens	Thickness of the putty [mm]
P-0-1	0
P-0-2	0
P-0-3	0
P-0.8-1	0.8
P-0.8-2	0.8
P-0.8-3	0.8
P-1.75-1	1.75
P-1.75-2	1.75
P-1.75-3	1.75

Note: 1 mm = 0.03937 in

The AFRP sheets used were AK60 Master Builders technologies with the following properties from the material characterization (see also section 4.1.6):

Tab. 4.39. Properties of AK60 Master builders technologies sheet

Rupture [MPa]	1880
Tensile Elastic Modulus [GPa]	121
Tensile strain [%]	1.63
Thickness [mm]	0.28*

Note: 1 MPa = 145 psi; 1 mm = 0.03937 in; * = value from manufacturer

The preparation of the specimens is represented in figure 4.68 where are shown all the specimens (a) and a particular sight of the specimen P-0.8-1 (b). All the phases of the preparation of the specimens are reported in appendix D.

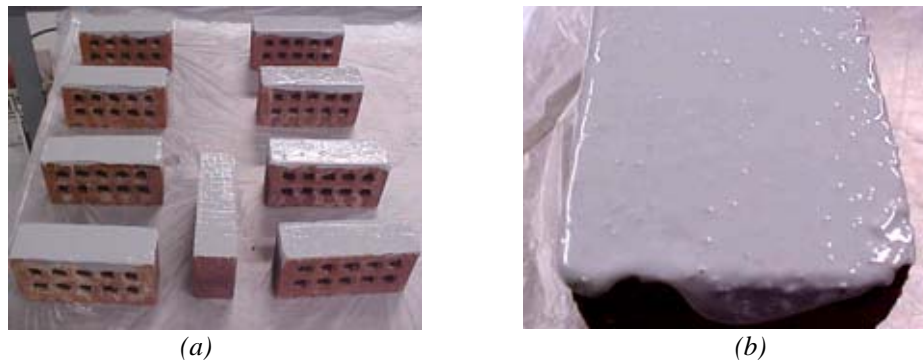


Fig. 4.68. Preparation of the specimens

In order to simplify the setup and to do fast tests, just two clay bricks were used for each test; figure 4.69 shows the configuration utilized.

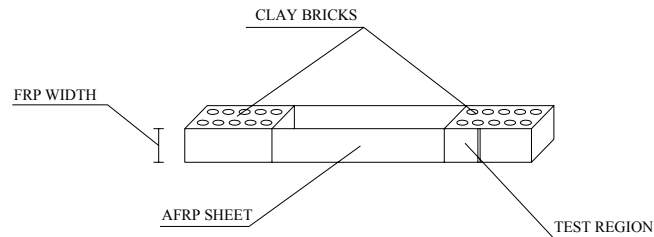


Fig. 4.69. Generic test configuration

One FRP sheet was applied to each face of the clay bricks in the longitudinal direction, connecting two clay bricks together. Only one clay brick was considered with a limited bonded length, called test region, of 50.8 mm (2 in); this was chosen to force the delamination only in that area. About a double bonded length, respect the test region, was chosen and made to avoid failure in others zones.

The specimens were prepared following the wet-lay-up technique (see section 3.1).

The specimens were left to cure for 4 days prior to testing.

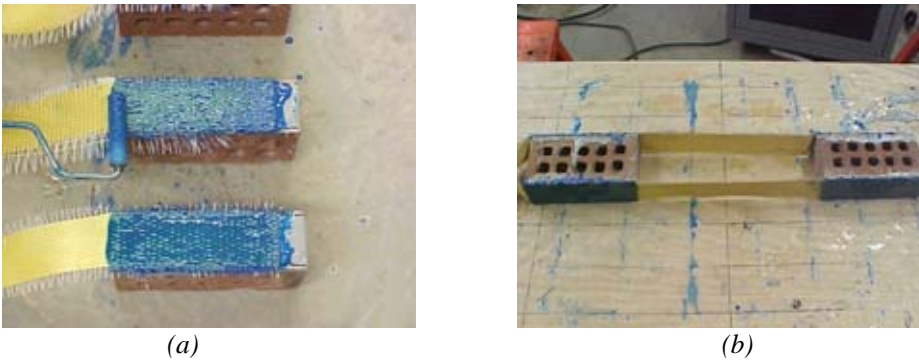


Fig. 4.70. Preparation of the specimens

4.4.2. Test Setup

The test bed consisted of a wood plate with four wood angles nailed on the plate to delimitate the position where the clay bricks had to be placed. The purpose of the plate was to ensure the proper positioning of the specimens during preparation and testing. Load was applied by means of a 12-ton hydraulic jack connected to a hydraulic pump. The jack was placed horizontally between the two blocks.

A Sensotek pressure transducer connected to the hydraulic jack recorded the load. Loads were all recorded with a one-Hertz sampling rate by a LABTECH data acquisition system. Figures 4.71 illustrate the test setup.

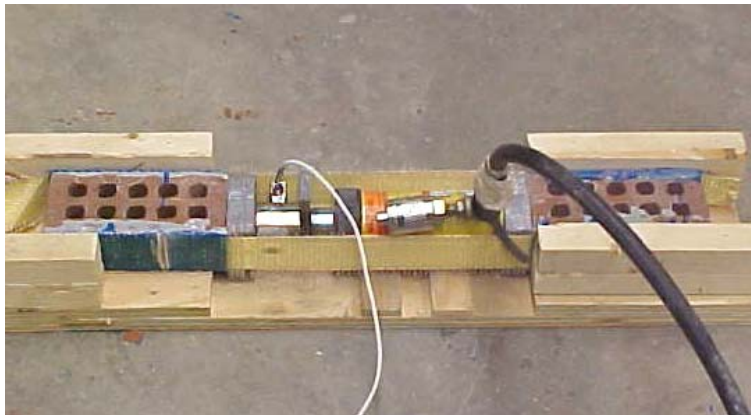


Fig. 4.71. Generic test configuration

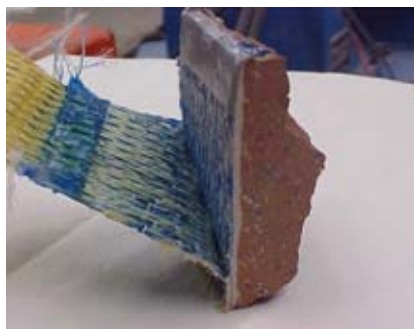
4.4.3. Test Results

All the results are summarized in the table 4.40.

Tab. 4.40. Values for the specimens

Specimens	Load [kN]	Load Average [kN]
P-0-1	13,5	11.8
P-0-2	n.d.	
P-0-3	10,1	
P-0.8-1	12,7	11.7
P-0.8-2	12,3	
P-0.8-3	13,5	
P-1.75-1	12,5	12.8
P-1.75-2	11,9	
P-1.75-3	14,1	

Two different types of delamination were observed; the first type in the specimens P-1.75-2, P-1.75-3, P-0.8-3 between the putty and the fiber and the second type for all the others specimens was between the putty and the brick with removal of a layer of brick. These phenomena are shown in figure 4.72.



(a)



(b)

Fig. 4.72. Different modes of failure

Anyway, issues were encountered in the test setup because of high tensile stresses in the brick due to the force transferred by means of FRP sheets. One of the specimens has been lost and there were also some problems with the others. In almost all the tests there was the rupture of the brick after the delamination.

Maybe the different mode of failure must be found in an imperfect setup.

In the figure 4.73 is shown the graph thickness of putty versus load.

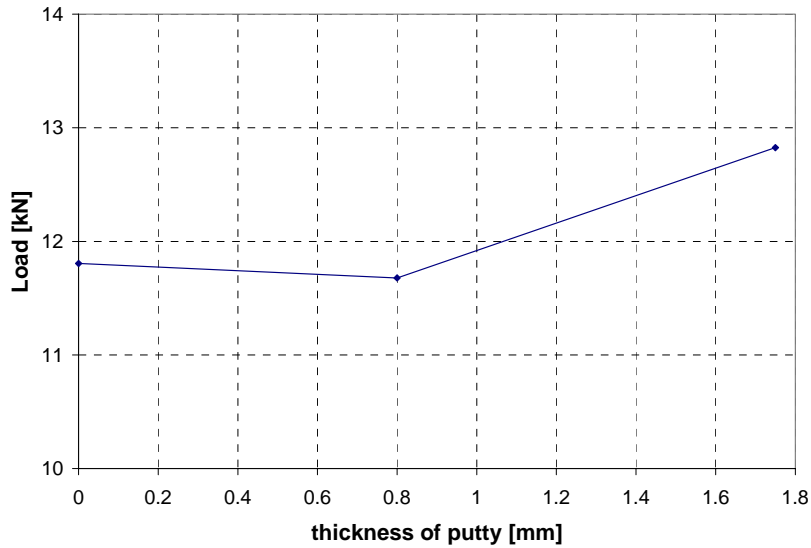


Fig. 4.73. Behavior of the load in function of the thickness of putty

4.4.4. Conclusions

Seeing the results, it can be observed a light increase of about 8% of the load between the specimens with the higher thickness of putty and the specimen without beads inside. However, setup issues and a limited number of tests do not allow to say whether the putty influences the bond behavior. Therefore, further investigations and a new setup are needed.

5. INFLUENCE OF ARCHING MECHANISM IN MASONRY WALLS STRENGTHENED WITH FRP LAMINATES

5.1. Previous Results

The previous results shown in this paragraph are researches on simply supported walls, meaning that boundary conditions such as presence of slabs or surrounded concrete frames are not taken into consideration; in other words, masonry walls with high slenderness ratio in which the arching effect (section 1.2) can be ignored.

Ehsani et al. (1996) investigated the flexural behavior of URM walls strengthened with GFRP sheets. Their dimensions were 0.22 m (8.5in) wide, 0.1 m (4in) high, and 1.48 m (57in) long. Two different kinds of mortars were used for their construction, type M with cement: lime sand ratios of 1:1/4:3 and a compressive strength of 32.04 MPa (4.65 ksi); and type M* with ratios of 1:1/4:5 and a compressive strength of 28.25 MPa (4.1 ksi). The specimens were subjected to four-point bending. The primary failure was a tension failure, which was observed when a low amount of strengthening was used. When the number of plies was increased, the masonry failed in compression. It was observed that the flexural capacity was increased up to 24 times compared to the control specimen. As observed in figure 5.1, the effect of the mortar strength appeared to be negligible, both specimens failed by crushing of the masonry.

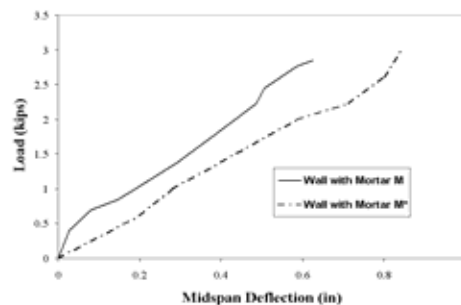


Fig. 5.1. Test results (Ehsani, 1996)

Hamilton et al. (1999) investigated the flexural behavior of URM walls strengthened with different composite materials. The walls were built with standard concrete blocks, with an overall dimension of 0.61 m (2 ft) by 1.83 m (6 ft). The use of high strength composite materials such as CFRP and AFRP led to undesirable modes of failure such as delamination and shear in the masonry. In order to use the material efficiently, two alternatives were recommended: the first one was to increase the spacing of the material until observing the rupture of the laminate and the second one was to use less expensive materials such as GFRP. Four modes of failure were identified: debonding, laminate rupture, shear, and face shell pull out. It was reported that debonding from the masonry substrate caused the failure of most of the test specimens (see figure 5.2).

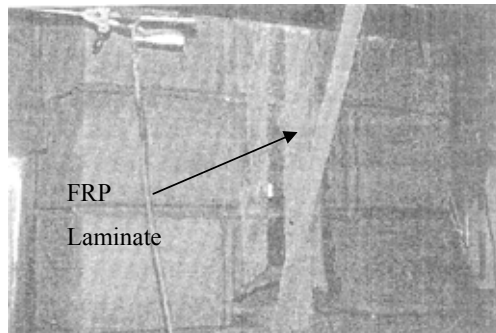


Fig. 5.2. Debonding of FRP laminate (Hamilton, 1999)

Velazquez et al. (2000) reported test results of half-scale URM walls tested under out-of-plane cyclic loading. The test specimens had a width of 1.22 m (48 in) and a height of 1.42 m (56 in), with a slenderness ratio of 28. Two of the walls were strengthened on both faces with GFRP strips. By understanding that the balanced condition represents the failure of masonry and rupture of composite laminate at the same time, one wall had the reinforcement equivalent to the balanced ratio (100% ρ_b). The other wall had three times the amount of reinforcement as compared to the first wall (300% ρ_b). The specimen reinforced with 100% ρ_b showed extensive delamination at failure. The first delaminated areas were observed on the central strip above the middle brick

course. The specimen with 300% ρ_b failed due to high in-plane shear stresses along the lower brick course. Substantial increases in strength and deformation capability were achieved. It was observed (see figure 5.3) that the retrofitted walls resisted pressures up to 24 times the weight of the wall and deflected as much as 5% of the wall height. To avoid very stiff behavior and improve the hysteretic response, it was recommended to limit the reinforcement ratio to two times the balanced condition.

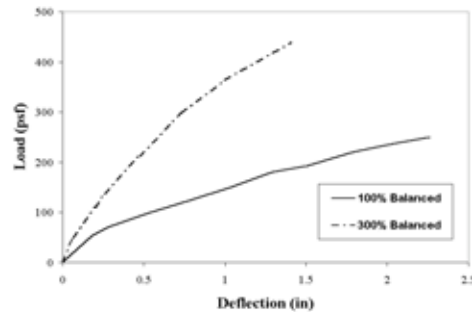


Fig. 5.3. Test results (Velazquez, 2000)

Albert et al (1999) tested ten full-scale masonry walls reinforced with externally applied FRP and subjected to primarily monotonically increasing lateral out-of-plane loads. One wall was loaded cyclically. Some walls were also concurrently subjected to moderate constant axial loads. All walls were 4 m (12 ft) high and 1.20 m (4 ft) wide, all tested in an upright position. Two out-of-plane concentrated loads were applied at two lines, 1.20 m (4 ft) from each reaction point. The parameters investigated were the type (carbon strap, carbon sheet and glass sheet), amount and layout of fiber reinforcement, axial load effects and cyclic behavior.

A full ancillary test series was performed. Masonry units showed a mean compressive strength of 19.90 MPa (2.88 ksi) and 15.90 MPa (2.30 ksi) respectively for the two series of walls investigated.

Each specimen was 20 courses high with #9 gauge joint reinforcement every third course. The walls were laid in running bond using factory mix Type S mortar.

Series 1 involved seven tests on the four walls and focused on varying the type of fiber reinforcement. Wall MU1 was first tested without fiber reinforcement, then tested again as a partially cracked wall reinforced with carbon straps, MCS2-1, and

finally as a fully cracked wall, MCS3-2. One was reinforced on one side with carbon sheet and tested until fully cracked, MCST4, then additional carbon sheet fiber reinforcement was placed on the opposite side and the wall was tested again in a cyclic manner, MCST7-4. One test in the series involved a wall reinforced with four carbon straps, MCS-6, and another was reinforced with two glass sheets, MGST5.

Overall results showed that the strength and ductility of the specimens were increased significantly when strengthened. The overall behavior of the specimens was similar.

The load-midspan deflection response for all the specimens was found to be divided into two phases. The first phase, nonlinear, represented the stiffness contribution of the masonry materials. The second phase was linear and represented the stiffness contribution from the fiber reinforcement.

The type and amount of reinforcement used affected the overall stiffness of a specimen. The layout of the fiber reinforcement had more of a direct effect on the local joint strain behavior than the overall behavior. The introduction of axial load increased the first phase stiffness and reduced the second phase stiffness. Series 2 involved six tests on the six walls and focused on varying the layout and amount of carbon fiber sheet. The fiber reinforcement was primarily oriented in the vertical direction to optimize the strength of the fibers. ICST12 was tested with the strips oriented diagonally. The purpose of this test was to determine the out-of-plane resistance of a wall reinforced primarily for in-plane loads. Axial load effects were also investigated in the series, ICST9 and ICST13.

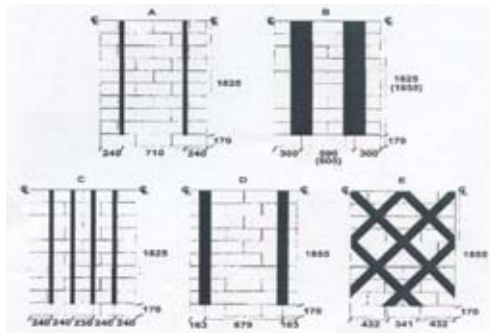


Fig. 5.4. Patterns and placement of FRP (Albert, 1999)

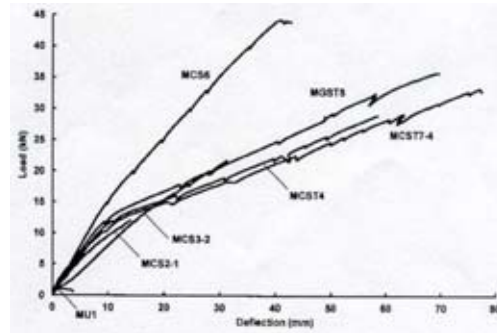


Fig. 5.5. Load-deflection response for series 1 (Albert, 1999)

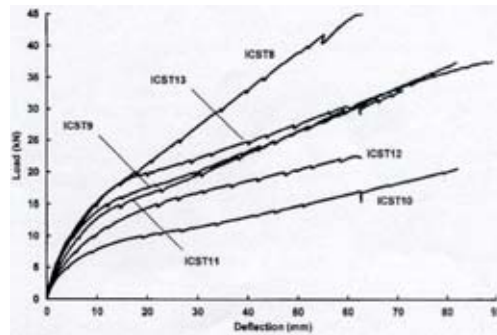


Fig. 5.6. Load-deflection response for series 2 (Albert, 1999)

Morbin A. et al. (2001) conducted work on simply supported walls at University of Missouri – Rolla just before the work shown in the next paragraphs.

Twenty unreinforced masonry walls were constructed for the experimental program: half of them were built with 0.102 by 0.203 by 0.305 m (4x8x12in) concrete blocks and half with 0.64 by 0.102 by 0.203m (2.5x4x8in) dark molded clay bricks in a running bond pattern, six and eighteen courses respectively. The specimens were 1.22 m (48 in) high, 0.61 m (24 in) wide and 0.102 m (4 in) thick. The mortar used was classified as Type N according to the standard ASTM C270.

The average compressive strength of the concrete masonry was 9.74 MPa (1414 psi) with a standard deviation of 1.04 MPa (151 psi), whereas the compressive strength of the clay masonry was 17.22 MPa (2500 psi) with a standard deviation of 0.35 MPa (50 psi). The reinforcement was applied just on one side of the walls. The fiber reinforcement strategy is shown in table 5.1 and 5.2; the amount of reinforcement was

chosen as a function of the balanced conditions ρ_b (It represents the failure of masonry and rupture of composite laminate at the same time. Further information is in section 5.2).

Tab. 5.1. Test matrix for series CO (concrete specimens) - Morbin, 2001

Specimen	Strengthening System	Reinforcing Scheme
COA3	AFRP laminates	One strip (w=3 in)
COG3	GFRP laminates	
COA5	AFRP laminates	One strip (w=5 in)
COG5	GFRP laminates	
COA7	AFRP laminates	One strip (w=7 in)
COG7	GFRP laminates	
COA9	AFRP laminates	One strip (w=9 in)
COG9	GFRP laminates	
COA12	AFRP laminates	One strip (w=12 in)
COG12	GFRP laminates	

Tab. 5.2. Test matrix for series CL (clay specimens) – Morbin, 2001

Specimen	Strengthening System	Reinforcing Scheme
CLA3	AFRP laminates	One strip (w=3 in)
CLG3	GFRP laminates	
CLA5	AFRP laminates	One strip (w=5 in)
CLG5	GFRP laminates	
CLA7	AFRP laminates	One strip (w=7 in)
CLG7	GFRP laminates	
CLA9	AFRP laminates	One strip (w=9 in)
CLG9	GFRP laminates	
CLA12	AFRP laminates	One strip (w=12 in)
CLG12	GFRP laminates	

Masonry specimens were tested under four point bending, following the ASTM standard E518. Each was tested as a simply supported beam, meaning that boundary conditions such as presence of corners or joint interferences were not taken into consideration. Figure 5.7 and 5.8 illustrates the test setup.

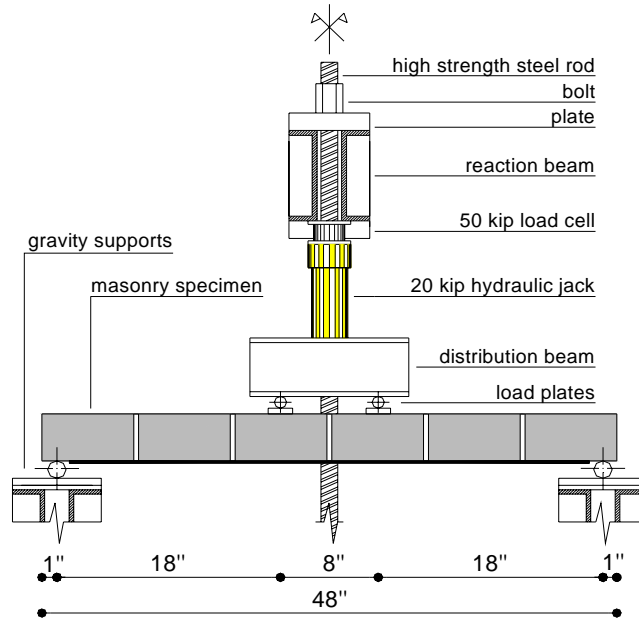


Fig. 5.7. Load scheme (Morbin, 2001)



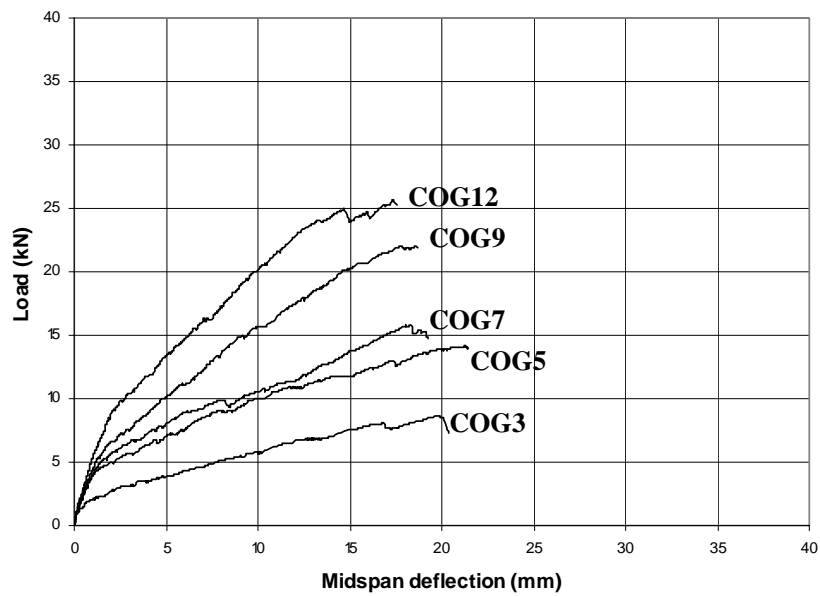
Fig. 5.8. Test set-up (Morbin, 2001)

The load was applied in cycles of loading and unloading. Table 5.3 illustrates a summary of the load cycles.

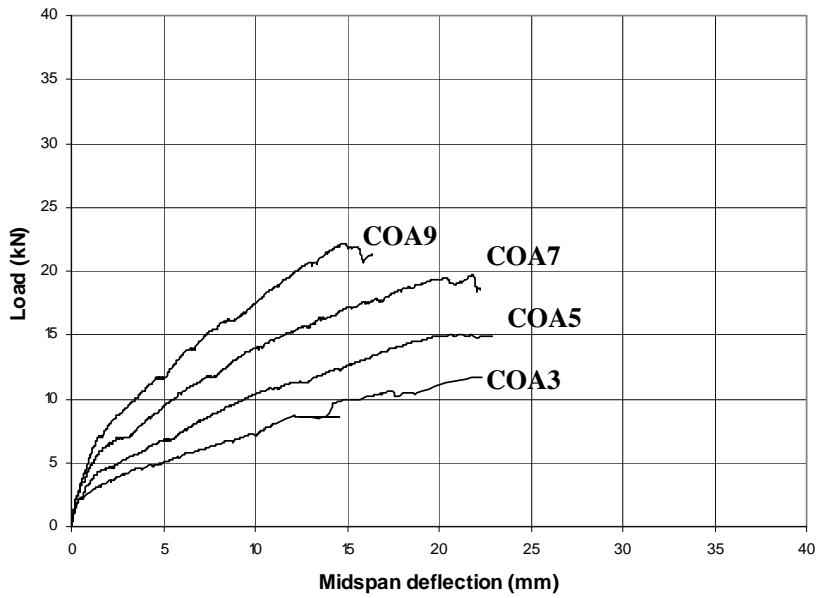
Tab. 5.3. Load cycles – Morbin, 2001

Cycle	Load Range (kips)
1	0-0.5
2	0.5-1.5-0.5
3	0.5-2.5-0.5
4	0.5-3.5-0.5
5	0.5-failure

In the figures 5.9 a and b, 5.10 a and b are shown the results for all the specimens tested.

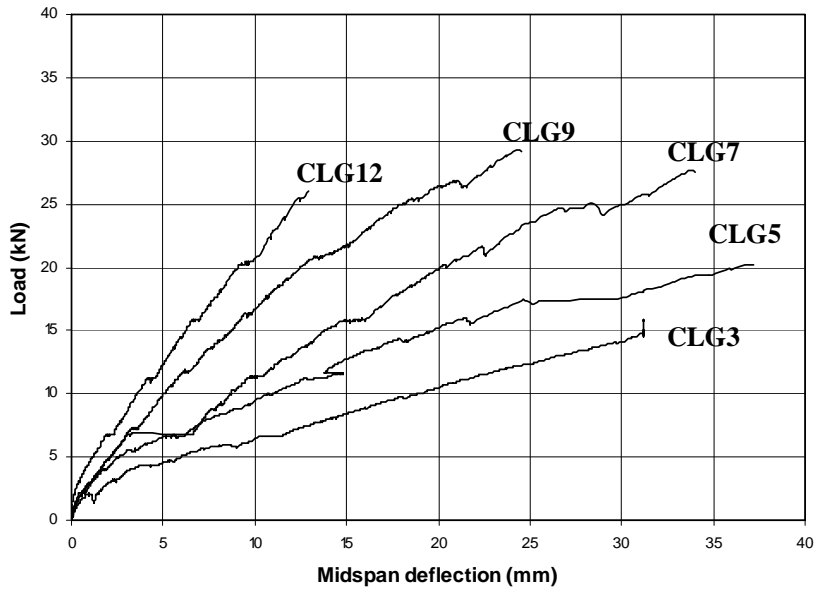


(a)



(b)

Fig. 5.9. Envelopes of series COG (a) and COA (b)



(a)

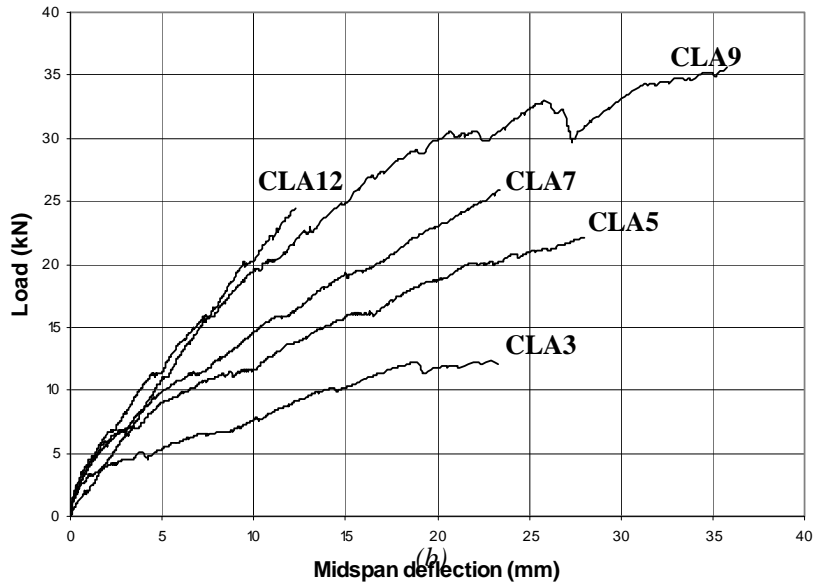


Fig. 5.10. Envelopes of series CLG (a) and CLA (b)

Out of the 20 tests, three general modes of failure were observed:

- (1) Debonding of the FRP laminates
- (2) Tension failure of the FRP reinforcement
- (3) Shear failure in the masonry units

All the experimental data are summarized in Table 5.4.

Tab. 5.4. Mode of failure (Morbin, 2001)

Wall	Failure	Wall	Failure
COG3	Delamination	CLG3	Delamination
COG5	Delamination	CLG5	Delamination
COG7	Delamination	CLG7	Delamination
COG9	Shear	CLG9	Shear
COG12	Shear	CLG12	Shear
COA3	Delamination	CLA3	Delamination
COA5	Delamination	CLA5	Rupture
COA7	Shear	CLA7	Delamination
COA9	Shear	CLA9	Rupture
COA12	Shear	CLA12	Shear

The conclusions are that FRP laminates have been proven to remarkably increase the flexural capacities of simply supported URM walls. Significant increases in flexural capacities, compared to the less strengthened wall, ranging between 50% and 300%,

can be achieved in concrete and clay walls. Test results showed that debonding of FRP laminates has been proven to be the controlling mechanism of failure. When a large amount of FRP is provided, shear failure occurred.

5.2. Experimental Program

URM walls depend on the tensile strength of masonry to resist out-of-plane loads (section 1.2) caused by high wind pressure or earthquakes. URM walls can collapse due to this limitation. In addition, relatively stiff frames may restrain the movement of the wall when subjected to out-of-plane loading. As a consequence, in-plane compressive forces are built, and produce a load resisting mechanism referred to as arching action (section 1.2) that improve the flexural behavior of the wall. The in-plane compression forces can delay cracking. Due to this action, the capacity of the wall can be much larger than that computed assuming simply supported conditions. Experimental works (Tumialan et al., 2001) have shown that the resultant force between the out-of-plane load and the induced membrane force could cause the crushing of the masonry units at the boundary. In this case, the application of the FRP did not exhibit the same effectiveness as in the case of walls having simply supported conditions. Thereby, the influence of arching mechanisms in the behavior of retrofitted walls needs to be taken into account to fully realize the effectiveness of strengthening strategies. Arching action becomes significant for height/thickness ratio less than 20 (Angel, 1994).

Ten specimens were built (five in concrete blocks and five in clay bricks) in order to investigate the FRP effectiveness in walls exhibiting arching action.

Standard hollow concrete blocks and clay bricks were used (see sections 4.1.2 and 4.1.3). The nominal dimensions of these walls were 1.22 m (48 in.) by 0.61 m (24 in.); their overall thickness was 0.095 m (3 3/4 in) for clay specimens and 0.092 m (3 5/8 in) for concrete specimens. Figure 5.11 illustrates the configuration of the walls.

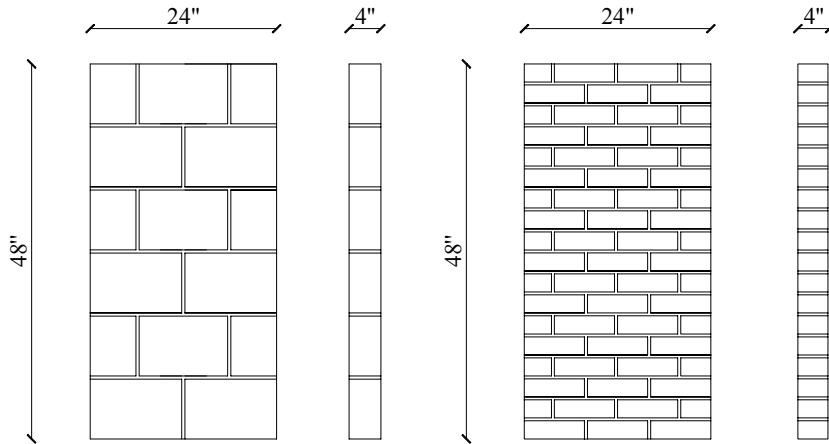


Fig. 5.11. Configuration of the walls

Generally, three ultimate states can be considered in flexural strengthening with FRP laminates:

- State 1: Debonding of the FRP laminate from the masonry substrate
- State 2: Rupture of the FRP laminate
- State 3: Crushing of masonry in compression

Previous investigations (Tumialan, 2000, Velazquez, 1998, Hamilton et al., 1999, Morbin, 2001) suggest that the controlling state is the state 1 (section 4). If a large amount of FRP is provided, shear failure may be observed. Theoretical flexural capacities of the strengthened walls were estimated based on the assumption that no premature failure was observed. This means that either rupture of the laminate or crushing of masonry would control the wall behavior. For simplicity and similarly to the flexural analysis of RC members, a parabolic distribution was used in the computation of the flexural capacity of the strengthened masonry. Thus:

$$f_m = f'_m \left[2 \left(\frac{\epsilon_m}{\epsilon'_m} \right) - \left(\frac{\epsilon_m}{\epsilon'_m} \right)^2 \right] \quad (5.1)$$

Where:

f_m' = Maximum compressive strength of the masonry

ϵ_m' = Maximum strain of the masonry

From the parabolic distribution, the coefficient α e β_1 that bound the equivalent compressive block can be determined from the following relationships:

$$\alpha \cdot \beta_1 = \left(\frac{\epsilon_m}{\epsilon_m'} \right) - \frac{1}{3} \left(\frac{\epsilon_m}{\epsilon_m'} \right)^2 \quad (5.2)$$

$$\alpha \cdot \beta_1 \left(1 - \frac{1}{2} \beta_1 \right) = \frac{2}{3} \left(\frac{\epsilon_m}{\epsilon_m'} \right) - \frac{1}{4} \left(\frac{\epsilon_m}{\epsilon_m'} \right)^2 \quad (5.3)$$

The strain and stress distribution in a masonry cross-section strengthened with FRP laminates is illustrated in figure 5.12.

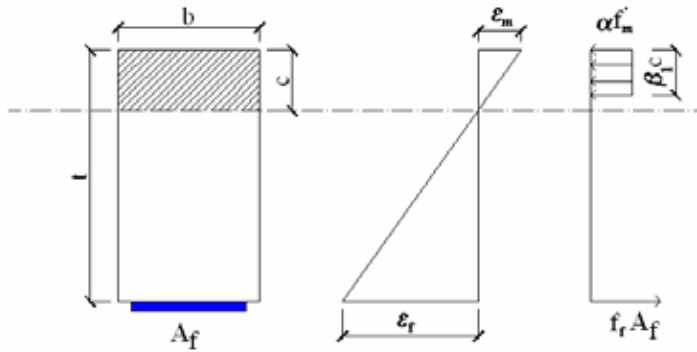


Fig. 5.12. Strain and stress distribution

The effective strain in the reinforcement “ ϵ_r ” and the strain in the masonry are related by:

$$\frac{\epsilon_m}{c} = \frac{\epsilon_r}{t - c} \quad (5.4)$$

where “c” is the height of the neutral axis. In order to satisfy the internal force equilibrium:

$$(\alpha f_m')(\beta_1 c)b = A_r f_r \quad (5.5)$$

$$f_r = E_r \varepsilon_r \quad (5.6)$$

where f_r , E_r and ε_r are the FRP strength, modulus of elasticity and strain.

Neglecting the tensile strength in the masonry, the theoretical flexural capacity can be estimated by:

$$M_{\text{theoretical}} = A_r f_r \left(t - \frac{\beta_1 c}{2} \right) \quad (5.7)$$

To study modes of failure, different amounts of glass (GFRP) reinforcement were chosen and expressed as a function of the balanced reinforced ratio ρ_b . The balanced condition was the parameter to determine the FRP amount. The balanced condition was assumed to occur when the compressive failure of the masonry is reached at the same time that the laminate fails in tension.

The following assumptions provided by Masonry Standards Joint Committee (MSJC) were considered:

- The maximum usable strain was assumed 0.0035 mm/mm (in/in) for clay masonry, and 0.0025 mm/mm (in/in) for concrete masonry.
- The tensile strength of masonry was neglected.
- The compressive strength of the clay masonry must be at least 17.0 MPa (2500 psi) for the clay masonry and 10.4 MPa (1500 psi) for the concrete masonry.

Table 5.5 Illustrates the material properties assumed in the design.

Tab. 5.5. Material properties for GFRP, clay masonry and concrete masonry

Material	Ultimate Strain [%]	Compr. Strength [MPa]	Tensile Strength [MPa]	E [GPa]
EG900 M.B.	2.1	-	1517	72
Clay Masonry	0.35	17	-	-
Concrete Masonry	0.25	10.4	-	-

Note: 1MPa = 145 psi; for the experimental values see section 4

Considering $\varepsilon_m = \varepsilon_m'$, from the equations 5.2 and 5.3 the α and β_1 coefficients for the ultimate state can be found.

$$\alpha = 0.89$$

$$\beta = 0.75$$

From the equation 5.4 the position of the neutral axis for clay masonry “c_b” and concrete masonry “c_c” at ultimate strength can be found.

$$c_b = 13.6 \text{ mm (0.536 in)}$$

$$c_c = 9.8 \text{ mm (0.385 in)}$$

Dividing the FRP area found from the equation 5.5 by the thickness of the laminate (section 4) the FRP width related to the balanced condition can be calculated.

$$W_{bb} = 178 \text{ mm (7 in)}$$

$$W_{bc} = 76 \text{ mm (3 in)}$$

Where:

W_{bb} = FRP width related to the clay masonry

W_{bc} = FRP width related to the concrete masonry

For simplicity, the different GFRP widths were chosen as multiples of inches.

Table 5.6 shows the test matrix.

Tab. 5.6. Test matrix

Specimen	Material	Dimensions [m]	GFRP width [mm]	% ρ_b	h/t ratio
Control B	Clay	1.22x0.61x0.095	-	-	12.8
BG3	Clay	1.22x0.61x0.095	76.2	43	12.8
BG5	Clay	1.22x0.61x0.095	127.0	72	12.8
BG7	Clay	1.22x0.61x0.095	177.8	100	12.8
BG9	Clay	1.22x0.61x0.095	228.6	130	12.8
Control C	Concrete	1.22x0.61x0.092	-	-	13.2
CG3	Concrete	1.22x0.61x0.092	76.2	100	13.2
CG5	Concrete	1.22x0.61x0.092	127.0	167	13.2
CG7	Concrete	1.22x0.61x0.092	177.8	233	13.2
CG9	Concrete	1.22x0.61x0.092	228.6	300	13.2

Note: 1 mm = 0.03937 in; ρ_b = balanced condition; h = height of the wall; t = thickness of the wall

The strengthening of the walls was positioned right in the middle of the bottom side of the specimens and, for the reinforcement installation, the wet-lay-up technique was followed (section 3.1). Two different surface preparation methods (with or without putty filler) were used. The surface preparation of all the masonry specimens built with clay units included the use of the putty. This was because the clay brick wall surfaces exhibited more unevenness than those with concrete blocks. In every case, the length of the FRP strip was 1170 mm (46 in); in this manner, the laminate would not touch the roller supports used for testing.

Five strain gages were applied to the GFRP laminates to monitor the strain distribution along the laminate during the tests. All the strain gages had a gage length of 12.7 mm (1/2 in) to ensure localized strain measurement. The surface of laminate was smoothed and conditioned to assure a perfect bond between strain gage and sheet. Figure 5.13 indicates the typical strain gages location on the GFRP laminates.

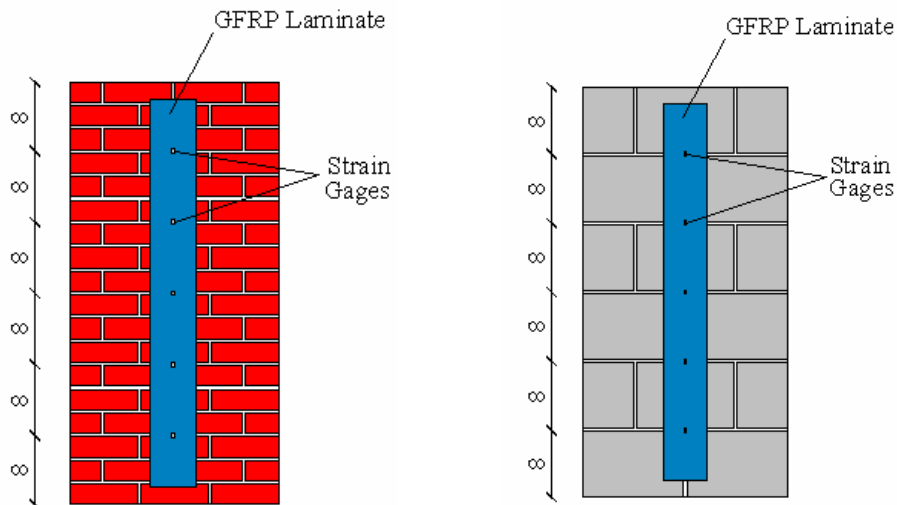


Fig. 5.13. Typical strain gage locations on the masonry walls



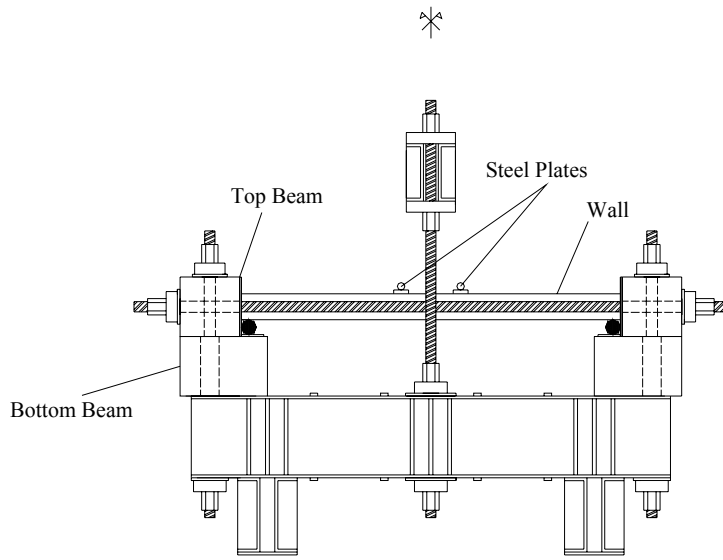
Fig. 5.14. Specimens ready

All the material properties are summarized in section 4.

5.3. Test Setup

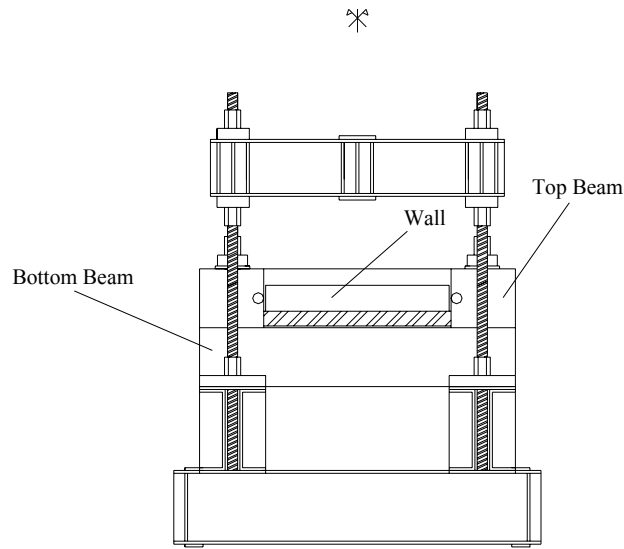
The masonry walls were tested under two out-of-plane loads, which were distributed by 50.8 x 609.6 x 12.7 mm (2 x 24 x ½ in.) steel plates to the external face of the wall (figure 5.15). Their distance was 101.6 mm (4 in.) from the midspan. The loads were generated by means of a 12 ton hydraulic jack activated by a manual pump. The force created by this jack reacted against a steel frame (figure 5.15).

To reproduce the real boundary conditions when the wall is restrained inside a reinforced concrete (RC) frame, and to separate the two reaction forces (F_v and F_h in section 1.2), four concrete beams were built. The bottom beams provided the vertical reaction. The top beams were built to be resistant at the horizontal load, created by the arching effect of the wall. Their design is reported in appendix A. High strength steel rods were used to connect these to the steel test frame. Figure 5.15 illustrates the test setup scheme and figure 5.16 illustrates a picture of the real test.



LONGITUDINAL VIEW

(a)



FRONT VIEW

(b)

Fig. 5.15. Test setup scheme

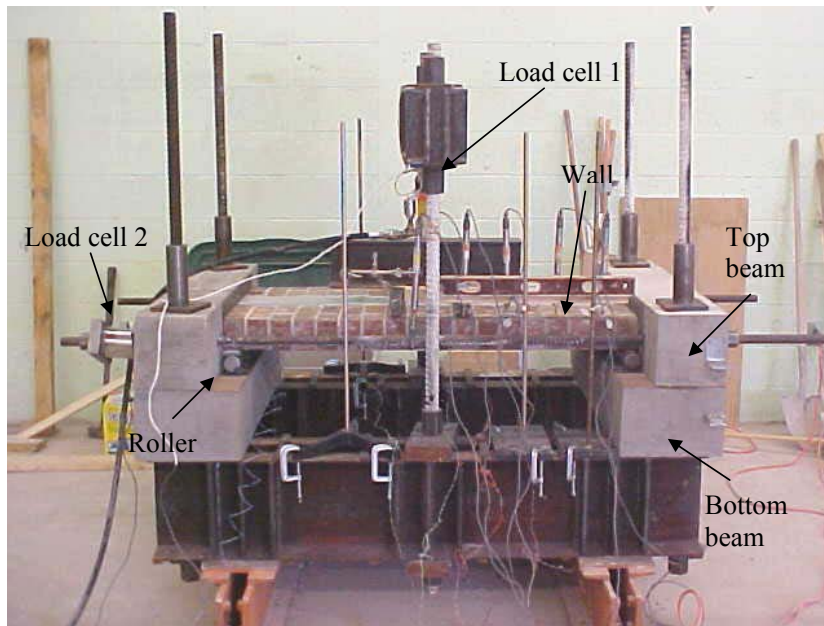


Fig. 5.16. Test setup

LVDTs were positioned in the middle of the walls to measure the midspan deflection during the tests. In the specimens “Control B”, “BG3”, and “BG5”, five LVDTs intended to record out-of-plane deflections along the walls (see appendix A).

Two load cells were used to record the in-plane (load cell 2) and the out-of-plane (load cell 1) loads. A horizontal load of 2.9 kN/m (200 lb/ft) was applied before testing to hold the walls in place. This load was selected in accordance with the Masonry Joint Standard Committee (MSJC, 1999) recommendations, which specify that level of load as the limit between non load-bearing and load-bearing walls.

In order to determine the cyclic behavior of the walls, different load cycles were chosen as a function of FRP width and masonry mechanical properties.

Tab. 5.7. Load cycles

Specimen	1 st cycle [kN]	2 nd cycle [kN]	3 rd cycle [kN]	4 th cycle [kN]	5 th cycle [kN]	6 th cycle [kN]
Control B	0-Failure	-	-	-	-	-
BG3	0-2.2	2.2-6.7-2.2	2.2-11.1-2.2	2.2-15.6-2.2	2.2-20.0-2.2	2.2-Failure
BG5	0-2.2	2.2-6.7-2.2	2.2-11.1-2.2	2.2-15.6-2.2	2.2-20.0-2.2	2.2-Failure
BG7	0-2.2	2.2-6.7-2.2	2.2-11.1-2.2	2.2-20.0-2.2	2.2-Failure	-
BG9	0-2.2	2.2-6.7-2.2	2.2-11.1-2.2	2.2-20.0-2.2	2.2-Failure	-
Control C	0-Failure	-	-	-	-	-
CG3	0-2.2	2.2-6.7-2.2	2.2-11.1-2.2	2.2-15.6-2.2	2.2-Failure	-
CG5	0-2.2	2.2-6.7-2.2	2.2-11.1-2.2	2.2-15.6-2.2	2.2-Failure	-
CG7	0-2.2	2.2-6.7-2.2	2.2-11.1-2.2	2.2-20.0-2.2	2.2-Failure	-
CG9	0-2.2	2.2-6.7-2.2	2.2-11.1-2.2	2.2-20.0-2.2	2.2-Failure	-

Note: 1 kN = 0.2248 Kip

5.4. Test Results

Three different modes of failure were observed:

- **Flexural failure:** after developing flexural cracks primarily located at mortar joints, a wall failed by either rupture (or debonding) of the FRP laminate or masonry crushing depending on the reinforcement ratio, ρ , and arching effect.
- **Crushing of the masonry at the supports:** this is the most common mode of failure in walls in which arching mechanism occurs. This kind of failure is due to the resultant force from shear and the in-plane forces at the supports.
- **Shear failure:** cracking started with a development of fine vertical cracks at the maximum bending region. Only flexural shear failure was observed. The sliding shear was not observed because of the in-plane force at the supports.

Tests results in terms of ultimate loads and maximum midspan deflection are summarized in table 5.8 and table 5.9. The average value of the two LVDTs was assumed for the midspan deflection. The horizontal load (H) values for the H/V_{\max} ratio were chosen at the corresponding values of V_{\max} (maximum vertical load).

Tab. 5.8. Test results for Clay Masonry

Specimen	FRP width [mm]	Horiz. Load [kN]	Vert. Load [kN]	H/V _{max} ratio	Midspan deflection [mm]
Control B	-	57.8	21.3	2.72	30.1*
BG3	76.2	115.6	52.2	2.21	31.7
BG5	127.0	101.4	45.6	2.22	28.9*
BG7	177.8	97.9	55.0	1.78	24.1
BG9	228.6	80.9	53.1	1.52	18.1

Note: 1 mm = 0.03937 in; 1 kN = 0.2248 kip.; * = Lost LVDTs

Tab. 5.9. Test results for Concrete Masonry

Specimen	FRP Width [mm]	Horiz. Load [kN]	Vert. Load [kN]	H/V _{max} ratio	Midspan deflection [mm]
Control C	-	83.6	22.4	3.74	31.1*
CG3	76.2	82.7	29.0	2.85	26.5
CG5	127.0	58.7	27.1	2.16	18.1
CG7	177.8	58.7	33.1	1.77	20.7
CG9	228.6	38.3	34.7	1.10	21.6

Note: 1 mm = 0.03937 in; 1 kN = 0.2248 kip.; * = Lost LVDTs

In the control specimens and in specimens BG3, BG5, CG3 and CG5, crushing of the masonry units at the boundary regions and of the mortar in the midspan were observed. Can be observed also that when failure is bond-controlled, debonding started from the middle of the walls. Figure 5.17 illustrates a series of pictures with the various mode of failure.



(a) BG5 – Crushing of the tile



(b) BG3 – Crushing of the tile



(c) Control C – Crushing of the midspan



(d) CG3 – Crushing of the tile



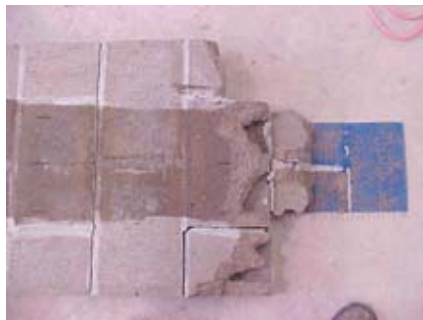
(e) BG3 – Fiber rupture + delam.



(f) Control B – Crushing of the midspan

Fig. 5.17. Failure of the specimens (I)

For the specimens BG7, BG9, CG7 and CG9, failure occurred due to shear. Figure 5.18 illustrates the mode of failure.



(a) CG9 – Shear failure



(b) BG9 – Shear failure



(c) CG9 – Shear Plan View



(d) BG9 – Shear Plan View

Fig. 5.18. Failure of the specimens (II)

The mode of failure for all the specimens are summarized in table 5.10.

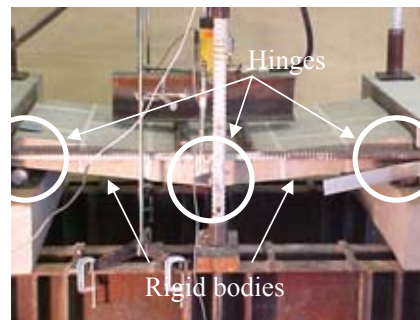
Tab. 5.10. Modes of failure for the specimens

Specimen	Mode of Failure	Specimen	Mode of Failure
Control B	Crushing of masonry units	Control C	Crushing of masonry units
BG3	Fiber rupture	CG3	Crushing of masonry units
BG5	Crushing of masonry units	CG5	Crushing of masonry units
BG7	Masonry shear	CG7	Masonry shear
BG9	Masonry shear	CG9	Masonry shear

In the specimens CG7, CG9, BG7, BG9, no crushing of the midspan was observed. By increasing the amount of FRP, due to the reduction of the displacement, the in-plane load decreased. A mechanism of three plastic hinged arch in all the specimens was observed. The specimens rotated as rigid bodies, like the theory showed in section 1.2. Figure 5.19 shows the phenomenon on different specimens.



(a) Specimen BG3



(b) Specimen Control C

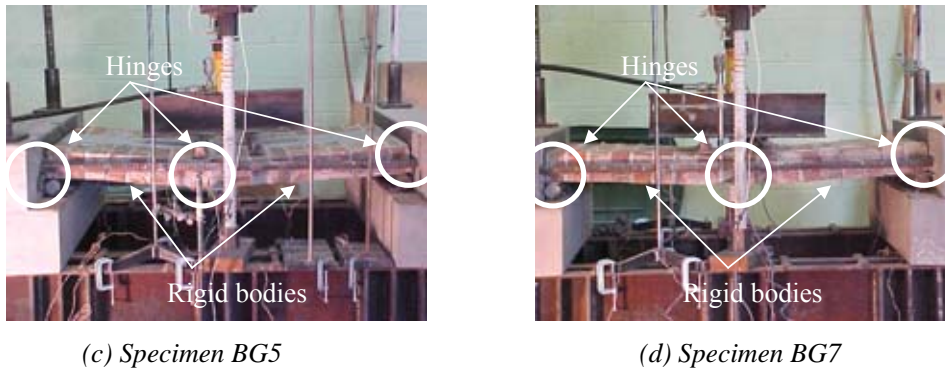


Fig. 5.19. Arch mechanism

It can be observed that the control walls had a great flexural capacity due to the arching action. If the wall is simply supported, the flexural capacity is related to the load at which corresponds the creation of the first crack. Generally, in Morbin's work, it happened when the vertical load was about 3.1 kN (0.7 kip). This means that the flexural capacity of the wall was increased about 7 times for concrete and clay masonry. From the data acquisition system, the vertical load versus mid-height deflection can be obtained for all the specimens. Figure 5.20 shows the cyclic behavior for the specimen BG3. The other cyclic behaviors are illustrated in appendix A.

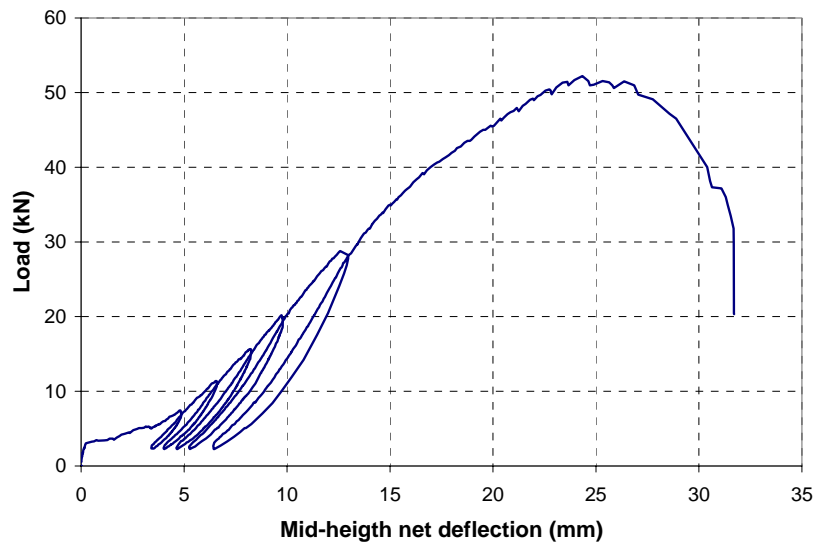
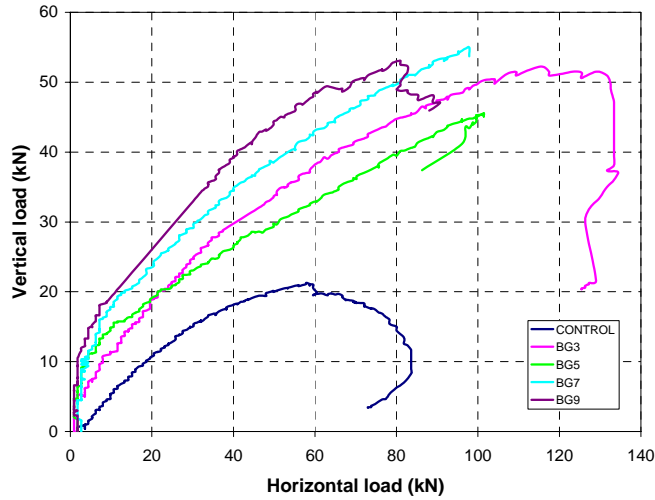


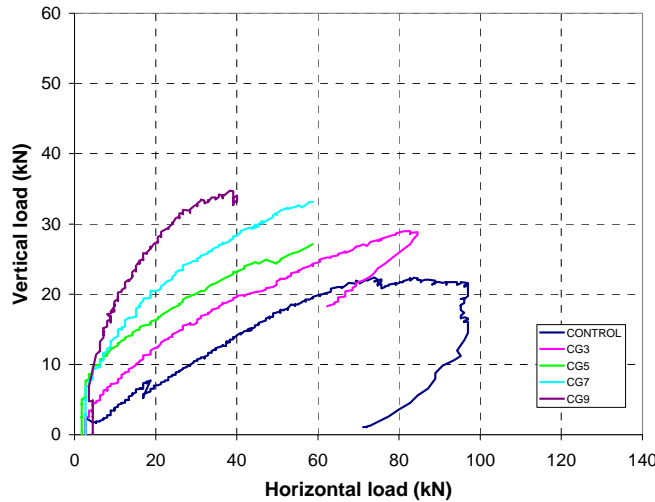
Fig. 5.20. Cyclic behavior for specimen BG3

By analyzing the experimental data, it is observed that when the first crack appeared in the walls, the in-plane restraining force suddenly increased. This can be referred to as the arching action.

By plotting the out-of-plane load (vertical load) versus the in-plane load (horizontal load), it can be observed that the in-plane load remains practically constant until the first crack appears in the specimens (Figure 5.21 a and b) and then grows almost linearly.



(a) Clay Masonry

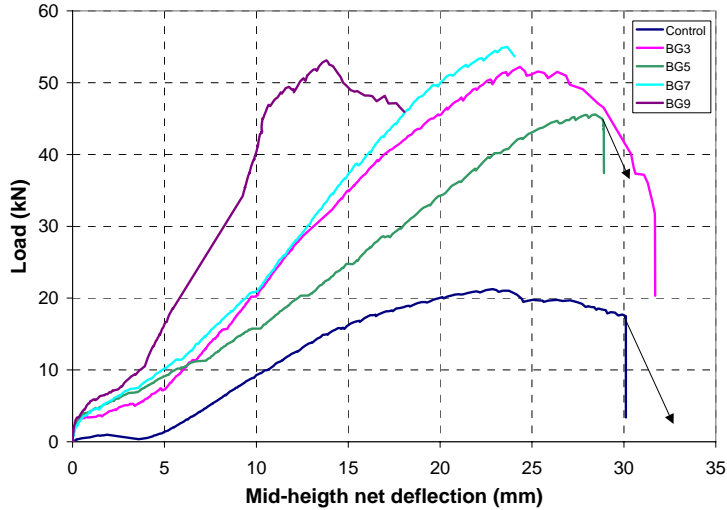


(b) Concrete Masonry

Fig. 5.21. Horizontal load vs. Vertical load.

From the experimental values, a comparison of vertical load (out-of-plane) versus mid-height deflection in terms of different FRP widths can be obtained.

Clay masonry. Figure 5.22 shows a comparison among the clay masonry specimens.



Note: In specimens control B and BG5 LVDTs were lost close to ultimate load

Fig. 5.22. Comparison among clay masonry

Table 5.11 illustrates the ratio between the ultimate vertical loads of the strengthened specimens and the ultimate load for the control wall.

Tab. 5.11. Comparison among clay masonry specimens

Specimen	FRP Width [mm]	Vertical load [kN]	Vertical load ratio
Control B	-	21.3	1
BG3	76.2	52.2	2.45
BG5	127.0	45.6	2.14
BG7	177.8	55.0	2.58
BG9	228.6	53.1	2.49

Note: 1 mm = 0.03937 in.; 1 kN = 0.2248 Kip

A remarkable increment of flexural capacity compared to the control wall can be observed. This increment may be overly optimistic because the arching was not completely developed in the control specimen due to set-up difficulties. Figure 5.23 illustrates the horizontal load versus FRP width behavior.

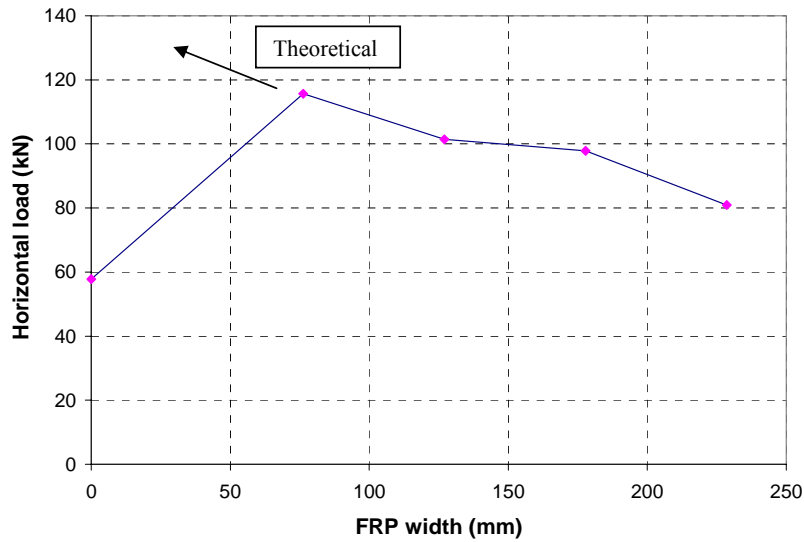


Fig. 5.23. Horizontal versus FRP width behavior (Clay masonry)

Figure 5.23 shows the differences between the real and the theoretical behavior of the control wall. This means that arching was not completely developed. Hence, a bigger vertical load for the control specimen could be expected.

From the comparison in figure 5.22, it can be observed that the different amounts of reinforcement do not influence dramatically the ultimate load. Higher reinforcement can only increase the stiffness and reduce the deflection. By increasing the amount of reinforcement, a drop in ductility was shown. Anyway, good performance under cyclic load can be obtained with small amounts of FRP reinforcement.

By plotting the graphic with the H/V_{\max} load ratio, it can be observed that if the FRP width increases, the ratio decreases linearly. Figure 5.24 illustrates the experimental behavior and a trend line shows the linear behavior.

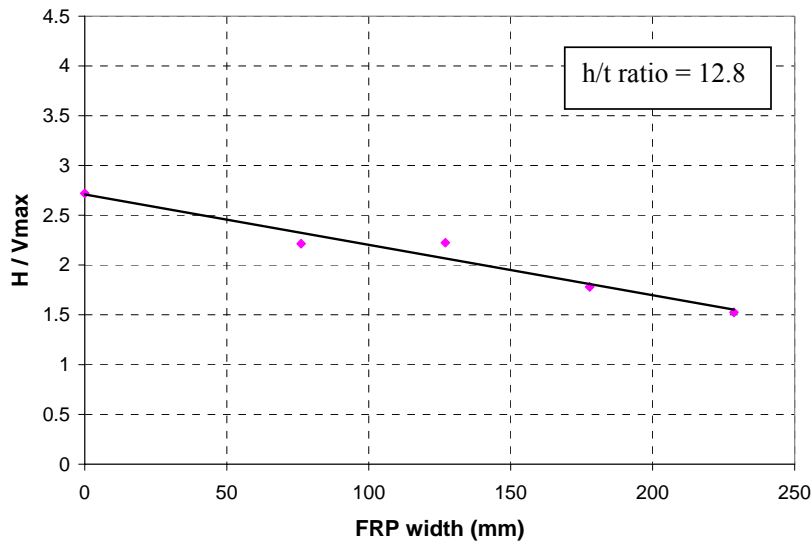
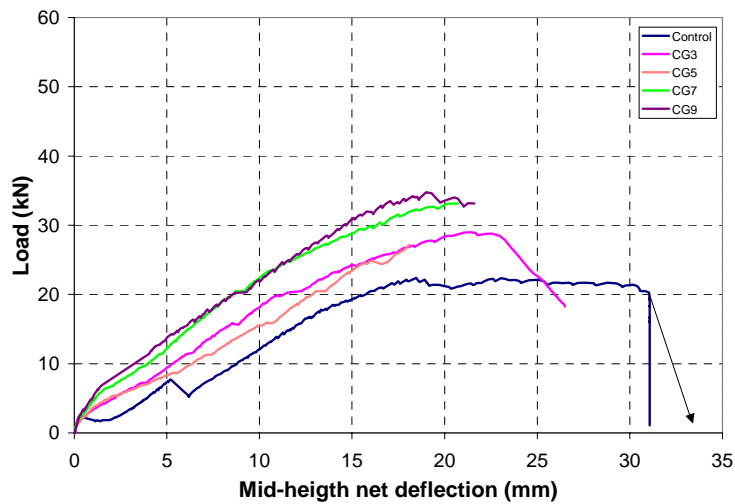


Fig. 5.24. H/V_{max} ratio in function of FRP width (Clay masonry)

However, it can be noted that for H/V_{max} ratio equal to 1.52, failure was due to shear-compression behavior. It is reasonable to think an H/V_{max} ratio limit for the reinforced masonry (It caused by shear-compression failure).

Concrete masonry. Figure 5.25 shows a comparison among the concrete masonry specimens.



Note: In specimen control C lost LVDTs close to ultimate load

Fig. 5.25. Comparison among concrete masonry

Table 5.12 illustrates the flexural capacity ratio compared to the control specimen.

Tab. 5.12. Comparison among concrete masonry specimens

Specimen	FRP Width [mm]	Vertical load [kN]	Vertical load ratio
Control C	-	22.4	1
CG3	76.2	29.0	1.29
CG5	127.0	27.1	1.21
CG7	177.8	33.1	1.48
CG9	228.6	34.7	1.55

Note: 1 mm = 0.03937 in; 1 kN = 0.2248 Kip

Issues were not encountered to setup the tests. Figure 5.26 illustrates the horizontal load versus FRP width behavior, close to the theoretical behavior.

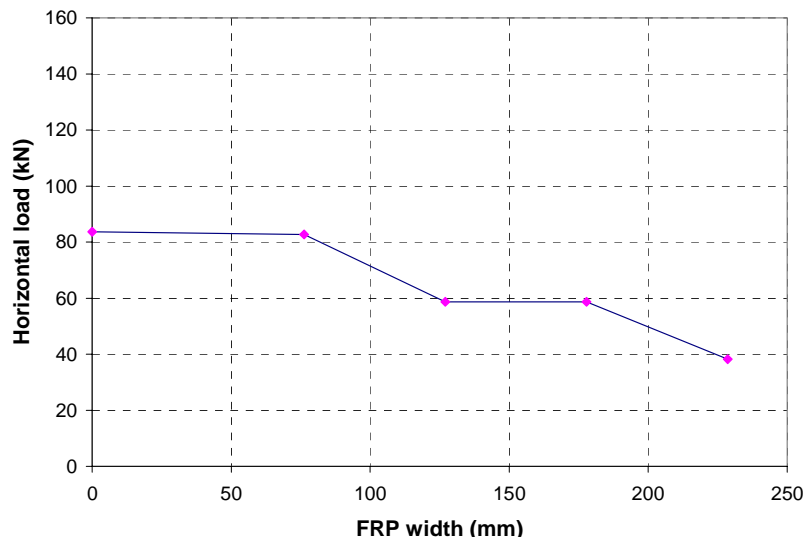


Fig. 5.26. Horizontal versus FRP width behavior (Concrete masonry)

From the comparison, it can be observed that the reinforcement does not influence dramatically the ultimate load. By increasing the amount of reinforcement, a drop in ductility was shown. Anyway, like for the clay masonry, good performance under cyclic load can be obtained with small amounts of reinforcement. Plotting the graphic with the H/V_{\max} load ratio, a linear behavior similar to the one obtained for clay masonry can be observed (Figure 5.27).

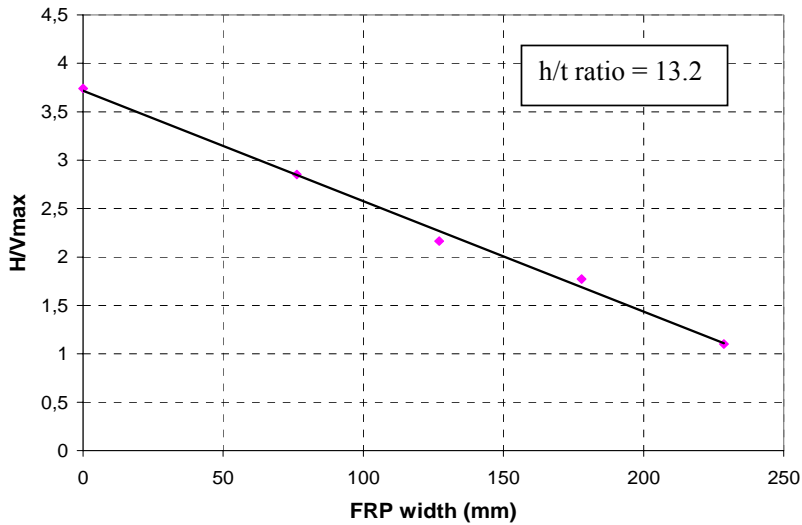


Fig. 5.27. H/V_{\max} ratio in function of FRP width (concrete masonry)

However, like for clay masonry, it can be noted that for H/V_{\max} ratio equal to 1.10, failure was due to shear-compression behavior. It is reasonable to think an H/V_{\max} ratio limit for the reinforced masonry (It caused by shear-compression failure).

Comparing the load-deflection curves obtained in the case of simply supported walls (Morbin, 2001) and walls with the end restrained, a significant influence of boundary conditions in the wall is observed. Figure 5.28 shows the comparison between several concrete specimens.

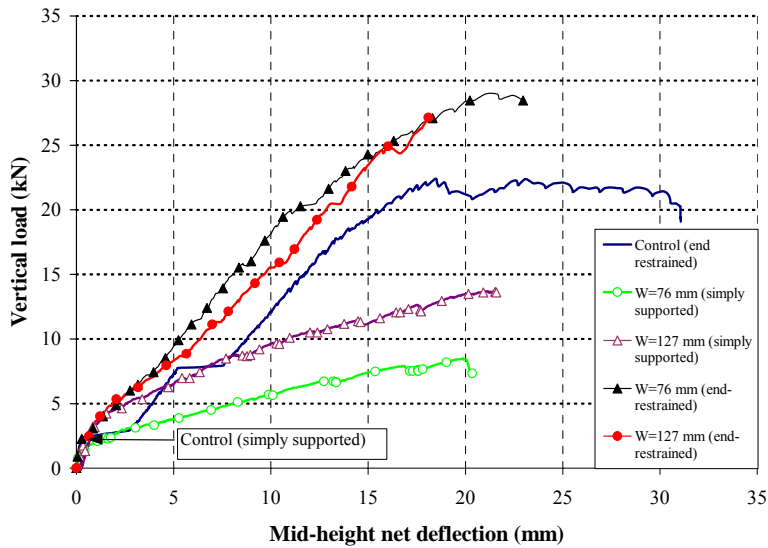


Fig. 5.28. Comp. among simply supported and restrained concrete specimens

If the wall behaves as a simply supported element (i.e. large slenderness ratio or upper end is not restrained), the FRP reinforcement is very effective since the wall is in pure flexure and the crack openings are bridged by the reinforcement. In the case of the simply supported unstrengthened specimens, the URM masonry wall collapsed when the vertical load was about 3.1 kN (0.7 kips). Figure 5.28 shows that the increase in the ultimate load for walls strengthened with 75 mm (3 in) and 125 mm (5 in) wide GFRP laminates were about 175 and 325% respectively. If the wall is restrained (i.e. arching mechanism is observed), the same effectiveness of FRP reinforcement is not observed because crushing of the masonry units at the boundary regions controls the behavior. In this case, the increase in the out-of-plane capacity for strengthened specimens with 75 mm (3 in) and 125 mm (5 in) wide GFRP laminates was about 25%. Table 5.13 illustrates the effectiveness of FRP reinforcement compared to the unstrengthened wall.

Tab. 5.13. Effectiveness of FRP reinforcement for walls with arching

Specimen	% increment of load
CG3	29
CG5	21
CG7	48
CG9	55

5.5. Analytical Study

In order to determine the plastic moment at the midspans and at the boundaries for all the specimens, interaction diagrams were built. The real dimensions of the cross section for clay and concrete masonry were assumed. In order to simplify the calculations, mortar joints were omitted. For the cross-section at the boundaries and for the unstrengthened specimens was assumed the unreinforced section, since the FRP was not present. Figure 5.29 shows the generic unreinforced section assumed to calculate the M-N diagram.

Unstrengthened section

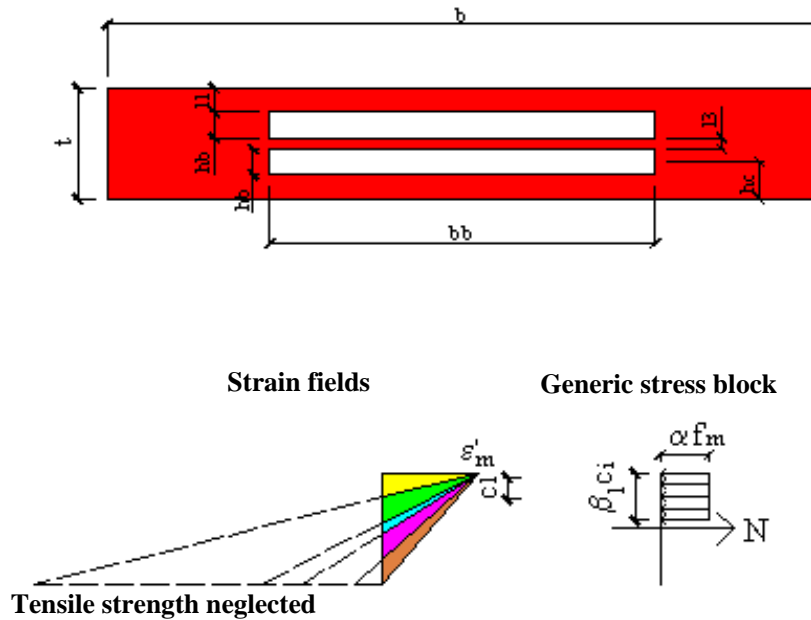


Fig. 5.29. Generic unreinforced section

The following assumptions were taken:

- The maximum strain ϵ'_m was assumed 0.0035 mm/mm (in/in) for clay masonry, and 0.0025 mm/mm (in/in) for concrete masonry.
- The tensile strength of masonry was neglected.

To determine the ultimate moment, the ultimate state $\epsilon_m = \epsilon'_m$ was considered. Thus, from the equations 5.2 and 5.3, α and β can be found.

$$\alpha = 0.89$$

$$\beta = 0.75$$

To take into account the hollow units, different strain fields were assumed. Thus, for each field M and N can be calculated with the equilibrium. As an example, the calculations for $\beta_1 c_1 \leq l_1$ (Figure 5.29) are reported below.

To satisfy the equilibrium:

$$N(c_i) = \alpha \cdot f'_m \beta_1 c_i \cdot b$$

$$M(c_i) = \alpha \cdot f'_m \beta_1 c_i \cdot b \cdot \left(h - \frac{\beta_1 c_i}{2}\right) - N(c_i) \cdot \frac{h}{2}$$

All the calculations are reported in appendix A. The experimental characteristics obtained from the material characterization (section 4) were considered.

For the midspan, the strengthened cross-section was assumed. In this case, another strain field had to be taken into account. FRP crisis was considered when FRP reached the ultimate strain ϵ_{fu} . Thus, the field when $\epsilon_m < \epsilon'_m$ has to be considered. In this field has to be considered also that α and β_1 coefficients are changing following the equations 5.2 and 5.3. Figure 5.30 illustrates the generic strengthened section assumed to calculate the M-N diagram.

Strengthened section

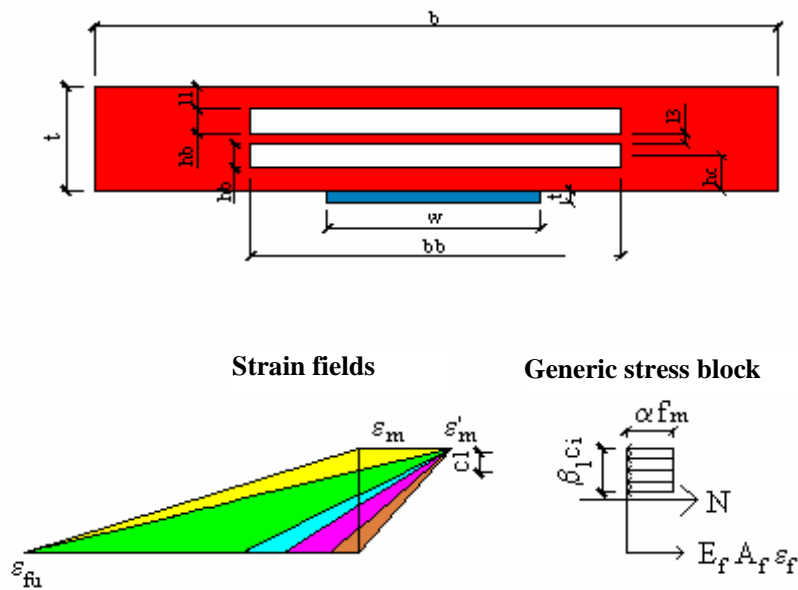
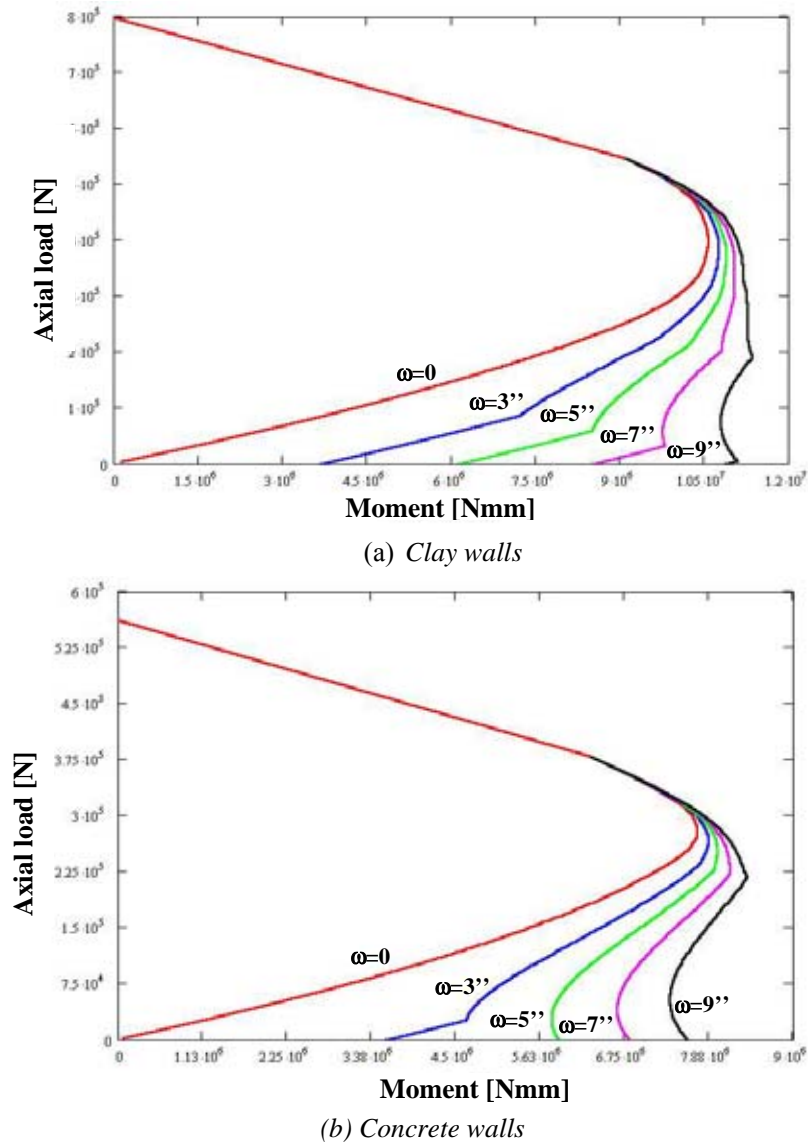


Fig. 5.30. Strengthened section

All the calculations are reported in appendix A. Figure 5.31 (a) and (b) show the interaction diagrams for the clay and concrete cross sections, considering the unstrengthened and reinforced sections with different amounts of reinforcement. The experimental characteristics obtained from the material characterization (section 4) were considered.



Note: 1 in = 25.4 mm; 1 N = 0.2248 pd

Fig. 5.31. Interaction diagrams for clay and concrete cross sections

From the experimental values of the horizontal forces “N”, corresponding to V_{\max} values, the experimental moments in the midspans and at the boundaries can be found, using the M-N interaction diagrams. Table 5.14 and 5.15 show the values for all the specimens.

Tab. 5.14. Experimental moments for the clay specimens

Specimen	N [kN]	M_{MID} [kN mm]	M_{BOUND} [kN mm]
Control B	57.8	2601	2601
BG3	115.6	7663	4895
BG5	101.4	8789	4359
BG7	97.9	9872	4223
BG9	80.9	10797	3554

Tab. 5.15. Experimental moments for the concrete specimens

Specimen	N [kN]	M_{MID} [kN mm]	M_{BOUND} [kN mm]
Control C	83.6	3406	3406
CG3	82.7	5238	3375
CG5	58.7	5888	2483
CG7	58.7	6683	2483
CG9	38.3	7372	1670

In order to find a relationship for all the specimens, both clay and concrete, an expression for the reinforcement ratio is introduced (Tumialan, 2000). The reinforcement ratio is expressed as:

$$\varpi_f = \frac{\rho_f E_f}{f_m'(h/t)}$$

Where:

$$\rho_f = \frac{A_f}{b \cdot t}$$

A_f = FRP area

The slenderness ratio h/t is justified since this parameter is identified as one of the most important in the out-of-plane behavior of masonry walls. The slenderness ratio and out-of-plane capacity are inversely proportional. Since the strength is directly proportional to the compressive strength, than the slenderness ratio and the compressive strength are inversely proportional. Therefore, it is reasonable to express the relation between the compressive strength and the slenderness ratio as a product.

With the experimental values from the characterizations, the reinforcement ratios can be calculated. Table 5.16 illustrates the values.

Tab. 5.16. Reinforcement ratio ω_f for clay and concrete masonry

Specimen	b [mm]	h [mm]	FRP width [mm]	A _f [mm ²]	ρ_f	ω_f
Control B	609.6	95.25	-	-	-	-
BG3	609.6	95.25	76.2	26.90	0.000463	0.149
BG5	609.6	95.25	127	44.84	0.000772	0.248
BG7	609.6	95.25	177.8	62.77	0.001081	0.348
BG9	609.6	95.25	228.6	80.71	0.00139	0.448
Control C	609.6	92.07	-	-	-	-
CG3	609.6	92.07	76.2	26.90	0.000479	0.206
CG5	609.6	92.07	127	44.84	0.000799	0.344
CG7	609.6	92.07	177.8	62.77	0.001118	0.481
CG9	609.6	92.07	228.6	80.71	0.001438	0.618

Note: 1 mm = 0.03937 in

In order to compare all the values a V/M_{\max} ratio was chosen. This ratio is representative of the behavior of the wall.

Figure 5.32 illustrates the behavior for the specimens tested.

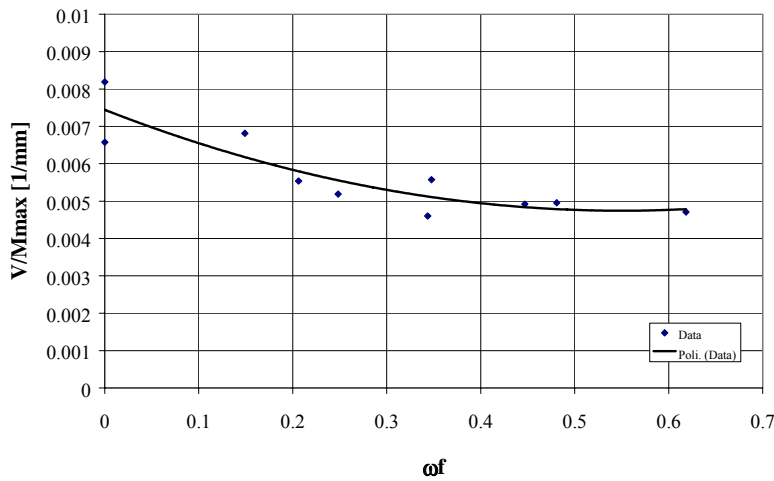


Fig. 5.32. Comparison for all the specimens

The figure 5.32 shows that there could be a limit for the V/M_{\max} ratio. It can be said that there could be a limit of the amount of the FRP reinforcement beyond which the behavior is governed by shear - compression failure.

Design considerations

The interaction diagrams were plotted to find the ultimate experimental moment for each kind of specimen, considering the hollow masonry units.

For design purposes this approach could be excessively rigorous, so, different solutions were investigated.

In order to maintain the slenderness ratio, two different cross sections were considered:

- A full section with unchanged dimensions
- An equivalent section with the same thickness and area of the hollow section, with a reduced base calculated using the following equation:

$$b_{eq} = \frac{A_h}{t}$$

Where: A_h = area of the hollow cross section

t = thickness of the wall

Figure 5.33 illustrates the comparison among the different kinds of approaches followed.

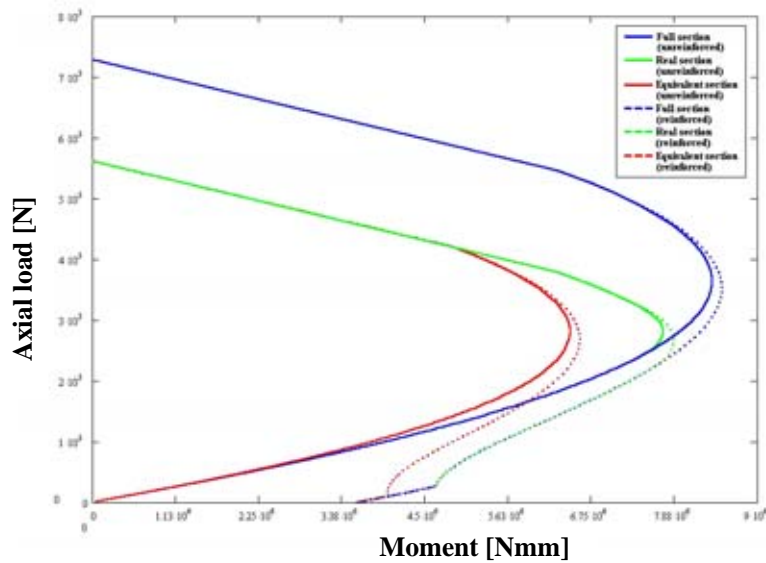


Fig. 5.33. Different approaches for design purposes

From the figure 5.33 can be seen that the most conservative approach is the one with the equivalent base.

It must be also taken into account that in designing phase the ultimate strain for the fiber should be limited to a value of $\epsilon_{ub} = 0.8\%$ (see also section 4) because of debonding issues.

6. IN-PLANE BEHAVIOR OF MASONRY WALLS STRENGTHENED WITH FRP LAMINATES AND RODS

6.1. Previous Results

The results presented in this section correspond to previous investigations conducted to study the in-plane behavior of masonry panels strengthened with FRP composites, which were intended to represent infill walls.

Schwegler (1995) investigated strengthening methods for masonry shear walls. The objectives of this study were to increase the system ductility, generate uniform crack distribution, and increase the load carrying capacity of the system. The dimensions of the walls were 3.66 m (12 ft) by 1.83 m (6 ft) by 0.2 m (8 in). CFRP sheets were bonded diagonally to the masonry walls as shown in figure 6.1, and mechanically anchored to the adjoining slabs.

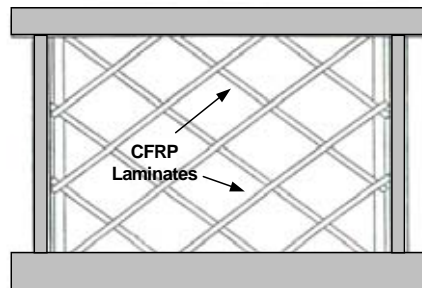


Fig. 6.1. Strengthened wall (Schwegler, 1995)

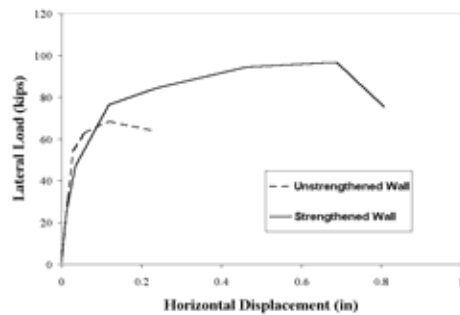


Fig. 6.2. Test results (Schwegler, 1995)

As observed in figure 6.2, the test results showed that the strengthened wall exhibited elastic behavior up to 70% of the maximum shear force. It was also observed that the carrying capacity decreased as a consequence of massive crack formation in the masonry. By comparing walls strengthened in one side and two sides, it was observed

that if only one side of the masonry wall is strengthened, the capacity could be halved. In addition, the eccentricities caused by this strengthening scheme had a minimum effect on the shear carrying capacity. In all the strengthened walls fine cracks were observed perpendicular to the sheets. The crack separation was constant and the crack widths remained small.

Laursen et.al. (1995) studied the shear behavior of masonry walls strengthened with CFRP laminates. The walls were built with concrete blocks and were fully grouted. The overall dimensions were 1.82 x 1.82 m (72 in x 72 in). The walls were internally reinforced; horizontally with a low shear reinforcement ratio of 0.14%, and vertically with a ratio of 0.54%. The “original” wall failed in shear. The specimen was re-tested after being repaired. The repair was performed by closing the large diagonal shear cracks with epoxy filler and epoxy injection, and repairing the crushed compression toes with epoxy mortar. The “repaired” wall was then strengthened with CFRP laminates, which covered the two sides of the wall; an additional layer was applied in the end regions as confinement. The amount of strengthening in the “retrofitted” wall was similar to the previous wall but applied to only one side of the wall.

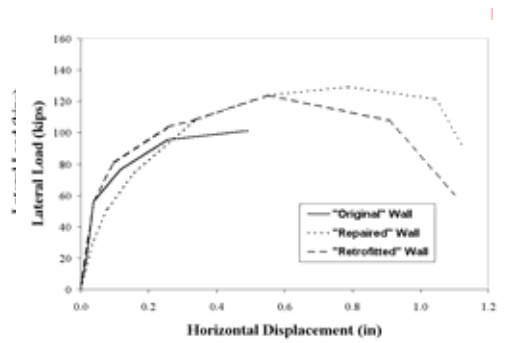


Fig. 6.3. Test results (Laursen, 1995)

It was observed that the presence of the FRP laminates improved the wall performance by changing the failure from a shear-controlled failure to a flexural-controlled failure. This change caused an increase in the capability of deformation of approximately 100% by preventing a brittle failure mode. The test results of this wall, shown in Figure 6.3, also proved that even though the wall failed in shear, it could be

repaired to restore the initial stiffness and strength compared to the standard of the “original” and “retrofitted” walls.

Tinazzi et al. (2000) introduced the term Structural Repointing and investigated the use of FRP rods to increase the shear capacity of masonry panels made of clay bricks. This technology consisted of placing # 2 GFRP rods in grooved horizontal joints as shown in Figure 6.4. The rods were embedded in an epoxy-based paste. The nominal dimensions of the panels were 0.09 m by 0.61 m by 0.61 m (3.5 in by 24in by 24 in). The failure of unreinforced panels consisted of the joint sliding along the compressed diagonal. In contrast, strengthened with FRP rods at each joint, showed increases in capacity of about 45% higher as compared to the unreinforced wall. The failure mode changed since joint sliding was prevented. The mechanism of failure indicated the sliding of the masonry-paste interface.



Fig. 6.4. GFRP rods in mortar bed joints (Tinazzi, 2000)

Morbin A. et al. (2001) conducted work on masonry panels built with concrete masonry blocks strengthened with GFRP laminates and rods at the University of Missouri - Rolla.

A total of six masonry walls were manufactured for this experimental program, which were built with 15.24 cm by 20.32 cm by 40.64 cm (6 in by 8 in by 16 in) concrete blocks following a running bond pattern. One Unreinforced Masonry (URM) wall, COW1, was the control specimen. COW2 was strengthened with GFRP bars at every horizontal joint only on one side. Walls COW2 and COW3 had similar amounts of reinforcement. In the latter specimen, the reinforcement was distributed in the two

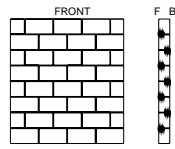
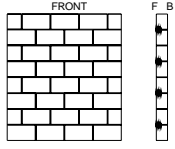
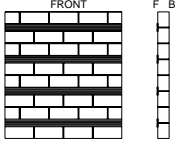
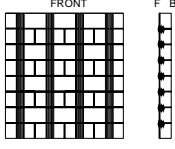
faces, following an alternate pattern, to observe the influence of the reinforcement eccentricity. Wall COW4 was strengthened with GFRP bars at every second horizontal joint to observe the behavior of a wall with half the amount of strengthening. Wall 5 was strengthened with GFRP laminates; the amount of strengthening reinforcement was equivalent to that of Wall 2 in terms of axial stiffness EA (Modulus of Elasticity \times Reinforcement Cross Sectional Area). Thus four GFRP strips, 1.63 m (64 in) long and 0.1 m (4 in) wide, were applied on the panel surface. Wall 6 was strengthened with a combination of GFRP bars and laminates. The bars were placed in every horizontal joint, whereas, the laminates were applied in the vertical direction. The amount of reinforcement for both directions was similar in terms of EA ; as for wall COW5, four strips 1.63 m (64 in) long and 0.1 m (4 in) wide were cut. The test matrix used in this investigation for Series COW is summarized in table 6.1.

Tab. 6.1. Test matrix for Series COW (Morbin, 2001)

Specimen	Strengthening	Front Side	Back Side	Layout
COW1	None	None	None	
COW2	#2 GFRP bars	1HJ	None	

Tab. 6.1. Test matrix (continued)

Specimen	Strengthening	Front Side	Back Side	Layout
----------	---------------	------------	-----------	--------

COW3	#2 GFRP bars	2HJ	2HJ	
COW4	#2 GFRP bars	2HJ	None	
COW5	4 in GFRP laminates	4HS	None	
COW6	#2 GFRP bars 4 in GFRP laminates	1HJ/4VS	None	

LEGEND: 1HJ= every horizontal joint, 2HJ= every second horizontal joint, 4HS=four horizontal glass strips @ 16 in o.c., 4VS= four vertical glass strips @ 16 in o.c.

The average compressive strength of concrete masonry obtained from the testing of prisms was 16.74 MPa (2430 psi) with a standard deviation of 2.37 MPa (345 psi). In order to determine the shear stresses along the mortar joints, two series of triplets were tested. Cohesion and coefficient of friction according to Coulomb criterion, expressed by the equation $\tau = \tau_o + \mu \sigma_n$, were obtained by means of linear interpolation of the experimental data. Thus for concrete blocks it was found $\tau = 57.43 + 0.6679\sigma_n$ (psi) for $\sigma_n < 216$ psi.

Masonry specimens were tested using the test setup illustrated in Figure 6.5 (see also section 6.3).



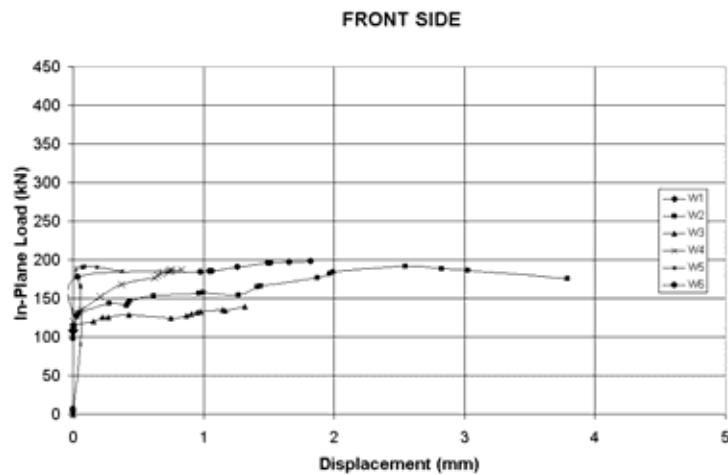
Fig. 6.5. Test setup (Morbin, 2001)

The load was applied in cycles of loading and unloading except for the control wall. Table 6.2 illustrates a summary of the load cycles.

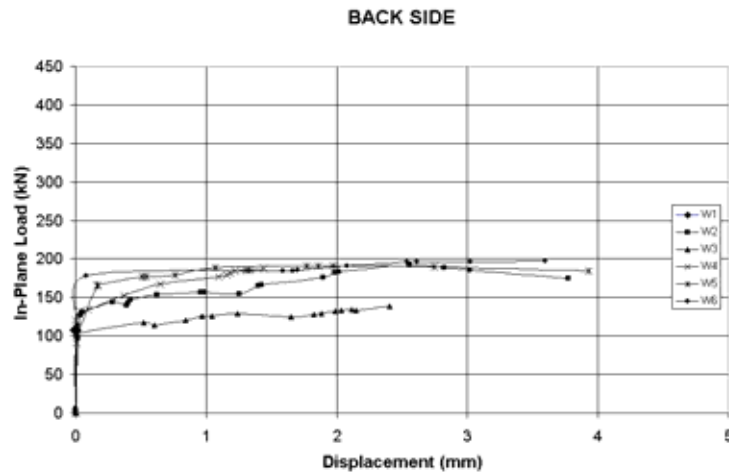
Tab. 6.2. Load cycles – Morbin, 2001

Cycle	Load Range (kips)
1	0-30-10
2	10-40-10
3	10-50-10
4	10-failure

In figure 6.6 (a), (b) and in table 6.3 are summarized the results for all the specimens tested.



(a)



(b)

Fig. 6.6. In-plane load vs. displacement (Morbin, 2001)

Tab. 6.3. Comparison of Pseudo-ductility for Series COW (Morbin, 2001)

Specimen	In-Plane Load [kN]	γ_u [°]	γ_y [°]	μ
COW1	108	0.09	0.09	1.0
COW2	200	1.71	0.13	13.1
COW3	195	1.82	0.09	20.2
COW4	189	0.40	0.08	5.0
COW5	137	0.94	0.17	5.5
COW6	191	0.72	0.14	5.1

The conclusions are that the masonry panels strengthened with FRP had a remarkable increase in shear capacity and pseudo-ductility, ranging between 30% and 85%.

It was observed that the mechanism of failure of walls strengthened with GFRP bars placed at every bed mortar joint consists of two phases. From the test observations, the in-plane phase was the most critical, and the out-of-plane phase is pronounced in walls having reinforcement eccentricity.

- **In-Plane Phase:** When the tensile strength of masonry is overcome, the wall cracks along the diagonal, following the mortar joints (stepped crack

vertical/horizontal). For the reinforcement placed in the horizontal joint, the crack is typically at the top side. Wall failure occurs only when a second crack develops below the reinforcement at the epoxy/block interface.

- **Out-of-Plane Phase:** This phase influences the stability of the wall, which is observed in specimens strengthened only on one side. Comparing the recorded crack openings on the front (strengthened) and back (unstrengthened) sides, the crack growth on the unstrengthened side increased at a higher rate than the strengthened side.

Moreover, in contrast with URM walls, strengthened walls are stable after failure. This fact can avoid injuries or loss of human life due to collapse of the wall.

6.2. Test Specimens

Infill walls may or not may resist lateral and vertical loads. In order to simplify the design, the potential interaction between the infill walls and the structural frame has been ordinarily ignored. Ignoring the contribution of the masonry infill walls does not always represent a conservative design. Their presence can lead to stiffening their frames and thereby cause a redistribution of the lateral loads in the building plan.

Infill walls can be totally enclosed in a surrounding frame of beams and columns, as typical in a multi story building. These walls can be subjected to high in-plane loads during exceptional events such as high wind or earthquake. These loads are due to the interaction between the infill walls and the surrounding structural frames.

Controlling shear failure is a key issue in masonry strengthening because after the wall is cracked due to in-plane loads, it can easily collapse due to movement perpendicular to the plane and jeopardize human lives. This kind of behavior has been evident from post-earthquake observations. In this context, FRP composites can provide viable solutions for the strengthening of URM walls subjected to stresses caused by wind or earthquake loads. The use of FRP materials offers important advantages in addition to their mechanical characteristics and ease of installation.

In order to demonstrate the effectiveness of the FRP strengthening of masonry walls subjected to in-plane loading, a research program was conducted to continue

Morbin's work. The specimens were built using clay bricks and were strengthened with different patterns and kinds of FRP materials.

This section describes an experimental program on shear strengthening of URM panels. FRP materials in the form of GFRP laminates, GFRP bars and carbon strips were used to strengthen the walls. In addition to the use of FRP laminates, a technique denominated **FRP Structural Repointing** is investigated. This technique consists of placing FRP bars in the mortar joints (Tumialan et al., 2000). Repointing is a traditional retrofitting technique commonly used in the masonry industry, which consists in replacing missing mortar in the joints. The term "structural" is added because the proposed method does not merely consist of filling the joints as the traditional technique, but allows for restoring the integrity and/or upgrading the shear and/or flexural capacity of walls.

Six specimens were built using light clay bricks (see also the description in section 4.1.4) in a common bond pattern. The nominal dimensions of these walls were 1630 mm (64 in) by 1630 mm (64 in), and the overall thickness was 200 mm (8 in).

Figure 6.7 illustrates the configuration of the walls.

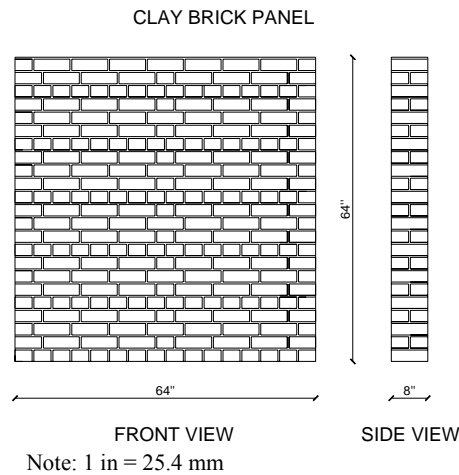


Fig. 6.7. Configuration of the walls

The engineering properties of masonry and strengthening materials were presented in section 4.

Wall CLW1 was selected as control specimen. For the first strengthened panel, CLW2, it was decided to put an amount of reinforcement equivalent to that of COW2 (See Section 6.1, Morbin, 2001), using the following equation:

$$A_{f,clay} = A_{f,concrete} \cdot \frac{A_{m,clay}}{A_{m,concrete}} \quad (6.1)$$

where:

$A_{f,clay}$ = cross area of FRP reinforcement in clay bricks panels

$A_{f,concrete}$ = cross area of FRP reinforcement in concrete block panels

$A_{m,clay}$ = net area of clay brick panels

$A_{m,concrete}$ = net area of concrete block panels

Following this procedure CLW2 was reinforced placing GFRP bars in the two faces, following an alternate pattern.

The testing of this wall showed that the amount of reinforcement calculated with equation 6.1 was not sufficient to increase the shear performance of the wall. It was observed that the wall failed suddenly right after the development of the first crack. This was attributed to the large amount of energy accumulated by the wall.

In light of this result, for the other specimens, the amount of FRP was decided in terms of ratio of the axial stiffness, which was defined as:

$$\rho = \frac{A_f \cdot E_f}{A_m \cdot f'_m} \quad (6.2)$$

where:

A_f = cross area of FRP reinforcement

A_m = net area of masonry

E_f = modulus of elasticity of FRP reinforcement

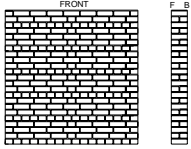
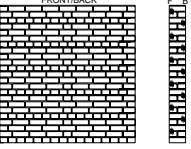
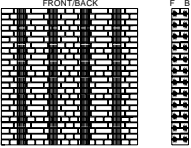
f'_m = compressive strength of masonry

For design considerations, according to MSJC Code (1999), the compressive strength of masonry must be at least 17.0 MPa (2500 psi) for clay masonry and 10.4 MPa (1500 psi) for concrete masonry.

Thus, CLW3 was reinforced placing GFRP rods and laminates on both sides of the panel in a symmetrical configuration. The strengthening layout consisted of GFRP rods every two joints and four vertical GFRP strips 1630 mm (64 in) long and 100

mm (4 in) wide. The amount of vertical reinforcement was the same used for the concrete block panel COW6 (see section 6.1, Morbin, 2001) considering that an amount of vertical reinforcement equal in terms of axial stiffness ($E_r A_f$) to the horizontal one would have been excessive. CLW4 presented the same amount of vertical GFRP laminates as CLW3 but half of the horizontal FRP reinforcement. Thus GFRP rods were placed every four mortar joints. The purpose was to observe the efficiency of the horizontal strengthening with the same amount of vertical. The last two specimens were strengthened with carbon strips. Because of its flat shape this kind of reinforcement is particularly suitable for old masonry building in which the joints are thin. The cross section is equivalent to that of a #2 rod. The amount of reinforcement was equivalent to that of CLW3 in terms of axial stiffness, but this was placed with two different patterns. For CLW5, seven horizontal strips were placed on one side of the wall and seven vertical strips were placed on the other side. For CLW6, five strips on each face were oriented diagonally equally spaced from the diagonal. The text matrix for series CLW is summarized in table 6.4.

Tab. 6.4. Test matrix for Series CLW

Specimen	Strengthening	Front Side	Back Side	Layout
CLW1	None	None	None	
CLW2	#2 GFRP bars	4HJ	4HJ	
CLW3	#2 GFRP bars 4 in GFRP laminates	2HJ/4VS	2HJ/4VS	

Tab. 6.4. Test matrix (continued)

Specimen	Strengthening	Front Side	Back Side	Layout
CLW4	#2 GFRP bars 4 in GFRP laminates	4HJ/4VS	4HJ/4VS	
CLW5	Carbon strips	3/4HC	3/4VC	
CLW6	Carbon strips	5D	5D	

LEGEND: 2HJ=every second mortar joint, 4HJ= every fourth mortar joint, 4VS= four vertical glass strips @ 16 in o.c., 3/4VC= vertical carbon strips every third/fourth mortar joint, 3/4HC= horizontal carbon strips every third/fourth mortar joint, 5D= five diagonal carbon strips simmetrically spaced from the diagonal

All the FRP strips (both glass and carbon) and rods were installed following the manual lay-up and NSM rods technique as described in Section 3.

Five strain gages were applied to the FRP reinforcement to monitor the strain distribution along the strip and the laminates in correspondence to the loaded diagonal of the panels. All the strain gages had a gage length of 12.7 mm (1/2 in) to ensure localized strain measurement. The surfaces on which they were applied were smoothed and conditioned to assure a perfect bond between strain gage and deformable support. Figure 6.8 indicate the typical strain gages location on the FRP reinforcement for the specimen CLW6 (see also Appendix B).

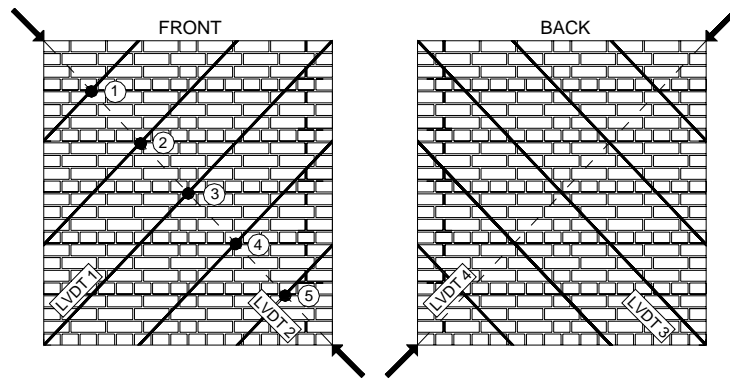
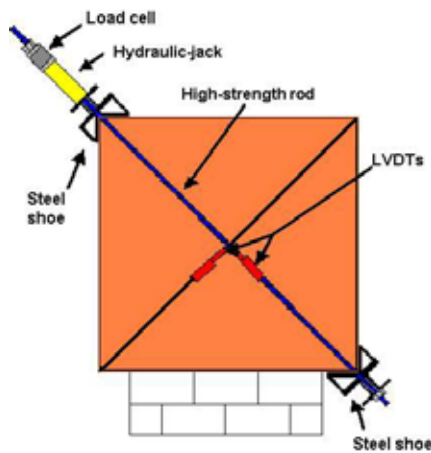


Fig. 6.8. Typical strain gages and LVDT's location

6.3. Test Setup

The specimens were tested in a close loop fashion, following the ASTM E518 standard protocol (Standard Test Method for Diagonal Tension in Masonry Assemblages). Two 30-ton-capacity hydraulic jacks activated by a manual pump were used to load the specimen along one diagonal. The force was applied to the wall by steel shoes placed at the top corner, and transmitted to similar shoes at the bottom corner through high-strength steel rods. Figures 6.9 (a) and (b) illustrate the test setup.



(a) Test setup scheme



(b) Test setup

Fig. 6.9. Test setup

The load was applied in cycles of loading and unloading, except for the control walls. An initial cycle for a low load was performed in every wall to verify that both the mechanical and electronic equipment was working properly. The data acquired by a 200 kip load cell and the Linear Variable Differential Transducers (LVDTs) were collected by a Daytronic Data Acquisition System at a frequency of one Hz. A total of four LVDTs were used to register displacements in the walls along the wall diagonals. Two LVDTs were placed on each side of the walls: one oriented along the force line to measure the wall shortening, and the other perpendicular to the force line to record the crack opening. Table 6.5 illustrates a summary of the load cycles.

Tab. 6.5. Test cycles

Cycle	Load Range [kN]
1	0-6.7-2.2
2	2.2-9.0-2.2
3	2.2-11.2-2.2
4	2.2-failure

Note: 1kN = 0.2248 kip

6.4. Test Results

Wall CLW1

This wall was selected as control specimen. After a low load cycle to verify the proper function of the monitoring instrumentation, the wall was taken to failure. Due to the brittle nature of the unstrengthened clay masonry the failure was caused by complete collapse of the loaded diagonal for splitting of the clay units. No visible cracks were detected until reaching the maximum load, which was 307 kN (69.0 kips). Figures 6.10 and 6.11 show, respectively, the load versus diagonal displacement behavior of the wall and a picture of the specimen after failure. In all the graphs, the positive displacement corresponds to the loaded diagonal.

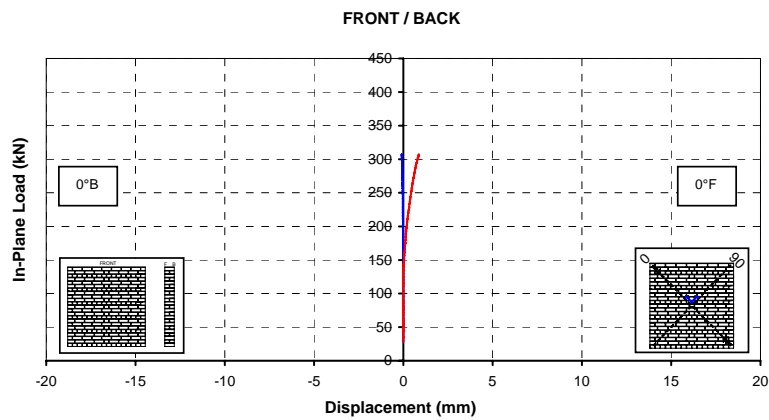


Fig. 6.10. Load vs. diagonal displacement



Fig. 6.11. Wall CLW1 after failure (front)

Wall CLW2

Wall CLW2 was strengthened with GFRP rods every two mortar joints distributed on the two faces of the panel. The peak load was reached at 306 kN (68.9 kips), less than the control wall and without showing any ductile behavior. This fact may be attributed to undesirable variables such as handwork or mortar workability. However, in this case, the GFRP rods had no effect in terms of increasing the shear capacity. The rods embedded in the joints provided the unique function to hold the wall at the ultimate stage. Figures 6.12 and 6.13 show, respectively, the load versus diagonal displacement behavior of the wall and a picture of the specimen after failure. During the test, the readings of the LVDTs in 90° directions were lost.

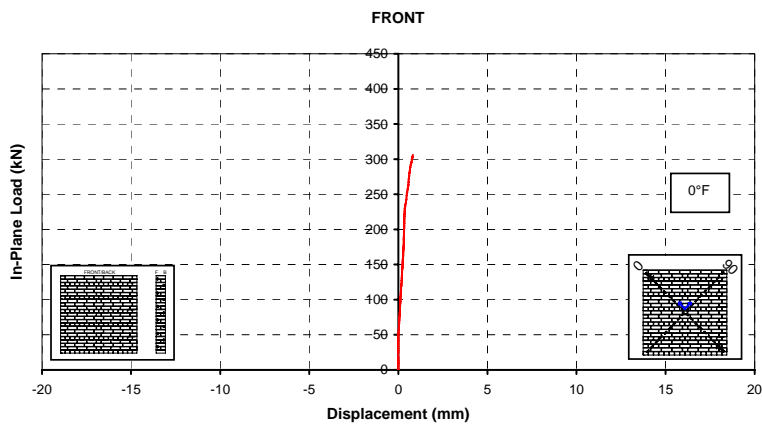


Fig. 6.12. Load vs. diagonal displacement



Fig. 6.13. Wall CLW2 after failure (front)

Wall CLW3

In Wall CLW3, the reinforcement was equally distributed in the horizontal and vertical direction. GFRP rods were used in the horizontal direction; whereas, GFRP laminates were used in the vertical direction. The first visible cracks were detected along the diagonal mortar joints and in the clay units at 300 kN (67 kips). The peak was reached at 406 kN (91 kips). The specimen, when compared to the control wall, exhibited a significant ductile behavior, which allowed the panel to keep the maximum load for a mean tensile displacement of 7.3 mm (0.29 in). Figures 6.14 and 6.15 show, respectively, the load versus diagonal displacement behavior of the wall and a picture of the specimen after failure.

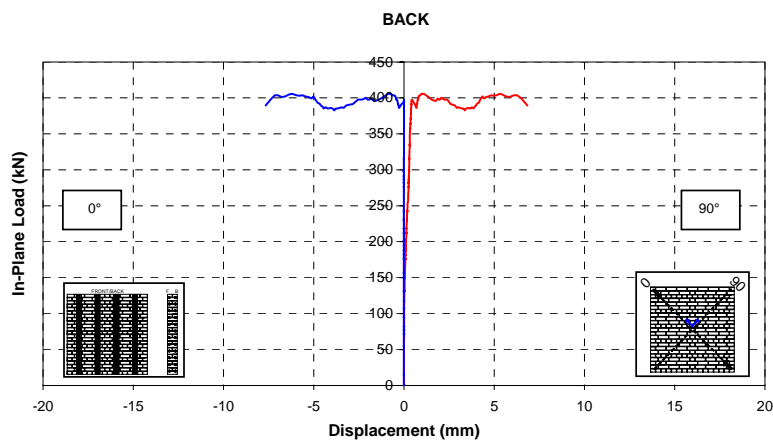


Fig. 6.14. Load vs. diagonal displacement

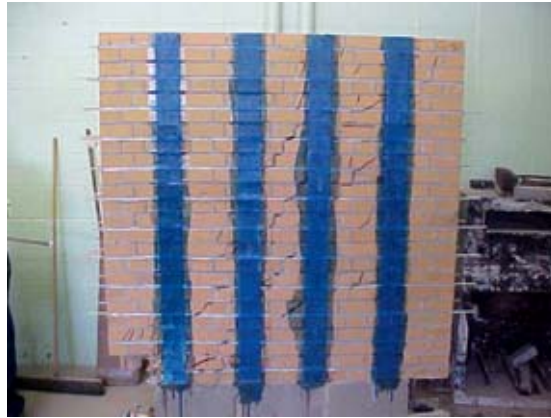


Fig. 6.15. Wall CLW3 after failure (front)

Wall CLW4

Wall CLW4 was strengthened with the same amount of vertical reinforcement of CLW3 but half amount of the horizontal reinforcement. Even though the increase of capacity and the ductile behavior observed for this specimen were less significant than the ones observed for wall CLW3, no substantial differences in the mechanical behavior during the load cycles and in the mode of failure were observed. The collapse was caused by the progressive debonding between the epoxy-based paste in the reinforced joints and the clay unit surfaces, which started from the loaded diagonal. Delamination of the GFRP laminates was also observed. The peak load was 319 kN (72 kips). Figures 6.16 and 6.17 show, respectively, the load versus diagonal displacement behavior of the wall and a picture of the specimen after failure.

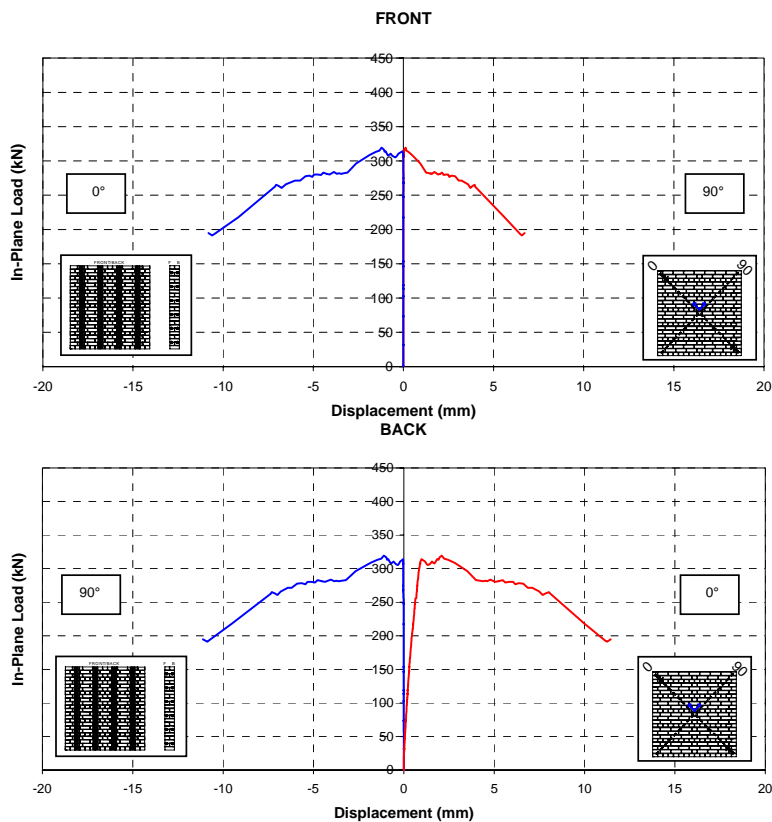


Fig. 6.16. Load vs. diagonal displacement



Fig. 6.17. Wall CLW4 after failure (front)

Wall CLW5

Wall CLW5 was strengthened with CFRP tapes strips. Due to the higher modulus of elasticity of this material, the amount of reinforcement in terms of axial stiffness was achieved with a lower number of strips. This wall was strengthened with seven horizontal tapes placed on one side of the wall and seven vertical tapes placed on the other side. The tapes were symmetrically spaced from the horizontal and the vertical axis.

Due to the high strength of the reinforcement, problems were encountered during this test. Failure due to diagonal cracking of the wall was not observed because of the sudden crushing of one corner of the specimen. This was caused by the fact that the contact area of the steel shoes used in the setup were not big enough to spread the high pressures originated by the diagonal load. Because of this problem, it was not possible to record the data needed to plot the load versus displacement graph up to shear failure.

However, the peak recorded before the corner crashed was 412 kN (93 kips), and the opening of fine cracks was also detected on the lower part of the wall. Figures 6.18 and 6.19 show, respectively, the load versus diagonal displacement behavior of the wall and pictures of the specimen after failure and of the crushed corner.

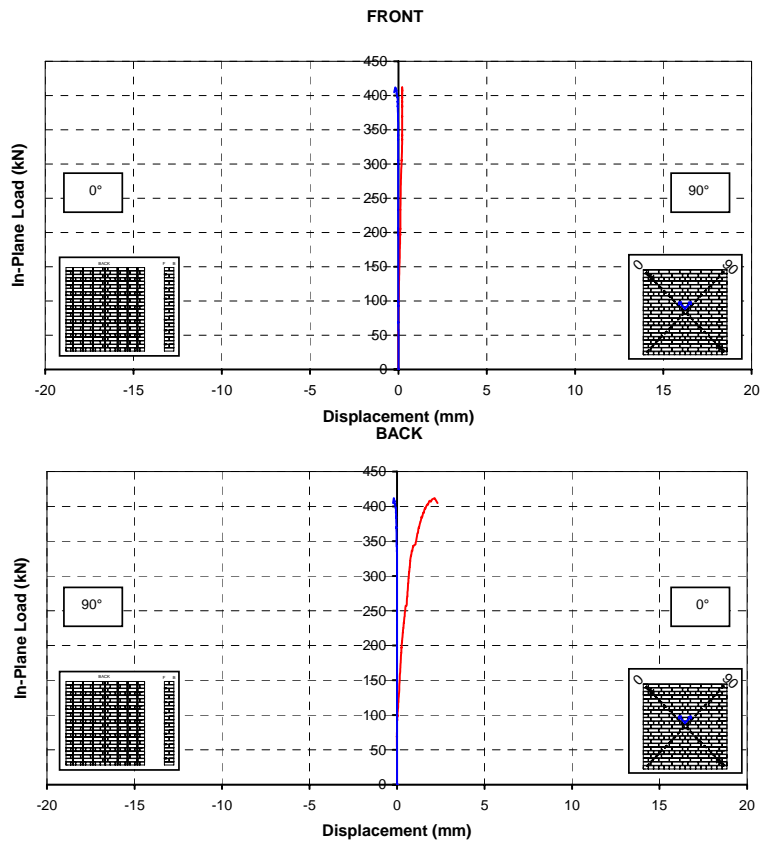


Fig. 6.18. Load vs. diagonal displacement



(a) Wall CLW5 after being tested (front)



(b) Crushing of the corner (back)

Fig. 6.19. Wall CLW5 after failure

Wall CLW6

Wall CLW6 was strengthened with five CFRP tapes on each face oriented diagonally and equally spaced from the diagonal. Because of the problems that occurred during the testing of Wall CLW5, the surface of the steel shoes were increased to spread the load on a larger masonry surface to avoid crushing of the corners. This led to an increment of the cross section of the diagonal compression strut. For this reason, the results obtained are plotted in a different plotting region and the graphs are not comparable with the one previously illustrated. After being tested, the wall did not show visible cracks. The two hydraulic jacks used to apply the load were not able to reach the failure load of the strengthened specimen. The peak was 591 kN (133 kips). Figures 6.20 and 6.21 show, respectively, the load versus diagonal displacement behavior of the wall and a picture of the specimen after failure.

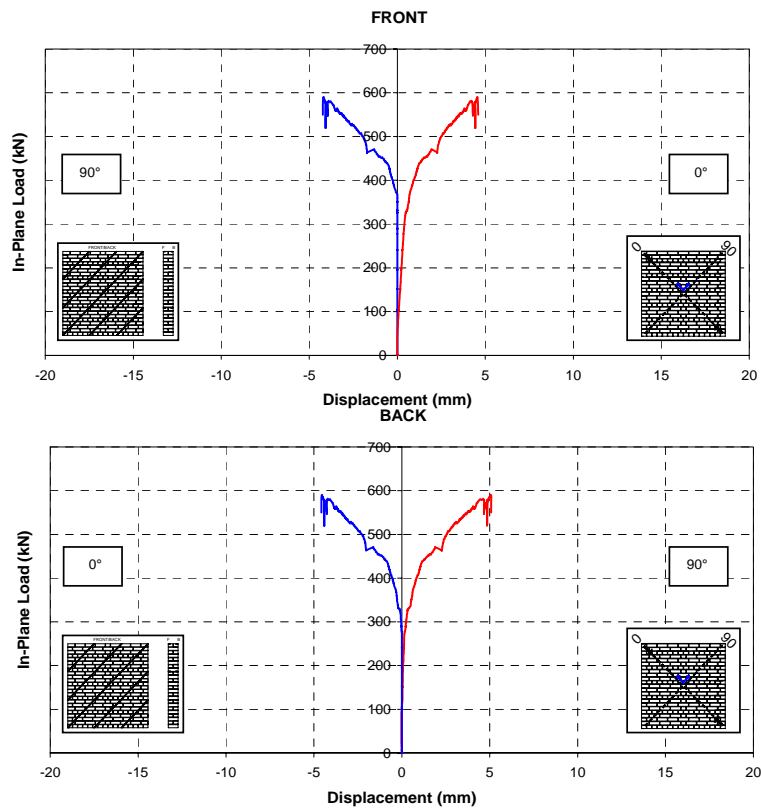


Fig. 6.20. Load vs. diagonal displacement



Fig. 6.21. Wall CLW6 after failure (front)

6.5. Mechanism of Failure

A critical in-plane mechanism of failure was detected in all the clay unit panels strengthened with GFRP rods and laminates. Test results demonstrated that in walls built with clay units, sliding shear failure is not observed. This can be attributed to better bonding between clay units and mortar. Wall CLW1 failed for splitting of the clay units, as observed in figures 6.22 (a) and (b).



(a)



(b)

Fig. 6.22. Splitting of clay units in wall CLW1

In CLW3 and CLW4 no substantial differences were observed in terms of development of cracks and mechanism of failure, which could be divided in two different phases that occurred at the same time:

- **Horizontal phase:** When the tensile strength of masonry is overcome, the wall cracks along the diagonal, following the mortar joints (stepped crack vertical/horizontal, see figure 6.23). For the reinforcement placed in the horizontal joint, the crack is typically at the top side (see item 1 in figure 6.23). Wall failure occurs only for a progressive loss of bonding due to a second crack, which develops in this case above and below the reinforcement at the epoxy/brick interface (see item 2 in figure 6.23).

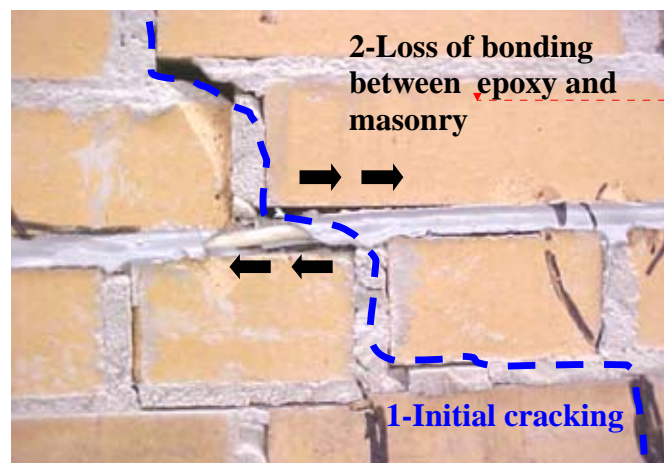


Fig. 6.23. Horizontal phase

- **Vertical phase:** Once the major diagonal crack is formed, simultaneously to the horizontal, a vertical phase, consisting of the progressive delamination of the GFRP sheets from the clay surface, starts moving from the loaded diagonal to the upper or lower borders of the panel. As described in section 4, it is assumed that an effective bonded length exists for Aramid but also for Glass fibers, and once the delamination occurs, it starts spreading to the

boundaries. Figure 6.24 shows the delamination of the GFRP laminates from clay surface.



Fig. 6.24. Delamination of GFRP laminates

Wall CLW2 was reinforced only with GFRP rods and no vertical reinforcement in the form of GFRP laminates was applied. Due to the presence of a low amount of GFRP rods, the wall did not exhibit more shear capacity compared to the control wall CLW1, but failed for the occurring of the horizontal phase previously explained. In order to achieve a significant increment in shear capacity, utilizing for an aesthetic purpose only the FRP Structural Repointing technique, a larger amount of glass rods embedded in the mortar joints should be provided for clay walls.

CLW4 exhibited the lowest shear capacity due to significant imperfections detected during the tests such as a large number of thick mortar joints and great differences in the mortar workability. For further researches, these types of imperfections that affected the average shear capacity should be avoided.

In the specimens strengthened with carbon tapes the mechanism previously described was not detected. For wall CLW5, the failure was due to the high stresses developed in the cross section of the diagonal compression strut that caused the crushing of the corner. Before failure, some slight cracks were developed and detected in the lower part of the panel.

The specimen reinforced with diagonal carbon strips (CLW6) showed no visible cracks after being tested and the data recorded by the strain gauges (see appendix B) showed that the strips worked up to 50% of the ultimate strain.

Figure 6.25 shows the cracks (highlighted with a marker) detected in the lower part of wall CLW5 after the test.

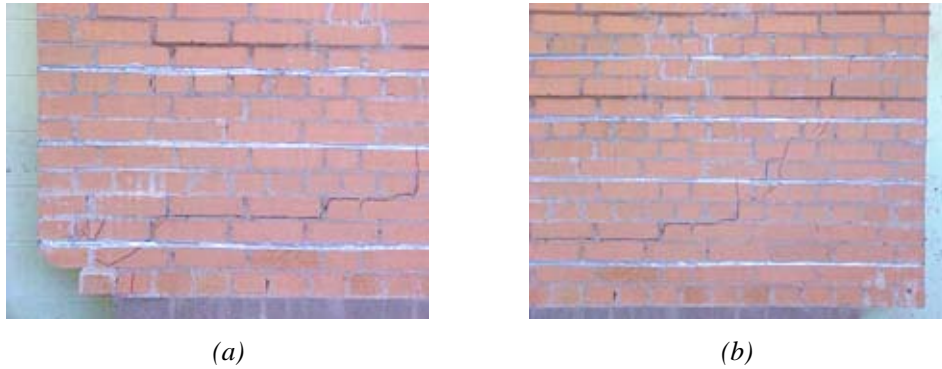


Fig. 6.25. Cracks detected in wall CLW5

The test setup configuration did not allow estimating ductility as conventionally done ($\mu = \delta_u / \delta_y$), where δ_u and δ_y are, respectively, the horizontal displacements at ultimate and “yielding” caused by an in-plane load. Instead, a criterion using the shear strain was adopted. Thus, the pseudo-ductility, ‘ μ ’, was quantified as the ratio γ_u / γ_y , where γ_u is the shear strain at ultimate and γ_y is the shear strain, corresponding to the point where the in-plane load vs. shear strain curve tends to be flat. Considering the strains generated by the diagonal in-plane load as principal strains, the maximum shear strain is expressed as:

$$\gamma = |\varepsilon_0| + |\varepsilon_{90}|$$

where ε_0 and ε_{90} are the strains associated with the shortening and lengthening of the wall diagonals.

In table 6.6 a comparison of the pseudo-ductilities is presented: the most strengthened specimens showed the highest values.

Tab. 6.6. Comparison of Pseudo-ductility for Series CLW

Specimen	In-Plane Load [kN]	γ_u [°]	γ_y [°]	μ
CLW1	307	0.03	0.03	1.0
CLW2	306	0.02	0.02	1.0
CLW3	406	0.38	0.05	7.6
CLW4	319	0.6	0.09	6.7

Note: 1kN = 0.2248 kip

The results regarding the specimens CLW5 and CLW6 are not included in table 6.6 because of the problems encountered during the test as previously described.

6.6. Conclusions

Overall, results for clay brick panels showed remarkable increases in shear capacity ranging between 4% and 30%. These percentages of increasing are lower than the one recorded for the concrete block panels (from 30% to 80%) (Morbin, 2001) because of different masonry characteristics (i.e. compressive strength) and wall geometries (i.e. number of wythes and number of layers).

The evaluation of the pseudo-ductilities demonstrates the effectiveness of the reinforcement. Increments in the amount of reinforcement led to increments in pseudo-ductility.

For the strengthened specimens, two different failure phases were identified: vertical and horizontal. Sliding shear failure was not observed in all the tested panels.

Due to the high compressive strength of clay masonry, and in order to have an effective strengthening in terms of shear capacity and ductility, a lower limit for FRP reinforcement should be identified. Under this limit, the reinforcement should not increase the shear capacity of the URM walls.

From the experimental evidences it can be said that the walls strengthened with carbon tapes showed significant increments of shear capacity ranging between 34% and 93% when compared to the control wall. Increments up to 46% in comparison with the specimen strengthened with GFRP laminates and rods were observed.

However, further experimental data obtained with a different test setup are needed to determine the real shear capacity and the load versus displacement behavior up to failure for the specimens strengthened with carbon tapes.

In contrast to URM walls, all the strengthened walls were stable after failure. In a real building, this fact can avoid injuries or loss of human life due to collapse.

7. POST - TENSIONING

7.1. Background

Post-tensioning is a method of reinforcing (strengthening) concrete or other materials with high-strength strands or bars, typically referred to as tendons. Post-tensioning applications include office and apartment buildings, parking structures, slabs-on-ground, bridges, sport stadiums, rock and soil anchors, and water-tanks. In many cases, post-tensioning allows construction that would otherwise be impossible due to either site constraints or architectural requirements.

A post-tensioning “tendon” is defined as a complete assembly consisting of the anchorages, the pre-stressing strand or bar, the sheathing or duct and any grout or corrosion-inhibiting coating (grease) surrounding the pre-stressing bar. There are two main types of post-tensioning: unbonded and bonded (grouted).

An unbonded tendon is one in which the pre-stressing bar is not actually bonded to the structure that surrounds it except at the anchorages.

In bonded systems, two or more strands are inserted into a metal or plastic duct that is embedded inside the structure. The strands are stressed with different techniques and anchored in an anchorage device. The duct is then filled with a cementitious grout that provides corrosion protection to the strand and bonds the tendon at the structure surrounding the duct.

In order for a pre-stressing tendon to be viable, it must attain and sustain the applied stresses. This ability relies on an anchorage system that is capable of developing the high levels of load without causing significant distress to the tendon that may result in failure. In the case of post-tensioning, the anchors must also be capable of sustaining these loads for the life of the structure. Anchorages for conventional steel pre-stressing strands typically employ a steel wedge to grip and secure the tendon (Nilson, 1987). The wedges commonly are serrated and grip the tendon or button-heads on the end of the steel tendon (Holte et al., 1993). The isotropy and strength of

the strand material are two of the main characteristics making this particular anchoring system feasible.

Uniaxially-reinforced FRP materials are highly anisotropic and show marked differences in strength and stiffness responses in directions parallel to and transverse to the fiber orientation. In order to accurately predict failure, special attention must be paid to areas of the material subjected to combined stresses, such as bends in stirrups, grid intersections and near tendon anchorages (Bank, 1993).

A major problem facing the use of fiber reinforced polymers (FRPs) in pre-stressing applications is the anchorage.

Issues like damage to the bars due to excessive grip force and slip of the bars out of the anchorages caused by weak friction forces and high tensile stress, clearly show that traditional methods for gripping metal rods, are not applicable for FRP bars.

Figure 7.1 illustrates the traditional anchors for metal rods.

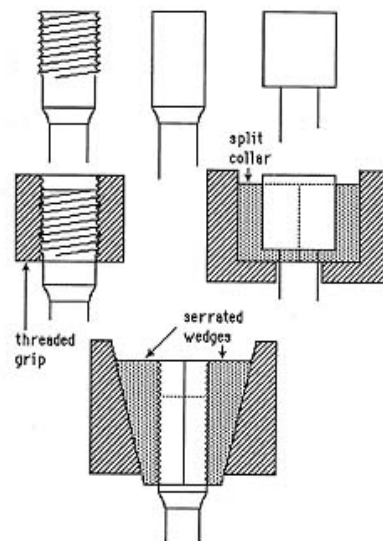


Fig. 7.1. Traditional anchor system for metal bars

Until recently, many anchorages included epoxy resins or expansive cements within the body of the system. The creep of these materials can make these anchorages inadequate for many applications through loss of pre-stress load with time.

On the other side, wedge systems that do not use resins are preferable if they do not cause premature failure of the tendon from their gripping action.

In wedge type anchors, failure is induced by the high shear at the leading edge of the wedge.

To take into consideration and solve the aforementioned problems, a variety of anchor system has been developed and in the following pages an overview of different commercially available FRP system and associated anchoring devices is reported. In general, the anchor devices are often supplied by producers for the same FRP tendons.

- *Arapree (ARAmid PREstressing Element)*

Arapree consists of round diameter 12 μm aramid filaments (Twaron) embedded in epoxy resin. There are two types of Arapree elements: one with a rectangular cross section and one with a circular cross section. Both consist of up to 400,000 aramid filaments. The former may be easier to grip with a wedge anchor system (Gerritse and Werner, 1988).

The systems developed for anchoring Arapree, both flat and round types, consist of a metal sleeve into which the tendon is either grouted (post-tensioning application) or clamped between two plastic wedges encased in an outer steel body. This system is made up of a terminal body comprised of steel and two semi-cylindrical tapered wedges of Polyamide.

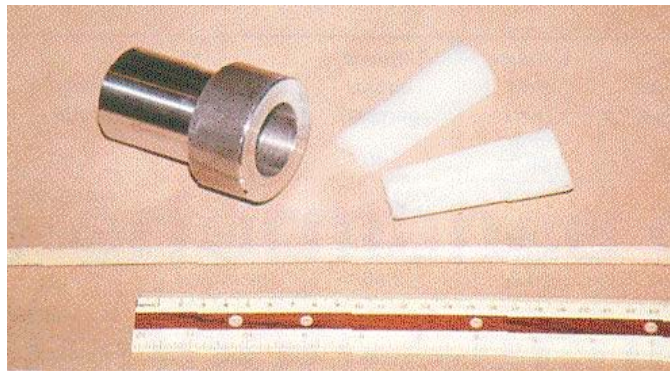


Fig. 7.2. Arapree tendon and anchor components

This anchoring system was designed for use primarily as pre-tensioning anchors. The manufacturer's literature states that another anchorage type consisting of a steel tube

filled with a cement mortar bond material was developed for long-term use (Gerritse and Werner, 1988).

The outer surface of the wedges and the inner surface of the metal terminal are non-coated. The inner surface of the wedge trough which holds the tendon is similarly smooth and gripping of the tendon rests solely on the frictional resistance provided by the plastic.

- *FiBRA (Fiber BRAiding)*

Mitsui Construction Company (MCC) produces an FRP tendon known by the trade name FiBRA. FiBRA is a continuous fiber rod formed by braiding high strength fibers in an epoxy resin. FiBRA rods have been used as reinforcement for concrete, soil or rock, and as pre-stressing tendons (Tamura, 1993).

FiBRA has two different types of anchoring systems: the R-type resin anchor used for single tendon anchoring, and the W-type wedge anchor for either single or multiple tendon anchoring. The resin anchor consists of a single tendon epoxied to a cylindrical steel cylinder. This cylinder is threaded on the exterior surface to allow securing with a simple nut.

The second pre-stressing anchorage is a steel wedge-type anchor. The steel anchor is comprised of four wedge units that slip inside a steel cylinder with a conical interior surface.

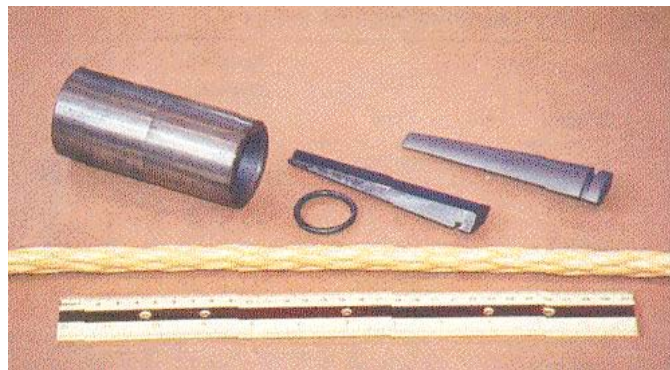


Fig. 7.3. FiBRA tendon and anchor components

Grit is applied to the inner surface of the wedges for better tendon gripping. The exterior surface, and the interior surface of the steel cylinder, is coated with a dry lubricant to assist in seating and removal of the anchor.

- Carbon Stress

Carbon Stress is the trade name for a prestressing tendon.

Both flat bars with rectangular cross sections and round bars with circular cross sections are currently available. Both bars are formed through pultrusion of carbon fibers with a binding matrix. The flat bar is dimpled with a hatched pattern to create a better bonding surface. The round bar is sanded to increase its bond characteristics.

Carbon Stress is similar in manufacturing to Arapree and employs similar anchoring devices.

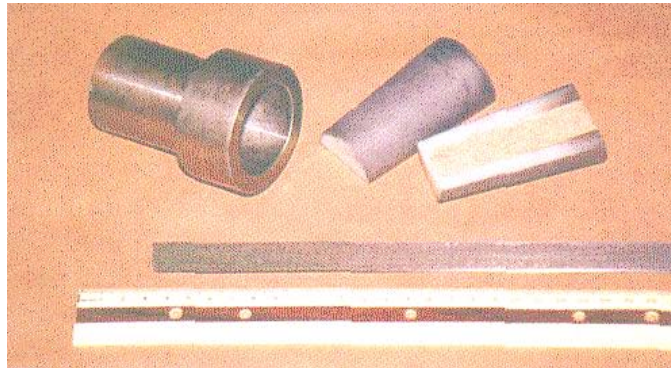


Fig. 7.4. Carbon Stress tendon and anchor components

A difference is in a dry lubricant coating on the exterior surface of the plastic wedges to assist in better setting of the wedges. This also aids in removal of the wedges after use. In addition, wedges for flat tendons are prepared by the manufacturer with a sanded surface for better gripping. The wedges for the round tendons come with instructions to apply a layer of epoxy and sand into the groove, which holds the tendon. In both cases, the function of the sand coating is to increase the gripping capability of the anchor.

- Leadline

Leadline is a carbon-based FRP rod, which is suitable for pre-stressing and ground anchor applications.

Several different varieties of surface deformations exist for the Leadline product. Smooth rods have no surface deformations. Indented rods have two shallow helical cuts in the surface that spiral in opposite directions continually down the length of the rod. The ribbed tendon has either raised helical windings similar to the indented pattern or a circumferential winding transverse to the longitudinal axis of the rod.

Leadline utilizes a modified wedge system to anchor the tendons. The modification comes in the form of a special metal sleeve, which fits between the wedges and the tendon to reduce the severity of shearing stresses induced in the rod by the wedges. The sleeve has four independent arms, which extend along the length of the tendon. The wedges are then placed around the sleeve such that the space between the wedges falls over the solid portion of the sleeve. A plastic film is placed around this to secure the multiple pieces together for insertion into the terminal body.



Fig. 7.5. Leadline tendon and anchor components

- Technora® Rods

Named for the brand of aramid fiber used in its manufacture, Technora® is a spiral wound rod that was developed as a substitute for high tensile strength steels. Bundles of aramid fibers impregnated with a vinyl ester resin are pultruded into rods, and hardened (Mukae et al., 1993).

Manufacturing a spiral wound tendon begins by impregnating a straight bundle of aramid fibers with vinylester resin and pulling the material through an unheated die to consolidate the composite. An identical fiber is wound spirally around the bundle of fibers to produce a deformed surface. Three longitudinal fiber bundles are added to the outer surface and a second spiral winding is added to secure these longitudinal fibers. The resin is then cured without pressure in an oven.

The Technora® tendons employ either wedge type or grout type anchorages. Anchorages for single rods and multiple bundles of rods numbering from 3 to 19 rods are available. The bond type anchors have been developed for use with the spiral wound rods, and are constructed so that the rod is inserted into a housing and then fixed with injected mortar. A screw thread is cut into the outer surface of the housing and the anchoring is secured with a nut.

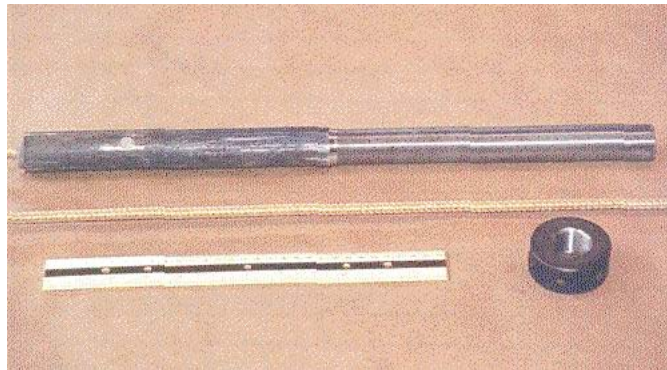


Fig. 7.6. Technora tendon and anchor components

- CFCC (Carbon Fiber Composite Cable)

Carbon Fiber Composite Cable (CFCC) is formed by twisting a number of strands of carbon fibers, much as conventional stranded steel tendon is manufactured.

The manufacturing process of CFCC begins with forming a prepreg consisting of 12,000 filaments impregnated with resin. The prepreg is then twisted to form a core of fibers, which is covered with a wrapping of synthetic yarns. These rods are then stranded to form a composite body, which is finally heated and cured. This process results in a single rod, which may be used singly, or combined in sets of seven, nineteen or thirty-seven to form multiple strand cables. The multiple strand cables

are twisted to better distribute forces throughout the cross section. The yarn covering protects the core from UV radiation and mechanical damage while simultaneously increasing bond characteristics (Erki and Rizkalla, 1993).

CFCC anchoring methods are classified as resin filling and diecast methods (Santoh 1993). The anchoring systems are chosen based on intended applications. The resin filling method bonds the cable to a steel cylinder utilizing a high performance epoxy. These tubes can be threaded, as necessary, to allow anchoring with nuts. The length of the fixing metal piece is resin dependent but the standard length is 13.5 times the CFCC diameter. The outer diameter of the cylinder varies by the material used.



Fig. 7.7. CFCC tendon and anchor components

The diecast method attaches the cable to a steel tube by means of a bronze alloy. Steel wedges are then utilized to clamp the cables to an anchor system much like steel cable systems.

- Lightline

This FRP tendon is stranded from individual Lightline rods, creating a twisted cable made up of seven individual rods (one central rod surrounded by six rods), mimicking a conventional 7-wire steel strand. The Lightline cable is a composite of E-glass and epoxy. The tendon is manufactured under a proprietary process that ensures a high degree of fiber alignment.

A resin-potted anchor with a parabolically tapered interior surface was chosen as the anchoring system. This steel anchor is threaded on the outside to receive a matching nut.

The anchor is an alternate design to the linearly tapered cone anchors currently available in industry. The parabolic taper has been demonstrated under laboratory investigation to reduce the peak shear stresses encountered at the front edge of linearly tapered anchors (Holte et al., 1993).

The preparation of the anchor for use with the Lightline tendon involved several steps as described in the literature.

- *Parafil (PARAllel FILaments)*

Linear Composites, Ltd. Yorkshire, England, is the producer of a parallel-lay rope composed of Kevlar high strength yarns or fibers contained within a protective polymeric sheath.

A variety of core yarns are used, the most common being polyester (known as Type A), Kevlar 29 (Type F) and Kevlar 49 (Type G). Those of primary interest for pre-stressing are the Type G ropes, which have the highest stiffness and lowest tendency for creep (Burgoyne, 1993).

The elimination of the resin leaves the possibility for a greater percentage of the cross-sectional area of this tendon to be fiber material. This advantage is balanced, however, by the decreased efficiency of the system due to lack of stress transfer resulting from resin impregnation.

Parafil has several features that distinguish it from most other pre-stressing systems: it cannot be bonded to concrete; it contains no resin; and it was not initially developed for pre-stressing. Nevertheless, it has been used for pre-stressing concrete on a number of occasions.

Parafil ropes are anchored by means of a barrel and spike fitting that grips the fibers between a central tapered spike and an external matching barrel. It has been suggested that aluminum alloy, galvanized mild steel, stainless steel and other

materials could be used for the anchors since this scheme takes advantage of the fibers of the rope simply being tightly packed in the protective outer sheathing.



Fig. 7.8. Parafill tendon and anchor components

Other particular anchors for different kinds of FRP tendons have been designed.

In the system developed by Rahman et al. (1993), epoxy paste is used to embed the bar end into an internal threaded bar.

Another system developed at West Virginia University consists of a 203.2 mm (8 in) long steel tube, with an internal diameter equal to that of the FRP bar, which is cut lengthwise into two pieces. The inner surfaces of the split tubes are roughened by sand blasting and coated with an epoxy adhesive. The tubes are then clamped to the FRP rod until the resin is cured. An extensive experimental study was carried out by Castro and Carino, (1998), in which the epoxy paste was substituted with a cement mortar.

Figure 7.9 shows the anchor systems developed by Rahman (a), by the West Virginia University (b) and the one developed by Castro and Carino (c).

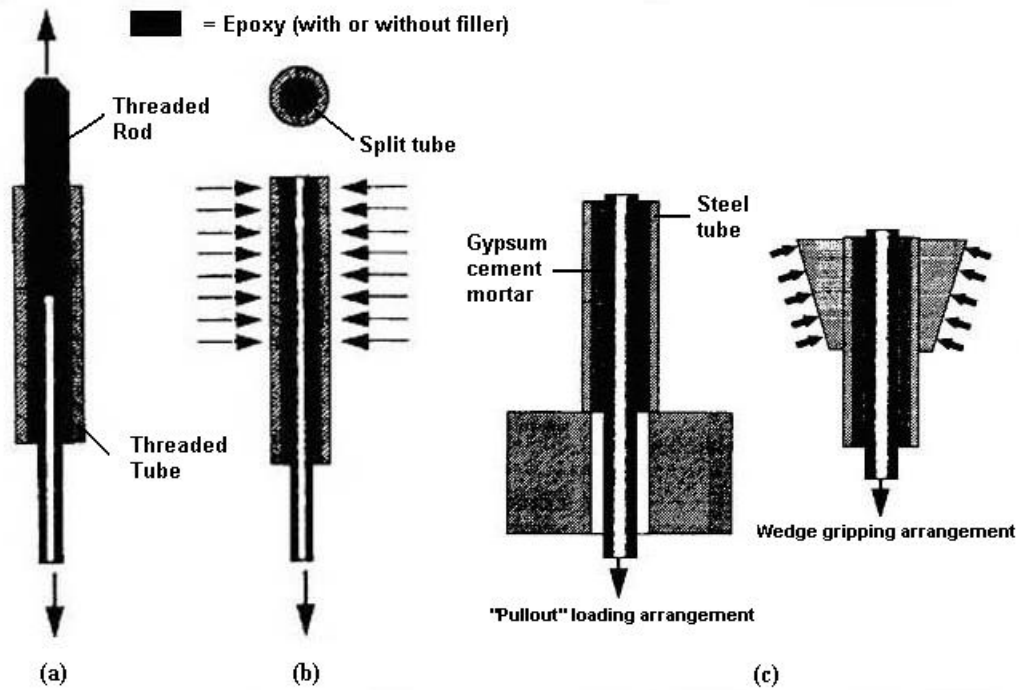


Fig. 7.9. Anchor systems used for FRP tendons

In this section, a new anchor system for the tensioning of GFRP bars used for structural strengthening will be described.

7.2. Tensioning and Anchor Devices

This post-tensioning technique addresses the solution of the tensioning problems of FRP bars used to take the place of steel rods for structural strengthening.

The bars can be manufactured with any fiber type embedded in a thermoplastic resin. The idea is based on the thermoplastic properties of the resin and consists of creating two temporary anchors at the end of the bar; with these anchors and a screw device the proper amount of tension can be introduced into the bar.

After this tensioning operation, one can bond the bar to the structure with any method used for composite materials such as Near Surface Mounted rods (Section 3.2) or drilled hole through transverse walls filled with epoxy-based paste.

This feature is very important particularly for historical masonry buildings, in which the strengthening system must be the least visible as possible.

All the devices were designed in order to obtain items easily machinable and that can be reused for several post-tensioning operations by removing them after the bar is bonded to the structure.

The first drawings for machining all the needed mechanical components consisted of eight steel items specifically designed for this particular post-tensioning technique.

The figure 7.10 shows all the items: (a) chuck; (b) teflon washer; (c) nut; (d) and (e) spreaders of load; (f) threaded pipe; (g) thrust bearing; (h) wedge.

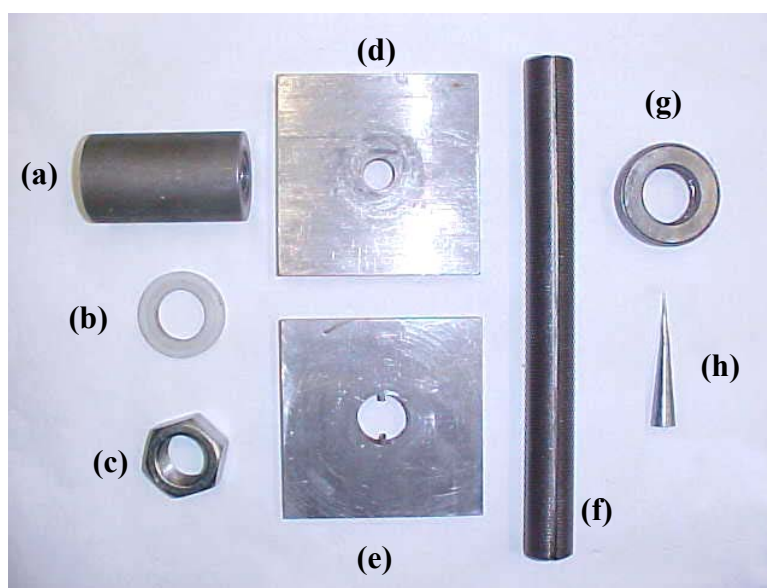


Fig. 7.10. Steel items

In order to anchor the rods, the thermoplastic properties of the resin used to pultrude some of the FRP bars available on the market, were taken into account.

Thermoplastic materials have the characteristic of becoming soft once they reach the glass transition temperature (T_g) and harden again once the source of heat is removed. To utilize this feature, a rope heater was used; it is a particular kind of heater that can be wrapped around objects even with small diameters.

The general procedure to load the GFRP bars used in these tests is described below. The first step consisted of heating one end of the bar with the rope heater. To reach and steadily maintain the T_g , the heater was connected with a temperature controller and a thermocouple that were able to switch off the rope heater when the temperature

was above the T_g and to switch it on again once the temperature was below the chosen threshold.

The main characteristics of the bars used are summarized in table 7.1.

Tab. 7.1. Material properties for GFRP G1 Rods

GFRP G1 RODS	
Ultimate Stress [MPa]	924
Modulus [MPa]	42574
Ultimate Strain	0.0217
T_g [°C]	138

Note: 1 Mpa = 145 psi

The amount of time needed to soften the end of the rod was between 210 and 240 seconds (data provided by the manufacturer of the rods). Both the temperature and the time to soften the rod should not be higher or lower than the aforementioned values, to avoid an excessive or an insufficient softening of the material that could cause problems at the moment of the insertion of the wedge.

Once the bar termination was soft, the rope heater was removed, and the steel wedge was gently driven into the bar by hand or hammer so as to avoid large cracking of the bar.

The softening of the thermoplastic resin enabled expansion of the bar as the wedge was driven into the end of the bar. This expansion was necessary for the bar to be anchored in the chuck (figure 7.12 (d)).

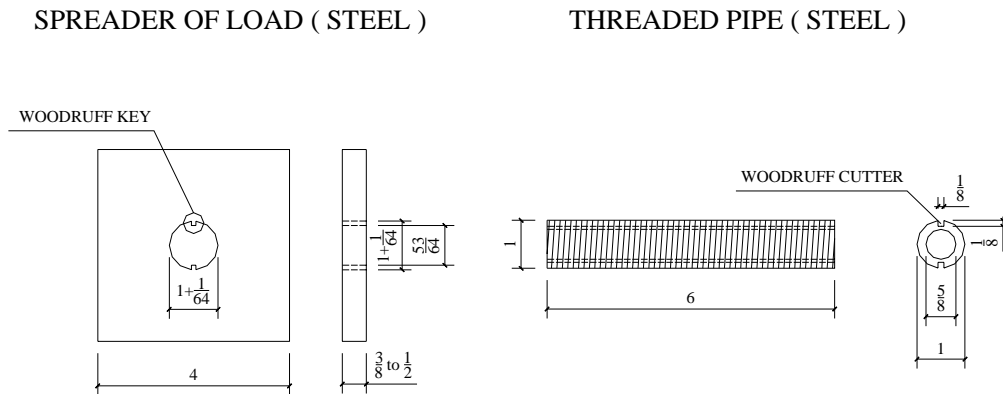
When the termination was cold again, the second step involved inserting the items to set up the dead end and the live end of the anchor system, in the following order:

for the dead end only the first chuck, the pipe, the first spreader of load (see figure 7.10 (d)) were inserted, and then, for the live end, the second spreader of load (see figure 7.10 (e)), the threaded pipe, the thrust bearing or the teflon washers, the nut and the second chuck were needed.

Now, repeating the first step, the insertion of the second wedge was done and when the FRP bar was cold, the rod was ready to be loaded by tightening the nut with a wrench. To avoid torsion stresses in the bar during the procedure of loading, caused by friction between the nut and the pipe, a “*woodruff key*” and a “*woodruff cutter*”

were machined respectively on one of the two spreaders of load and on the threaded pipe.

Figure 7.11 illustrates the loading procedure and the design drawings for the spreader of load and for the pipe.

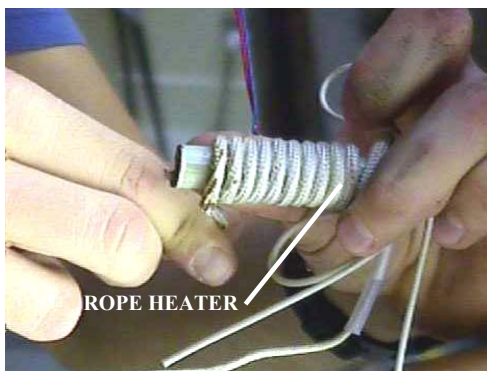


Note: 1 inch = 25.4 mm

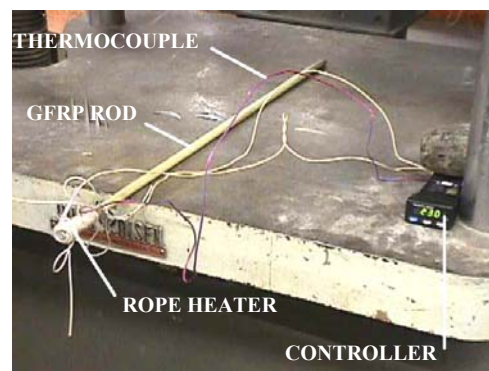
Fig. 7.11. Design drawings for spreader plate and threaded pipe

After loading, the bar can be positioned and embedded with an epoxy-based paste into a previously prepared groove in the structure. This installation could follow the steps of the NSM rods or by drilling a hole in the transverse wall and embedding only the end of the bar, as is often used for masonry bell towers.

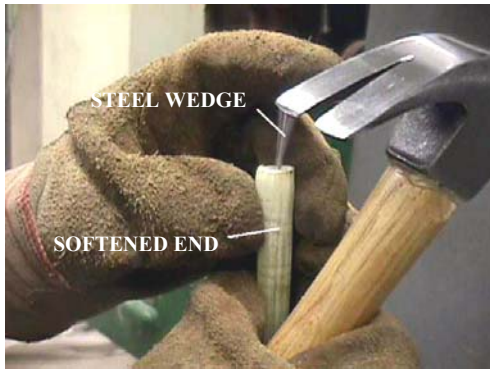
Figure 7.12 shows the general procedure for loading the FRP bars in all the different phases.



(a) Wrapping the bar



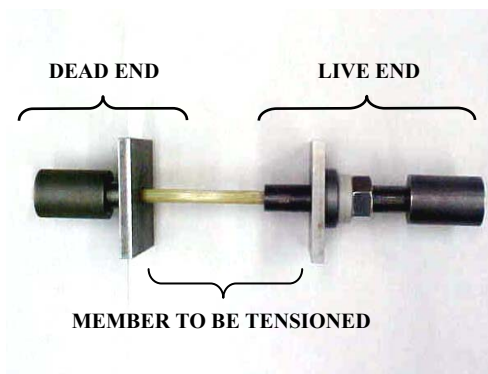
(b) Thermal setup



(c) Insertion of the wedge



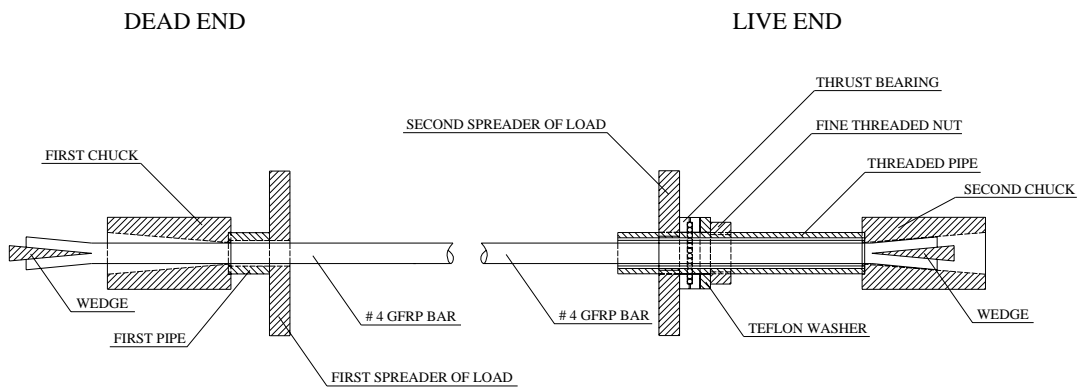
(d) Anchoring of the bar in the chuck



(e) Assembled items: details in (g)



(f) Loading procedure



(g) Assembled items

Fig. 7.12. General procedure for loading: different phases

Some tensile tests were performed in order to check the reliability of the anchors.

According to the specification of the ACI 440, because long-term exposure to various type of environments can reduce the tensile strength and creep rupture and fatigue endurance of FRP bars, the material properties used in design equations should be reduced based on the type and the level of environmental exposure.

The following equation gives the tensile properties that should be used in all design equations. The design tensile strength should be determined by:

$$f_{fu} = C_E \cdot f_{fu}^* \quad (7.1)$$

Where:

f_{fu} = design tensile strength of FRP, considering reductions for service environment;

C_E = environmental reduction factor, given in table 7.2 for various fiber type and exposure conditions;

f_{fu}^* = guaranteed tensile strength of an FRP bar defined as the mean tensile strength of a sample of test specimens minus three times the standard deviation ($f_{fu}^* = f_{u,ave} - 3\sigma$).

Tab. 7.2. C_E factor for various fibers and exposure conditions

Exposure Condition	Fiber Type	Environmental reduction factor, C_E
Concrete not exposed to earth and weather	Carbon	1
	Glass	0.8
	Aramid	0.9
Concrete exposed to earth and weather	Carbon	0.9
	Glass	0.7
	Aramid	0.8

Furthermore, to avoid failure of an FRP reinforced member due to creep rupture of the FRP, stress limits should be imposed on the FRP reinforcement.

Values for safe sustained stress levels are given in table 7.3. These values are based on the creep rupture stress limits stated in the ACI 440 (section 3.3.1) with an imposed safety factor.

Tab. 7.3. Creep rupture stress limits in FRP reinforcement

Fiber type	Glass FRP	Aramid FRP	Carbon FRP
Creep rupture stress limit, $F_{f,s}$	$0.20 f_{fu}$	$0.30 f_{fu}$	$0.55 f_{fu}$

Assuming the following values:

$$f_{fu}^* = 924 \text{ MPa (134000 psi) (Section 4.1.10)}$$

$$C_E = 0.8$$

Diameter of the bar = $\phi = 12 \text{ mm (0.472 in)}$

The stress limit for the Glass FRP bars used was:

$$F_{f,s} = 0.20 \cdot C_E \cdot f_{fu}^* = 148 \text{ MPa (21460 psi)}$$

Which corresponds to an axial load equal to:

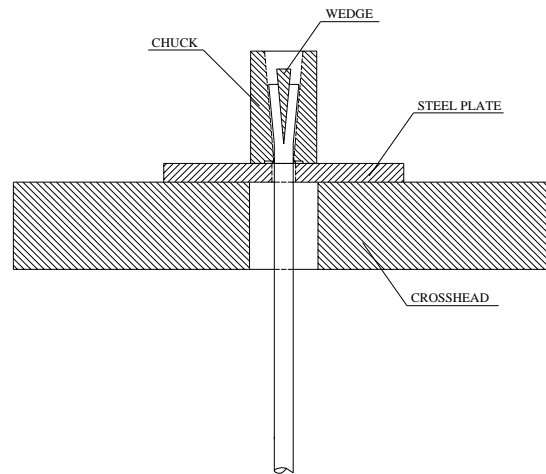
$$N = F_{f,s} \cdot \frac{\phi^2 \pi}{4} = 16.74 \text{ kN (3.76 kips)}$$

Tensile tests were performed using the Tinius-Olsen Universal Testing Machine. The bar was set up across the two crossheads of the machine and aligned with the axis of the grips. The anchor at one end rested on the top crosshead.

On both ends, steel plates with dimensions 203.2 mm (8 in) by 203.2 mm (8 in) and thickness of 12.7 mm (0.5 in) with a 13 mm (33/64 in) diameter hole in the middle, were inserted between the anchors and the crossheads to spread the load. The movable crosshead of the testing machine was positioned so that the plate at the lower end was snug without stressing the bar.

The load was read on the graduate scale present on the testing machine.

Figure 7.13 shows the testing machine used for the tests and the positioning of the anchors.



(a) Universal testing machine

(b) Positioning of the anchors

Fig. 7.13. Universal testing machine and anchor positioning

The failure of the bars occurred when the load was about 22.24 kN (\cong 5 kips).

Failure occurred within the chuck where the material was subjected to combined stresses such as transverse compression and longitudinal shear (in addition to the axial load).

A total slipping of the chuck around the bar was also observed, because of the small dimensions of the wedge that allowed the bar to pass through the chuck.

In order to avoid this type of failure and to increase the ultimate load tolerable by the anchors so as to apply a reasonable safety factor, the design of the chuck and of the wedge were changed and new items were machined to take the place of the previous ones.

The dimensions of the wedge were increased and also the internal shape of the chuck was changed, in order to increase the contact surface between the deformed bar and the chuck and to avoid excessive stress concentration around the cross section of the bar. For this purpose the bigger hole of the chuck was designed so as to have the same surface area of the bar plus that of the wedge.

The new items were again tested in tensile with the Tinius-Olsen Universal Testing Machine. In the new run of tests a load of about 40.00 kN (\cong 9 kips) was reached, and the bar, after being tested, showed no damage.

Because of safety issues, the failure of the bar was never reached with this setup. Figure 7.14 shows the modification between the first and the final design of the steel chuck.

Figure 7.15 illustrates the bar after the tensile tests with the two different chucks.

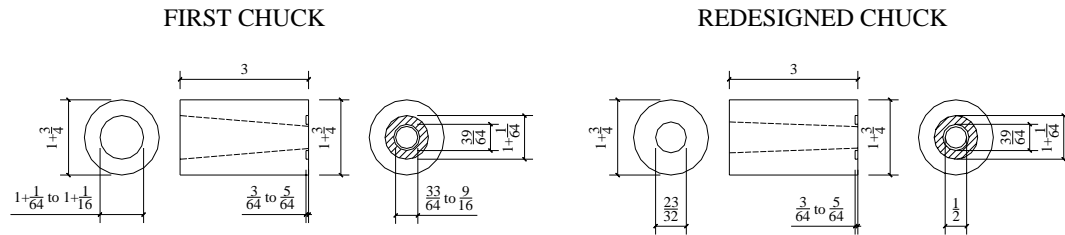


Fig. 7.14. Chuck designs



(a) Test with the first chuck



(b) Test with the redesigned chuck

Fig. 7.15. Bar after failure

7.3. Test Setup

Once it was proven that the anchors were able to carry the right amount of load, long-term tests were performed. A GFRP tendon-anchor system was stressed and subjected to sustained load, to determine ease of installation, mechanical performance, and anchor seating losses.

In order to find the amount of time after which the load was steady, different testing times (6, 12 and 24 hours) were chosen.

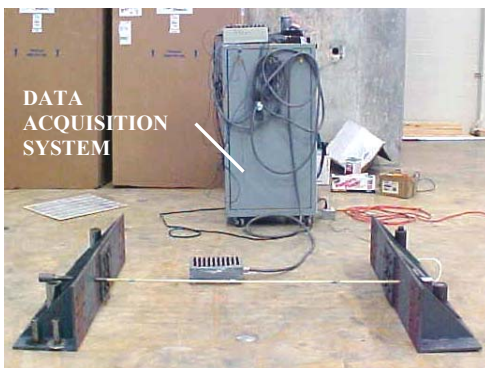
The anchor system was tested using two 1.270 m (50 in) long steel angulars with dimensions 304.8 mm (12 in) by 304.8 mm (12 in) and a thickness of 12.7 mm (0.5 in) bolted to the floor of the laboratory with 38.1 mm (1.5 in) diameter Dywidag rods. The two steel beams were stiffened with three triangular steel plates with dimensions 279.4 mm (11 in) by 279.4 mm (11 in) and a thickness of 12.7 mm (0.5 in).

In both angulars a 25.8 mm (65/64 in) diameter hole was drilled to allow the positioning of the pipe and the bar during the test.

The free length between the two beams was 1.524 m (60 in).

A Sensotek pressure transducer placed between two steel plates on the dead end of the device measured the load that was recorded by means of a LABTECH data acquisition system with a one-Hertz sampling rate.

Figure 7.16 illustrates the test setup.



(a) Test setup: general view



(b) Detail of the pressure transducer

Fig. 7.16. Test setup

7.4. Test Results

General Results.

All the results in terms of time and load losses are summarized in tables 7.4 and 7.5.

Tab. 7.4. Test results for sustained load test

Test Name	Testing Time [h]	Initial Load [kN]	Final Load [kN]	Losses of Load [%]
6h	6	22.33	16.98	24.0
12h-1*	12	24.12	21.19	12.1
12h-2	12	23.86	18.98	20.5
24h	24	21.07	15.73	25.3

Note: 1 kN = 0.2248 kip * = Reloaded specimen

Tab. 7.5. Losses of load during the test

Test Name	Losses of Load [%]				
	At 1 h	At 2 h	At 3 h	At 4 h	At 5 h
6h	16.7	19.4	20.6	21.6	23.0
12h-2	16.1	17.7	18.4	19.0	19.0
24h	19.3	20.7	22.0	22.0	22.9

For the specimen 12h-1, testing problems occurred during the procedure of loading, so the bar was unloaded and reloaded again when the ends were already engaged in the chuck. Because of this, losses of load significantly smaller than the other specimens were recorded.

As indicated in table 7.4 the final losses of load in percentage, are all approximately around the same value for all the tests.

Furthermore, from the data shown in table 7.5, it could be said that about 83% of the final losses of load due to the anchor seating happened in the first two hours and then they stabilize to a constant value after about six hours.

It must also be noted that the anchor seating losses during short-term use are generally small and could become insignificant depending on the length of the tendon.

Figure 7.17 illustrates the load versus time graph for a testing time of 24 hours (see also fig. C.3 - 2,3,4 in Appendix C).

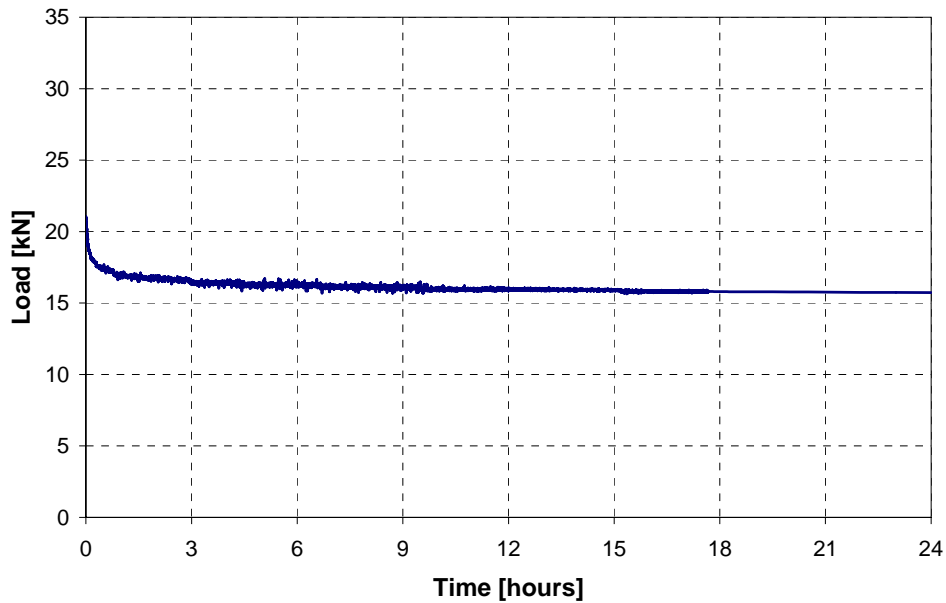


Fig. 7.17. Load vs. time for testing time equal to 24 hours

7.5. Validation of the System

The main area of application of this system is the structural rehabilitation of damaged concrete, masonry, timber members; it consists of restoring the original structure function and closing the cracks due to different causes such as seismic events or differential settlements.

The application of tensioned FRP bars to a damaged structure induces a state of compression and can close existing cracks.

Figure 7.18 shows a schematic drawing of the post-tensioned tendons used to close cracks in a masonry structure.

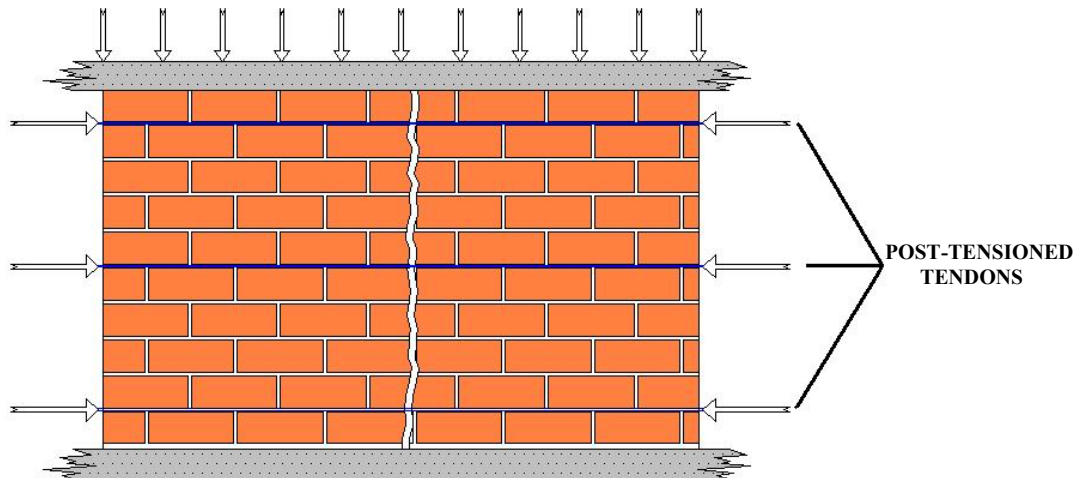


Fig. 7.18. Post-tensioning of a cracked masonry wall

7.5.1. Test Setup

In order to validate the system and to calibrate the load on the GFRP bar as a function of the torque furnished by a torque wrench, additional tests in the laboratory were performed.

A reinforced concrete beam with dimensions 267 mm (10.5 in) by 419 mm (16.5 in) by 2134 mm (84 in) long was casted.

The steel cage consisted of a 9.5 mm (3/8 in) diameter steel rebar and of stirrups with the same size at 254 mm (10 in).

A PVC pipe with the internal diameter equal to 38.1 mm (1.5 in) was positioned directly above the steel rebar, to allow the positioning of the threaded pipe during the post-tensioning procedure.

Two kinds of tests were performed using this RC beam: the first one (test 1) to check the variations of the mid span deflection during a certain amount of time while the beam was subjected to the post-tensioning load, and the second one (test 2) to find the ultimate load for this kind of device, loading the rod until reaching failure.

Figure 7.19 shows the RC beam used for the tests.



(a) Steel cage and PVC pipe



(b) RC beam after curing

Fig. 7.19. RC beam used for validation test and detail of the construction

After 28 days of curing, 10 grooves were done on both sides of the beam and were filled with weak mortar in order to see, as well as possible, the opening and closing of the cracks during the procedures of respectively loading and post-tensioning.

The beam was cracked using the Baldwin Universal Testing Machine with a four point flexural test, according with the standards dictated by the ASTM E 72-98.

Once the cracks were opened, the post-tensioning device was used to reduce the mid span deflection due to the vertical load previously applied.

In order to measure the midspan deflection and the load, an LVDT and a pressure transducer were used. The load was applied to the rod using a torque wrench that was calibrated after the tests.

Figure 7.20 shows the test setup and a detail of the dead end of the device.



(a) Test setup: general view



(b) Dead end and pressure transducer

Fig. 7.20. Test setup

7.5.2. Test Results

General Results.

The results of the two kinds of tests (test1 and test 2) are summarized in figures 7.21 and 7.22.

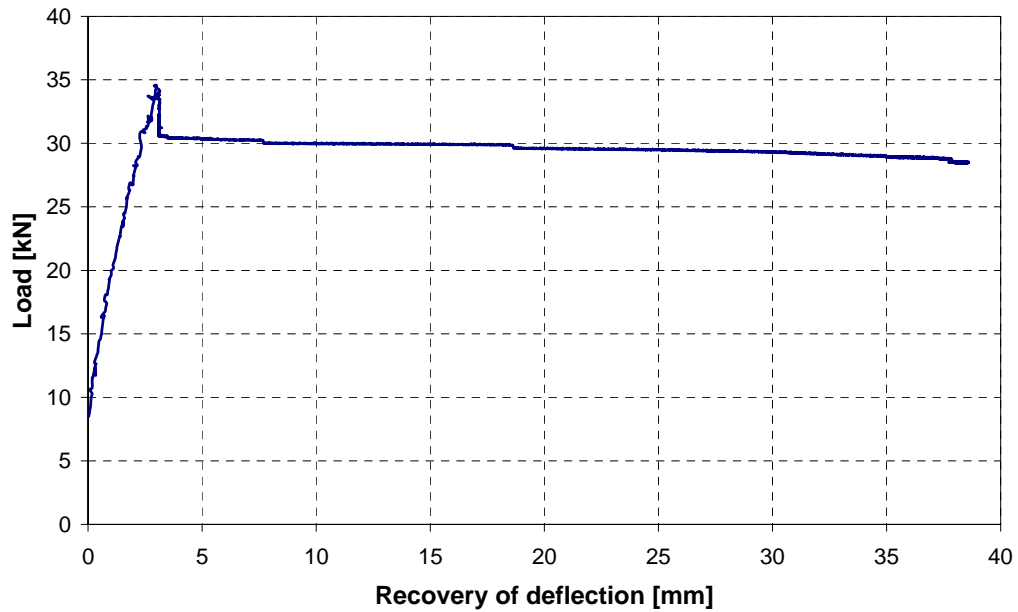


Fig. 7.21. Test 1: load vs. recovery of deflection

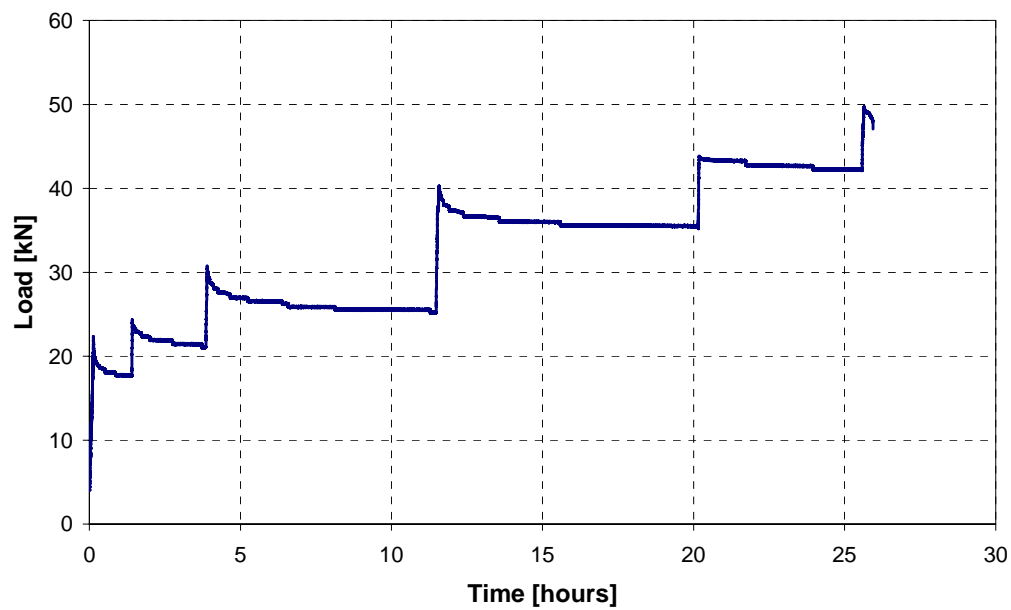


Fig. 7.22. Test 2: load vs. time: loading to failure

In figure 7.21, once reached a value of load of 35 kN (7.87 kips), two different regions can be recognized: the very first part of the curve after the loading branch is due to the anchor seating losses that represent the main part (66% of the total loss in about an hour). The second part represent the decreasing of load due to the recovery of deflection obtained by means of the sustained load carried by the post-tensioned rod. This second loss occurred in about five hours.

The recovery of deflection is obtained as difference between the value recorded in a moment and the value recorded at the beginning of the test with no load in the rod.

Figure 7.23 shows the position of the LVDT during the test and the recovery of deflection measured in a generic moment.

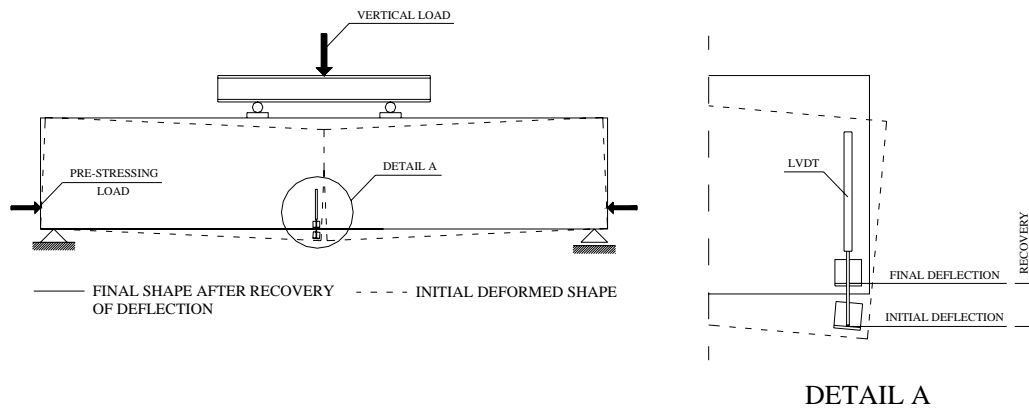
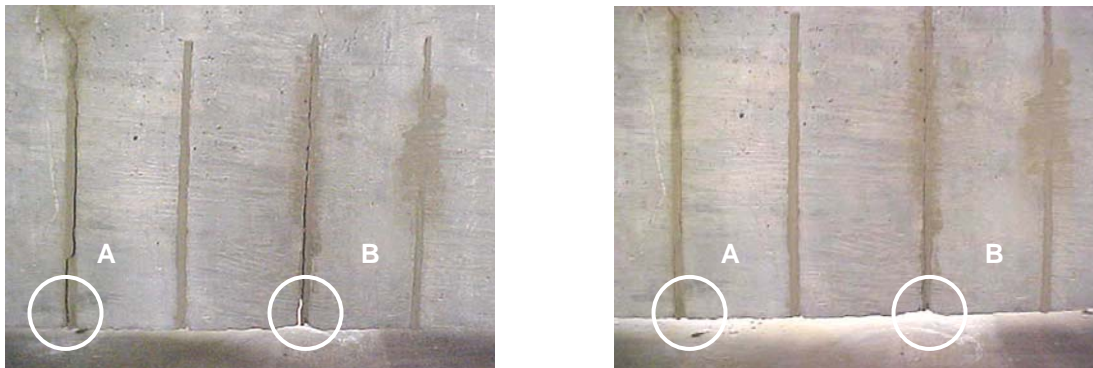


Fig. 7.23. LVDT position and detail of the valuation of recovery of deflection

During the whole test a total recovery of deflection of 38.1 mm (1.5 in) was recorded by the LVDT, and the cracks opened on the sides of the beam were totally closed.

Figure 7.24 illustrates the crack before and after the post-tensioning procedure.



(a) Cracks before post-tensioning

(b) Cracks after post-tensioning

Fig. 7.24. Effectiveness of the post-tensioning technique

Figure 7.22 shows the different loading cycles of a GFRP bar loaded up to failure.

The bar was loaded during a period of time of about 26 hours, increasing the load after six different periods of time, to check which was the ultimate capacity of the device and determine if the prestressing load would be maintained..

It can be noticed from the collected data that the ratio between the losses of load in percentage and the time during which they occur, was decreasing.

This phenomenon can be explained with a first contribution to the losses of load due to the anchor seating and a second one due to the recovery of deflection at mid span that decreased during the test because of the closing of the cracks.

The contribution due to the anchor seating losses affected the first three cycles of loading during a period of time which lasted about eleven hours, whereas the last part of the test was affected mainly by the decreasing recovery of deflection.

It can be noticed that during the very last cycle, the losses of load were very low meaning that the aforementioned contributions were almost completely developed.

Once the load of 49.62 kN (11.15 kips) was reached, the failure of the bar due to creep-rupture effects occurred in the part of the bar just outside the chuck.

Two additional tests of this type (test 2) were performed to define the ultimate capacity of the device and to collect the data in order to calibrate the torque wrench.

The test results in terms of ultimate load are summarized in table 7.6.

Tab. 7.6. Ultimate loads

Test Number	Ultimate Load [kN]
1	49.62
2	44.84
3	48.35
Mean	47.60

Note: 1 kN = 0.2248 kip

In order to calibrate the load on the GFRP bar as a function of the torque furnished by a torque wrench, additional data were collected during the tests, to find a relationship between the load measured by the pressure transducer and the moment read on the scale of the wrench.

The relationship is illustrated in figure 7.25.

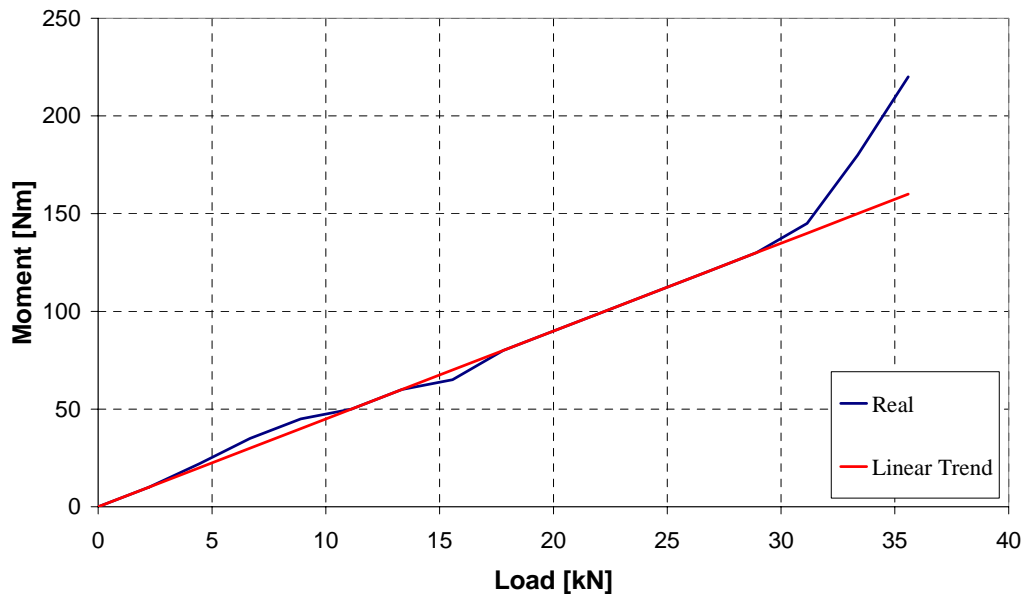


Fig. 7.25. Load vs. torque wrench moment graph

In figure 7.24 two different regions can be recognized: in the first part of the graph, up to 30 kN (7 kips), the behavior obtained from the data recorded during the test is very close to the linear trend, but in the second branch, the gap between the two curves increases with the increasing of the load in the rod.

This phenomenon can be explained by the increasing of the friction between the nut and the threaded pipe due to the damage that occur in the screw devices when the load increases to high values.

This problem can be avoided by using tough steel for the devices and suitable grease during the loading operation. In many cases, the torque wrench can be used up to loads two times bigger than the admissible value stated by the ACI code.

The following equation can be used to determine the value of the moment that must be read on the scale of the wrench used to load the rod in the field applications:

$$M = \frac{10}{2.224} \cdot N_{\text{rod}} \quad \text{with: } 0 \leq N_{\text{rod}} \leq 30 \text{ kN (7 kips)}$$

Where: N_{rod} is the design load to apply at the rod [kN]

M is the value of the moment that must be read on the wrench [N·m]

7.6. Conclusions

Several different kinds of tests were run to verify the effectiveness of the devices and the applicability of the method in the real field.

The results of the work done in the laboratory demonstrate that the post-tensioning devices allow for loading the rod up to loads almost three times larger than the threshold stated by the ACI code.

The anchors are also able to carry a steady load for the period of time needed to fully embed the rod in the member with the use of an epoxy-based paste.

The tests with the RC beam shows that the technique is capable of solving the problems concerning the structural rehabilitation such as damage and cracks due to seismic events or differential settlements, maintaining the integrity of structural assemblages while preserving aesthetics.

Furthermore, due to the light weight of the material and the devices involved, site equipment and handling requirements are reduced and simplified.

For these particular technique and devices, a patent disclosure was filed (see Appendix C.5).

8. CONCLUSIONS AND FUTURE WORKS

8.1. Conclusions

The present investigation has demonstrated that FRP composites offer benefits for the strengthening of masonry elements. FRP systems have been proven to increase flexure and shear capacities of URM elements. Analytical studies were presented for determining the flexural capacity limit of the strengthened walls and the effective bonded length of the AFRP laminates.

The new anchor system showed in Section 7 demonstrated that FRP can be successfully used also for the post-tensioning of masonry with composites in substitution of steel tendons.

Results on durability tests on putty are a warning with respect to long-term durability. An in-depth investigation of this and other types of putty may be warranted.

Specific conclusions and recommendations for both engineering and installation procedures have been presented in all the sections of this thesis.

8.2. Future works

Bond

Debonding of the FRP laminate from the masonry surface is the controlling mechanism of failure. The previous work intended to establish a limit for the FRP strain and for the minimum bonded length but is not sufficient for the calibration of the model since debonding has a direct relationship with the porosity of the masonry, the type of masonry, the humidity, the type of fiber, the quantity of saturant used, etc. Different representative types of masonry, FRP and other parameters would be investigated.

Out-of-plane with arching effect

In order to develop a design protocol for the flexural strengthening of URM walls subjected to arching effect, different types of FRP materials and different values of slenderness ratio would be studied. University of Missouri - Rolla is ready to build full-scale walls to evaluate all these parameters.

Arching effect appeared to influence significantly RC beams in concrete frames. This aspect could change ACI guidelines in terms of beam design.

In-plane behavior of masonry walls

For this behavior, it is important to investigate the interaction of strengthened walls with the surrounding structural elements (i.e. beams and columns) since the effectiveness of the strengthening may be dangerously overestimated due to premature failures in the masonry or structural elements. For FRP structural repointing, more economical embedding materials to encapsulate the FRP rods in the mortar joints need to be explored. These materials might be mortars with improved bond properties, which can transfer tensile stresses to the reinforcement.

Post-tensioning

University of Missouri – Rolla is ready to test the anchor system for the thermoplastic bars in the field to validate the effectiveness and the speed of installation.

Note: a general issue is represented to a lack of material standardization that cause many design difficulties because of large differences between the same type of FRP materials.

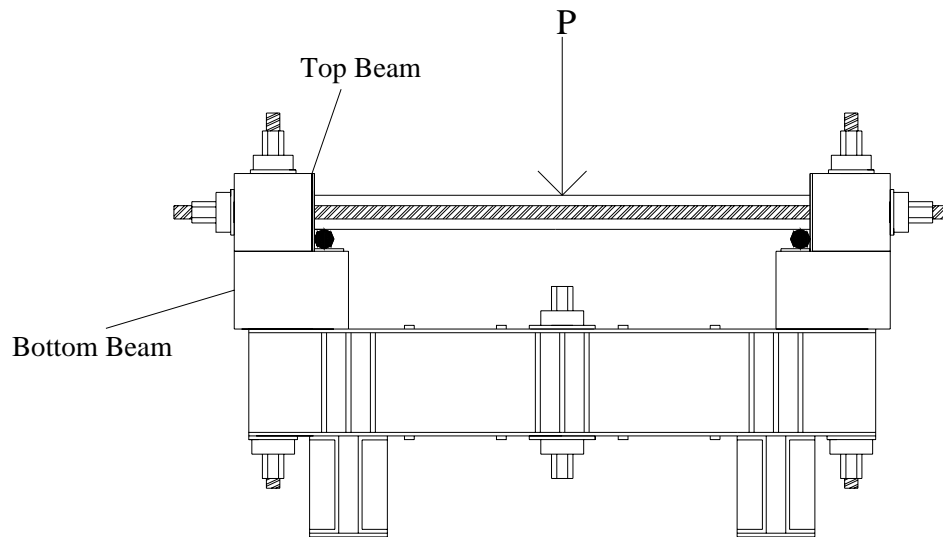
8.3. New frontiers for FRP composites (Blast upgrading)

Terrorist attacks have shown to be a dangerous threat for civilian and military facilities. Because of the high casualties experienced in the Oklahoma City and Khobar Towers (Saudi Arabia) bombings, and in the Pentagon with aerial attack, force protection is considered by the US Department of Defense (DOD) to be a critical mission parameter. In particular, the blast scenario from a structural point of view can be subdivided in three phases. In the first phase, exterior walls and columns and windows are affected, in the second phase floor slabs and roofs, and in the third and last phase, the lateral load-resisting frame. Amongst building components, masonry walls possess a reduced capacity against out-of-plane blast loading. Their capacity can be upgraded by placing internal or external steel reinforcement. However, these procedures require significant labor during installation. An alternative is to attach FRP composite materials to the surfaces of the walls to increase the blast capacity. University of Missouri – Rolla is working in collaboration with Fort Leonard Wood (Missouri) in a project consisting of design, verification and upgrade with FRP composites.

APPENDIX A: ARCHING EFFECT

Appendix A.1: Beams design

Testing frame



Material Properties:

Concrete: $f_{cu} = 23.4 \text{ N/mm}^2 = 3400 \text{ psi}$

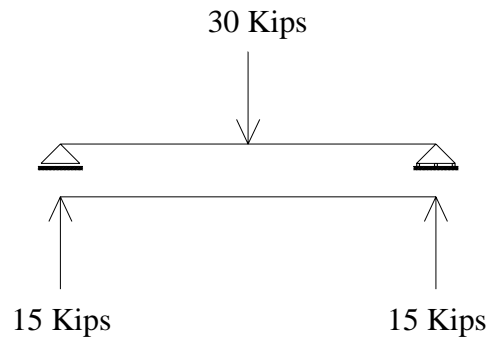
$f_{ctd} = 3.6 \text{ N/mm}^2 = 525 \text{ psi}$

$\epsilon_u = 0.0035$

Steel: $f_{yd} = 359 \text{ N/mm}^2 = 52.2 \text{ ksi}$

$\epsilon_{yd} = 0.002$

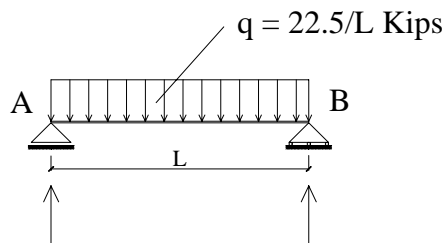
$\epsilon_u = 0.01$

BOTTOM BEAM DESIGN**Load on bottom beam**

$$P = 30 \cdot 1.5 = 45 \text{ kips} \cong 200 \text{ kN}$$

$$V_A = V_B = \frac{200}{2} = 100 \text{ kN} = 22.5 \text{ kips}$$

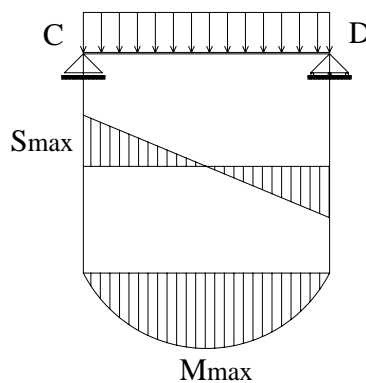
Load sketch for bottom beam:



$$L = 0.8128 \text{ m} = 32''$$

$$q = \frac{100000}{0.8128} = 123 \text{ kN/m} = 0.703 \text{ kips/in}$$

Shear and flexure diagram:



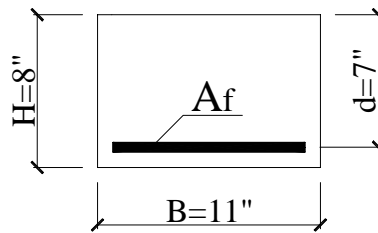
$$V_c = V_d = \frac{qL}{2} = \frac{123 \cdot 0.8128}{2} = 50 \text{ kN} = 11.25 \text{ kips}$$

$$S_{\max} = \frac{qL}{2} = \frac{123 \cdot 0.8128}{2} = 50 \text{ kN} = 11.25 \text{ kips}$$

$$M_{\max} = \frac{qL^2}{8} = \frac{123 \cdot 0.8128^2}{8} = 10.16 \text{ kN} \cdot \text{m} = 90 \text{ kips} \cdot \text{in}$$

The design is influenced from the frame's dimensions

FLEXURE DESIGN:



- $B = 279.4 \text{ mm} = 11''$
- $H = 203.2 \text{ mm} = 8''$
- $D = 177.8 \text{ mm} = 7''$

$$A_f = \frac{M_{\max}}{0.9 \cdot d \cdot f_{yd}} = \frac{10157400}{0.9 \cdot 177.8 \cdot 359.7} = 176 \text{ mm}^2 = 0.27 \text{ in}^2$$

- N° 3 Rebars #3 $A_f = 213 \text{ mm}^2 = 0.33 \text{ in}^2$

$$\omega_s = \frac{A_s \cdot f_{yd}}{B \cdot d \cdot f_{cu}} = \frac{213 \cdot 359.7}{279.4 \cdot 177.8 \cdot 23.4} = 0.0658 = \text{field "a"}$$

$$\xi = 0.066 + 0.924\omega_s = 0.127$$

$$x = \xi d = 0.127 \cdot 177.8 = 22.6 \text{ mm} = 0.89''$$

$$\beta = \frac{4.57 - 11.10 \cdot \xi}{(1 - \xi)^2} \cdot \xi = \frac{4.57 - 11.10 \cdot 0.127}{(1 - 0.127)^2} \cdot 0.127 = 0.527$$

$$k = \frac{0.33 - 0.13 \cdot \xi}{1 - \xi} = \frac{0.33 - 0.13 \cdot 0.127}{1 - 0.127} = 0.359$$

$$\zeta = 1 - k \cdot \xi = 1 - 0.359 \cdot 0.127 = 0.95$$

$$M_{rd} = f_{yd} \cdot A_f \cdot \zeta \cdot d = 359.7 \cdot 213 \cdot 0.95 \cdot 177.8 = 12941220 \text{ N} \cdot \text{mm} = 12.9 \text{ kN} \cdot \text{m}$$

$$= 114.49 \text{ Kips} \cdot \text{in} \geq M_{\max}$$

Strain Control:

$$\epsilon_c = \frac{x \cdot 0.01}{d - x} = \frac{22.6 \cdot 0.01}{17.78 - 2.26} = 0.00145 \leq 0.0035$$

SHEAR DESIGN:

$$S_{\max} = 50 \text{ kN} = 11.25 \text{ Kips} = V_{sd}$$

$$V_{rd1} = 0.25 \cdot f_{ctd} \cdot r \cdot (1 + 50\rho_t) \cdot b_w \cdot d \cdot \delta$$

- $r = 1.6 \cdot d = 1.42 \text{ m}$
- $f_{ctd} = 3.6 \text{ N/mm}^2 = 525 \text{ Psi}$
- $\rho_t = \frac{A_f}{b_w \cdot d} = \frac{213}{279.4 \cdot 177.8} = 4.3 \cdot 10^{-3} \leq 0.02$
- $\delta = 1$
- $b_w = 279.4 \text{ mm} = 11''$
- $d = 177.8 \text{ mm} = 7''$

$$V_{rd1} = 77.13 \text{ kN} = 17.34 \text{ Kips} \geq 50 \text{ kN} = 11.25 \text{ Kips} \quad \text{NO STIRRUPS NEEDED}$$

- N° Stirrups 1 # 3 - 2 Arms / 254 mm (10'')

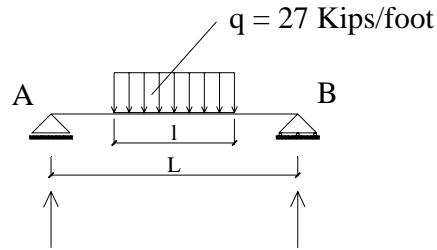
Checking compressed concrete:

$$V_{rsu} = 0.30 \cdot f_{cu} \cdot b_w \cdot d = 0.30 \cdot 23.4 \cdot 279.4 \cdot 177.8 = 348 \text{ kN} = 78 \text{ Kips} \geq V_{sd}$$

TOP BEAM DESIGN

The load on this beam was calculated considering that the wall cannot rotate.

Load sketch for top beam:

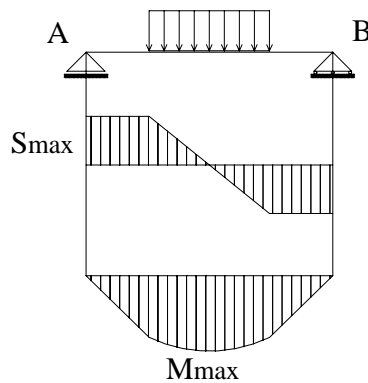


$$L = 812.8 \text{ mm} = 32''$$

$$l = 609.6 \text{ mm} = 24''$$

$$q = \frac{240 \cdot 1.5}{0.6096} = 591 \text{ kN/m} = 3.375 \text{ Kips/in}$$

Shear and flexure diagram:

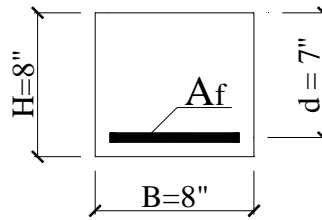


$$V_A = V_B = \frac{ql}{2} = \frac{591 \cdot 0.6096}{2} = 180 \text{ kN} = 40.5 \text{ Kips}$$

$$S_{\max} = V_A = V_B = 180 \text{ kN} = 40.5 \text{ Kips}$$

$$M_{\max} = V_A \cdot \frac{L}{2} - \frac{ql^2}{8} = 180 \cdot \frac{0.8128}{2} - \frac{591 \cdot 0.6096^2}{8} = 45.75 \text{ kN} \cdot \text{m} = 401 \text{ Kips} \cdot \text{in}$$

The design is influenced from the frame's dimensions

FLEXURE DESIGN:

- $B = 203.2 \text{ cm} = 8''$
- $H = 203.2 = 8''$
- $d = 177.8 = 7''$

$$A_f = \frac{M_{\max}}{0.9 \cdot d \cdot f_{yd}} = \frac{45756000}{0.9 \cdot 177.8 \cdot 359.7} = 795 \text{ mm}^2 = 1.23 \text{ in}^2$$

- N° 3 Rebars #6 $A_f = 852 \text{ mm}^2 = 1.32 \text{ in}^2$

$$\omega_s = \frac{A_s \cdot f_{yd}}{B \cdot d \cdot f_{cu}} = \frac{852 \cdot 359.7}{203.2 \cdot 177.8 \cdot 23.4} = 0.362 = \text{field "b"}$$

$$\beta_0 = 0.8$$

$$k_0 = 0.4$$

$$\xi = \frac{\omega_s}{\beta_0} = \frac{0.362}{0.8} = 0.453$$

$$x = \xi d = 0.453 \cdot 177.8 = 80.6 \text{ mm} = 3''.171$$

$$\zeta = 1 - k \cdot \xi = 1 - 0.4 \cdot 0.453 = 0.82$$

$$M_{rd} = f_{yd} \cdot A_f \cdot \zeta \cdot d = 359.7 \cdot 852 \cdot 0.82 \cdot 177.8 = 44.7 \text{ kN} \cdot \text{m} = 395.5 \text{ Kips} \cdot \text{in} \cong M_{\max}$$

Strain Control:

$$\epsilon_{sd} = \frac{\epsilon_{cu} \cdot (d - x)}{x} = \frac{0.0035 \cdot (177.8 - 80.6)}{80.6} = 0.0042 \leq 0.01$$

SHEAR DESIGN:

$$S_{\max} = 180 \text{ kN} = 40.5 \text{ Kips} = V_{sd}$$

$$V_{rd1} = 0.25 \cdot f_{ctd} \cdot r \cdot (1 + 50\rho_t) \cdot b_w \cdot d \cdot \delta$$

- $r = 1.6 - d = 1.42 \text{ m}$
- $f_{ctd} = 3.6 \text{ N/mm}^2 = 525 \text{ psi}$
- $\rho_t = \frac{A_f}{b_w \cdot d} = \frac{850}{203.2 \cdot 177.8} = 0.023 \cong 0.02$
- $\delta = 1$
- $b_w = 203.2 \text{ mm} = 8''$
- $d = 177.8 \text{ mm} = 7''$

$$V_{rd1} = 101 \text{ kN} = 12.21 \text{ Kips} \leq 180 \text{ kN} = 40.5 \text{ Kips} \quad \text{NEED STIRRUPS}$$

$$V_{cd} = 0.6 \cdot f_{ctd} \cdot b_w \cdot d \cdot \delta$$

$$\delta = 1$$

$$V_{cd} = 0.6 \cdot 3.6 \cdot 203.2 \cdot 177.8 = 78.04 \text{ kN}$$

$$V_{wd} = V_{sd} - V_{cd} = 180 - 78 = 102 \text{ kN}$$

N° Stirrups 1 # 4 - 2 Arms

$$A_{st} = 2 \cdot 129 = 258 \text{ mm}^2 = 0.40 \text{ in}^2$$

$$s = \frac{A_{st} \cdot f_{yd} \cdot 0.9 \cdot d}{V_{wd}} = \frac{258 \cdot 359.7 \cdot 0.9 \cdot 177.8}{102000} = 145 \text{ mm} \cong 5'' \frac{3}{4}$$

- N° Stirrups 1 # 4 - 2 Arms/ 14 cm (5'' ½)

Checking compressed concrete:

$$V_{rsu} = 0.30 \cdot f_{cu} \cdot b_w \cdot d = 0.30 \cdot 23.4 \cdot 203.2 \cdot 177.8 = 253.6 \text{ kN} = 57 \text{ Kips} \geq V_{sd}$$



(a) Beam forms



(b) Beams casting

Fig. A.1. – 1 Preparation of the beams

Appendix A.2: Strengthening scheme

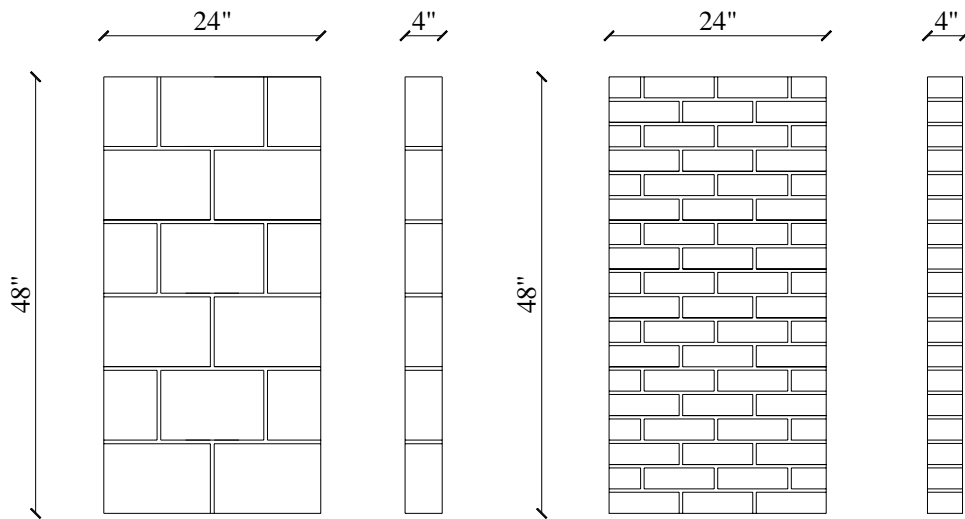


Fig. A.2 – 1. Configuration of the walls

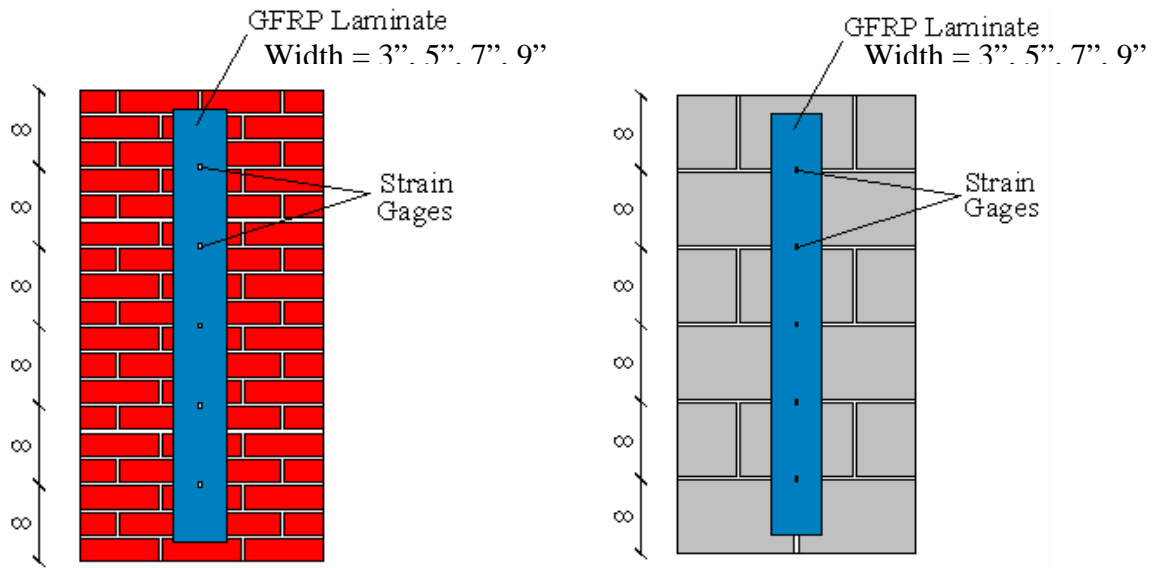


Fig. A.2 – 2. Strengthening scheme with the typical location of the strain gages



(a) Application of primer



(b) Application of putty



(c) Application of GFRP sheet



(d) Removing of air bubbles

Fig. A.2 – 3. Specimens preparation

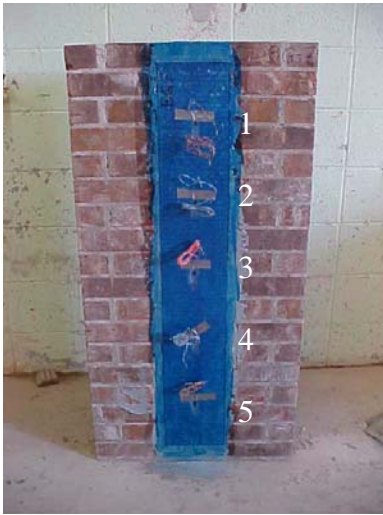


Fig. A.2 – 4. Specimens ready to be tested

Appendix A.3: Test Setup

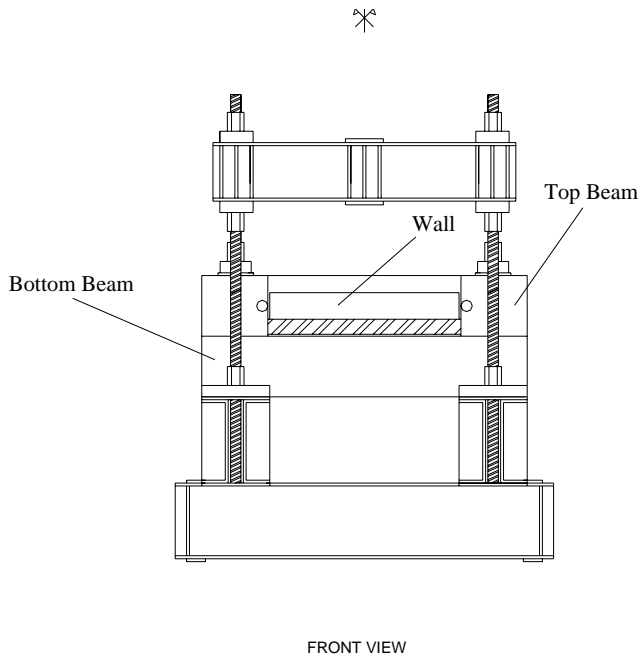
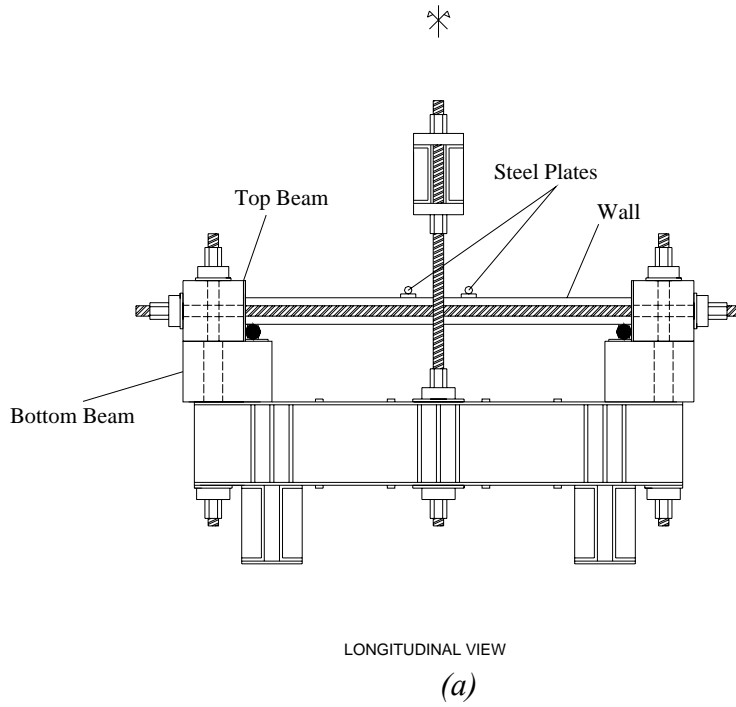


Fig. A.3 – 1. Test setup



Fig. A.3 – 2. Picture test setup

Appendix A.4: Test results

CLAY MASONRY

Specimen Control B

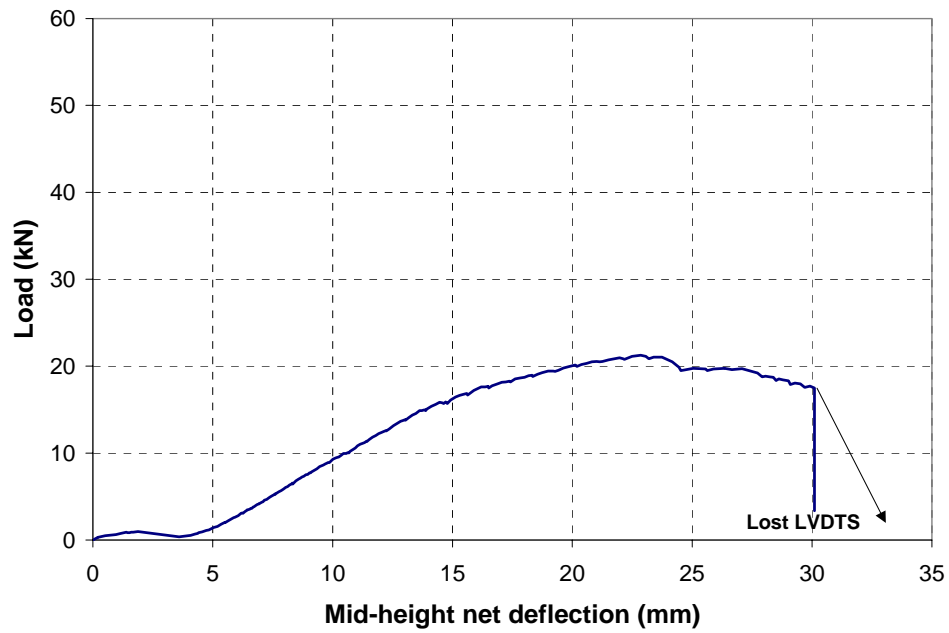


Fig. A.4 – 1. Mid-height deflection vs. Load – Control B

Specimen BG3

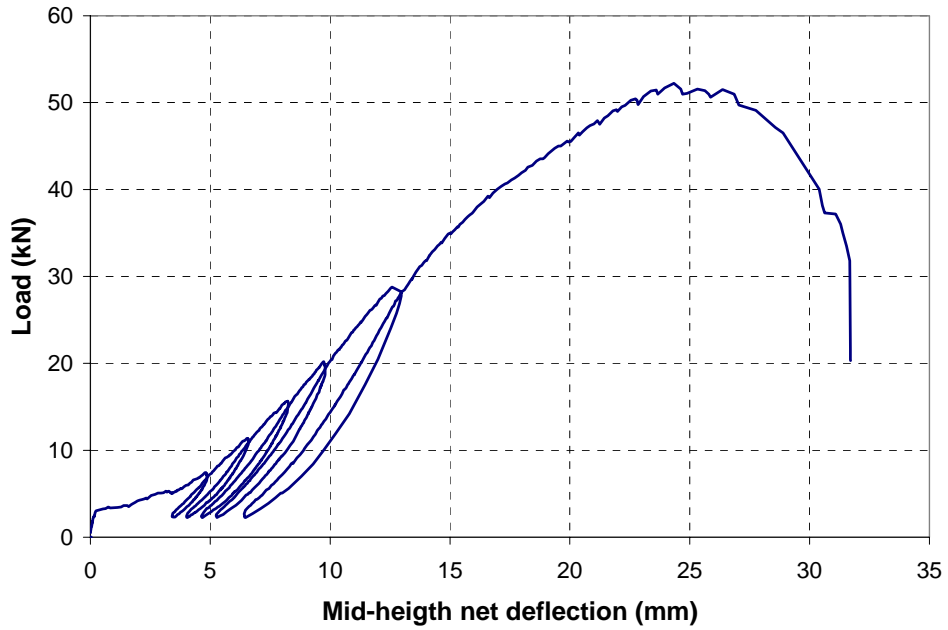


Fig. A.4 – 2. Mid-height deflection vs. Load – BG3

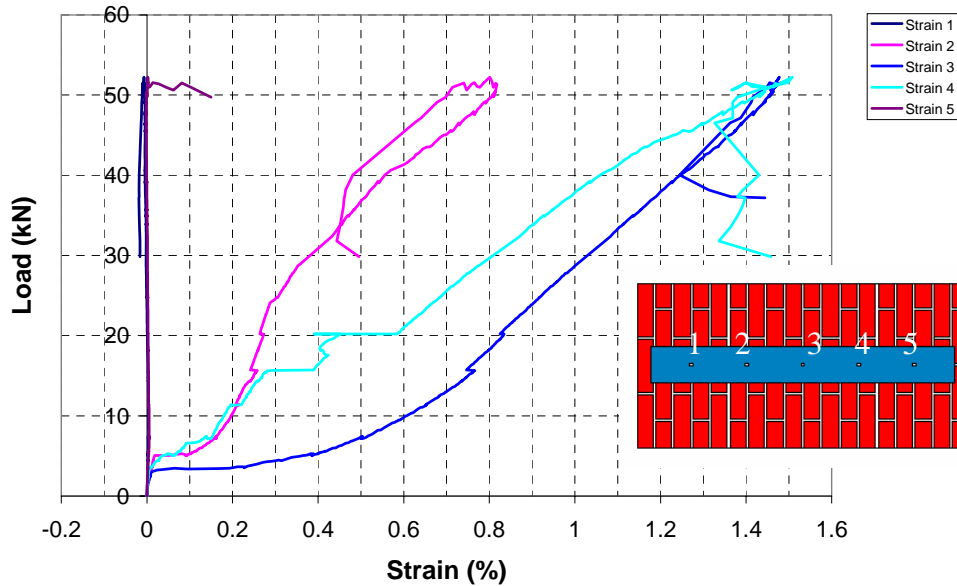


Fig. A.4 – 3. Strain vs. Load – BG3

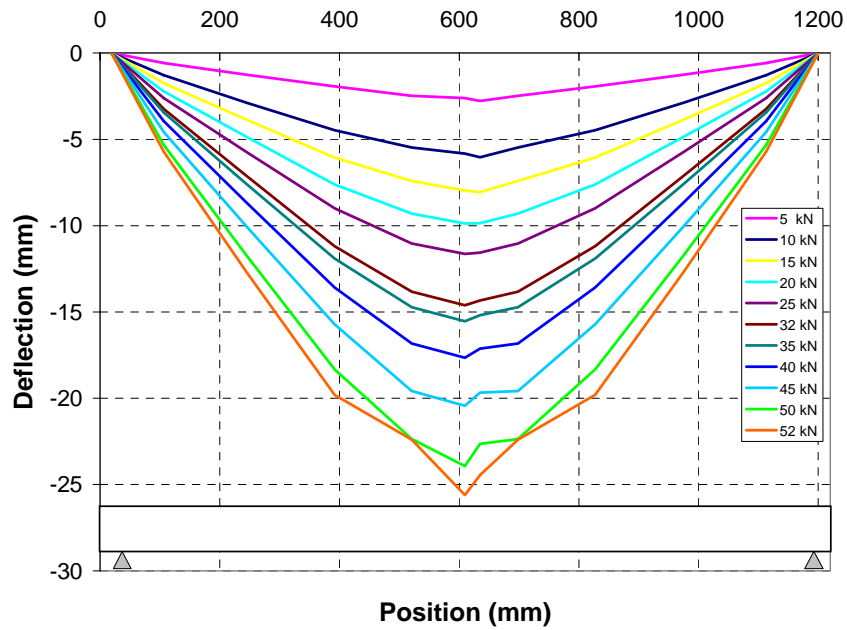


Fig. A.4 – 4. Height vs. deflection– BG3

Specimen BG5

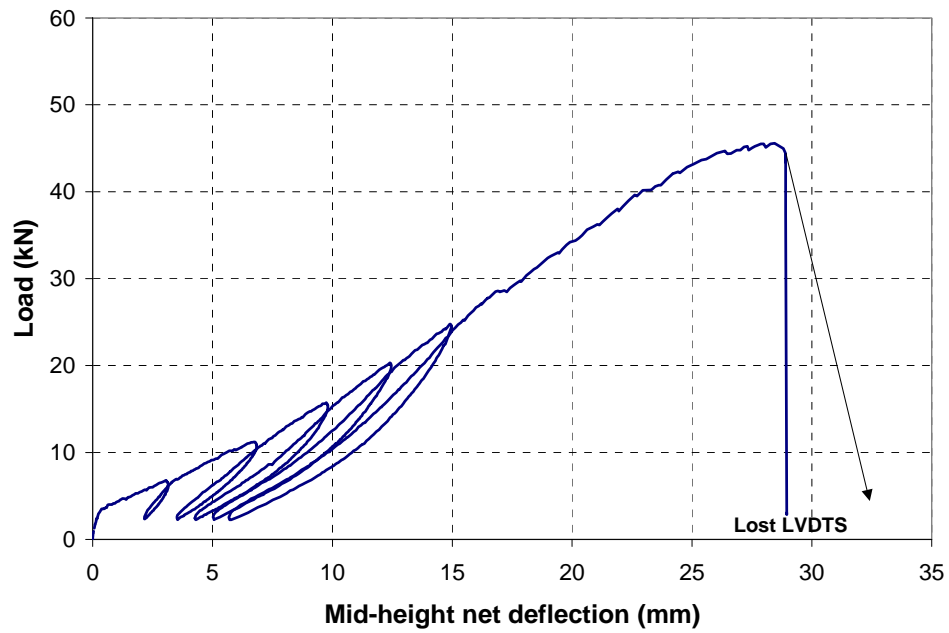


Fig. A.4 – 5. Mid-height deflection vs. Load – BG5

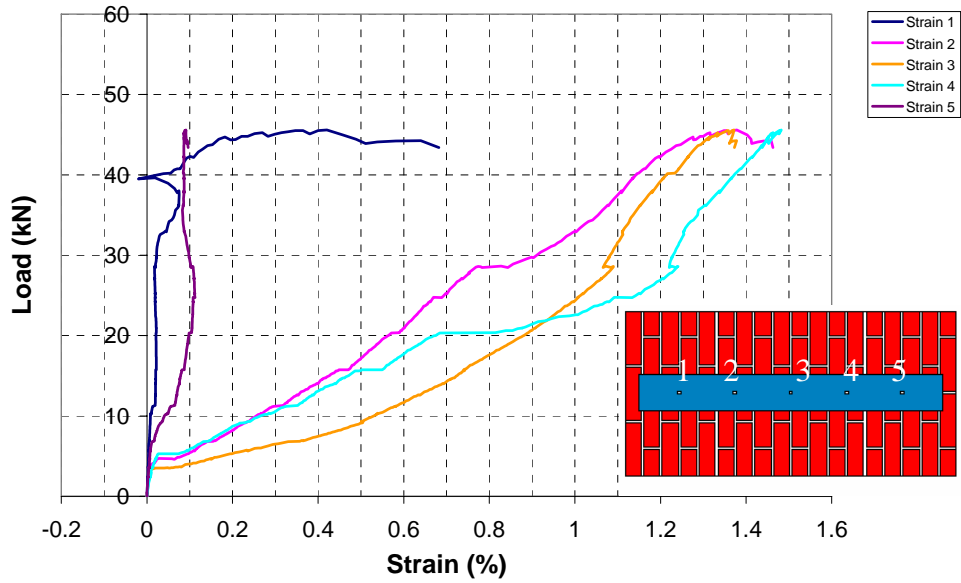


Fig. A.4 – 6. Strain vs. Load – BG5

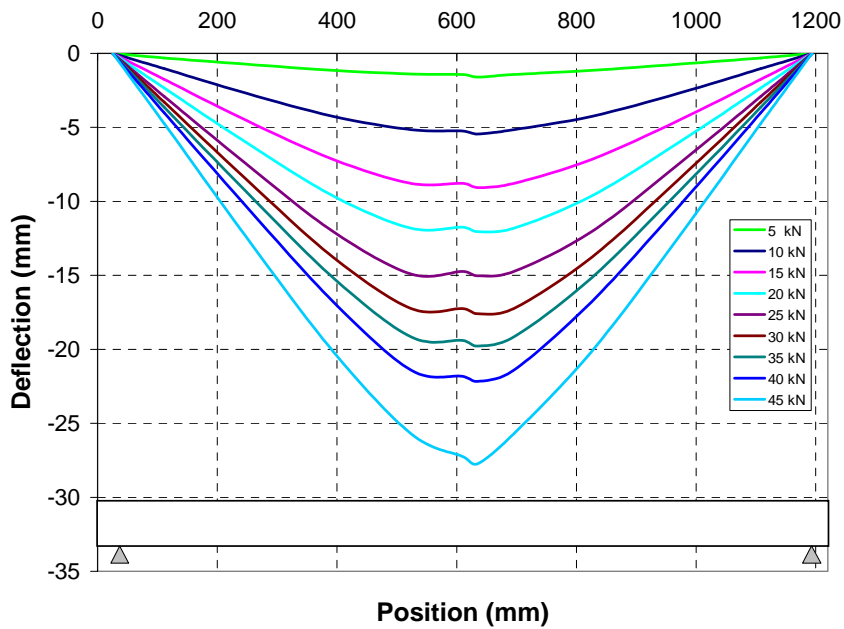


Fig. A.4 – 7. Height vs. deflection– BG5

Specimen BG7

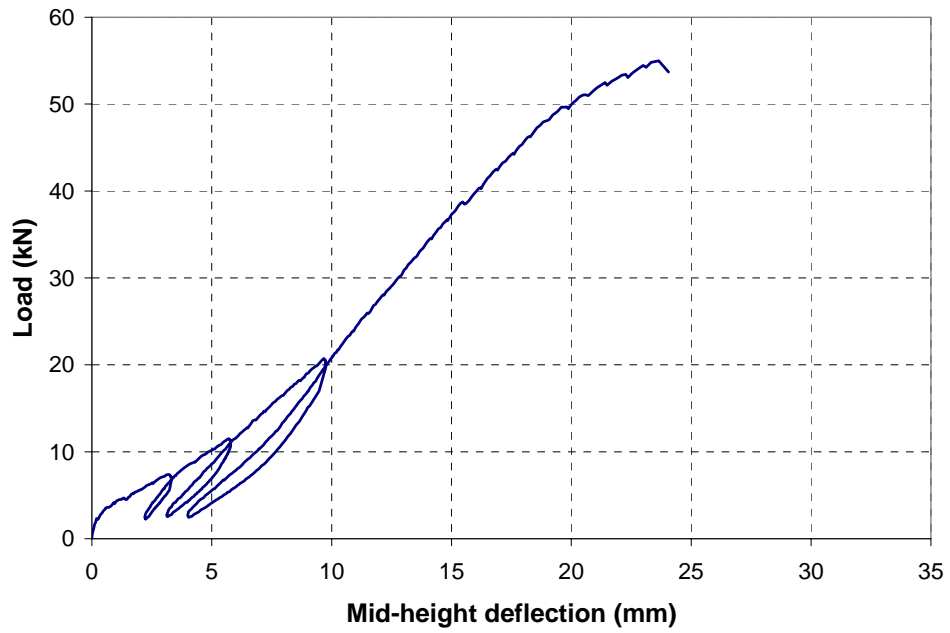


Fig. A.4 – 8. Mid-height deflection vs. Load – BG7

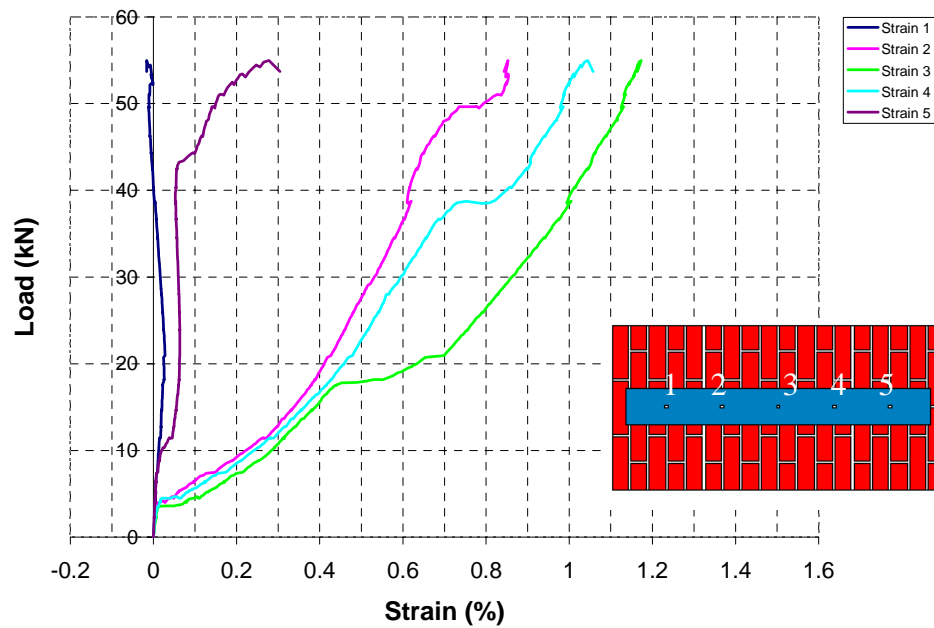


Fig. A.4 – 9. Strain vs. Load – BG7

Specimen BG9

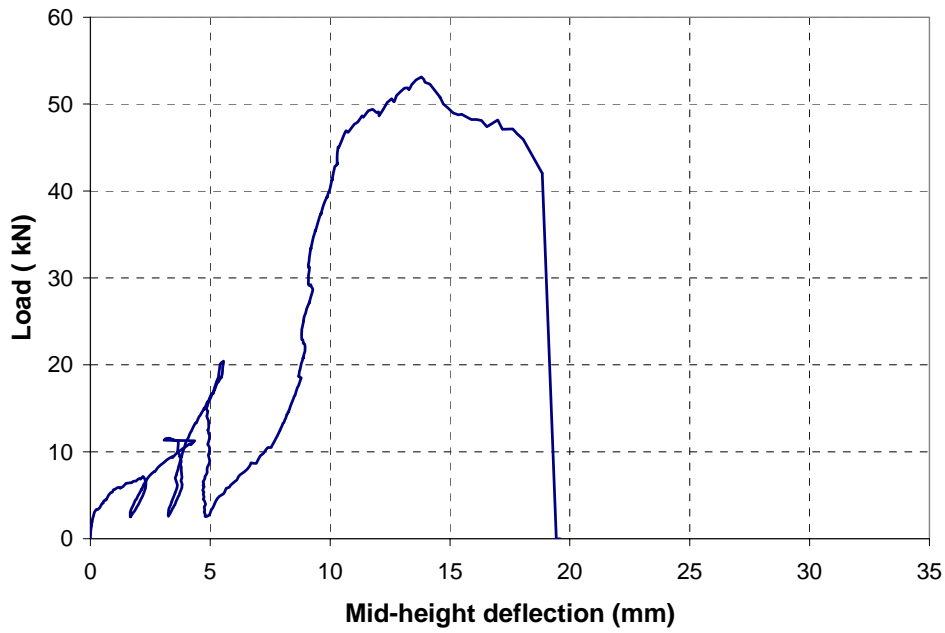


Fig. A.4 – 10. Mid-height deflection vs. Load – BG9

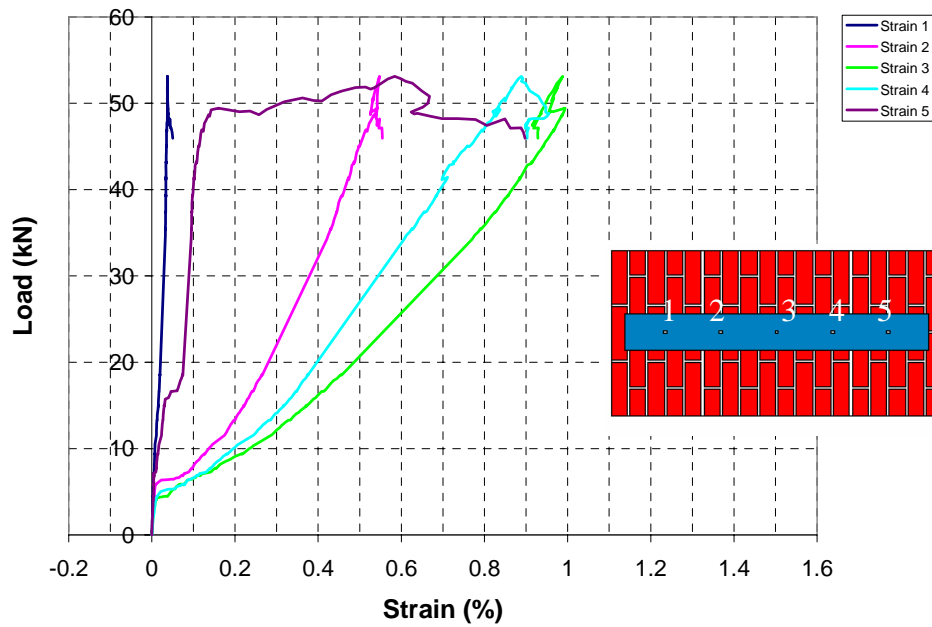


Fig. A.4 – 11. Strain vs. Load – BG9

Comparisons among clay masonry specimens

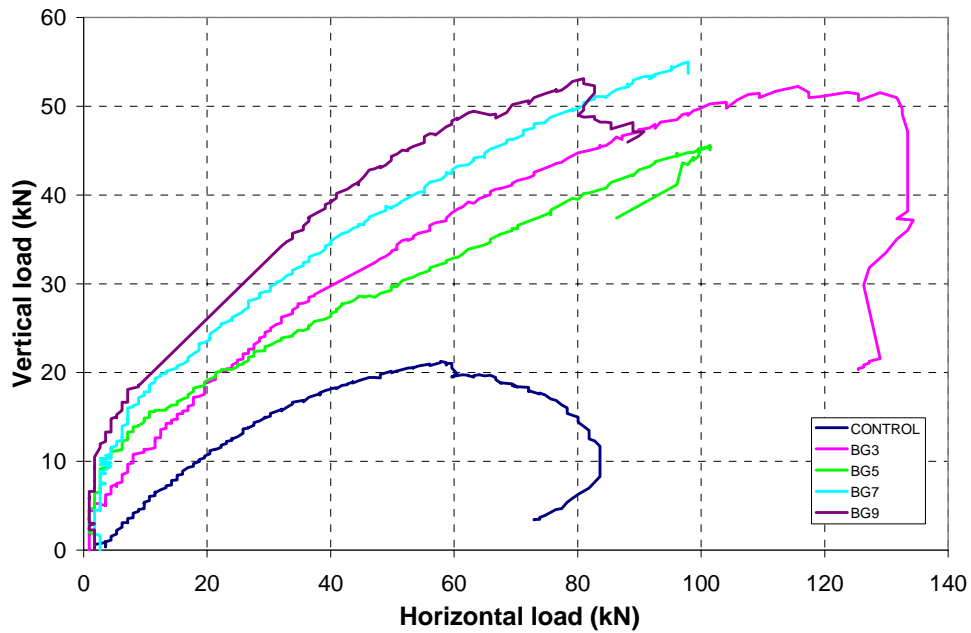


Fig. A.4 – 12. Vertical load vs. horizontal load – Comparison Clay masonry

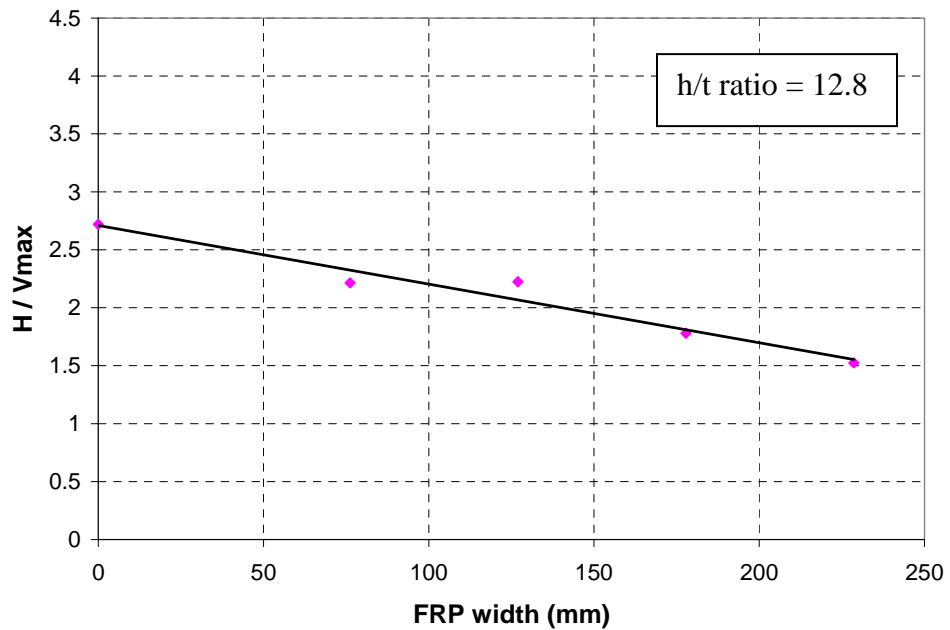
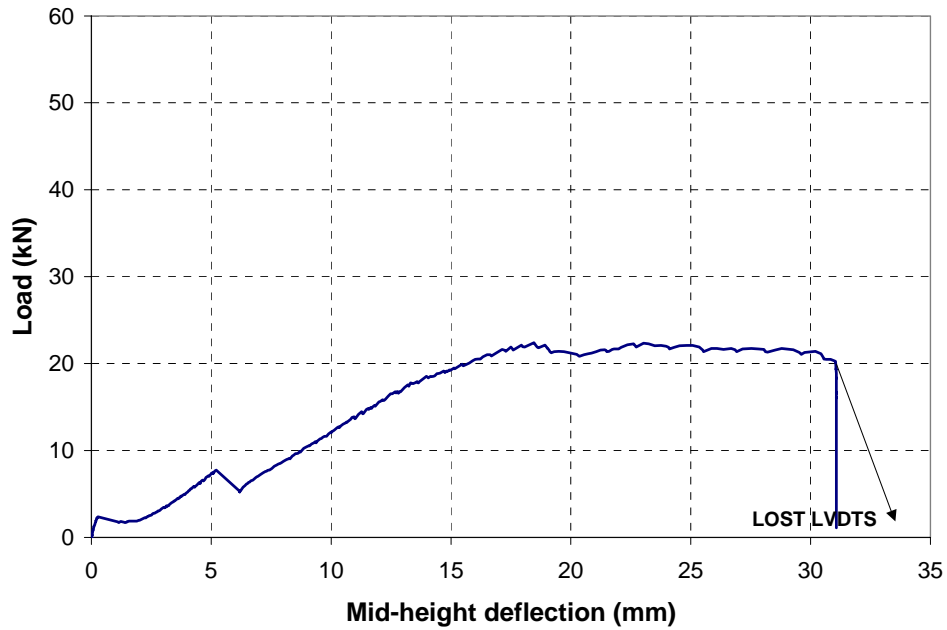
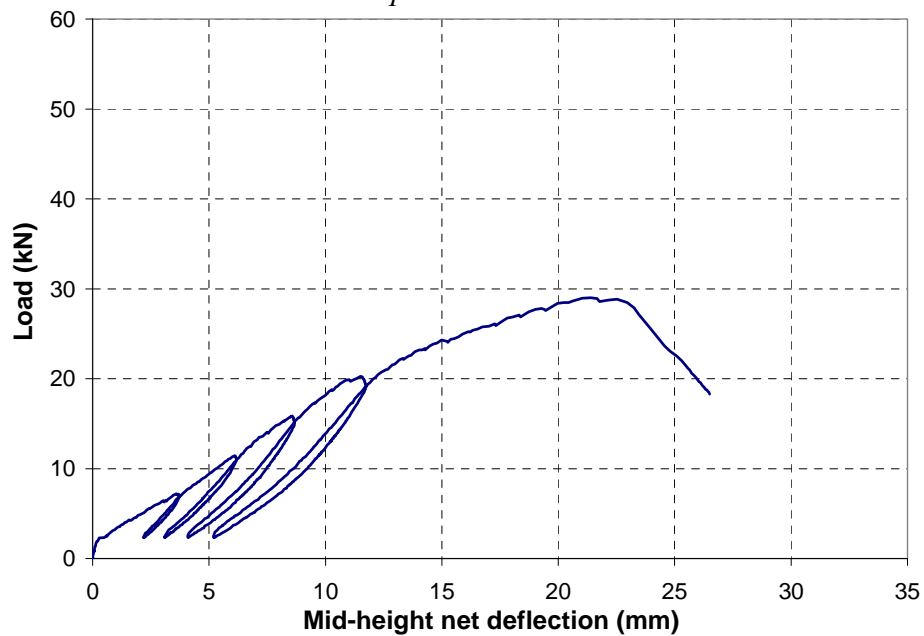


Fig. A.4 – 13. H/V_{max} vs. FRP width – Comparison Clay masonry

CONCRETE MASONRY

Specimen Control C*Fig. A.4 – 14. Mid-height deflection vs. Load – Control C**Specimen CG3**Fig. A.4 – 15. Mid-height deflection vs. Load – CG3*

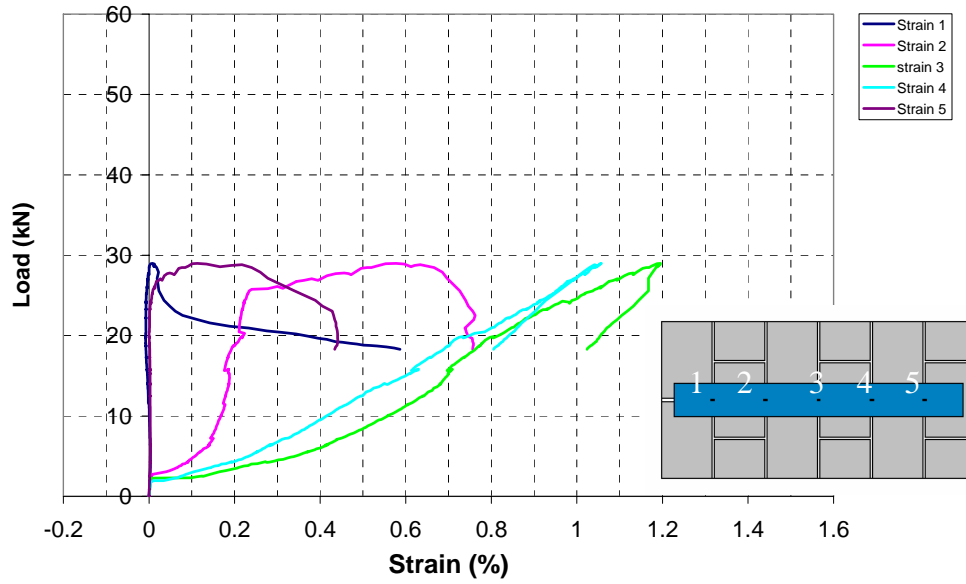


Fig. A.4 – 16. Strain vs. Load – CG3

Specimen CG5

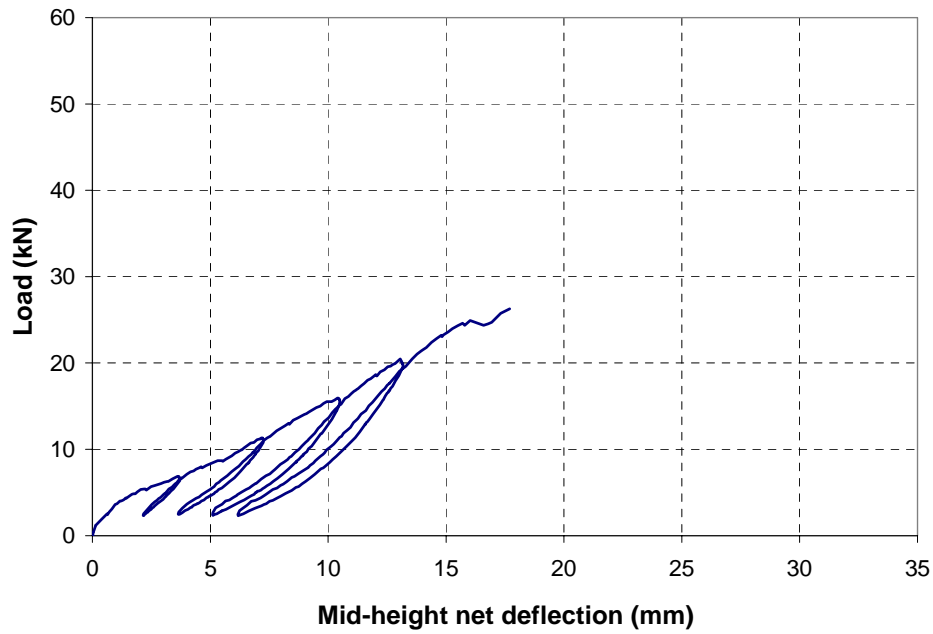


Fig. A.4 – 17. Mid-height deflection vs. Load – CG5

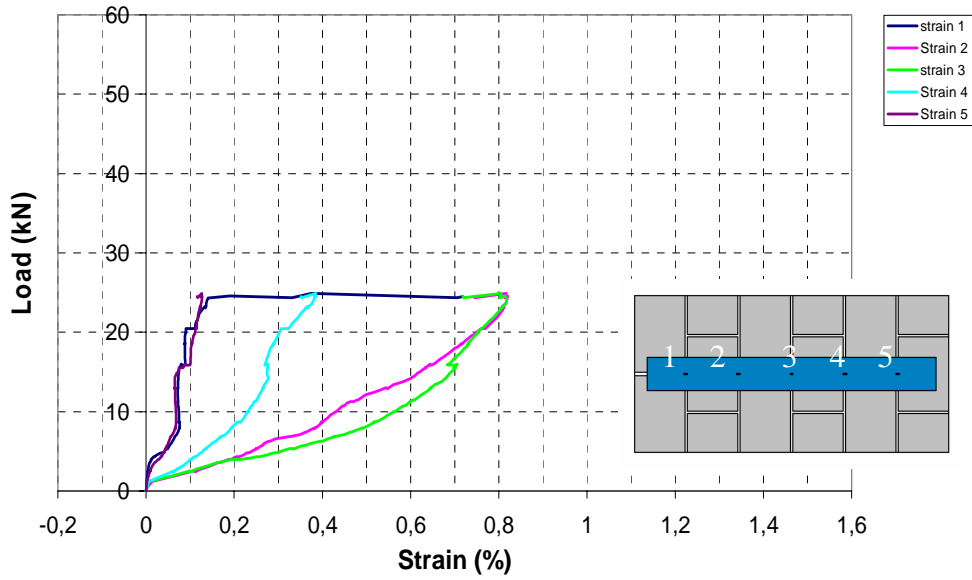


Fig. A.4 – 18. Strain vs. Load – CG5

Specimen CG7

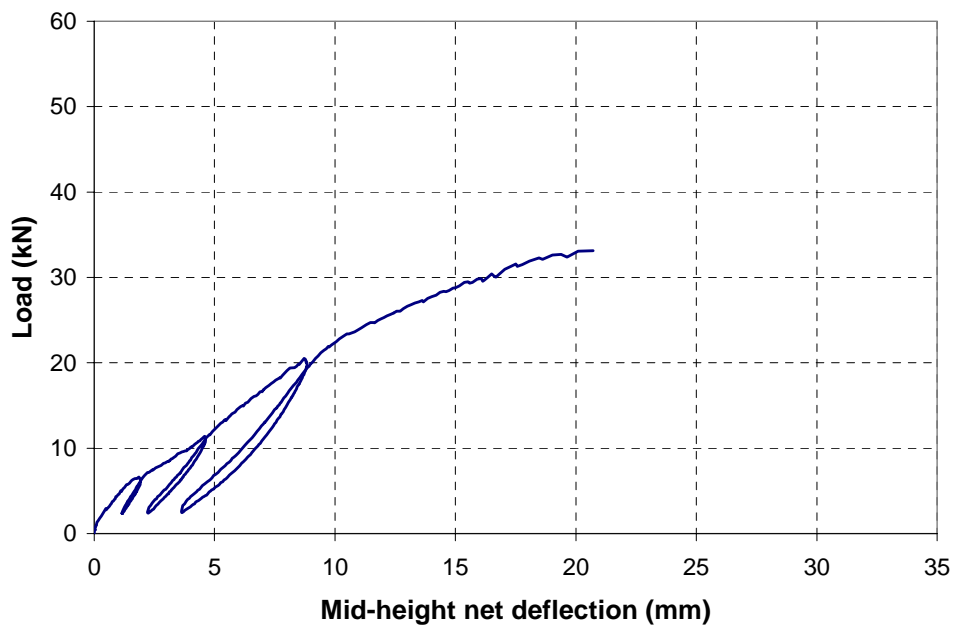


Fig. A.4 – 19. Mid-height deflection vs. Load – CG7

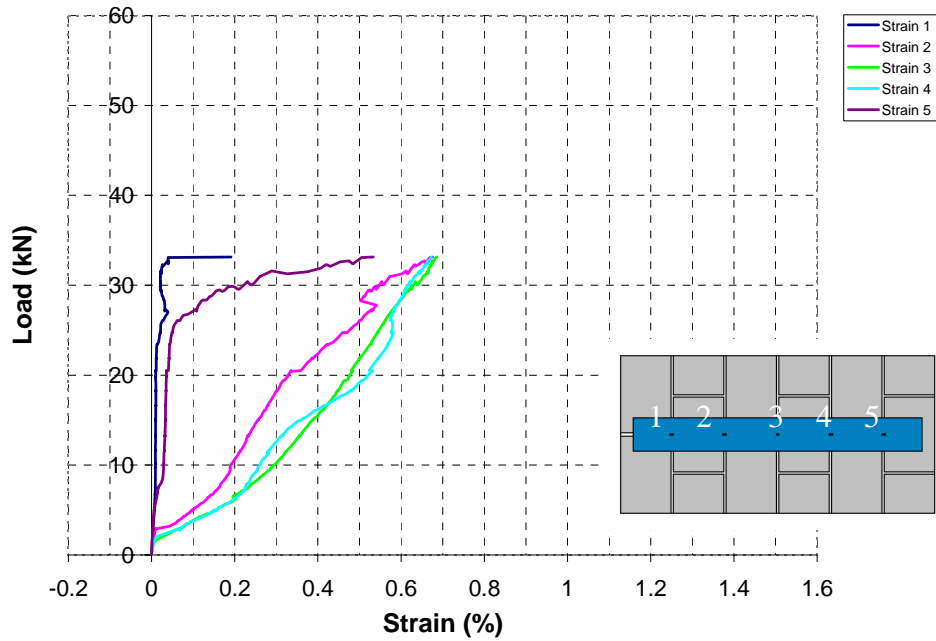


Fig. A.4 – 20. Strain vs. Load – CG7

Specimen CG9

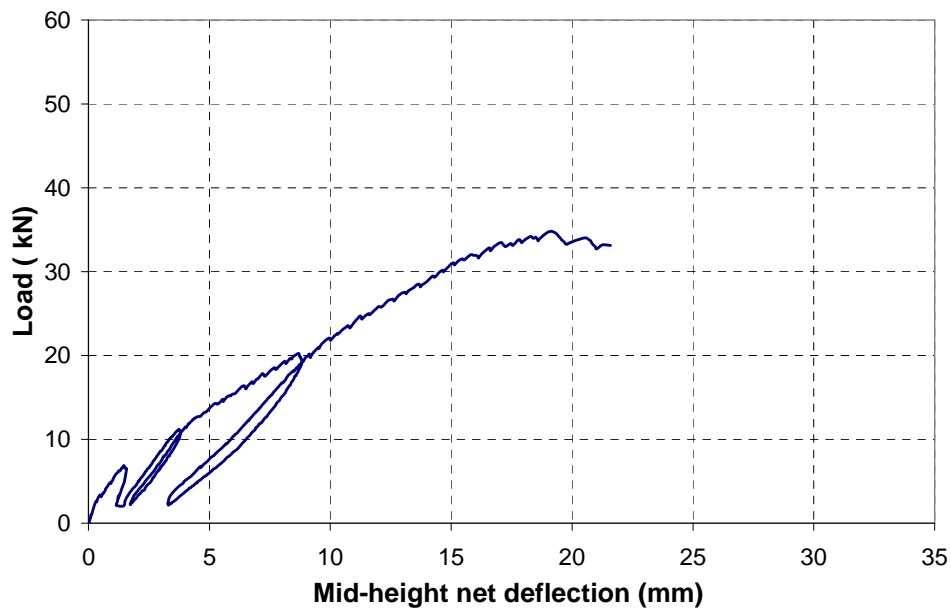


Fig. A.4 – 21. Mid-height deflection vs. Load – CG9

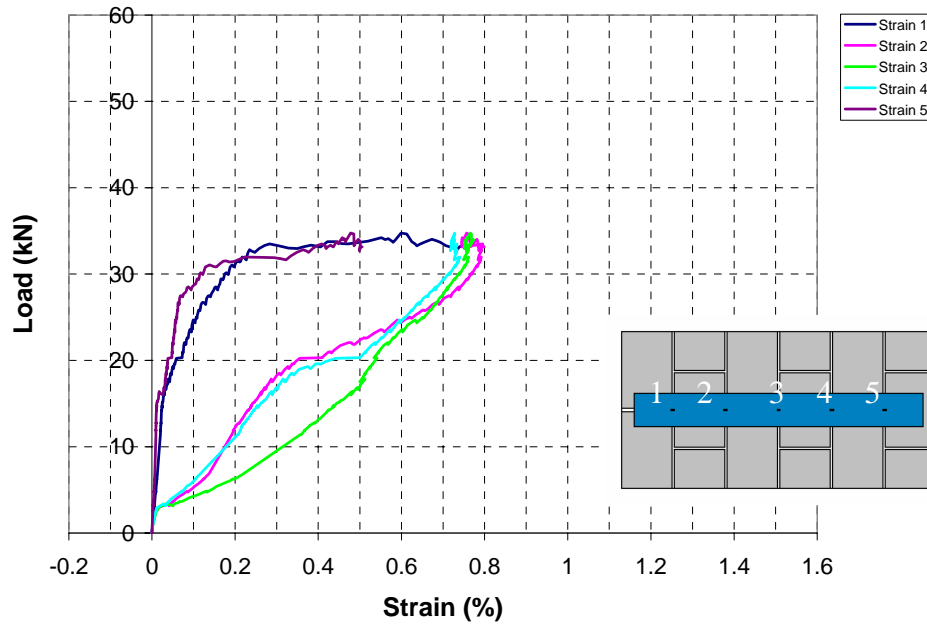


Fig. A.4 – 22. Strain vs. Load – CG9

Comparisons among concrete masonry specimens

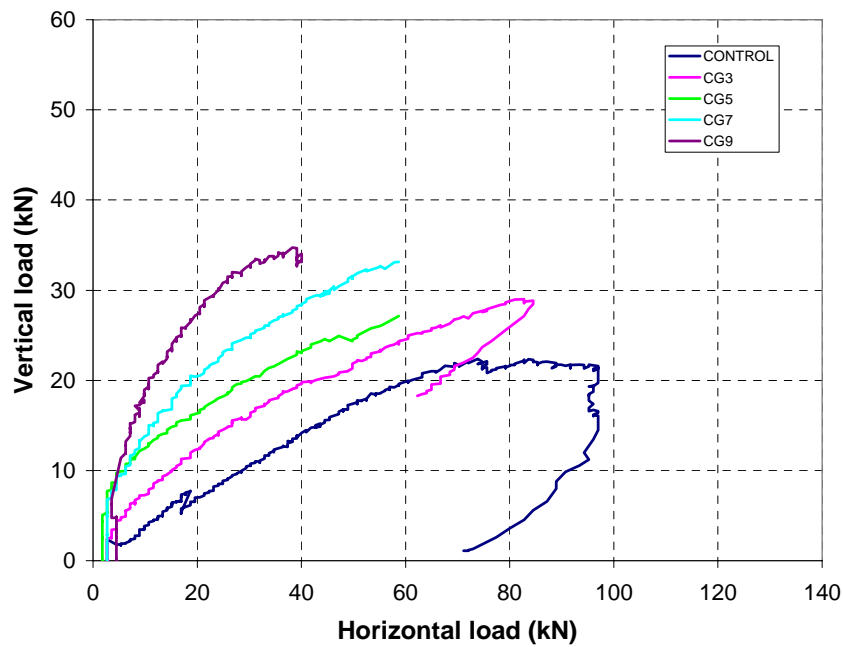


Fig. A.4 – 23. Vertical load vs. horizontal load – Comparison Concrete masonry

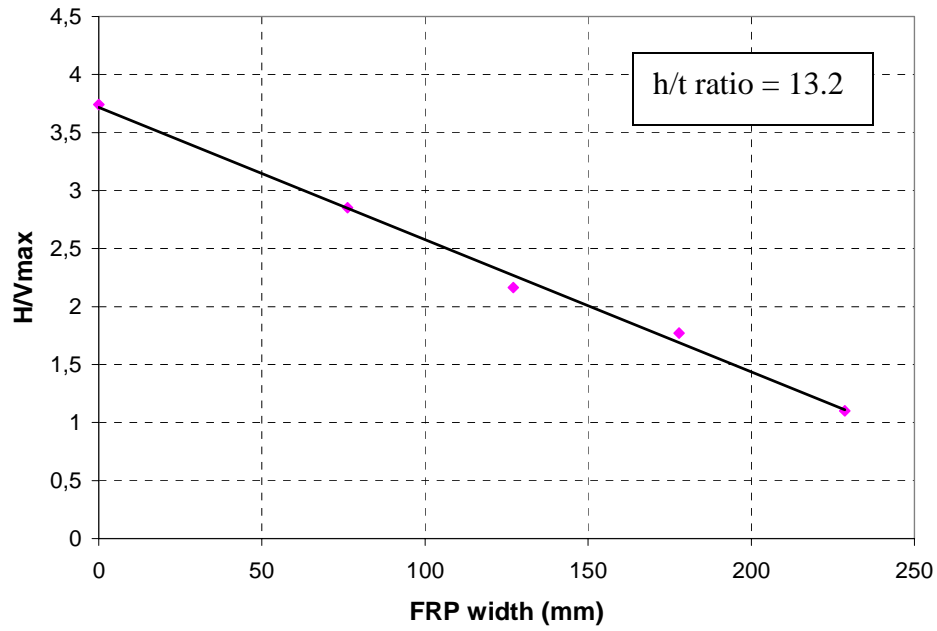


Fig. A.4 – 24. H/V_{max} vs. FRP width – Comparison Concrete masonry

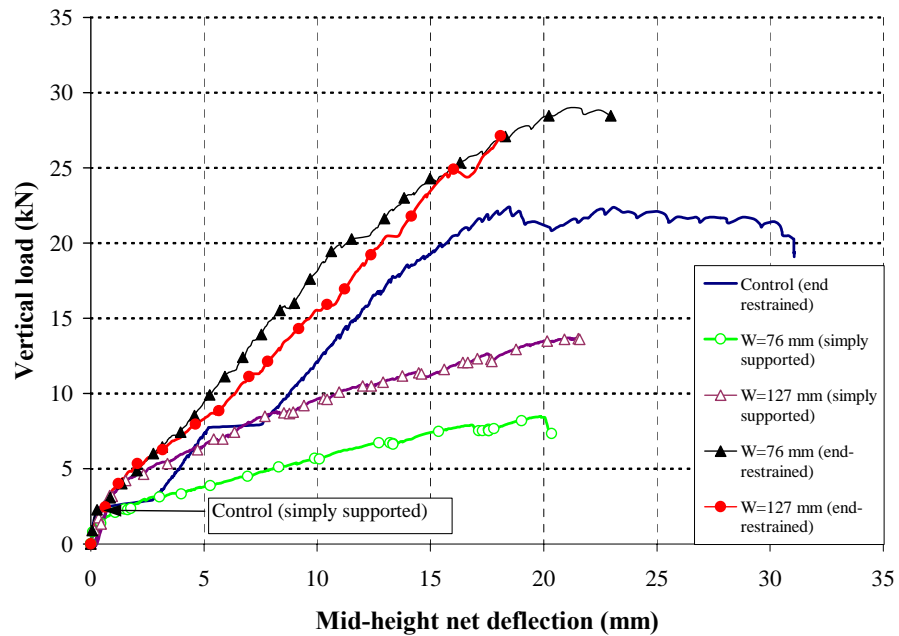


Fig. A.4 – 25. Comparison among simply supported and restrained concrete specimens

Appendix A.5: Analytical study

Unstrengthened section

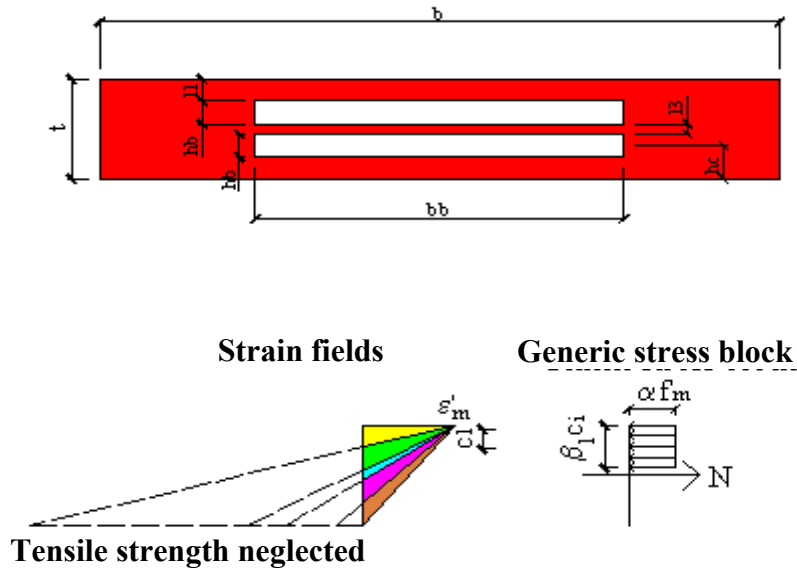


Fig. A.5 - 1. Unstrengthened section

Strengthened section

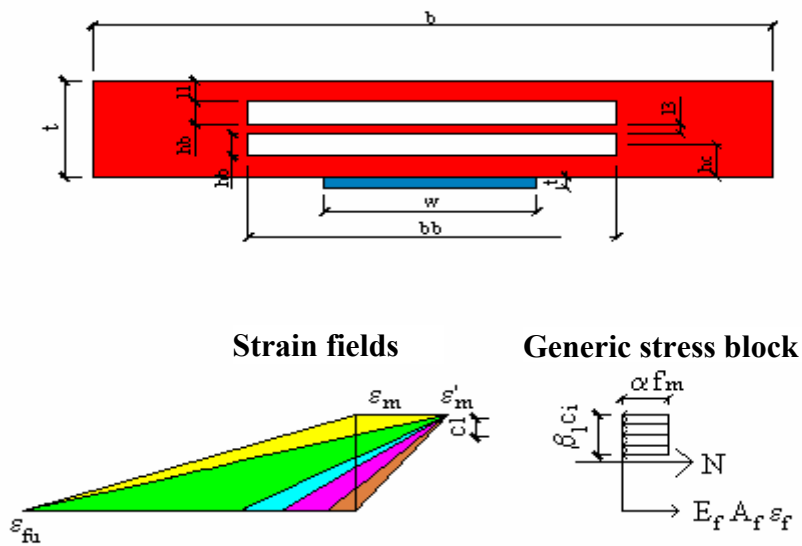


Fig. A.5 - 2. Strengthened section

FILE MATHCAD FOR THE M-N DIAGRAMS

Geometrical properties of the section:

$$\begin{array}{llll}
 b := 609.6 & h := 95.25 & bb := 330.2 & hb := 20.6375 \\
 t := 0.35306 & l1 := 22.225 & hc := l1 + \frac{hb}{2} & l3 := h - 2 \cdot l1 - 2 \cdot hb \\
 bf := 76.2 & bf1 := 127 & bf2 := 177.8 & bf3 := 228.6 \\
 Af := bf \cdot t & Af1 := bf1 \cdot t & Af2 := bf2 \cdot t & Af3 := bf3 \cdot t
 \end{array}$$

Material properties:

$$\begin{array}{llll}
 Ef := 83129.98 & Em := 14119.77 & n1 := \frac{Ef}{Em} & \epsilon mu := 0.0035 \\
 \epsilon fu := 0.0182 & fmu := 20.17406 & ffu := Ef \cdot \epsilon fu &
 \end{array}$$

Crushing of the masonry:

$$\begin{array}{l}
 \alpha := 0.89 \\
 \beta := 0.75 \\
 n := 1 \dots 10000 \\
 \epsilon x(n) := \frac{(n-1)1}{10000-1} \\
 c(\epsilon x) := \epsilon mu \frac{h}{(\epsilon x + \epsilon mu)}
 \end{array}$$

Determination of the strain limits:

$$\begin{array}{llll}
 c1 := \frac{(h-11)}{\beta} & c2 := \frac{(h-11-hb)}{\beta} & c3 := \frac{(h-11-hb-l3)}{\beta} & c4 := \frac{(h-11-2 \cdot hb-l3)}{\beta} \\
 \epsilon 1 := \epsilon mu \frac{(h-c1)}{c1} & \epsilon 2 := \epsilon mu \frac{(h-c2)}{c2} & \epsilon 3 := \epsilon mu \frac{(h-c3)}{c3} & \epsilon 4 := \epsilon mu \frac{(h-c4)}{c4}
 \end{array}$$

Unstrengthened cross-section:

$$N(\epsilon x) := \begin{cases} \alpha \cdot fmu \cdot [b \cdot c(\epsilon x) \cdot \beta - 2 \cdot (bb \cdot hb)] & \text{if } \epsilon x \leq \epsilon 1 \\ \alpha \cdot fmu \cdot [b \cdot c(\epsilon x) \cdot \beta - bb \cdot hb - bb \cdot (\beta \cdot c(\epsilon x) - 11 - hb - l3)] & \text{if } \epsilon 1 < \epsilon x \leq \epsilon 2 \\ \alpha \cdot fmu \cdot (b \cdot c(\epsilon x) \cdot \beta - bb \cdot hb) & \text{if } \epsilon 2 < \epsilon x \leq \epsilon 3 \\ \alpha \cdot fmu \cdot [b \cdot c(\epsilon x) \cdot \beta - bb \cdot (\beta \cdot c(\epsilon x) - 11)] & \text{if } \epsilon 3 < \epsilon x \leq \epsilon 4 \\ \alpha \cdot fmu \cdot \beta \cdot c(\epsilon x) \cdot b & \text{otherwise} \end{cases}$$

$$K1(\epsilon x) := \beta \cdot b \cdot c(\epsilon x) \cdot \alpha \cdot fmu \cdot \left[h - \left(\beta \cdot \frac{c(\epsilon x)}{2} \right) \right]$$

$$K(\epsilon x) := K1(\epsilon x) - bb \cdot hb \cdot \alpha \cdot fmu \cdot (h - hc)$$

$$M(\epsilon x) := \begin{cases} K1(\epsilon x) - bb \cdot hb \cdot \alpha \cdot fmu \cdot (h - hc) - bb \cdot hb \cdot \alpha \cdot fmu \cdot hc - N(\epsilon x) \frac{h}{2} & \text{if } \epsilon x \leq \epsilon 1 \\ K(\epsilon x) - bb \cdot \alpha \cdot fmu \cdot (\beta \cdot c(\epsilon x) - 11 - hb - 13) \cdot [(h - 11 - hb - 13) - 0.5 \cdot (\beta \cdot c(\epsilon x) - hb - 11 - 13)] - N(\epsilon x) \frac{h}{2} & \text{if } \epsilon 1 < \epsilon x \leq \epsilon 2 \\ K(\epsilon x) - N(\epsilon x) \frac{h}{2} & \text{if } \epsilon 2 < \epsilon x \leq \epsilon 3 \\ K1(\epsilon x) - \alpha \cdot fmu \cdot bb \cdot (\beta \cdot c(\epsilon x) - 11) \cdot \left[h - 11 - \left[\frac{(\beta \cdot c(\epsilon x) - 11)}{2} \right] \right] - N(\epsilon x) \frac{h}{2} & \text{if } \epsilon 3 < \epsilon x \leq \epsilon 4 \\ K1(\epsilon x) - N(\epsilon x) \frac{h}{2} & \text{otherwise} \end{cases}$$

Strengthened cross-section:

$$N1(\epsilon x) := \begin{cases} \alpha \cdot fmu \cdot [b \cdot c(\epsilon x) \cdot \beta - 2 \cdot (bb \cdot hb)] - Af \cdot \epsilon x \cdot Ef & \text{if } \epsilon x \leq \epsilon 1 \\ \alpha \cdot fmu \cdot [b \cdot c(\epsilon x) \cdot \beta - bb \cdot hb - bb \cdot (\beta \cdot c(\epsilon x) - 11 - hb - 13)] - Af \cdot \epsilon x \cdot Ef & \text{if } \epsilon 1 < \epsilon x \leq \epsilon 2 \\ \alpha \cdot fmu \cdot (b \cdot c(\epsilon x) \cdot \beta - bb \cdot hb) - Af \cdot \epsilon x \cdot Ef & \text{if } \epsilon 2 < \epsilon x \leq \epsilon 3 \\ \alpha \cdot fmu \cdot [b \cdot c(\epsilon x) \cdot \beta - bb \cdot (\beta \cdot c(\epsilon x) - 11)] - Af \cdot \epsilon x \cdot Ef & \text{if } \epsilon 3 < \epsilon x \leq \epsilon 4 \\ (\alpha \cdot fmu \cdot \beta \cdot c(\epsilon x) \cdot b) - Af \cdot \epsilon x \cdot Ef & \text{if } \epsilon 4 < \epsilon x \leq \epsilon fu \\ (\alpha \cdot fmu \cdot \beta \cdot c(\epsilon fu) \cdot b) - Af \cdot \epsilon fu \cdot Ef & \text{otherwise} \end{cases}$$

$$M1(\epsilon x) := \begin{cases} K1(\epsilon x) - bb \cdot hb \cdot \alpha \cdot fmu \cdot (h - hc) - bb \cdot hb \cdot \alpha \cdot fmu \cdot hc - N1(\epsilon x) \frac{h}{2} & \text{if } \epsilon x \leq \epsilon 1 \\ K(\epsilon x) - bb \cdot \alpha \cdot fmu \cdot (\beta \cdot c(\epsilon x) - 11 - hb - 13) \cdot [(h - 11 - hb - 13) - 0.5 \cdot (\beta \cdot c(\epsilon x) - hb - 11 - 13)] - N1(\epsilon x) \frac{h}{2} & \text{if } \epsilon 1 < \epsilon x \leq \epsilon 2 \\ K(\epsilon x) - N1(\epsilon x) \frac{h}{2} & \text{if } \epsilon 2 < \epsilon x \leq \epsilon 3 \\ K1(\epsilon x) - \alpha \cdot fmu \cdot bb \cdot (\beta \cdot c(\epsilon x) - 11) \cdot \left[h - 11 - \left[\frac{(\beta \cdot c(\epsilon x) - 11)}{2} \right] \right] - N1(\epsilon x) \frac{h}{2} & \text{if } \epsilon 3 < \epsilon x \leq \epsilon 4 \\ K1(\epsilon x) - N1(\epsilon x) \frac{h}{2} & \text{if } \epsilon 4 < \epsilon x \leq \epsilon fu \\ K1(\epsilon fu) - N1(\epsilon fu) \frac{h}{2} & \text{otherwise} \end{cases}$$

$$N2(\epsilon x) := \begin{cases} \alpha \cdot fmu \cdot [b \cdot c(\epsilon x) \cdot \beta - 2 \cdot (bb \cdot hb)] - Af1 \cdot \epsilon x \cdot Ef & \text{if } \epsilon x \leq \epsilon 1 \\ \alpha \cdot fmu \cdot [b \cdot c(\epsilon x) \cdot \beta - bb \cdot hb - bb \cdot (\beta \cdot c(\epsilon x) - 11 - hb - 13)] - Af1 \cdot \epsilon x \cdot Ef & \text{if } \epsilon 1 < \epsilon x \leq \epsilon 2 \\ \alpha \cdot fmu \cdot (b \cdot c(\epsilon x) \cdot \beta - bb \cdot hb) - Af1 \cdot \epsilon x \cdot Ef & \text{if } \epsilon 2 < \epsilon x \leq \epsilon 3 \\ \alpha \cdot fmu \cdot [b \cdot c(\epsilon x) \cdot \beta - bb \cdot (\beta \cdot c(\epsilon x) - 11)] - Af1 \cdot \epsilon x \cdot Ef & \text{if } \epsilon 3 < \epsilon x \leq \epsilon 4 \\ (\alpha \cdot fmu \cdot \beta \cdot c(\epsilon x) \cdot b) - Af1 \cdot \epsilon x \cdot Ef & \text{if } \epsilon 4 < \epsilon x \leq \epsilon fu \\ (\alpha \cdot fmu \cdot \beta \cdot c(\epsilon fu) \cdot b) - Af1 \cdot \epsilon fu \cdot Ef & \text{otherwise} \end{cases}$$

$$\begin{aligned}
m &:= 1 \dots 10000 \\
\epsilon m(m) &:= \frac{(m-1) \cdot \epsilon mu}{10000 - 1} \\
\alpha 1(m) &:= \frac{-2 \cdot \epsilon m(m) \cdot (-3 \cdot \epsilon mu + \epsilon m(m))^2}{3(-4 \cdot \epsilon mu + \epsilon m(m)) \cdot \epsilon mu^2} \\
\beta 1(m) &:= \frac{1 \cdot (-4 \cdot \epsilon mu + \epsilon m(m))}{2(-3 \cdot \epsilon mu + \epsilon m(m))} \\
cm(m) &:= \frac{\epsilon m(m) \cdot h}{\epsilon fu + \epsilon m(m)} \\
Na1(m) &:= \alpha 1(m) \cdot fmu \cdot \beta 1(m) \cdot cm(m) \cdot b - Af \cdot \epsilon fu \cdot Ef \\
Ma1(m) &:= \alpha 1(m) \cdot fmu \cdot \beta 1(m) \cdot cm(m) \cdot b \cdot \left(h - \beta 1(m) \frac{cm(m)}{2} \right) - Na1(m) \frac{h}{2} \\
Na2(m) &:= \alpha 1(m) \cdot fmu \cdot \beta 1(m) \cdot cm(m) \cdot b - Af1 \cdot \epsilon fu \cdot Ef \\
Ma2(m) &:= \alpha 1(m) \cdot fmu \cdot \beta 1(m) \cdot cm(m) \cdot b \cdot \left(h - \beta 1(m) \frac{cm(m)}{2} \right) - Na2(m) \frac{h}{2} \\
Na3(m) &:= \alpha 1(m) \cdot fmu \cdot \beta 1(m) \cdot cm(m) \cdot b - Af2 \cdot \epsilon fu \cdot Ef \\
Ma3(m) &:= \alpha 1(m) \cdot fmu \cdot \beta 1(m) \cdot cm(m) \cdot b \cdot \left(h - \beta 1(m) \frac{cm(m)}{2} \right) - Na3(m) \frac{h}{2} \\
Na4(m) &:= \alpha 1(m) \cdot fmu \cdot \beta 1(m) \cdot cm(m) \cdot b - Af3 \cdot \epsilon fu \cdot Ef \\
Ma4(m) &:= \alpha 1(m) \cdot fmu \cdot \beta 1(m) \cdot cm(m) \cdot b \cdot \left(h - \beta 1(m) \frac{cm(m)}{2} \right) - Na4(m) \frac{h}{2} \\
Nu &:= \alpha \cdot fmu \cdot [b \cdot h - 2 \cdot (bb \cdot hb)] \\
rx &:= N(0) \dots Nu \\
ry(rx) &:= \frac{M(0) \cdot rx}{N(0) - Nu} + \frac{-Nu \cdot M(0)}{N(0) - Nu}
\end{aligned}$$

M function of N for unstrengthened section:

$$\begin{aligned}
ex1 &:= 0 \dots 2 \\
cm(ex1) &:= \epsilon mu \frac{h}{(\epsilon x1 + \epsilon mu)} \\
Nm(ex1) &:= \begin{cases} \alpha \cdot fmu \cdot [b \cdot cm(ex1) \cdot \beta - 2 \cdot (bb \cdot hb)] & \text{if } ex1 \leq \epsilon 1 \\ \alpha \cdot fmu \cdot [b \cdot cm(ex1) \cdot \beta - bb \cdot hb - bb \cdot (\beta \cdot cm(ex1) - l1 - hb - l3)] & \text{if } \epsilon 1 < ex1 \leq \epsilon 2 \\ \alpha \cdot fmu \cdot (b \cdot cm(ex1) \cdot \beta - bb \cdot hb) & \text{if } \epsilon 2 < ex1 \leq \epsilon 3 \\ \alpha \cdot fmu \cdot [b \cdot cm(ex1) \cdot \beta - bb \cdot (\beta \cdot cm(ex1) - l1)] & \text{if } \epsilon 3 < ex1 \leq \epsilon 4 \\ \alpha \cdot fmu \cdot \beta \cdot cm(ex1) \cdot b & \text{otherwise} \end{cases}
\end{aligned}$$

$$N1 := N(\epsilon 1)$$

$$N2 := N(\epsilon 2)$$

$$N3 := N(\epsilon 3)$$

$$N4 := N(\epsilon 4)$$

$$C1(N) := \frac{\frac{N}{\alpha \cdot fmu} + 2 \cdot bb \cdot hb}{b \cdot \beta}$$

$$C2(N) := \frac{\frac{N}{\alpha \cdot fmu} - (bb \cdot l1 + bb \cdot l3)}{b \cdot \beta - \beta \cdot bb}$$

$$C3(N) := \frac{\frac{N}{\alpha \cdot fmu} + bb \cdot hb}{b \cdot \beta}$$

$$C4(N) := \frac{-bb \cdot l1 + \frac{N}{\alpha \cdot fmu}}{b \cdot \beta - bb \cdot \beta}$$

$$C5(N) := \frac{N}{\alpha \cdot fmu \cdot \beta \cdot b}$$

$$K1m1(N) := \beta \cdot b \cdot C1(N) \cdot \alpha \cdot fmu \cdot \left[h - \left(\beta \frac{C1(N)}{2} \right) \right]$$

$$K1m2(N) := \beta \cdot b \cdot C2(N) \cdot \alpha \cdot fmu \cdot \left[h - \left(\beta \frac{C2(N)}{2} \right) \right]$$

$$K1m3(N) := \beta \cdot b \cdot C3(N) \cdot \alpha \cdot fmu \cdot \left[h - \left(\beta \frac{C3(N)}{2} \right) \right]$$

$$K1m4(N) := \beta \cdot b \cdot C4(N) \cdot \alpha \cdot fmu \left[h - \left(\beta \frac{C4(N)}{2} \right) \right]$$

$$K1m5(N) := \beta \cdot b \cdot C5(N) \cdot \alpha \cdot fmu \left[h - \left(\beta \frac{C5(N)}{2} \right) \right]$$

$$Km2(N) := K1m2(N) - bb \cdot hb \cdot \alpha \cdot fmu \cdot (h - hc)$$

$$Km3(N) := K1m3(N) - bb \cdot hb \cdot \alpha \cdot fmu \cdot (h - hc)$$

$$Mu(N) := \begin{cases} K1m1(N) - bb \cdot hb \cdot \alpha \cdot fmu \cdot (h - hc) - bb \cdot hb \cdot \alpha \cdot fmu \cdot hc - N \frac{h}{2} & \text{if } N \geq N1 \\ Km2(N) - bb \cdot \alpha \cdot fmu \cdot (\beta \cdot C2(N) - 11 - hb - 13) \cdot [(h - 11 - hb - 13) - 0.5 \cdot (\beta \cdot C2(N) - hb - 11 - 13)] - N \frac{h}{2} & \text{if } N1 > N \geq N2 \\ Km3(N) - N \frac{h}{2} & \text{if } N2 > N \geq N3 \\ K1m4(N) - \alpha \cdot fmu \cdot bb \cdot (\beta \cdot C4(N) - 11) \left[h - 11 - \left[\frac{(\beta \cdot C4(N) - 11)}{2} \right] \right] - N \frac{h}{2} & \text{if } N3 > N \geq N4 \\ K1m5(N) - N \frac{h}{2} & \text{otherwise} \end{cases}$$

N := 0 .. Nu

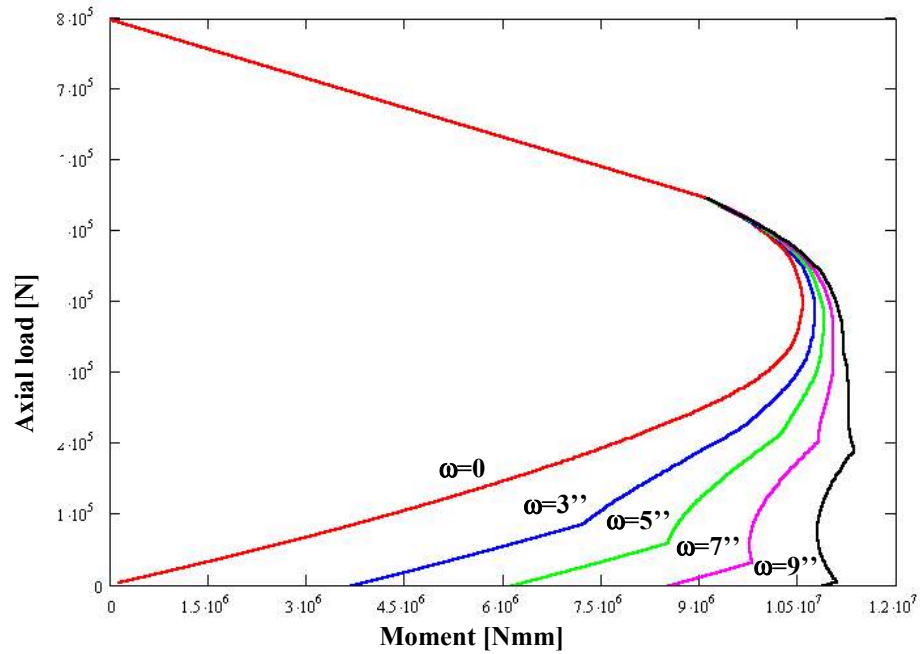


Fig. A.5 – 3. Interaction diagrams for clay cross sections

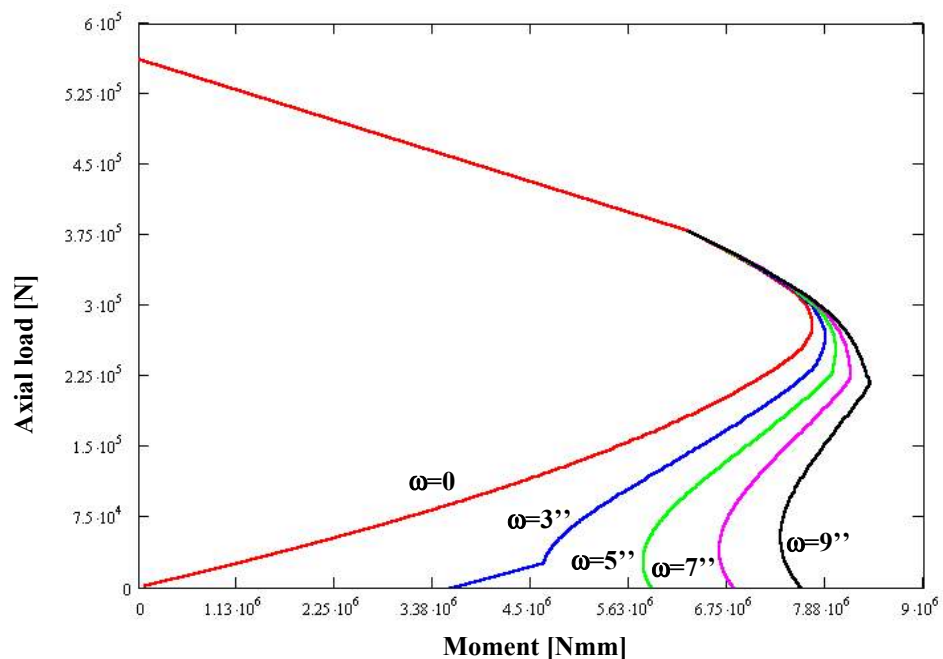


Fig. A.5 – 4. Interaction diagrams for concrete cross sections

Tab. A.5 – 1. Experimental moments for the clay specimens

Specimen	N [kN]	M _{MID} [kN mm]	M _{BOUND} [kN mm]
Control B	57.8	2601	2601
BG3	115.6	7663	4895
BG5	101.4	8789	4359
BG7	97.9	9872	4223
BG9	80.9	10797	3554

Tab. A.5 – 2. Experimental moments for the concrete specimens

Specimen	N [kN]	M _{MID} [kN mm]	M _{BOUND} [kN mm]
Control C	83.6	3406	3406
CG3	82.7	5238	3375
CG5	58.7	5888	2483
CG7	58.7	6683	2483
CG9	38.3	7372	1670

Tab. A.5 – 3. Reinforcement ratio ω_f for clay and concrete masonry

Specimen	b [mm]	h [mm]	FRP width [mm]	Af [mm ²]	ρ_f	ω_f
Control B	609.6	95.25	-	-	-	-
BG3	609.6	95.25	76.2	26.90	0.000463	0.149
BG5	609.6	95.25	127	44.84	0.000772	0.248
BG7	609.6	95.25	177.8	62.77	0.001081	0.348
BG9	609.6	95.25	228.6	80.71	0.00139	0.448
Control C	609.6	92.07	-	-	-	-
CG3	609.6	92.07	76.2	26.90	0.000479	0.206
CG5	609.6	92.07	127	44.84	0.000799	0.344
CG7	609.6	92.07	177.8	62.77	0.001118	0.481
CG9	609.6	92.07	228.6	80.71	0.001438	0.618

Note: 1 mm = 0.03937 in

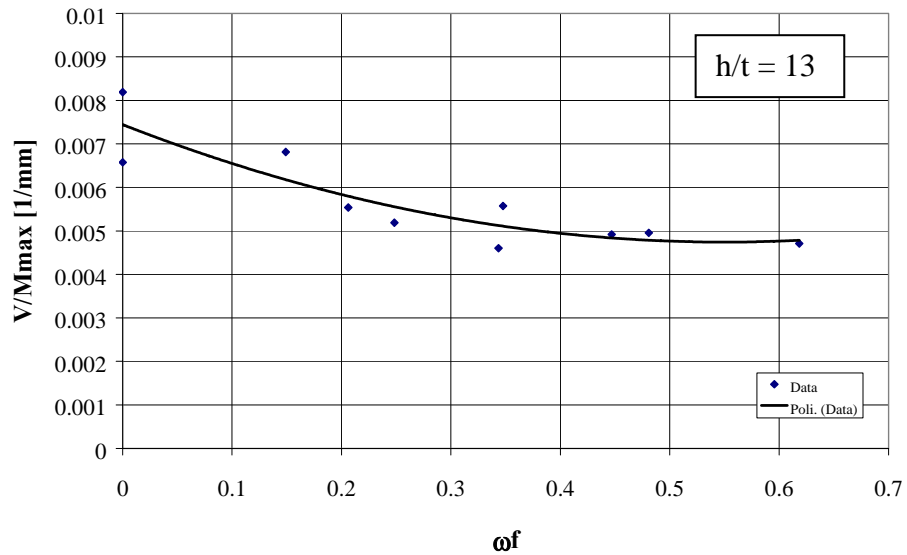


Fig. A.5 – 5. Comparison for all the specimens

FILE MATHCAD FOR DESIGN PURPOSES

Geometrical properties of the section:

$$\begin{aligned}
 b &:= 609.6 & h &:= 92.075 & bb &:= 405.60625 & hb &:= 31.75 \\
 t &:= 0.35306 & l1 &:= 30.1625 & hc &:= l1 + \frac{hb}{2} & l3 &:= h - 2 \cdot l1 - hb \\
 bf &:= 76.2 & bf1 &:= 76.2 & Af &:= bf \cdot t & Af1 &:= bf1 \cdot t \\
 Ac &:= b \cdot h - bb \cdot hb
 \end{aligned}$$

Material properties:

$$\begin{aligned}
 Ef &:= 83129.66 & Em &:= 13125.66 & n1 &:= \frac{Ef}{Em} & \epsilon_{mu} &:= 0.0025 \\
 \epsilon_{fu} &:= 0.0182 & f_{mu} &:= 14.58241 & f_{fu} &:= Ef \cdot \epsilon_{fu}
 \end{aligned}$$

Crushing of the masonry:

$$\begin{aligned}
 \alpha &:= 0.89 \\
 \beta &:= 0.75 \\
 \epsilon_x &:= 0, 0.0001 .. 1 \\
 c(\epsilon_x) &:= \epsilon_{mu} \frac{h}{(\epsilon_x + \epsilon_{mu})}
 \end{aligned}$$

Determination of the strain limits:

$$\begin{aligned}
 c1 &:= \frac{(h - l1)}{\beta} & c2 &:= \frac{(h - l1 - hb)}{\beta} \\
 \epsilon1 &:= \epsilon_{mu} \frac{(h - c1)}{c1} & \epsilon2 &:= \epsilon_{mu} \frac{(h - c2)}{c2}
 \end{aligned}$$

Unstrengthened cross-section:**Real section:**

$$N(\epsilon_x) := \begin{cases} \alpha \cdot f_{mu} \cdot (b \cdot c(\epsilon_x) \cdot \beta - bb \cdot hb) & \text{if } \epsilon_x \leq \epsilon1 \\ \alpha \cdot f_{mu} \cdot [b \cdot c(\epsilon_x) \cdot \beta - bb \cdot (\beta \cdot c(\epsilon_x) - 11)] & \text{if } \epsilon1 < \epsilon_x \leq \epsilon2 \\ \alpha \cdot f_{mu} \cdot \beta \cdot c(\epsilon_x) \cdot b & \text{otherwise} \end{cases}$$

$$K1(\epsilon_x) := \beta \cdot b \cdot c(\epsilon_x) \cdot \alpha \cdot f_{mu} \cdot \left[h - \left(\beta \cdot \frac{c(\epsilon_x)}{2} \right) \right]$$

$$K(\epsilon_x) := K1(\epsilon_x) - bb \cdot hb \cdot \alpha \cdot f_{mu} \cdot (h - hc)$$

$$M(\epsilon_x) := \begin{cases} K1(\epsilon_x) - bb \cdot hb \cdot \alpha \cdot f_{mu} \cdot hc - N(\epsilon_x) \cdot \frac{h}{2} & \text{if } \epsilon_x \leq \epsilon1 \\ K1(\epsilon_x) - bb \cdot \alpha \cdot f_{mu} \cdot (\beta \cdot c(\epsilon_x) - 11) \cdot \left[h - 11 - \frac{(\beta \cdot c(\epsilon_x) - 11)}{2} \right] - N(\epsilon_x) \cdot \frac{h}{2} & \text{if } \epsilon1 < \epsilon_x \leq \epsilon2 \\ K1(\epsilon_x) - N(\epsilon_x) \cdot \frac{h}{2} & \text{otherwise} \end{cases}$$

Full section:

$$Np(\varepsilon x) := \begin{cases} \alpha \cdot fmu \cdot (b \cdot c(\varepsilon x) \cdot \beta) & \text{if } \varepsilon x \leq \varepsilon 2 \\ \alpha \cdot fmu \cdot \beta \cdot c(\varepsilon x) \cdot b & \text{otherwise} \end{cases}$$

$$Mp(\varepsilon x) := \begin{cases} K1(\varepsilon x) - Np(\varepsilon x) \frac{h}{2} & \text{if } \varepsilon x \leq \varepsilon 2 \\ K1(\varepsilon x) - Np(\varepsilon x) \frac{h}{2} & \text{otherwise} \end{cases}$$

Equivalent section:

$$b1 := \frac{Ac}{h}$$

$$Nc(\varepsilon x) := \begin{cases} \alpha \cdot fmu \cdot (b1 \cdot c(\varepsilon x) \cdot \beta) & \text{if } \varepsilon x \leq \varepsilon 2 \\ \alpha \cdot fmu \cdot \beta \cdot c(\varepsilon x) \cdot b1 & \text{otherwise} \end{cases}$$

$$K2(\varepsilon x) := \beta \cdot b1 \cdot c(\varepsilon x) \cdot \alpha \cdot fmu \left[h - \left(\beta \frac{c(\varepsilon x)}{2} \right) \right]$$

$$Mc(\varepsilon x) := \begin{cases} K2(\varepsilon x) - Nc(\varepsilon x) \frac{h}{2} & \text{if } \varepsilon x \leq \varepsilon 2 \\ K2(\varepsilon x) - Nc(\varepsilon x) \frac{h}{2} & \text{otherwise} \end{cases}$$

Strengthened cross-sections:**Real section:**

$$N1(\varepsilon x) := \begin{cases} \alpha \cdot fmu \cdot (b \cdot c(\varepsilon x) \cdot \beta - bb \cdot hb) - Af \cdot Ef \cdot \varepsilon x & \text{if } \varepsilon x \leq \varepsilon 1 \\ \alpha \cdot fmu \cdot [b \cdot c(\varepsilon x) \cdot \beta - bb \cdot (\beta \cdot c(\varepsilon x) - 11)] - Af \cdot Ef \cdot \varepsilon x & \text{if } \varepsilon 1 < \varepsilon x \leq \varepsilon 2 \\ (\alpha \cdot fmu \cdot \beta \cdot c(\varepsilon x) \cdot b - Af \cdot Ef \cdot \varepsilon x) & \text{if } \varepsilon 2 \leq \varepsilon x \leq \varepsilon fu \\ (\alpha \cdot fmu \cdot \beta \cdot c(\varepsilon fu) \cdot b - Af \cdot Ef \cdot \varepsilon fu) & \text{otherwise} \end{cases}$$

$$K(\varepsilon x) := K1(\varepsilon x) - bb \cdot hb \cdot \alpha \cdot fmu \cdot (h - hc)$$

$$K1(\varepsilon x) := \beta \cdot b \cdot c(\varepsilon x) \cdot \alpha \cdot fmu \left[h - \left(\beta \frac{c(\varepsilon x)}{2} \right) \right]$$

$$M1(\varepsilon x) := \begin{cases} K1(\varepsilon x) - bb \cdot hb \cdot \alpha \cdot fmu \cdot hc - N1(\varepsilon x) \frac{h}{2} & \text{if } \varepsilon x \leq \varepsilon 1 \\ K1(\varepsilon x) - bb \cdot \alpha \cdot fmu \cdot (\beta \cdot c(\varepsilon x) - 11) \left[h - 11 - \frac{(\beta \cdot c(\varepsilon x) - 11)}{2} \right] - N1(\varepsilon x) \frac{h}{2} & \text{if } \varepsilon 1 < \varepsilon x \leq \varepsilon 2 \\ K1(\varepsilon x) - N1(\varepsilon x) \frac{h}{2} & \text{if } \varepsilon 2 \leq \varepsilon x \leq \varepsilon fu \\ K1(\varepsilon fu) - N1(\varepsilon fu) \frac{h}{2} & \text{otherwise} \end{cases}$$

Full section:

$$N2p(\varepsilon x) := \begin{cases} \alpha \cdot fmu \cdot (b \cdot c(\varepsilon x) \cdot \beta) - Af \cdot Ef \cdot \varepsilon x & \text{if } \varepsilon x \leq \varepsilon 2 \\ (\alpha \cdot fmu \cdot \beta \cdot c(\varepsilon x) \cdot b - Af \cdot Ef \cdot \varepsilon x) & \text{if } \varepsilon 2 \leq \varepsilon x \leq \varepsilon fu \\ (\alpha \cdot fmu \cdot \beta \cdot c(\varepsilon fu) \cdot b - Af \cdot Ef \cdot \varepsilon fu) & \text{otherwise} \end{cases}$$

$$K1(\varepsilon x) := \beta \cdot b \cdot c(\varepsilon x) \cdot \alpha \cdot fmu \cdot \left[h - \left(\beta \cdot \frac{c(\varepsilon x)}{2} \right) \right]$$

$$M2p(\varepsilon x) := \begin{cases} K1(\varepsilon x) - N2p(\varepsilon x) \frac{h}{2} & \text{if } \varepsilon x \leq \varepsilon 2 \\ K1(\varepsilon x) - N2p(\varepsilon x) \frac{h}{2} & \text{if } \varepsilon 2 \leq \varepsilon x \leq \varepsilon fu \\ K1(\varepsilon fu) - N2p(\varepsilon fu) \frac{h}{2} & \text{otherwise} \end{cases}$$

Equivalent section:

$$N2c(\varepsilon x) := \begin{cases} \alpha \cdot fmu \cdot (b1 \cdot c(\varepsilon x) \cdot \beta) - Af \cdot Ef \cdot \varepsilon x & \text{if } \varepsilon x \leq \varepsilon 2 \\ (\alpha \cdot fmu \cdot \beta \cdot c(\varepsilon x) \cdot b1 - Af \cdot Ef \cdot \varepsilon x) & \text{if } \varepsilon 2 \leq \varepsilon x \leq \varepsilon fu \\ (\alpha \cdot fmu \cdot \beta \cdot c(\varepsilon fu) \cdot b1 - Af \cdot Ef \cdot \varepsilon fu) & \text{otherwise} \end{cases}$$

$$K1c(\varepsilon x) := \beta \cdot b1 \cdot c(\varepsilon x) \cdot \alpha \cdot fmu \cdot \left[h - \left(\beta \cdot \frac{c(\varepsilon x)}{2} \right) \right]$$

$$M2c(\varepsilon x) := \begin{cases} K1c(\varepsilon x) - N2c(\varepsilon x) \frac{h}{2} & \text{if } \varepsilon x \leq \varepsilon 2 \\ K1c(\varepsilon x) - N2c(\varepsilon x) \frac{h}{2} & \text{if } \varepsilon 2 \leq \varepsilon x \leq \varepsilon fu \\ K1c(\varepsilon fu) - N2c(\varepsilon fu) \frac{h}{2} & \text{otherwise} \end{cases}$$

$$Nup := \alpha \cdot fmu \cdot b \cdot h$$

$$rxp := Np(0), Nup.. Nup$$

$$ryp(\text{rxp}) := \frac{Mp(0) \cdot \text{rxp}}{Np(0) - Nup} + \frac{-Nup \cdot Mp(0)}{Np(0) - Nup}$$

$$Nuc := \alpha \cdot fmu \cdot b1 \cdot h$$

$$rxc := Nc(0), Nuc.. Nuc$$

$$ryc(\text{rxc}) := \frac{Mc(0) \cdot \text{rxc}}{Nc(0) - Nuc} + \frac{-Nuc \cdot Mc(0)}{Nc(0) - Nuc}$$

$$Nu := \alpha \cdot fmu \cdot (b \cdot h - bb \cdot hb)$$

$$rx := N(0), Nu.. Nu$$

$$ry(\text{rx}) := \frac{M(0) \cdot \text{rx}}{N(0) - Nu} + \frac{-Nu \cdot M(0)}{N(0) - Nu}$$

$$\varepsilon m := 0, 0.000001 .. 0.0025$$

$$\alpha 1(\varepsilon m) := \frac{-2 \cdot \varepsilon m \cdot (-3 \cdot \varepsilon m u + \varepsilon m)^2}{3(-4 \cdot \varepsilon m u + \varepsilon m) \cdot \varepsilon m u^2}$$

$$\beta 1(\varepsilon m) := \frac{1 \cdot (-4 \cdot \varepsilon m u + \varepsilon m)}{2(-3 \cdot \varepsilon m u + \varepsilon m)}$$

$$cm(\varepsilon m) := \frac{\varepsilon m \cdot h}{\varepsilon fu + \varepsilon m}$$

Real section:

$$N_{a1}(\varepsilon_m) := \alpha_1(\varepsilon_m) \cdot f_{mu} \cdot \beta_1(\varepsilon_m) \cdot c_m(\varepsilon_m) \cdot b - A_f \cdot \varepsilon_{fu} \cdot E_f$$

$$M_{a1}(\varepsilon_m) := \alpha_1(\varepsilon_m) \cdot f_{mu} \cdot \beta_1(\varepsilon_m) \cdot c_m(\varepsilon_m) \cdot b \cdot \left(h - \beta_1(\varepsilon_m) \cdot \frac{c_m(\varepsilon_m)}{2} \right) - N_{a1}(\varepsilon_m) \cdot \frac{h}{2}$$

Full section:

$$N_{ap}(\varepsilon_m) := \alpha_1(\varepsilon_m) \cdot f_{mu} \cdot \beta_1(\varepsilon_m) \cdot c_m(\varepsilon_m) \cdot b - A_f \cdot \varepsilon_{fu} \cdot E_f$$

$$M_{ap}(\varepsilon_m) := \alpha_1(\varepsilon_m) \cdot f_{mu} \cdot \beta_1(\varepsilon_m) \cdot c_m(\varepsilon_m) \cdot b \cdot \left(h - \beta_1(\varepsilon_m) \cdot \frac{c_m(\varepsilon_m)}{2} \right) - N_{ap}(\varepsilon_m) \cdot \frac{h}{2}$$

Equivalent section:

$$N_{ac}(\varepsilon_m) := \alpha_1(\varepsilon_m) \cdot f_{mu} \cdot \beta_1(\varepsilon_m) \cdot c_m(\varepsilon_m) \cdot b_1 - A_f \cdot \varepsilon_{fu} \cdot E_f$$

$$M_{ac}(\varepsilon_m) := \alpha_1(\varepsilon_m) \cdot f_{mu} \cdot \beta_1(\varepsilon_m) \cdot c_m(\varepsilon_m) \cdot b_1 \cdot \left(h - \beta_1(\varepsilon_m) \cdot \frac{c_m(\varepsilon_m)}{2} \right) - N_{ac}(\varepsilon_m) \cdot \frac{h}{2}$$

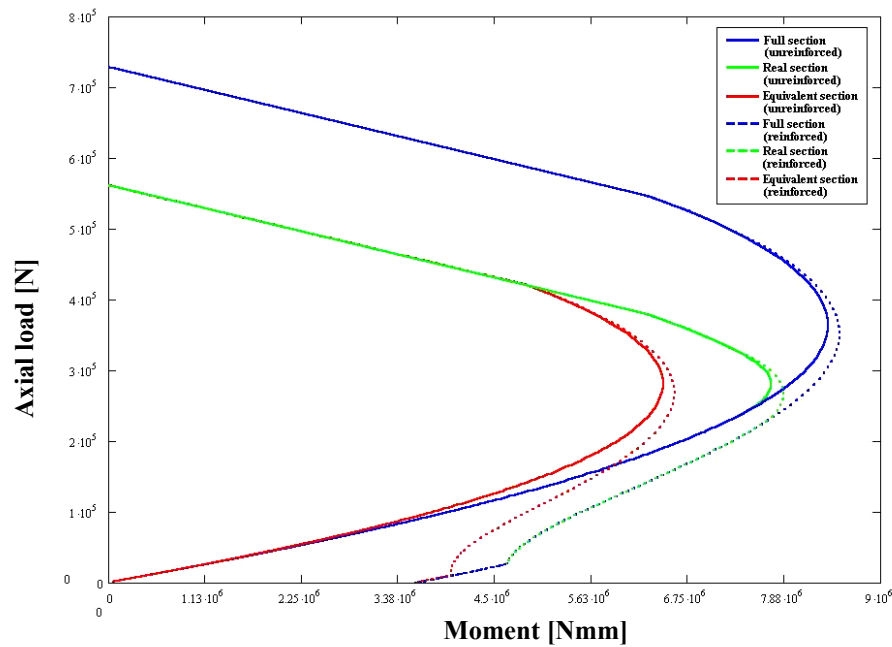


Fig. A.5 – 6. Different approaches for design purposes

APPENDIX B: IN - PLANE

APPENDIX B.1: Test Specimens

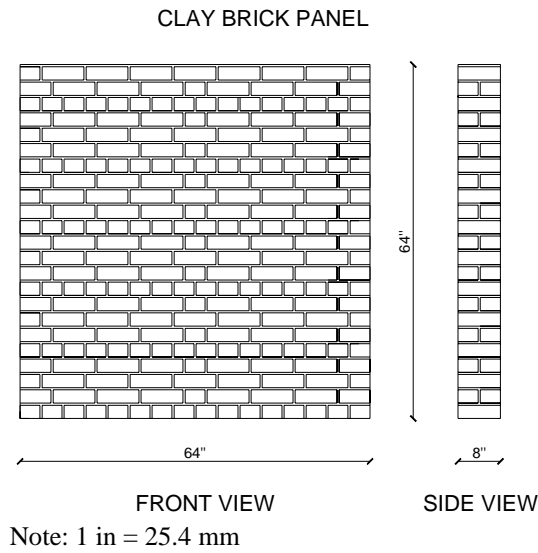
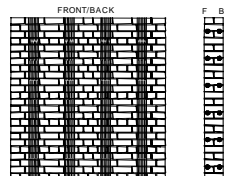
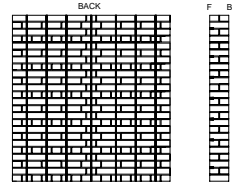
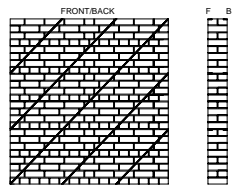


Fig.B.1 - 1. Configuration of the walls

Tab. B.1 - 1. Test matrix for Series CLW

Specimen	Strengthening	Front Side	Back Side	Layout
CLW1	None	None	None	
CLW2	#2 GFRP bars	4HJ	4HJ	
CLW3	#2 GFRP bars 4 in GFRP laminates	2HJ/4VS	2HJ/4VS	

Tab. B.1 - 1. Test matrix (continued)

Specimen	Strengthening	Front Side	Back Side	Layout
CLW4	#2 GFRP bars 4 in GFRP laminates	4HJ/4VS	4HJ/4VS	
CLW5	Carbon strips	3/4HC	3/4VC	
CLW6	Carbon strips	5D	5D	

LEGEND: 2HJ=every second mortar joint, 4HJ= every fourth mortar joint, 4VS= four vertical glass strips @ 16 in o.c., 3/4VC= vertical carbon strips every third/fourth mortar joint, 3/4HC= horizontal carbon strips every third/fourth mortar joint, 5D= five diagonal carbon strips symmetrically spaced from the diagonal

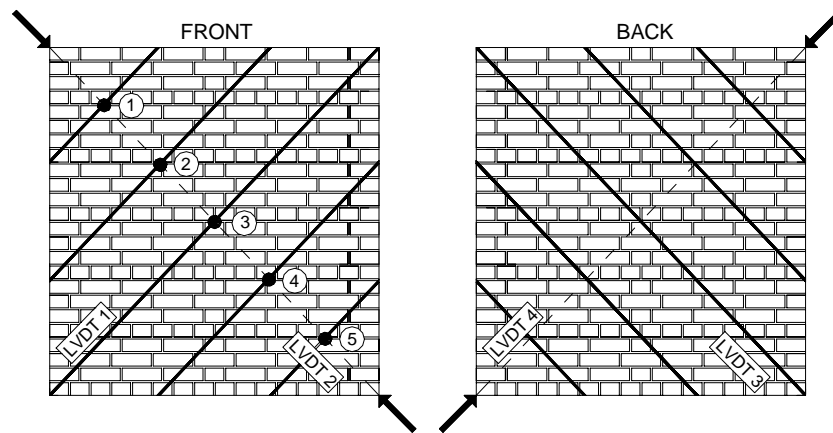
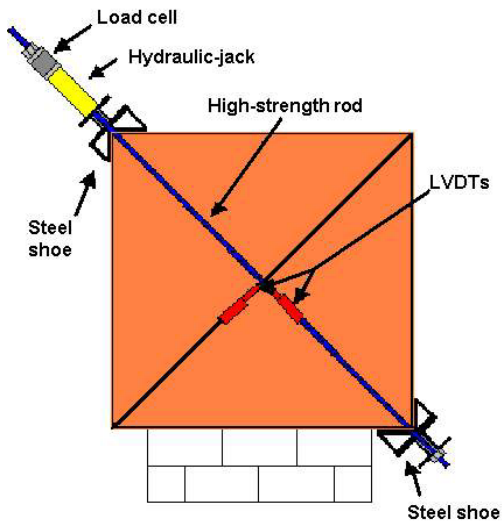


Fig.B.1 - 2. Typical strain gages and LVDT's location

APPENDIX B.2: Test Setup



(a) Test setup scheme

(b) Test setup

Fig.B.2 - 1. Test setup



Fig.B.2 - 2. Steel shoe

Tab. B.2 - 1. Test cycles

Cycle	Load Range (kips)
1	0-6.7-2.2
2	2.2-9.0-2.2
3	2.2-11.2-2.2
4	2.2-failure

Note: 1kN = 0.2248 kip

APPENDIX B.3: Test Results

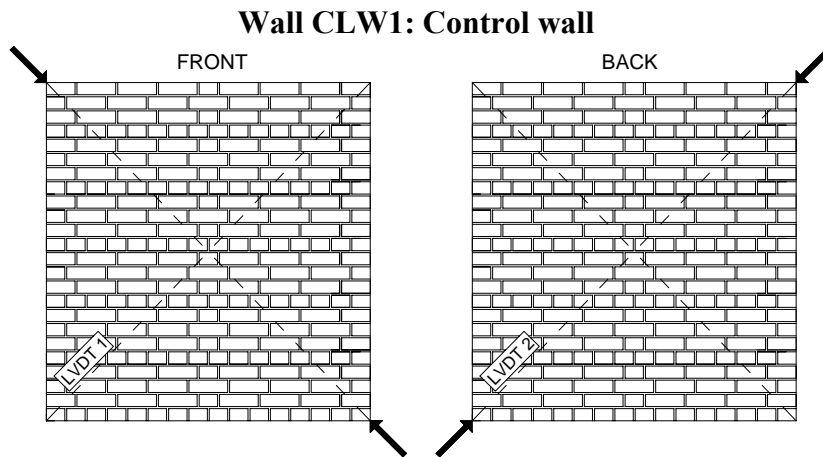


Fig.B.3 - 1. LVDTs location and loaded diagonal

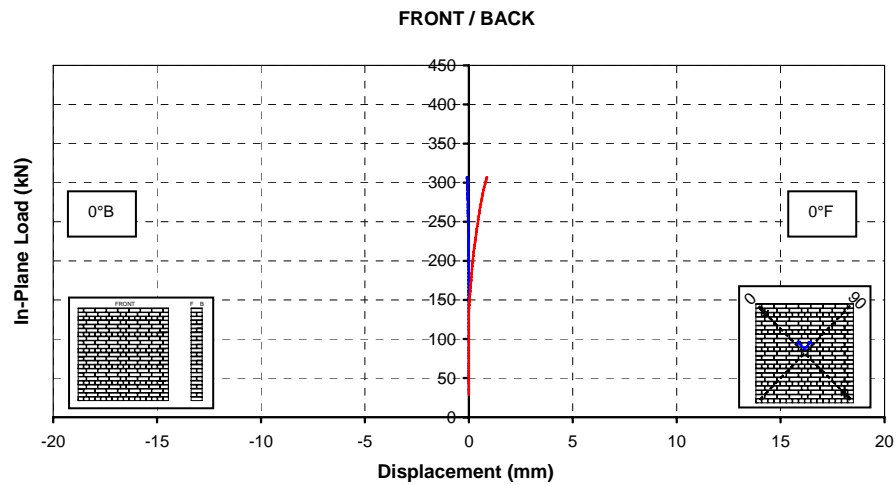


Fig.B.3 - 2. Load vs. diagonal displacement



Fig.B.3 - 3. Wall CLW1 after failure (front)

Wall CLW2

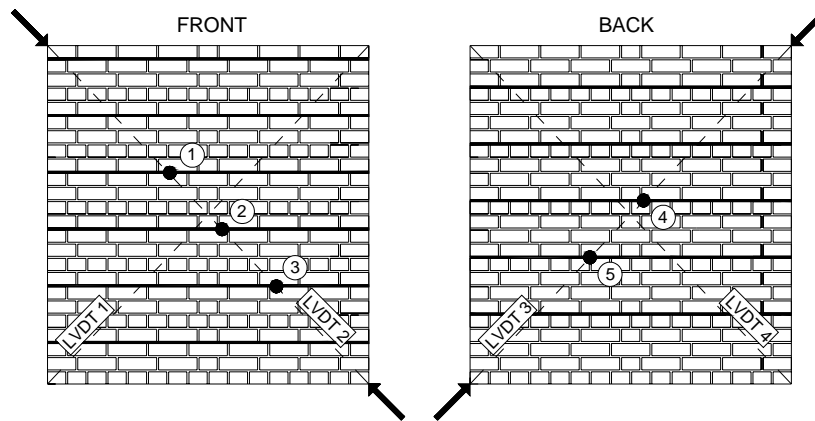


Fig.B.3 - 4. Strain gauges, LVDTs locations and loaded diagonal

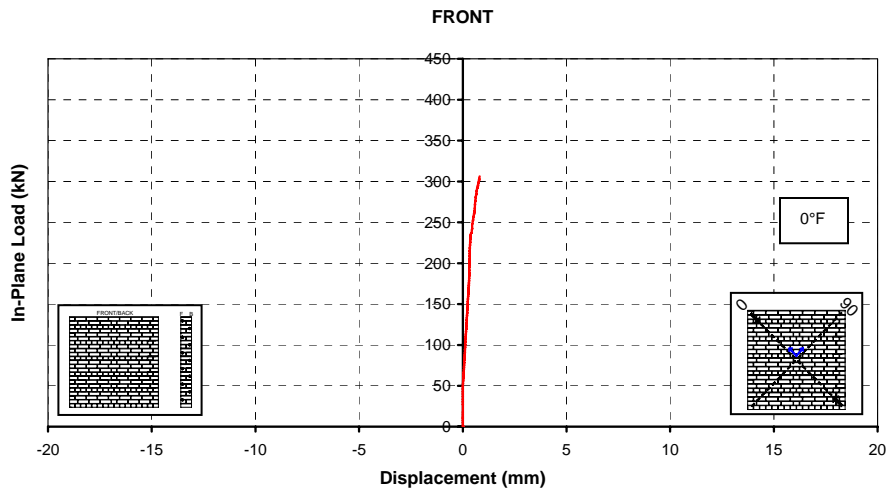


Fig.B.3 - 5. Load vs. diagonal displacement



Fig.B.3 - 6. Wall CLW2 after failure (front)

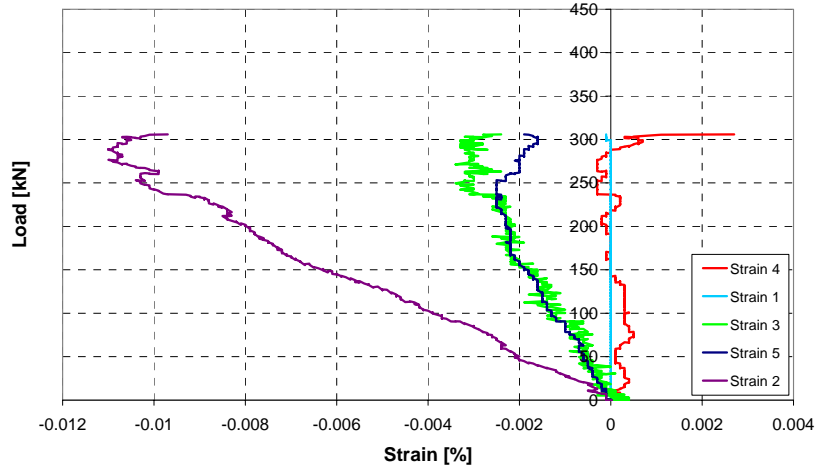


Fig.B.3 - 7. Load vs. strain

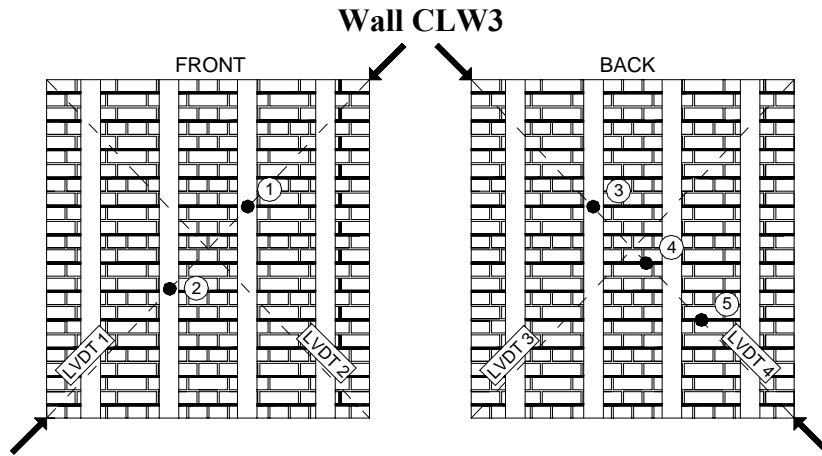


Fig.B.3 - 8. Strain gauges, LVDTs locations and loaded diagonal

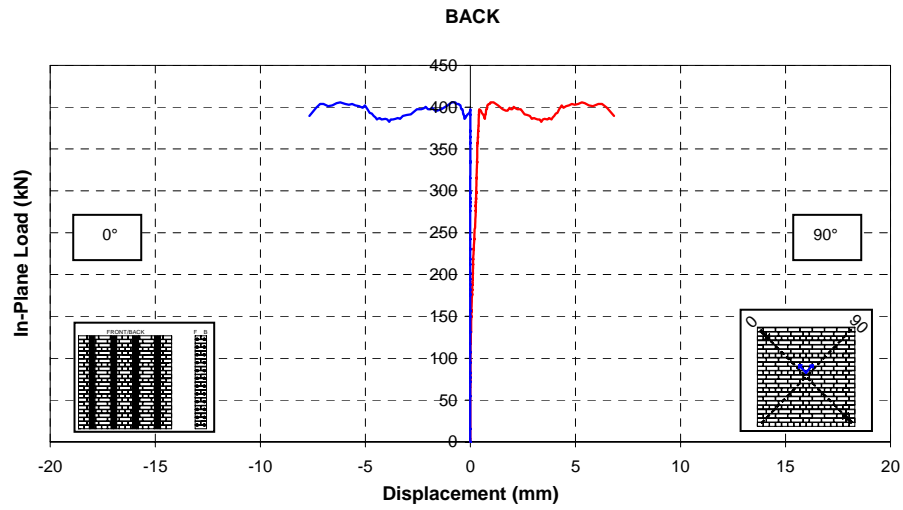


Fig.B.3 - 9. Load vs. diagonal displacement



Fig.B.3 - 10. Wall CLW3 after failure (front)

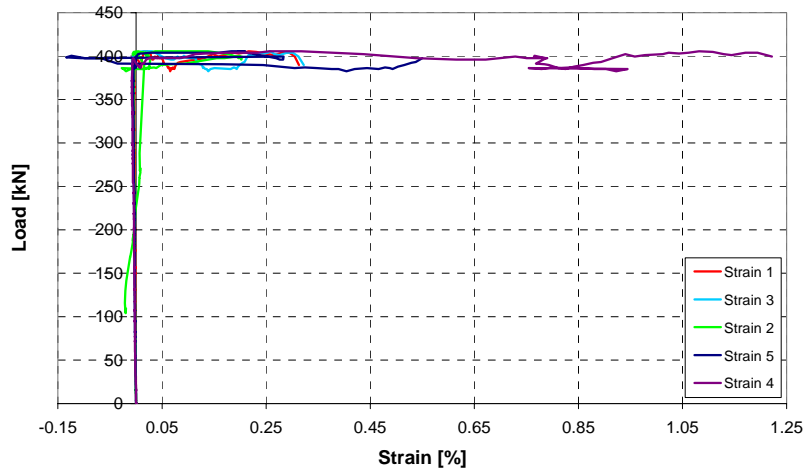


Fig.B.3 - 11. Load vs. strain

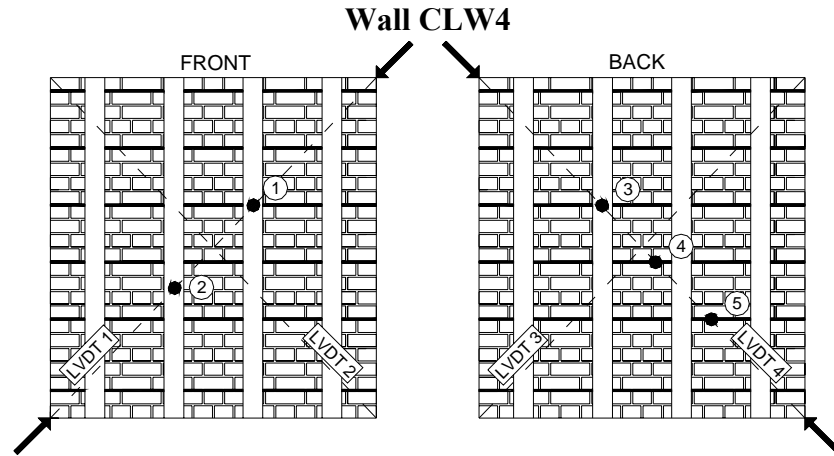


Fig.B.3 - 12. Strain gauges, LVDTs locations and loaded diagonal

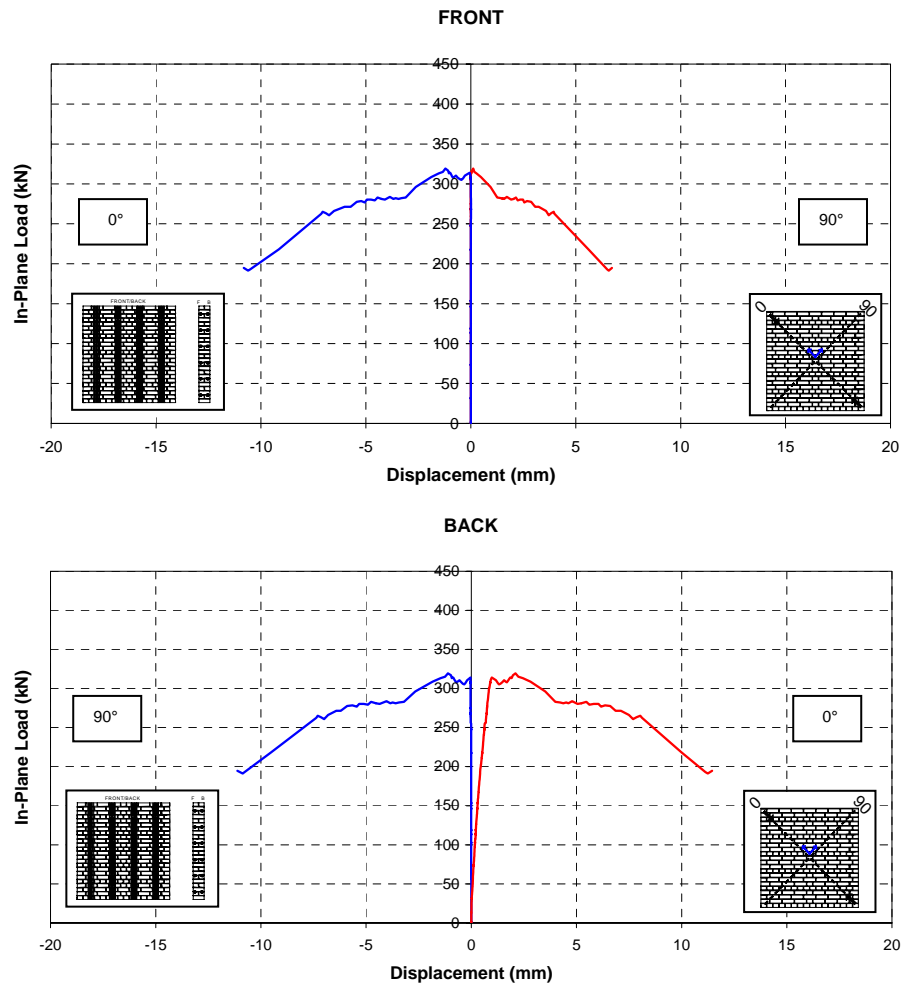


Fig.B.3 - 13. Load vs. diagonal displacement

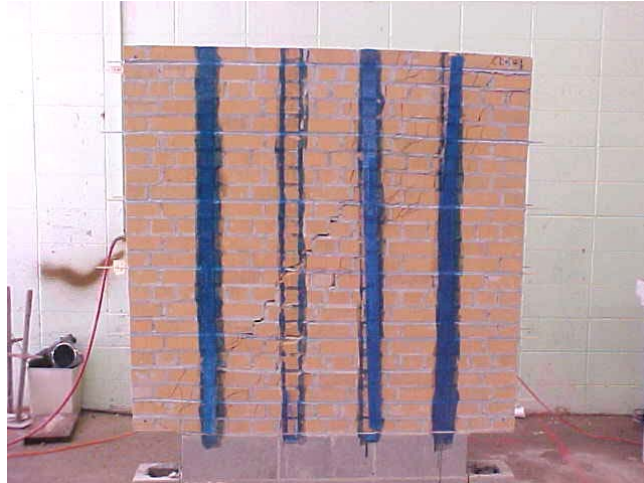


Fig.B.3 - 14. Wall CLW4 after failure (front)

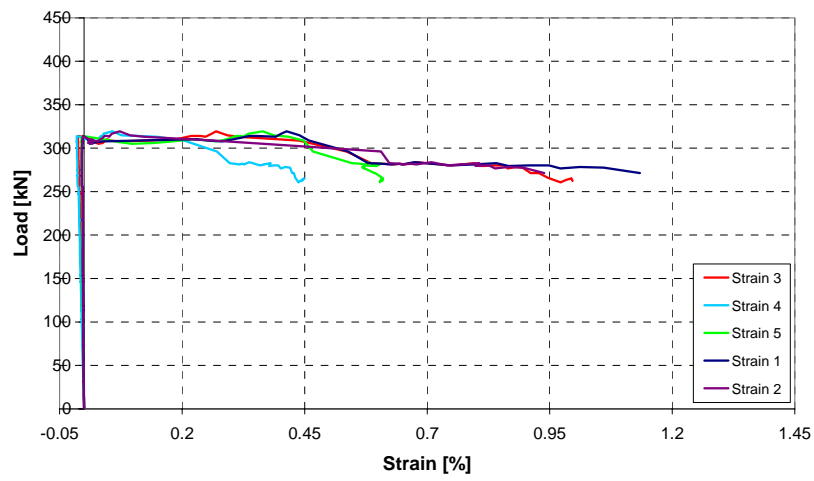


Fig.B.3 - 15. Load vs. strain

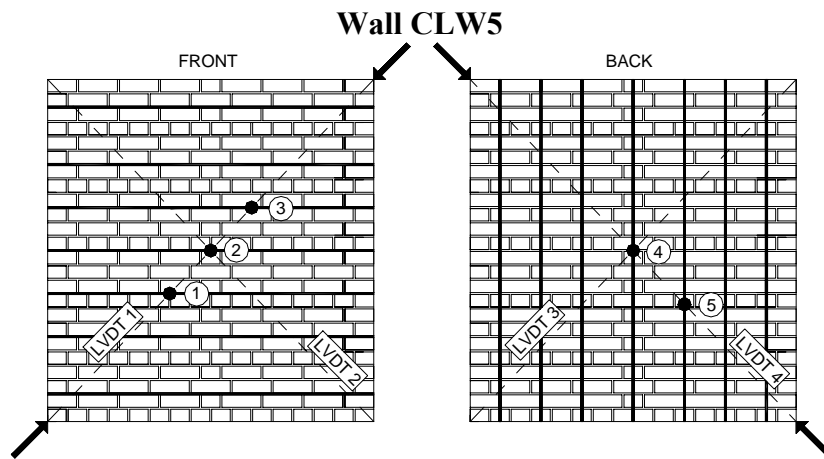


Fig.B.3 - 16. Strain gauges, LVDTs locations and loaded diagonal

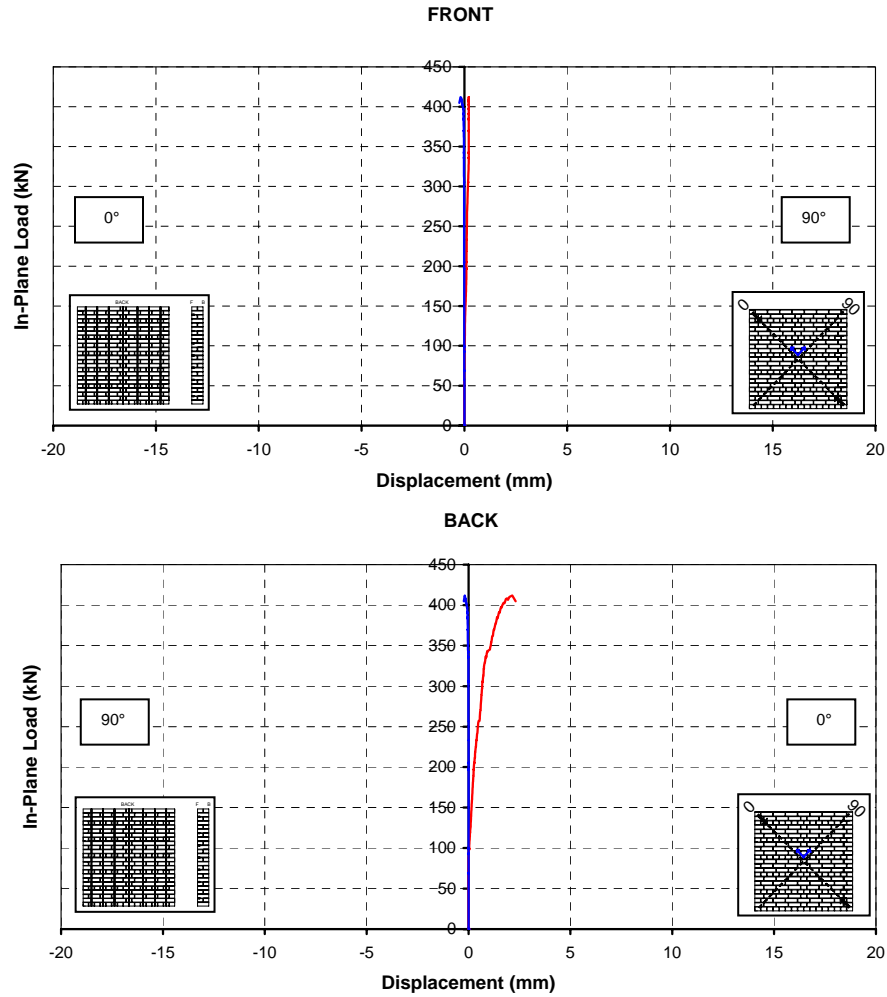
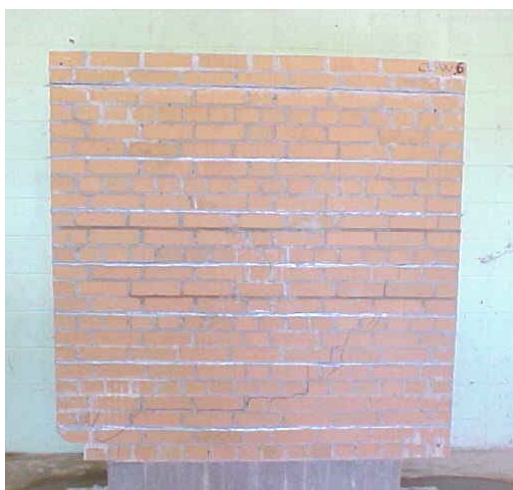


Fig. B.3 – 17. Load vs. diagonal displacement



(a) Wall CLW5 after being tested (front)



(b) Crushing of the corner (back)

Fig.B.3 - 18. Wall CLW5 after failure

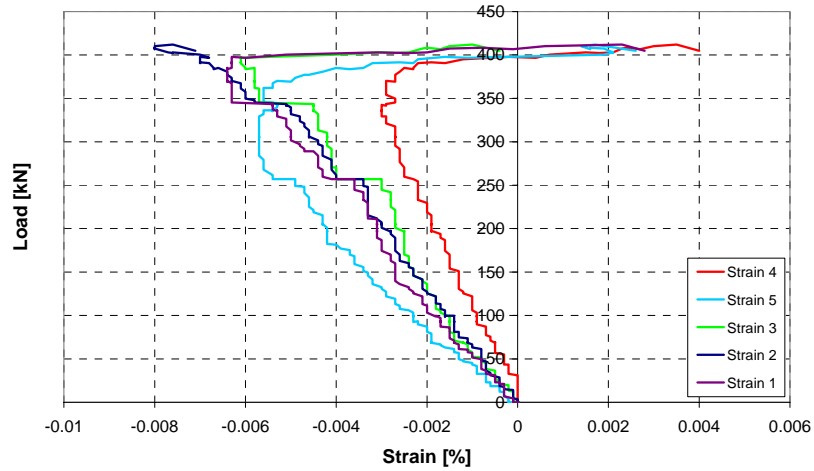


Fig.B.3 - 19. Load vs. strain

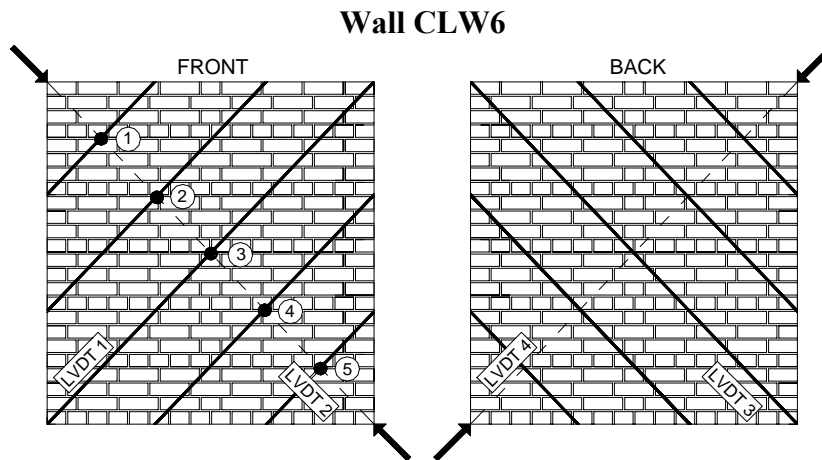
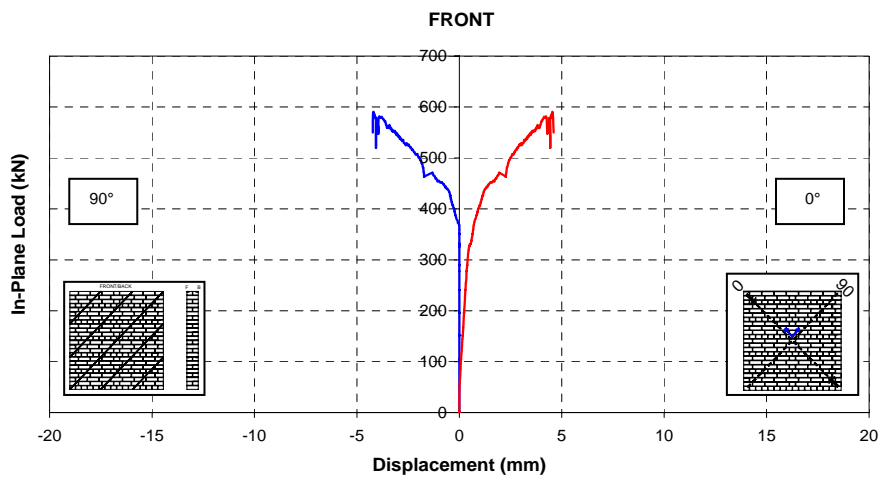


Fig.B.3 - 20. Strain gauges, LVDTs locations and loaded diagonal



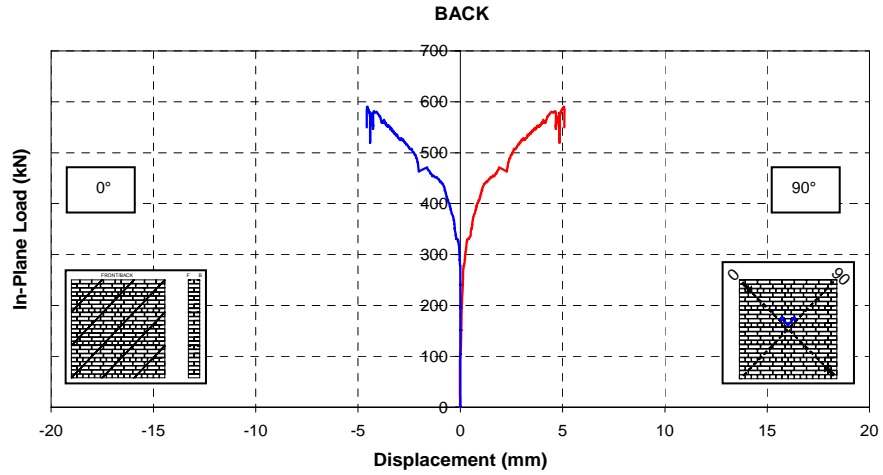


Fig.B.3 - 21. Load vs. diagonal displacement



Fig.B.3 - 22. Wall CLW6 after failure (front)

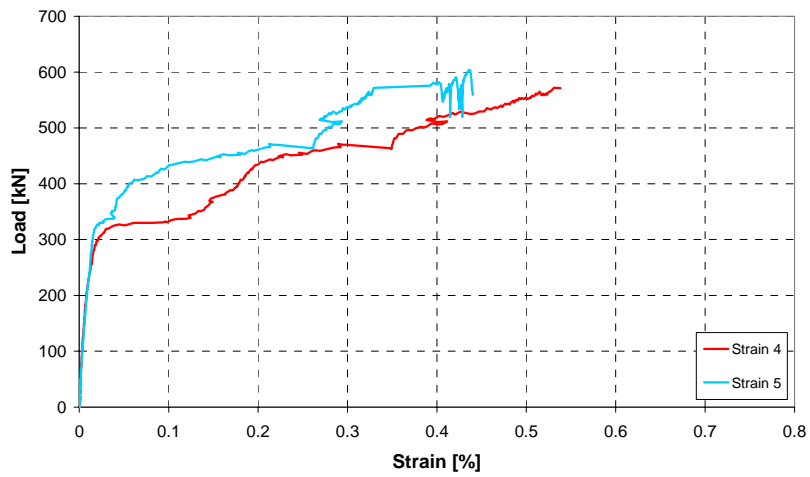


Fig.B.3 - 23. Load vs. strain

APPENDIX B.4: Mechanism of Failure



Fig.B.4 - 1. Splitting of clay units in wall CLW1

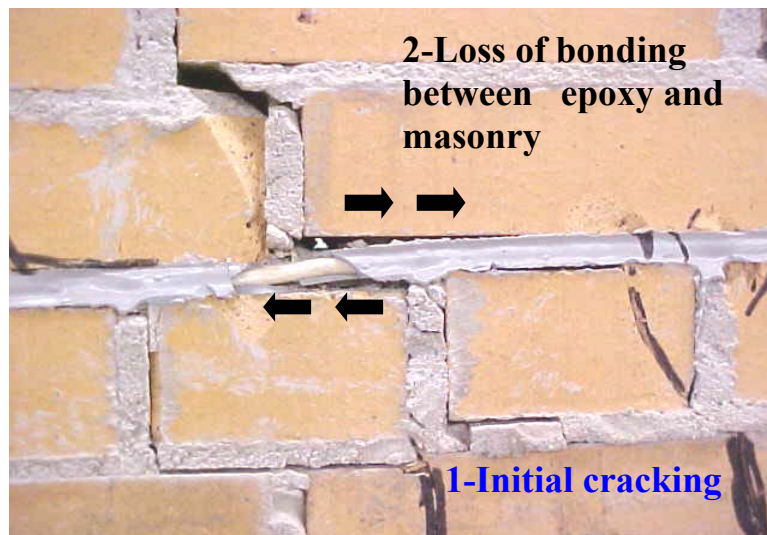
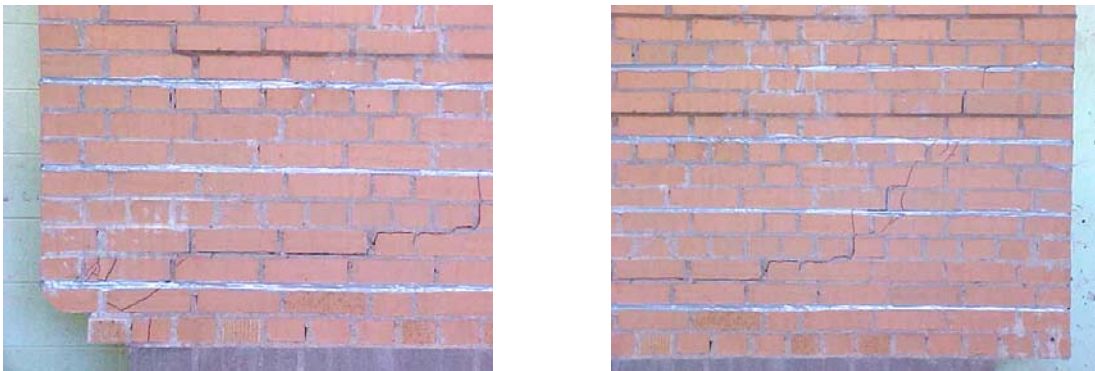


Fig.B.4 - 2. Horizontal phase



Fig.B.4 - 3. Delamination of GFRP laminates



(a)

(b)

Fig.B.4 - 4. Cracks detected in wall CLW5

Tab. B.4 - 1. Comparison of Pseudo-ductility for Series CLW

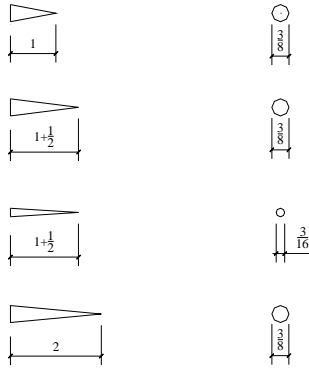
Specimen	In-Plane Load [kN]	γ_u [°]	γ_y [°]	μ
CLW1	307	0.03	0.03	1.0
CLW2	306	0.02	0.02	1.0
CLW3	406	0.38	0.05	7.6
CLW4	319	0.6	0.09	6.7

Note: 1kN = 0.2248 kip

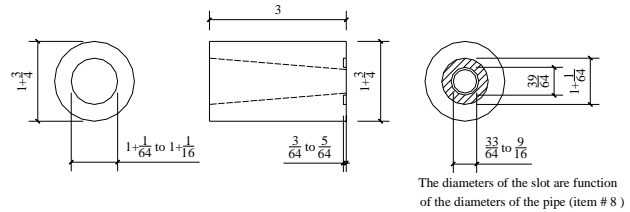
APPENDIX C: POST -TENSIONING

APPENDIX C.1: Tensioning and Anchor Devices

ITEM # 1: WEDGE

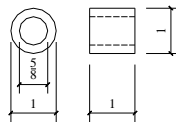


ITEM # 2: CHUCK

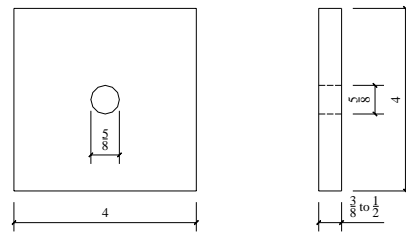


ITEM # 3: PIPE

Can be the same pipe as item # 8 without woodruff cutter



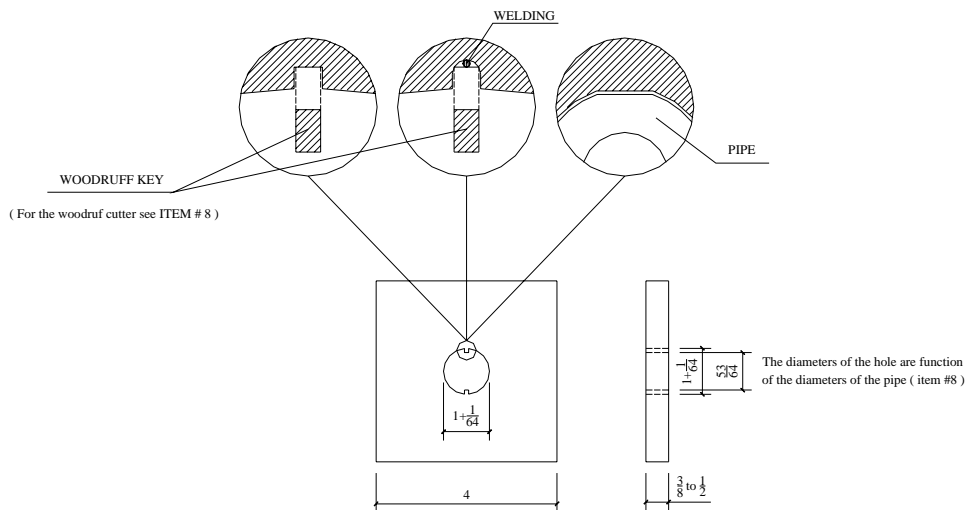
ITEM # 4: SPREADER OF LOAD



ITEM # 5: SPREADER OF LOAD

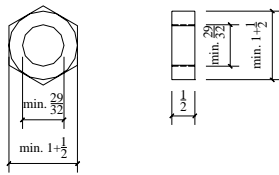
(Choose the cheaper option)

OPTION 1 OPTION 2 OPTION 3



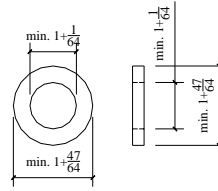
ITEM # 6: FINE THREAD NUT

(The dimensions of the nut are function of the diameters of the pipe (ITEM # 8))



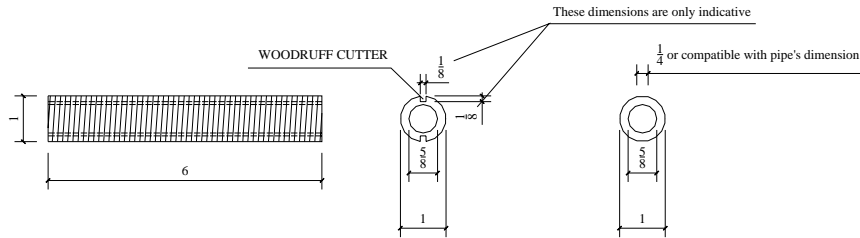
ITEM # 7: TEFLON WASHER

(The dimension of the washers are function of the diameters of the pipe (ITEM # 8))



ITEM # 8: THREADED PIPE

(The shape of the pipe is function of the choosen option for ITEM # 5)

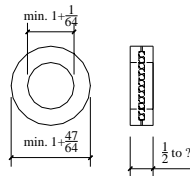


OPTION 1 AND 2

OPTION 3

ITEM # 9: THRUST BEARING

(The dimensions of this item are function of the thrust bearings available on the market and it must carry a load of about 15 to 20 kips)



DEAD END

LIVE END

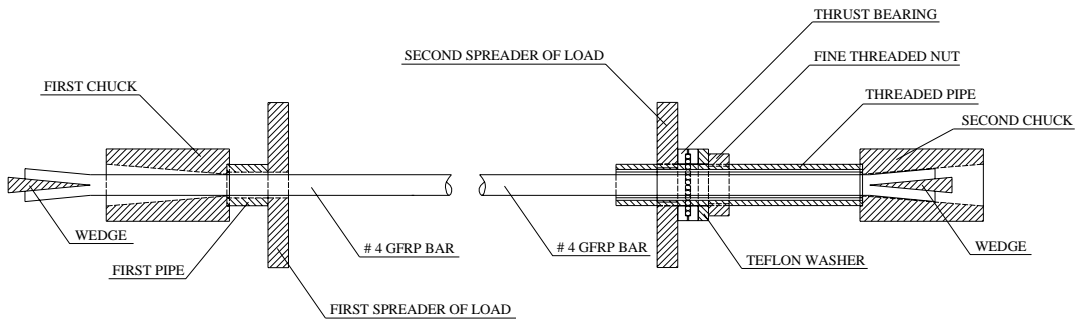


Fig.C.1 - 1. Autocad drawings



Fig. C.1 - 2. The chuck



Fig. C.1 - 3. The wedges

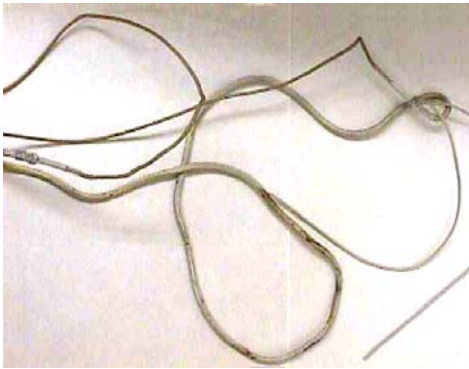


Fig.C.1 - 4. The rope heater



Fig.C.1 - 5. The thermo controller

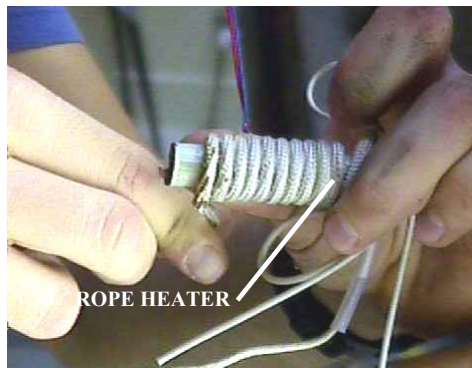
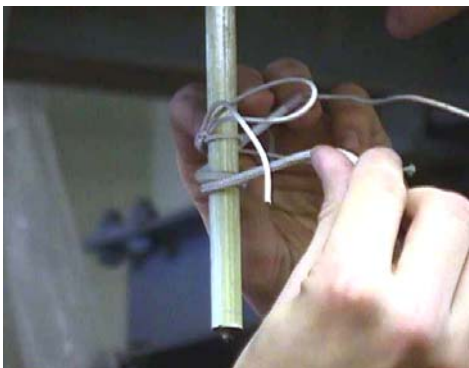


Fig.C.1 - 6. Wrapping of the GFRP Rod

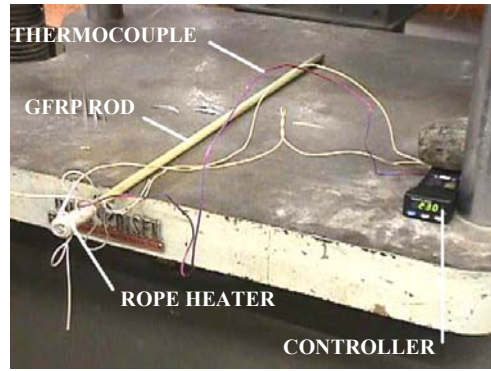


Fig.C.1 - 7. Test setup

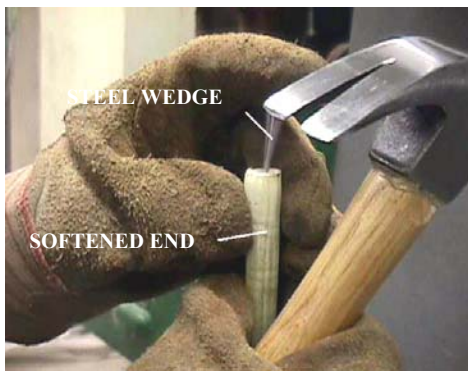


Fig.C.1 - 8. Driving the wedge



Fig.C.1 - 9. Final results with different heating times



Fig.C.1 - 10. Anchoring of the bar in the chuck

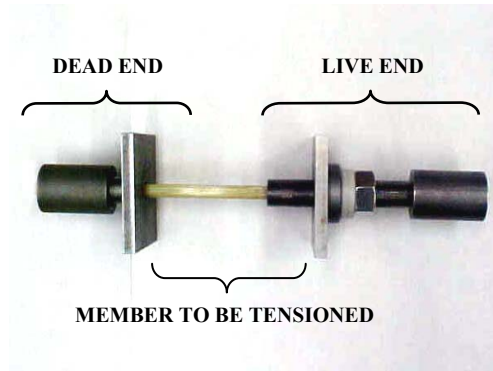


Fig.C.1 - 11. Assembled items

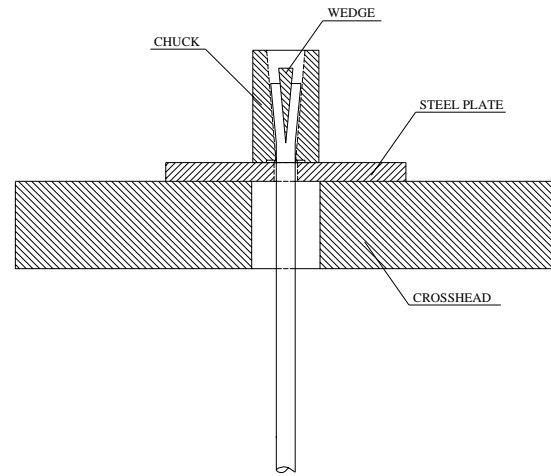


Fig.C.1- 12. Loading procedure

APPENDIX C.2: Tensile Tests



(a) Universal testing machine



(b) Positioning of the anchors

Fig. C.2 - 1. Universal testing machine and anchor positioning

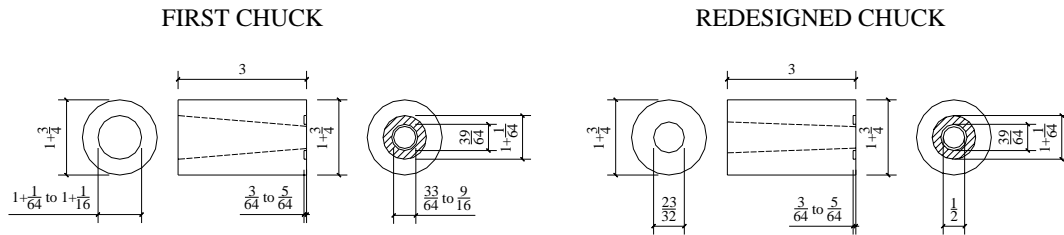


Fig. C.2 - 2. Chuck drawings



(a) Test with the first chuck

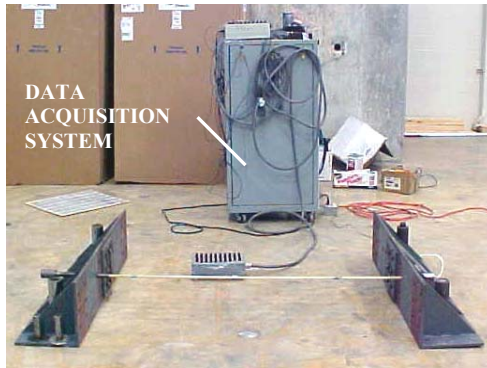


(b) Test with the redesigned chuck

Fig. C.2 - 3. Bar after failure

APPENDIX C.3: Long Term Tests

Test Setup



(a) Test setup: general view



(b) Detail of the pressure transducer

Fig. C.3 - 1. Test setup

Test Results

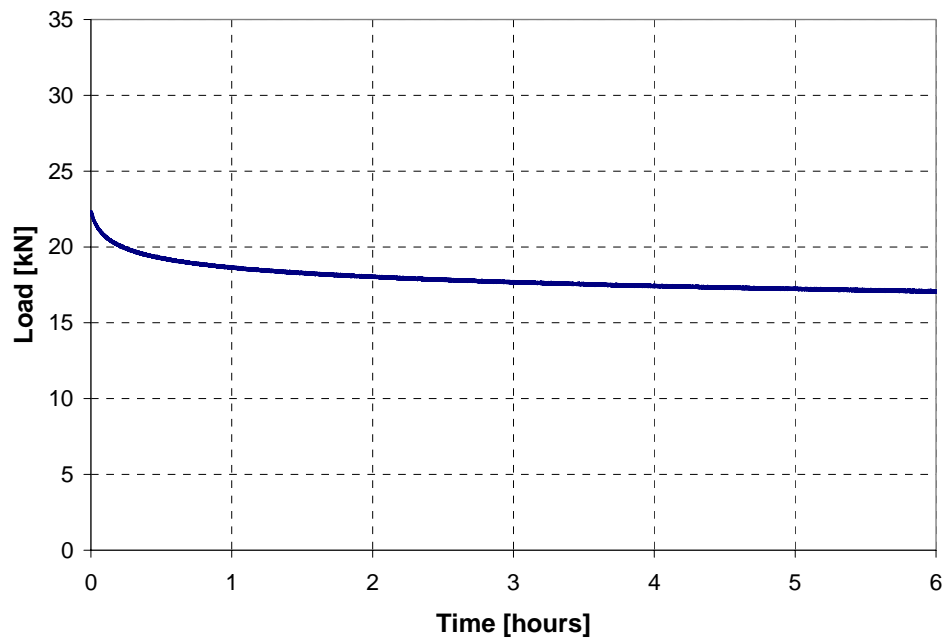


Fig. C.3 - 2. Load vs. time for testing time equal to 6 hours

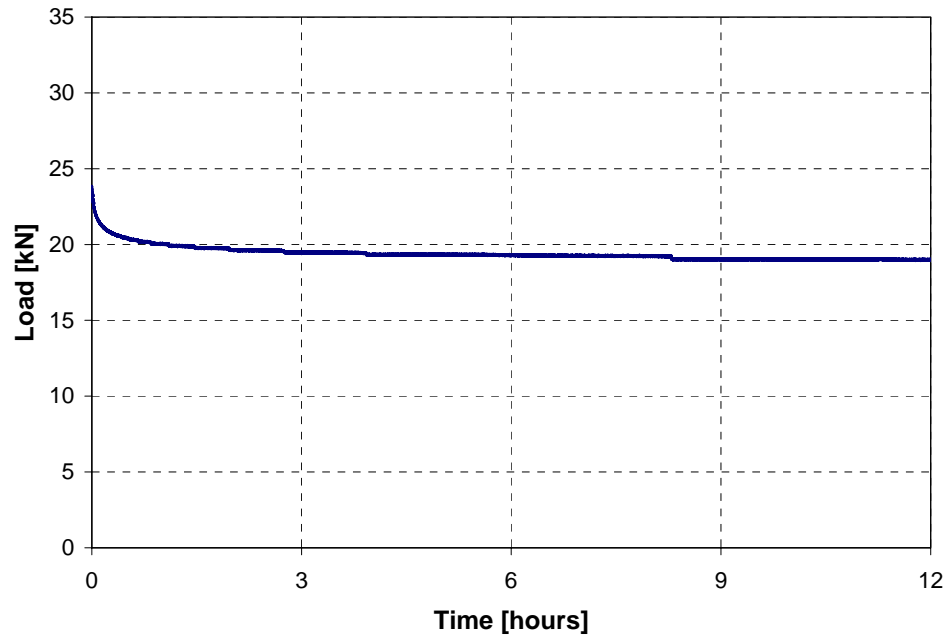


Fig. C.3 - 3. Load vs. time for testing time equal to 12 hours

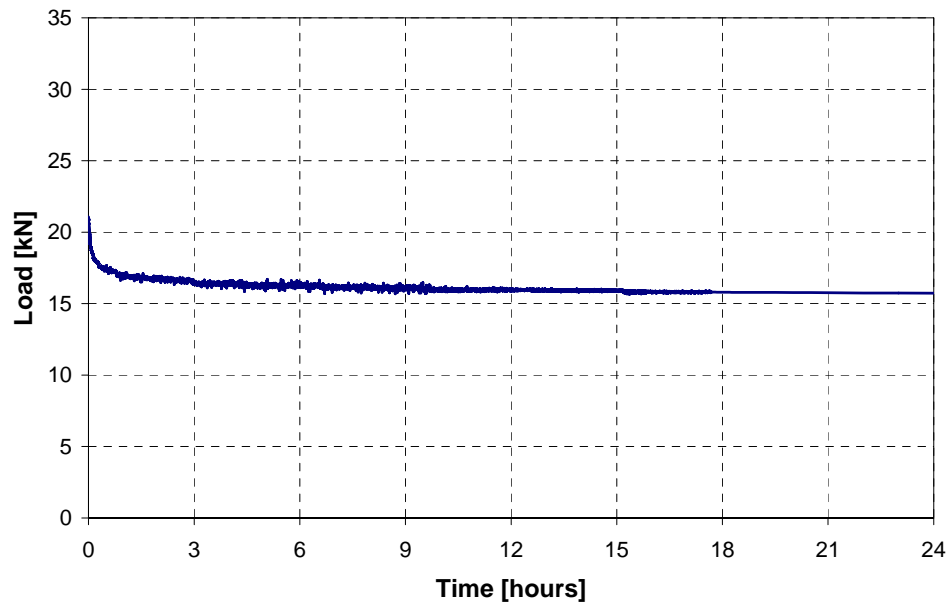


Fig. C.3 - 4. Load vs. time for testing time equal to 24 hours

APPENDIX C.4: Validation of the System

Test Setup



(a) Test setup: general view



(b) Dead end and pressure transducer

Fig. C.4 - 1. Test setup

Test Results

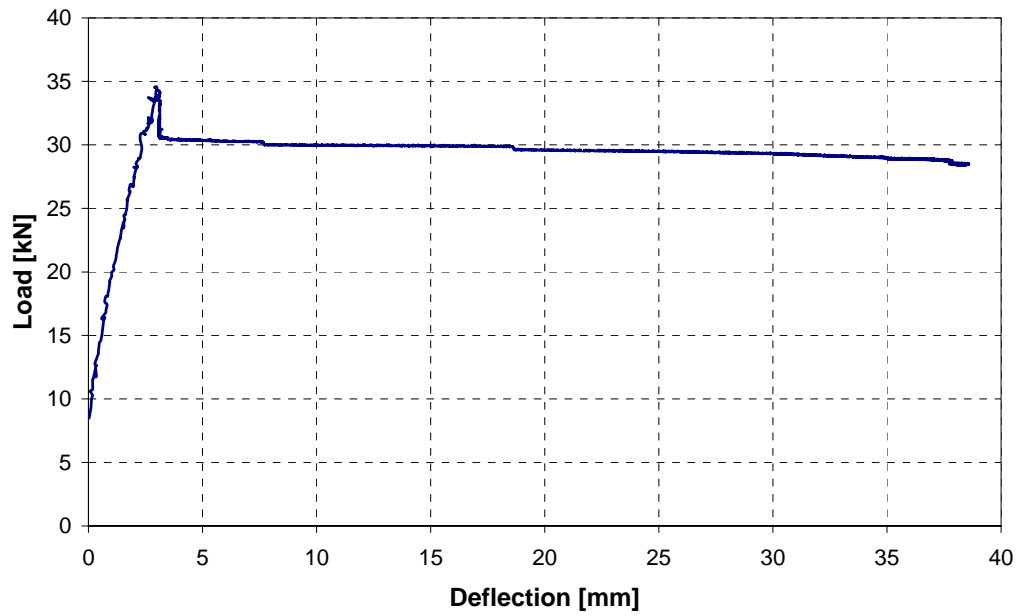


Fig. C.4 - 2. Load vs. mid span deflection

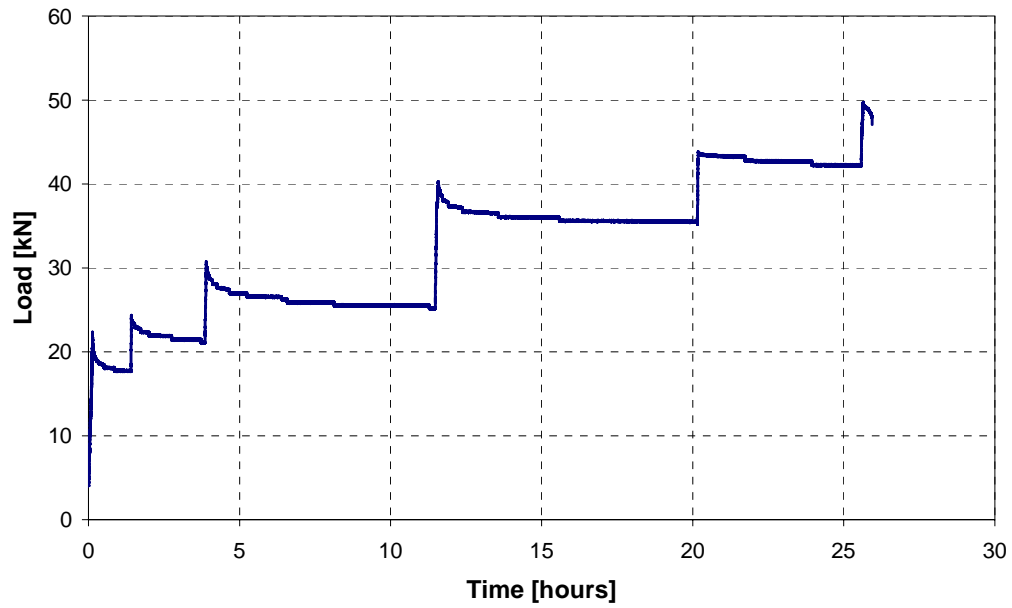


Fig. C.4 - 3. Load vs. time: loading to failure

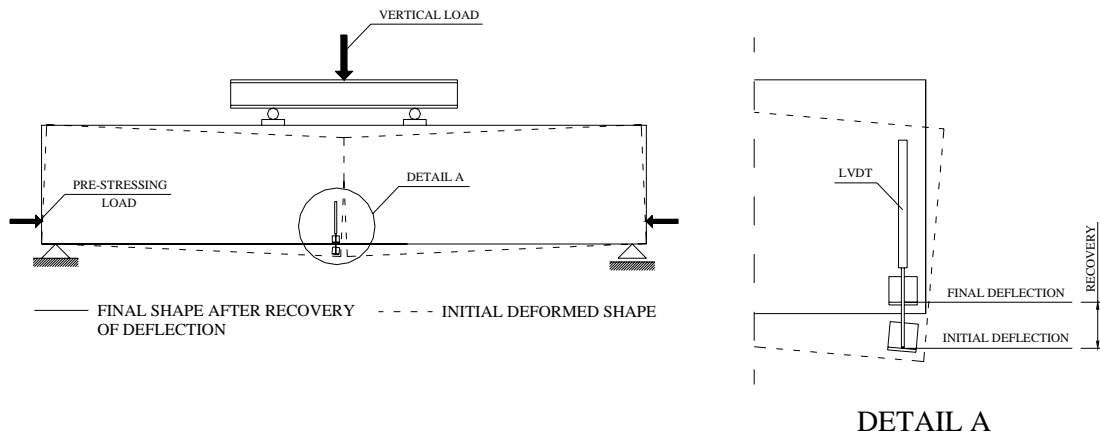
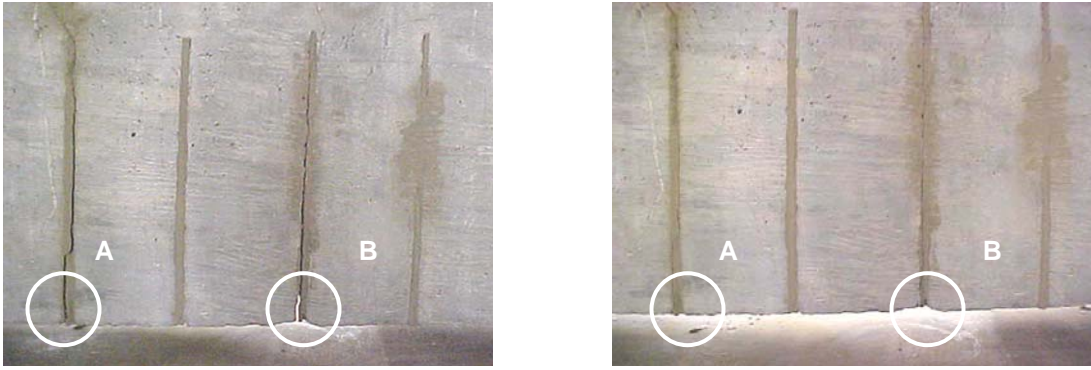


Fig. C.4 - 4. Position of the LVDT and detail of the valuation of recovery of deflection



(a) Cracks before post-tensioning

(b) Cracks after post-tensioning

Fig. C.4 - 5. Effectiveness of the post-tensioning technique

Tab. C.4 – 1. Ultimate loads

Test Number	Ultimate Load [kN]
1	49.62
2	44.84
3	48.35
Mean	47.60

Note: 1 kN = 0.2248 kip

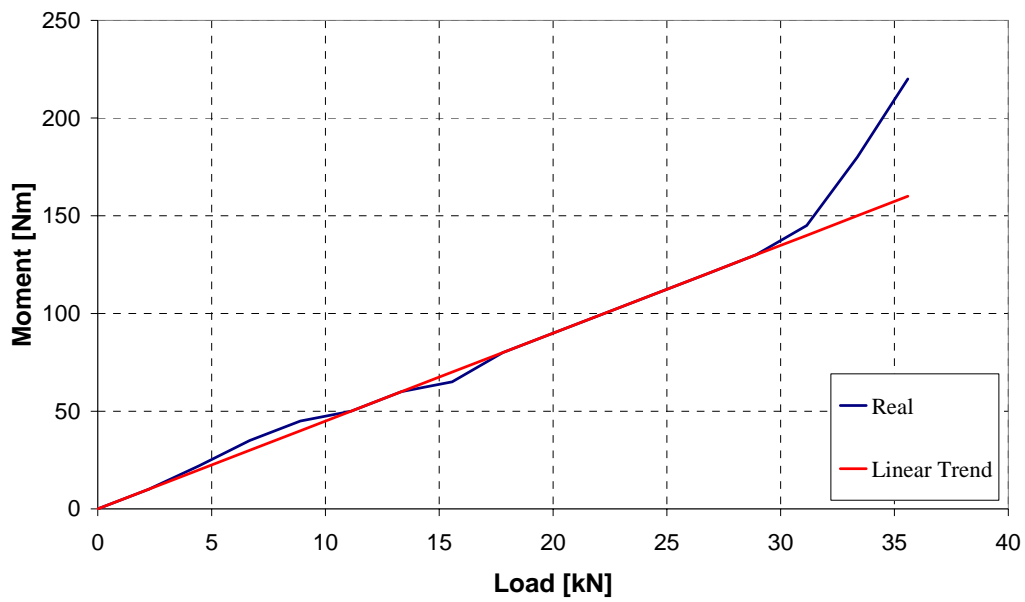


Fig. C.4 - 6. Load vs. torque wrench moment

APPENDIX C.5: Patent Disclosure

UMUW FORM 16C
CAMPUS _____

UP&L DISCLOSURE NO:
DATE RECEIVED UP&L:

UNIVERSITY OF MISSOURI SYSTEM

PROPRIETARY INFORMATION/INVENTION DISCLOSURE

NOTE: This statement shall be treated as confidential information except for specific sections as noted. Except for individuals engaged in the evaluation and approval process, the information will not be divulged to others without proper confidentiality agreements in place, except as required by law. The objective of the form is to obtain the information necessary to determine whether to pursue patent protection for your invention.

SECTION I NONCONFIDENTIAL INFORMATION

1. Nonconfidential title of the work:

ANCHOR SYSTEM FOR THE TENSIONING OF FIBER-REINFORCED POLYMER BARS USED FOR STRUCTURAL STRENGTHENING

2. Nonconfidential lay abstract of invention:

This invention addresses the solution of the tensioning problems of Fiber-Reinforced Polymer (FRP) bars used to take the place of steel rods for structural strengthening.

The bars can be manufactured with any fiber type embedded in a thermoplastic resin.

The idea is based on the thermoplastic properties of the resin and consists of creating two temporary anchorages at the end of the bar; with these anchors and a screw device the proper amount of tension can be introduced into the bar.

After this tensioning operation, one can bond the bar to the structure with any method used for composite materials (e.g. Near Surface Mounted (NSM) rods or drilled hole through transverse walls filled with epoxy-based paste).

After bonding is completed, one can remove the anchors and the screw device to use them for another bar. In this way, one can cut the bars in situ as desired, and the tendon can be hidden inside the structure. This feature is very important particularly for historical masonry buildings, in which the strengthening system must be the least visible as possible.

3. Nature of work: Machine ___ Process Utility ___ Software ___

If Software: Have proper copyright markings been utilized? Yes__No__

UNIVERSITY PATENTS & LICENSING OFFICE
509 LEWIS HALL
COLUMBIA, MO 65211
(573)882-2821

APPENDIX D: MATERIALS AND BOND CHARACTERIZATION

APPENDIX D.1: Specimens Preparation (Bond Tests)



(a) Application of primer



(b) Application first coat of saturant



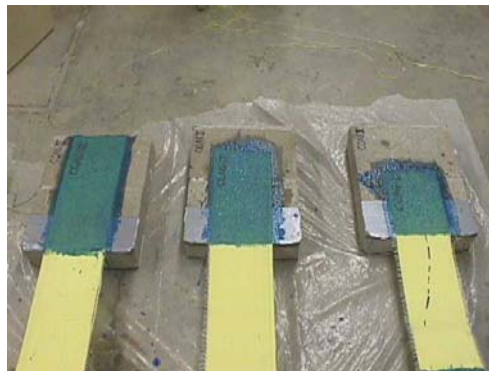
(c) Application of AFRP sheets



(d) Application of second coat of saturant



(e) Specimens ready



(e) Test regions

Fig. D.1 – 1. Specimens preparation

APPENDIX D.2: Test Setup (Bond Tests)

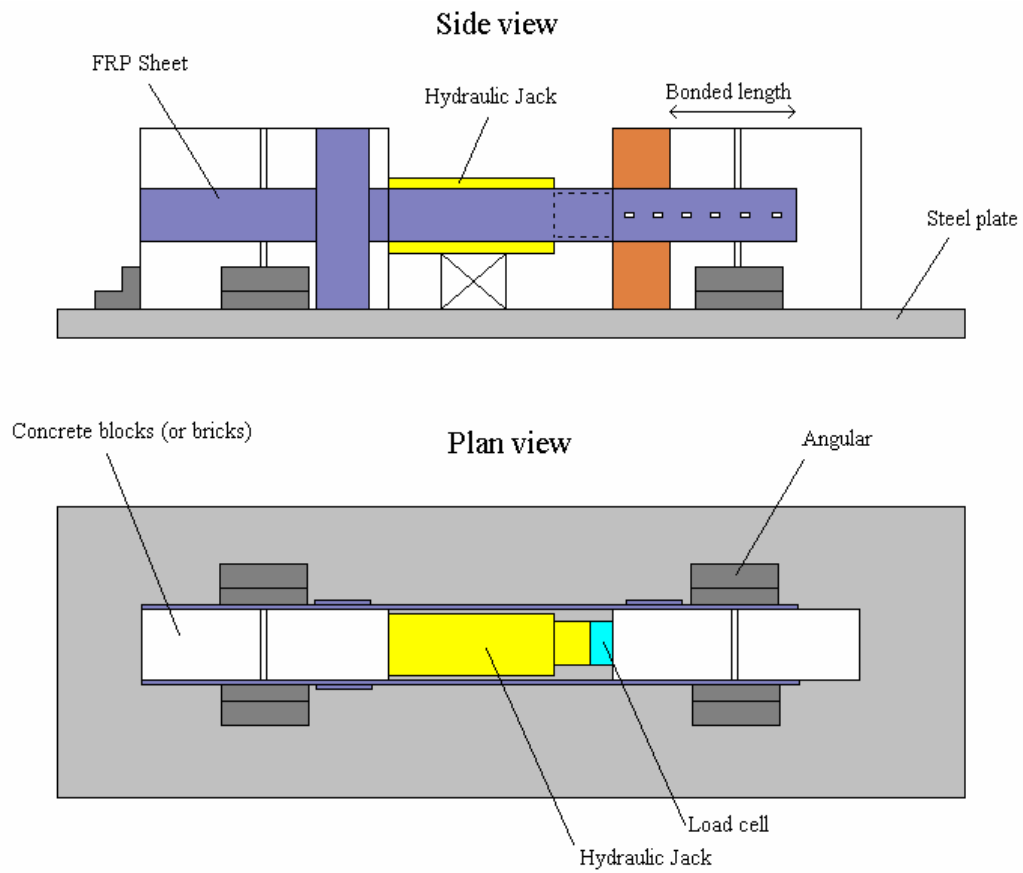


Fig. D.2 – 1. Test setup

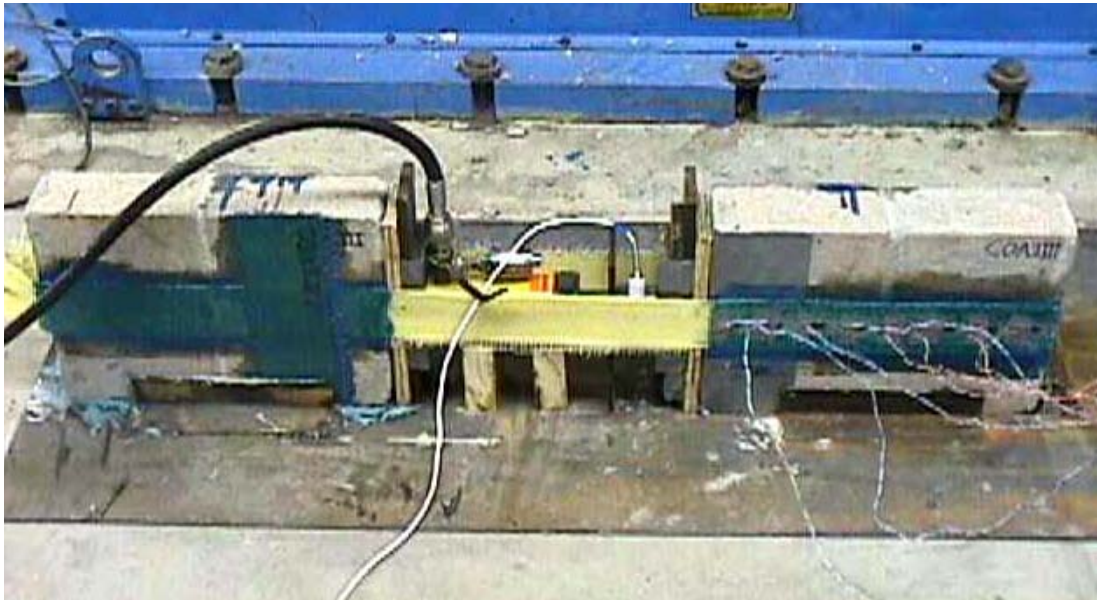


Fig. D.2 – 2. Picture test setup

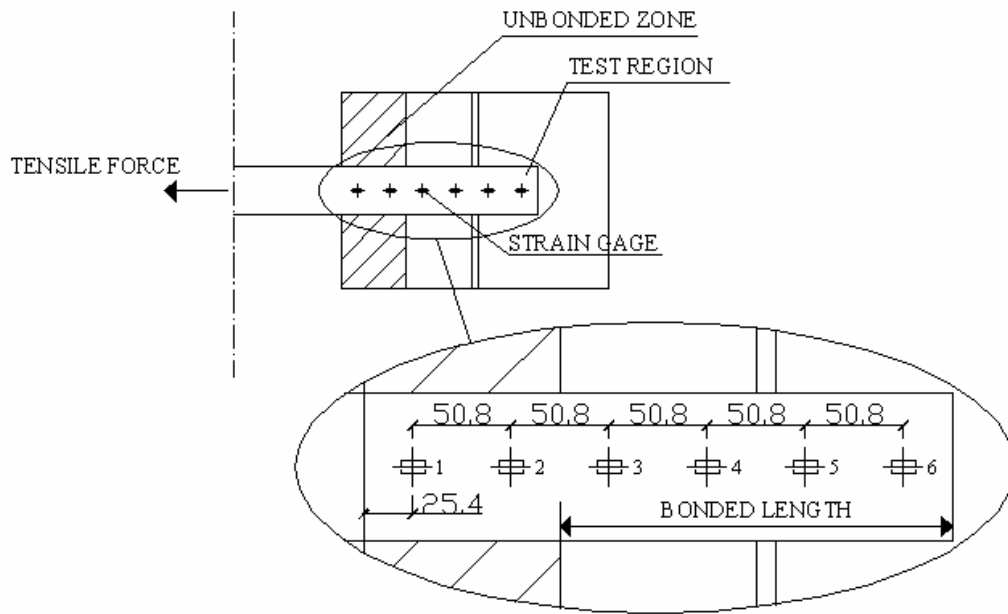


Fig. D.2 – 3. Typical strain gages location

APPENDIX D.3: Test Results (Bond Tests)

Series CA

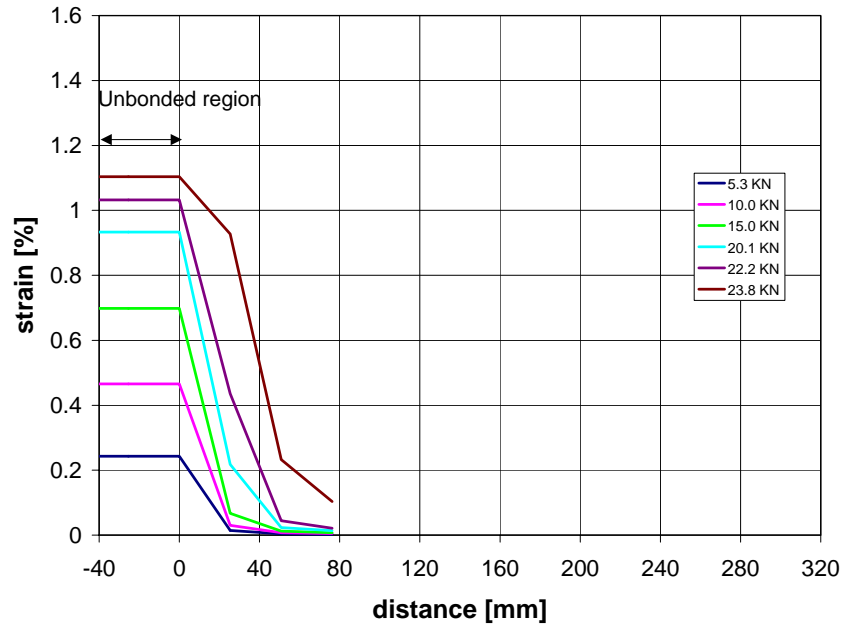


Fig. D.3 – 1. Strain vs. location – Test CA3-4

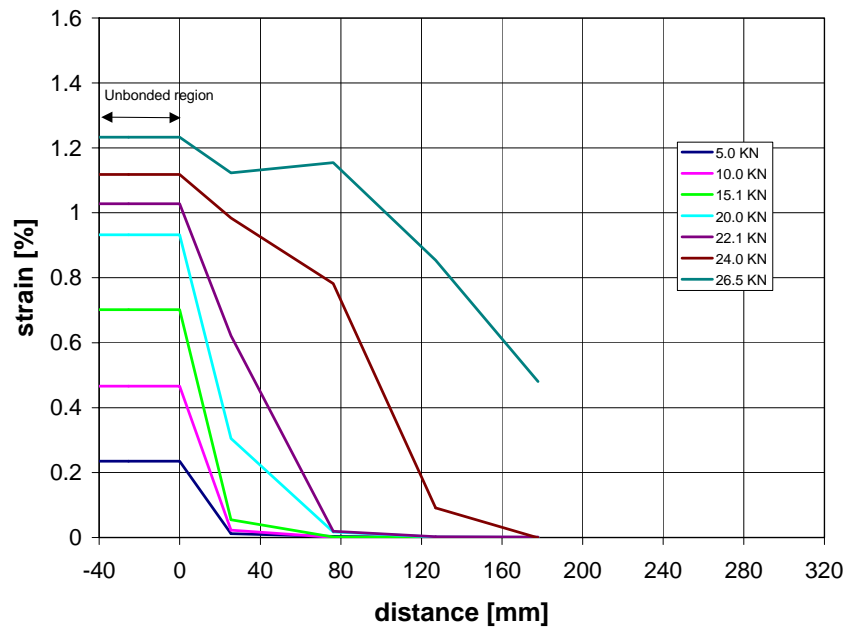


Fig. D.3 – 2. Strain vs. location – Test CA3-8

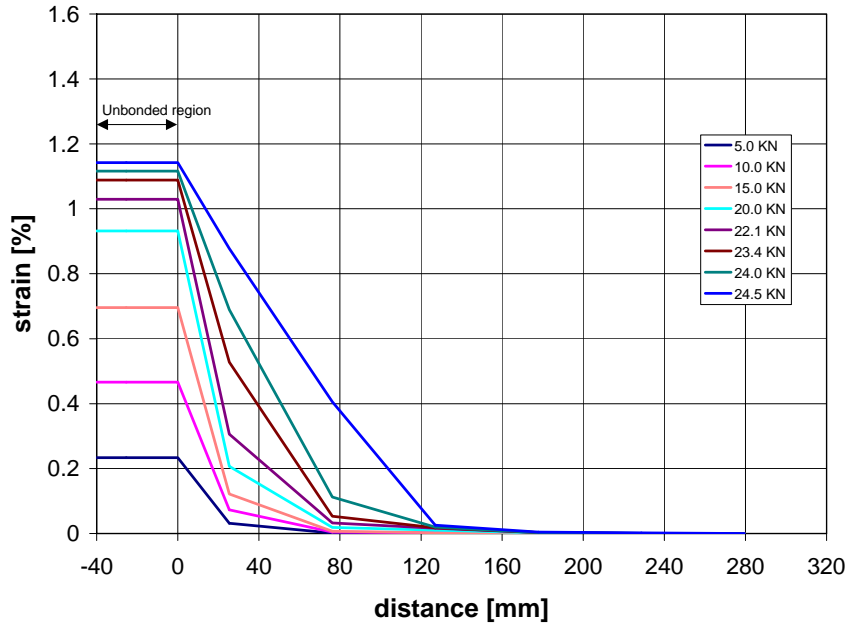


Fig. D.3 – 3. Strain vs. location – Test CA3-12

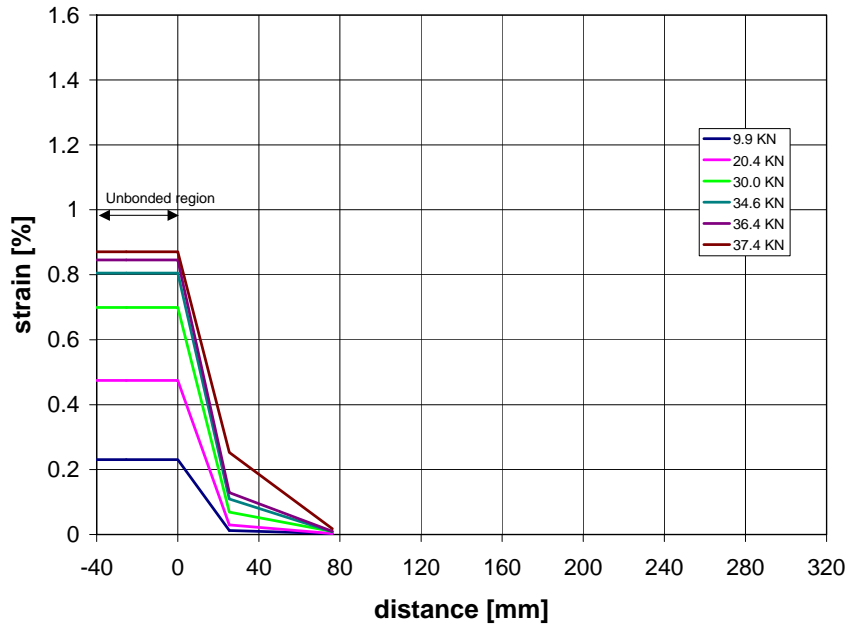


Fig. D.3 – 4. Strain vs. location – Test CA6-4

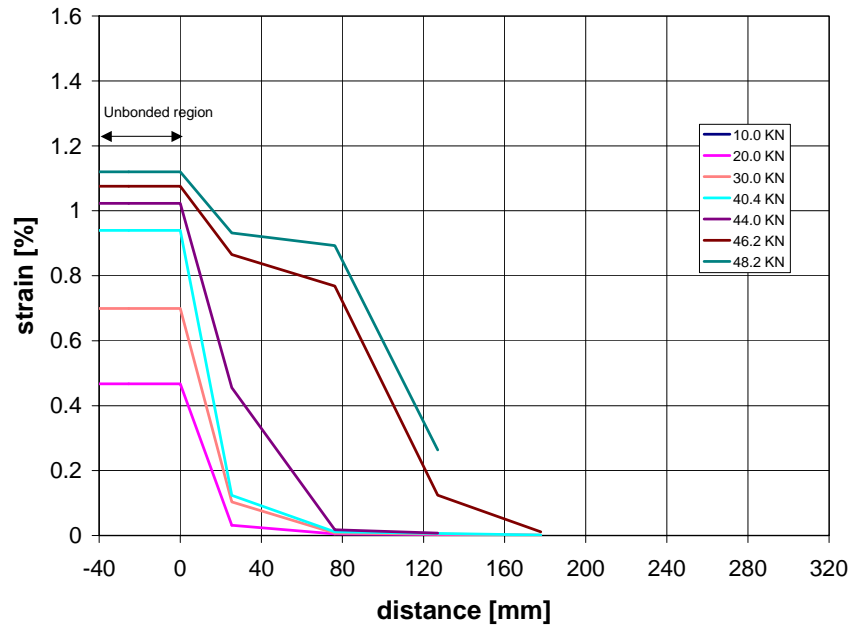


Fig. D.3 – 5. Strain vs. location – Test CA6-8

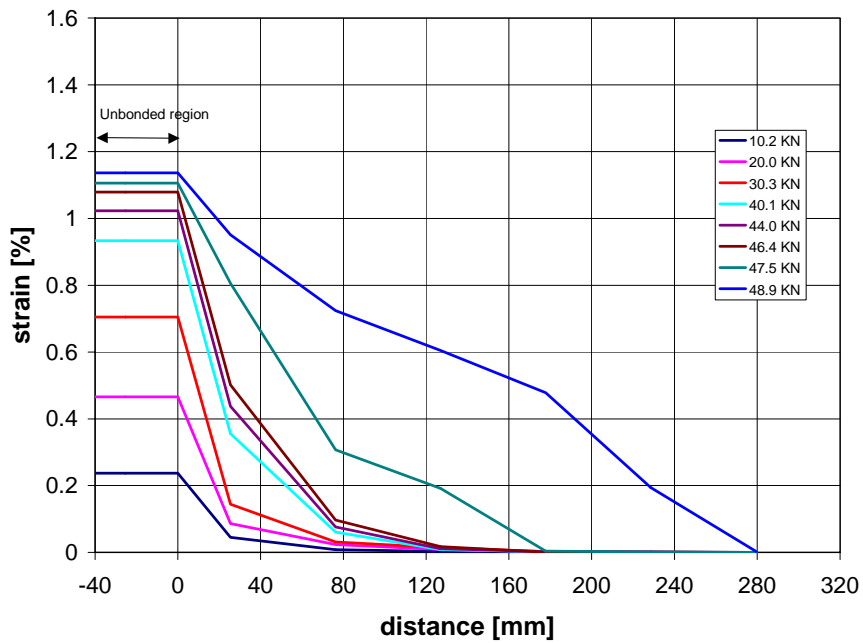


Fig. D.3 – 6. Strain vs. location – Test CA6-12

Series BA

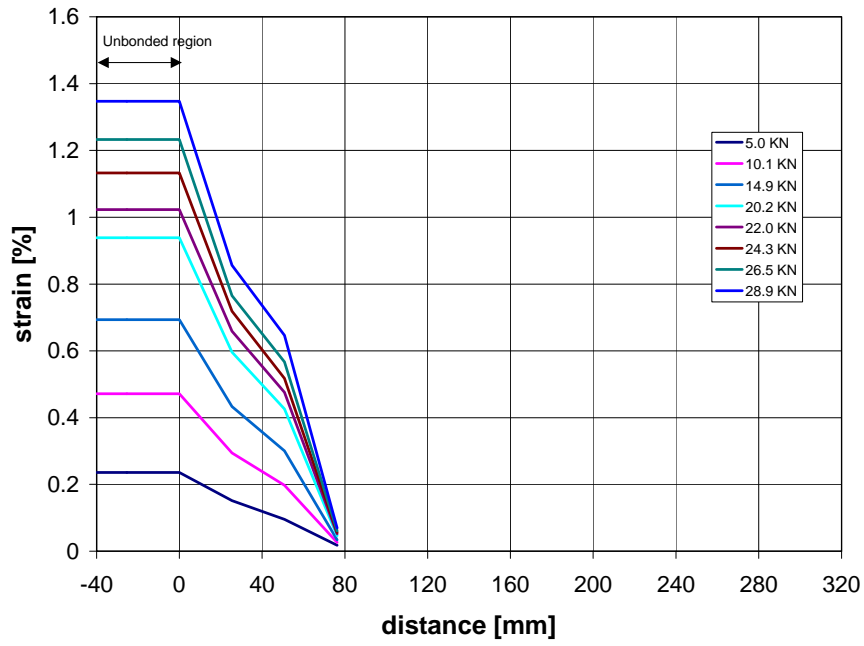


Fig. D.3 – 7. Strain vs. location – Test BA3-4

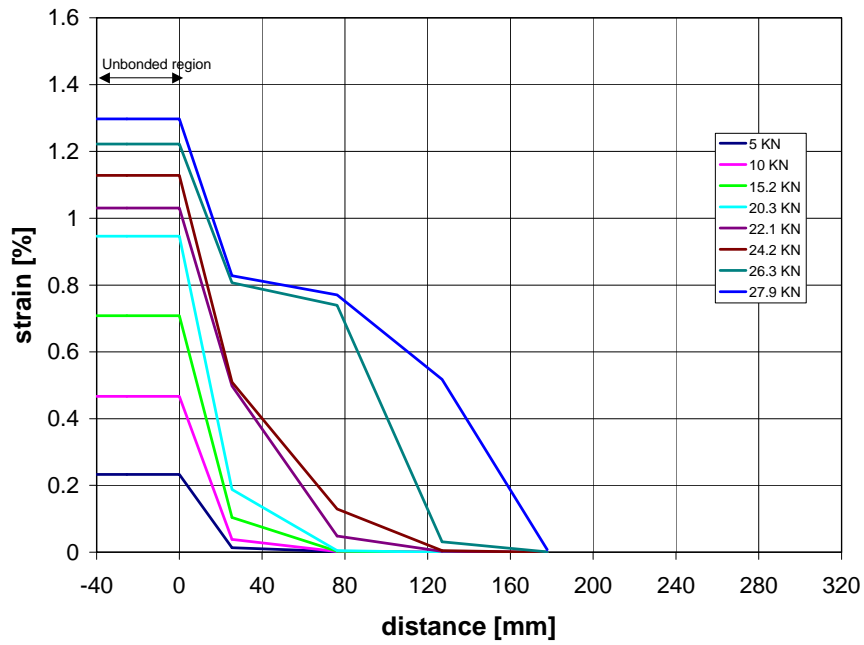


Fig. D.3 – 8. Strain vs. location – Test BA3-8

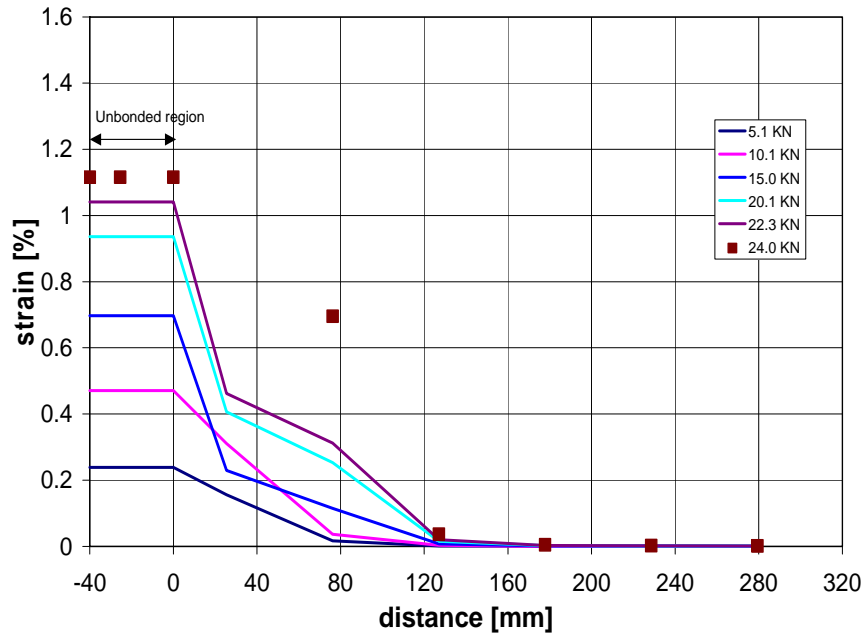


Fig. D.3 - 9. Strain vs. location - Test BA3-12

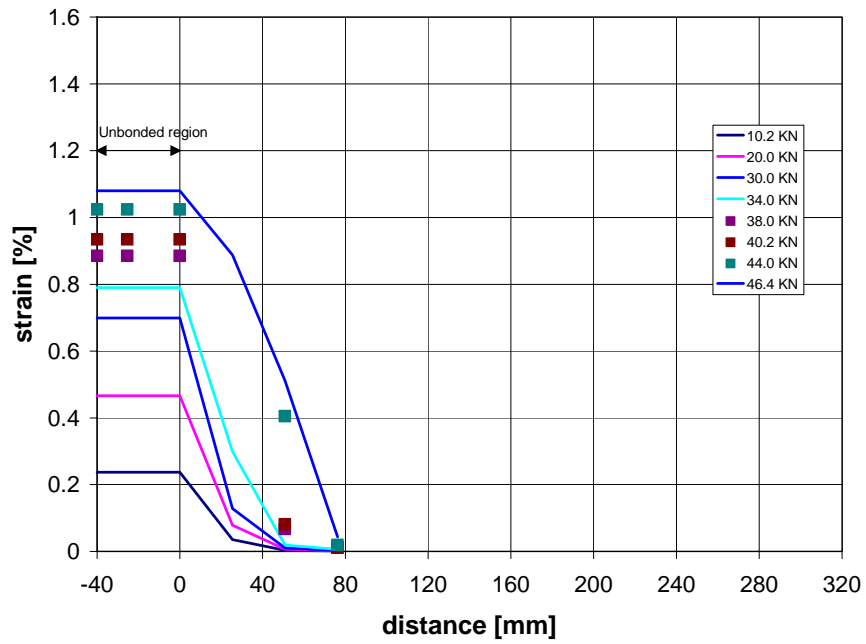


Fig. D.3 - 10. Strain vs. location - Test BA6-4

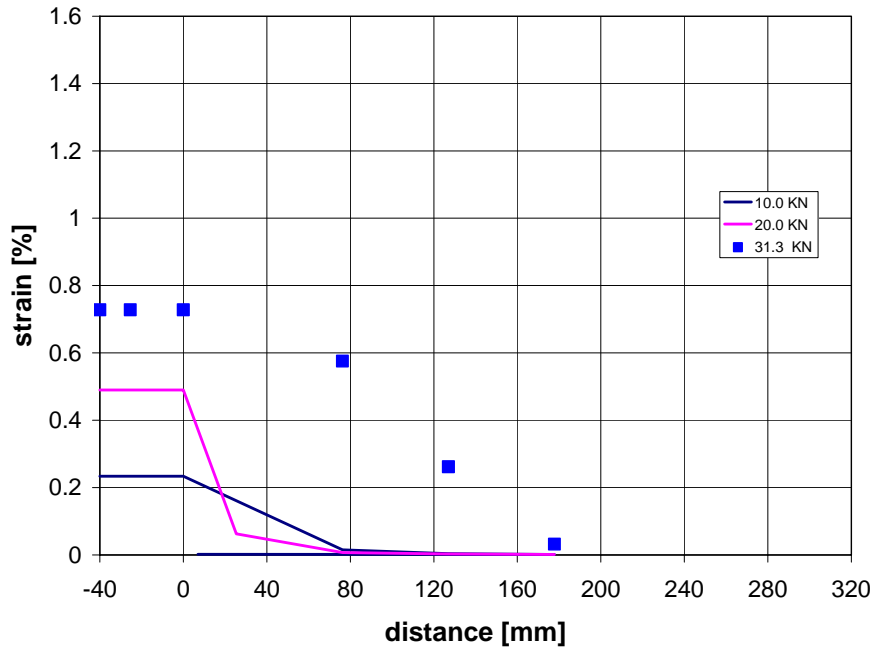


Fig. D.3 – 11. Strain vs. location – Test BA6-8

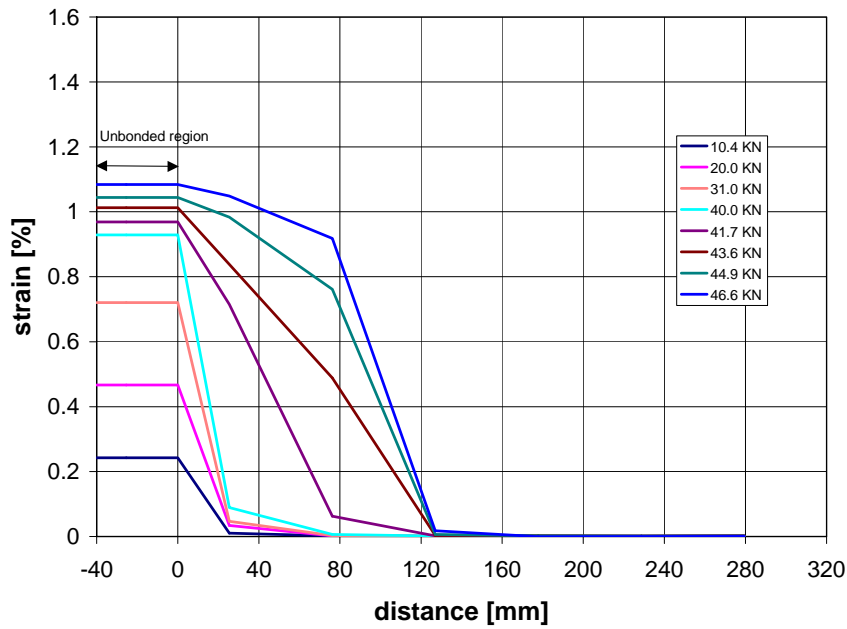


Fig. D.3 – 12. Strain vs. location – Test BA6-8

APPENDIX D.4: Photographs (Bond Tests)



(a) Specimen CA3-4



(b) Specimen CA3-8



(c) Specimen CA3-12



(d) Specimen CA6-4



(f) Specimen CA6-8



(d) Specimen CA6-12

Fig. D.4 – 1. Failure of the concrete specimens



(a) Specimen BA3-4



(b) Specimen BA3-12



(c) Specimen BA6-4



(d) Specimen BA6-8



(e) Specimen BA6-12



(g) Specimen BA6-12

Fig. D.4 – 2. Failure of the clay specimens

APPENDIX D.5: Specimens Preparation (Putty Tensile Tests)



(a)



(b)

Fig. D.5 – 1. Beads



(a)



(b)

Fig. D.5 – 2. Preparation of the specimens

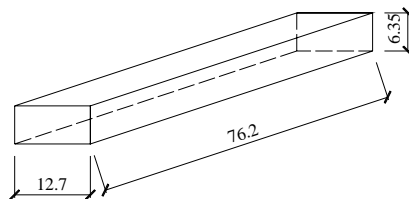


Fig. D.5 – 3. Specimen configuration

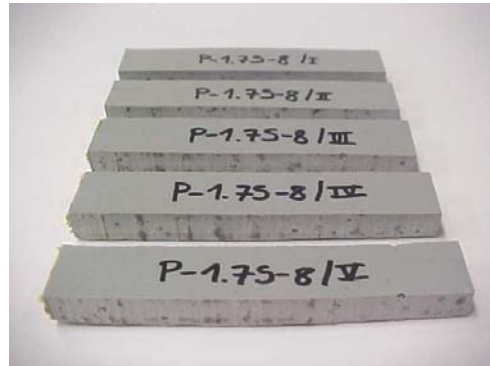


Fig. D.5 – 4. Specimens ready to test

APPENDIX D.6: Test Setup (Putty Tensile Tests)

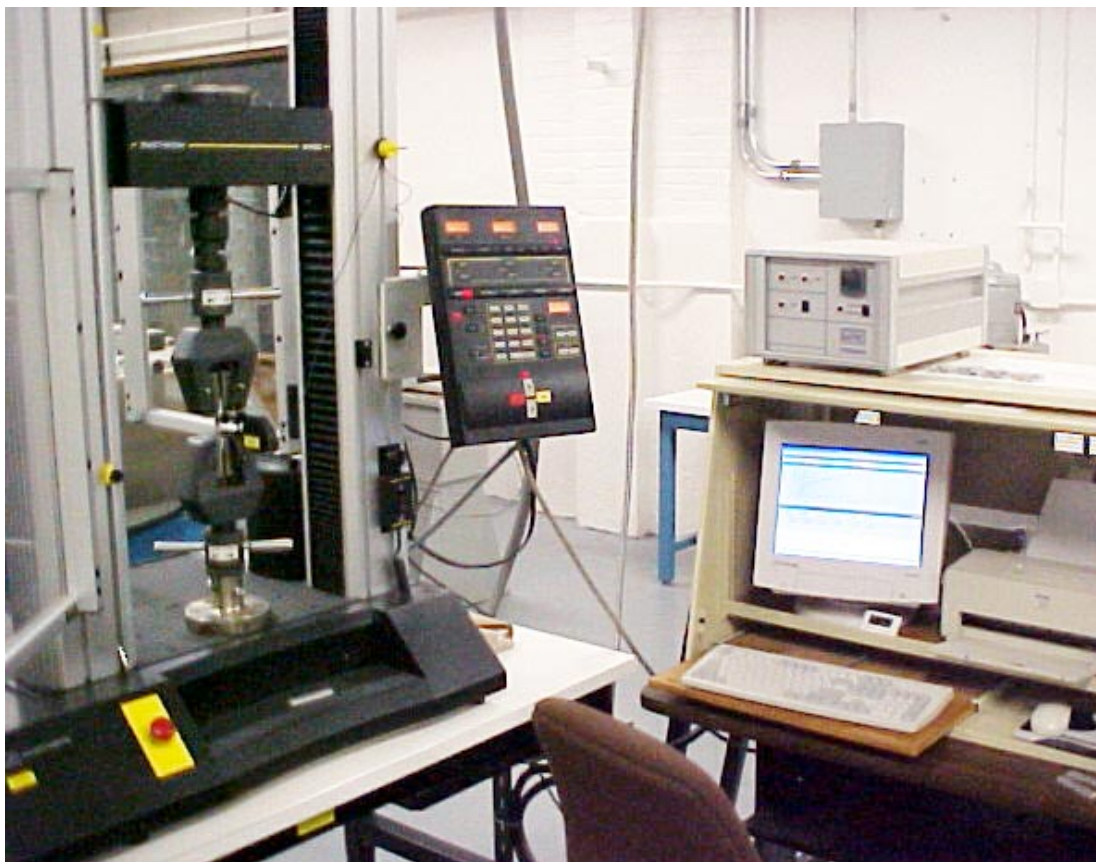
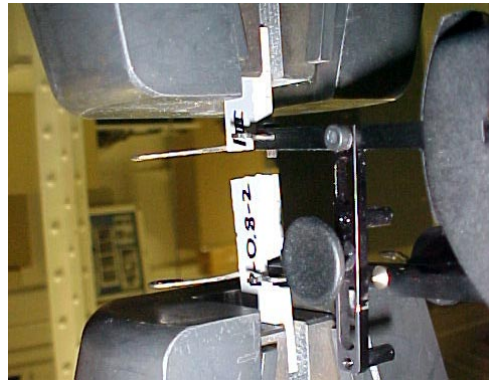


Fig. D.6 – 1. Test apparatus

APPENDIX D.7: Test Results (Putty Tensile Tests)



(a)

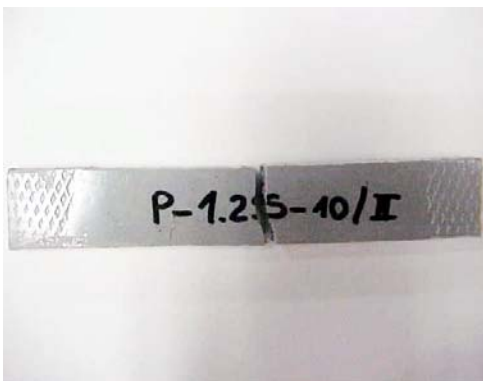


(b)

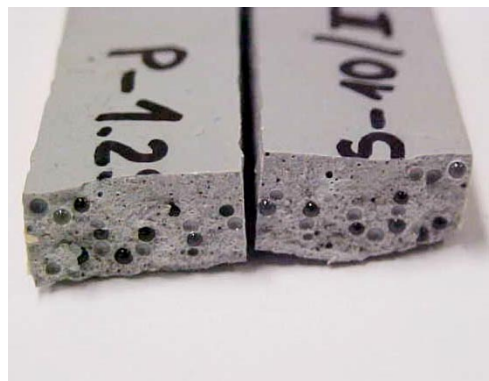


(c)

Fig. D.7 – 1. Failure of the specimens



(a)



(b)

Figure D.7 – 2. Specimens after the test

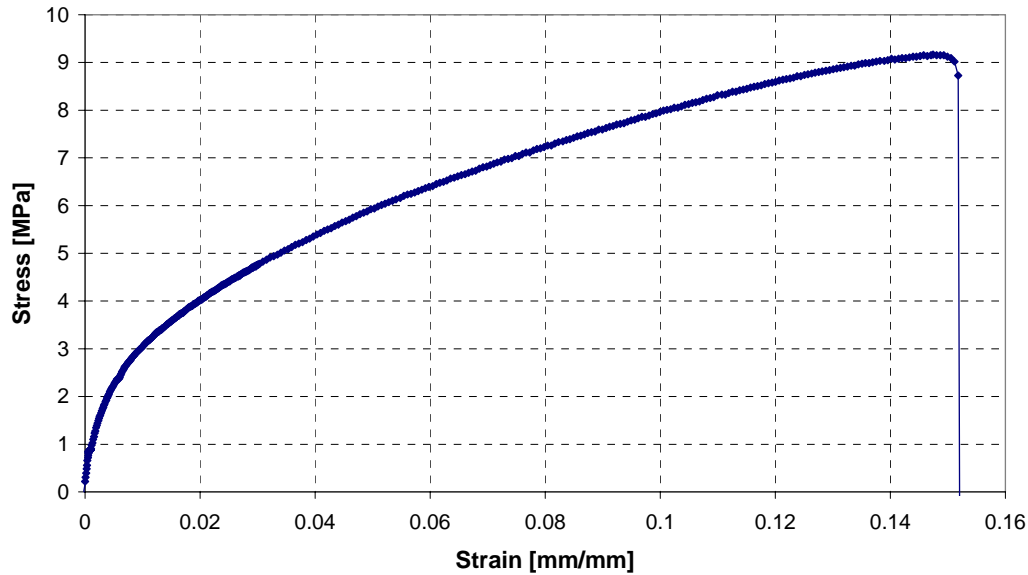


Fig. D.7 – 3. Example of experimental behavior of the specimens

Tab. D.7. – 1. Young's Modulus values [MPa]

Beads %								
Beads diameters	0	1	2	3	4	5	8	10
0.8 mm	1319	1352	1250	1191	1214	1203	1312	1309
1 mm		1237	1376	1251	1167	1256	1413	1299
1.25 mm		1078	1134	1053	1249	1218	1437	1286
1.75 mm		1275	1200	1352	1256	1180	1375	1228
2.25 mm		1239	1350	1373	1433	1050	1233	1070

Note: 1 MPa = 145 psi; 1 mm = 0.03937 in

Tab. D.7. – 2. Stress values [MPa]

Beads %								
Beads diameters	0	1	2	3	4	5	8	10
0.8 mm	10.398	9.595	9.485	9.368	9.407	9.464	9.835	9.896
1 mm		10.650	9.817	9.675	8.295	7.960	9.585	9.272
1.25 mm		9.037	8.610	8.041	9.441	9.284	9.369	9.551
1.75 mm		9.004	9.626	9.160	9.473	9.429	9.467	9.378
2.25 mm		10.070	8.188	8.079	8.422	7.608	6.999	7.485

Note: 1 MPa = 145 psi; 1 mm = 0.03937 in

Tab. D.7 – 3. Strain values [mm/mm]

Beads %								
Beads diameters	0	1	2	3	4	5	8	10
0.8 mm	0.190	0.202	0.199	0.200	0.194	0.189	0.138	0.143
1 mm		0.174	0.178	0.180	0.223	0.221	0.162	0.153
1.25 mm		0.225	0.232	0.232	0.182	0.149	0.147	0.116
1.75 mm		0.177	0.172	0.173	0.165	0.149	0.175	0.172
2.25 mm		0.196	0.145	0.136	0.136	0.121	0.107	0.135

Note: 1 MPa = 145 psi; 1 mm = 0.03937 in

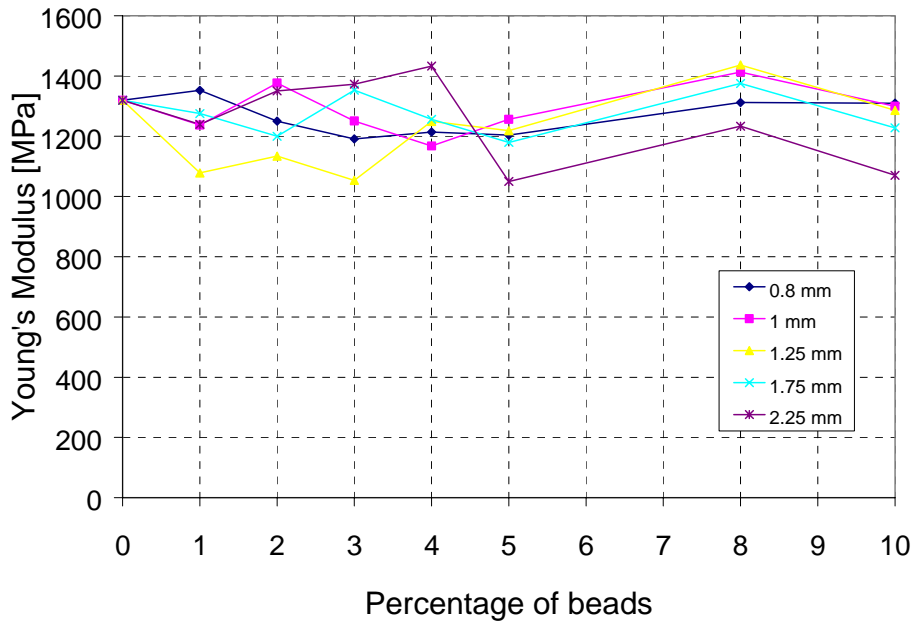


Fig. D.7. – 4. Comparison between Young's Modulus for specimens with and without beads.

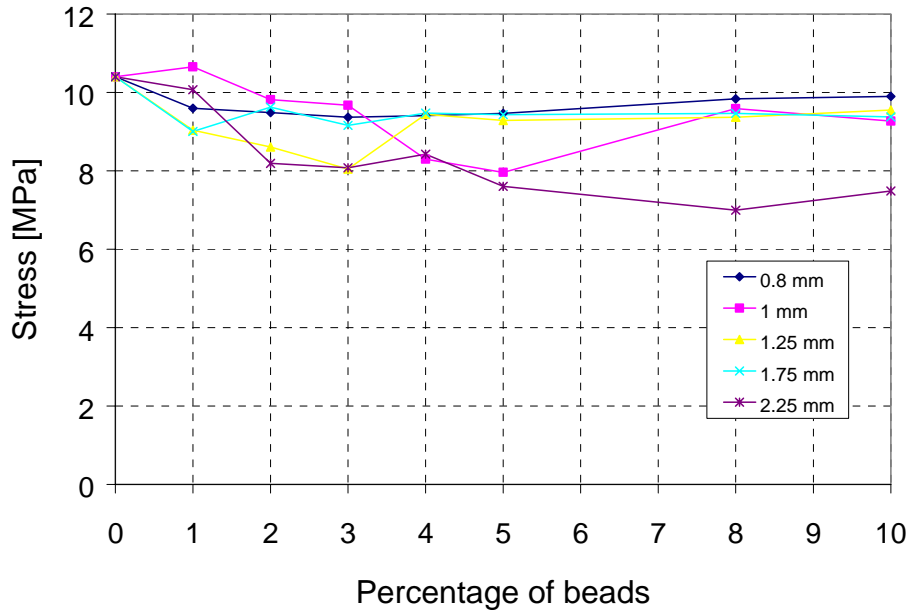


Fig. D.7 – 5. Comparison between stresses for specimens with and without beads

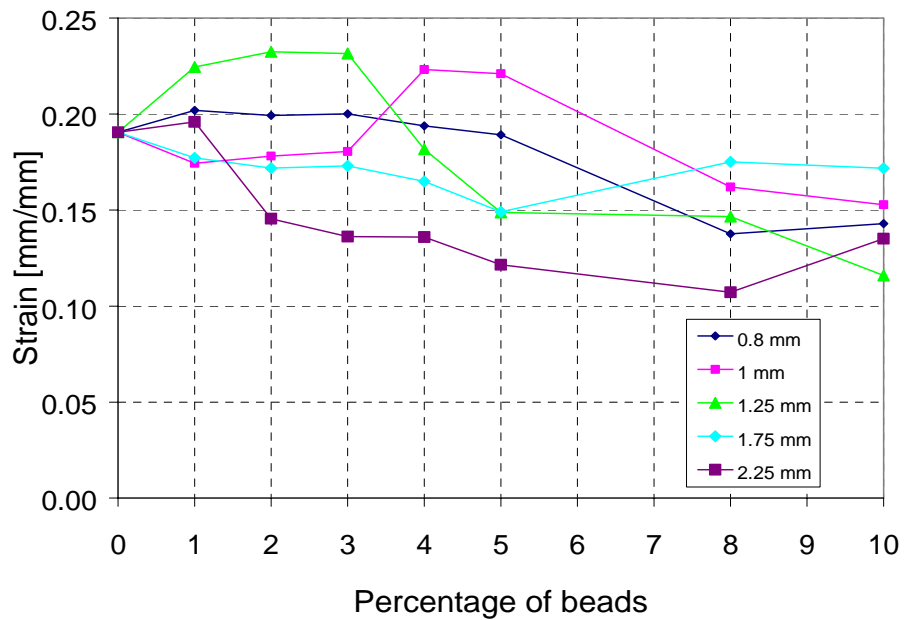


Fig. D.7 – 6. Comparison between strains for specimens with and without beads

Tab. D.7 – 4. Losses of mechanical properties

	Virgin Specimen	20% Sand	Loss (%)
Young’s Modulus [MPa]	1319	1096	17
Stress [MPa]	10.40	8.52	18
Strain [mm/mm]	0.190	0.126	34

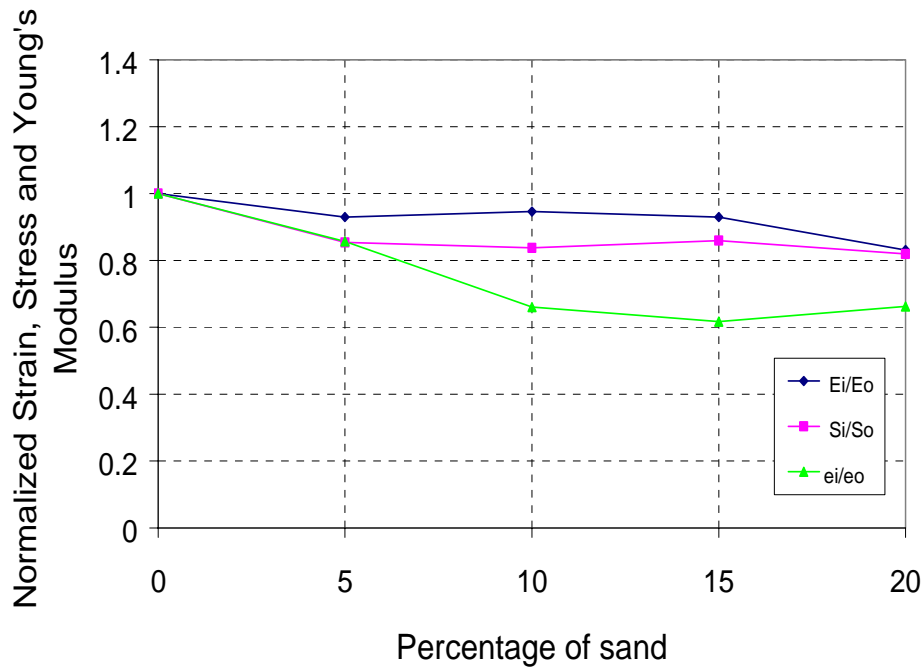


Fig. D.7 – 7. Young’s Modulus, strength and strain as a function of sand percentage

Tab. D.7 – 5. Young’s Modulus values [MPa]

Beads %		0	1	2	3	4	5	8	10
Beads diameters									
0.8 mm	687		561	552	581	587	547	687	581
1 mm			676	685	631	594	587	576	606
1.25 mm			569	596	554	698	658	616	685
1.75 mm			629	608	692	564	552	495	522
2.25 mm			656	658	641	621	601	565	502

Note: 1 MPa = 145 psi; 1 mm = 0.03937 in

Tab. D.7 – 6. Stress values [MPa]

Beads %								
Beads diameters	0	1	2	3	4	5	8	10
0.8 mm	4.497	4.742	4.492	4.663	4.655	4.337	4.113	4.058
1 mm		4.960	4.775	4.764	3.822	4.224	4.150	4.384
1.25 mm		3.731	3.835	4.150	4.303	4.442	4.415	3.571
1.75 mm		4.122	3.644	3.463	3.879	3.489	3.378	3.252
2.25 mm		3.307	3.152	2.901	3.408	3.066	3.313	2.672

Note: 1 MPa = 145 psi; 1 mm = 0.03937 in

Tab. D.7 – 7. Strain values [mm/mm]

Beads %								
Beads diameters	0	1	2	3	4	5	8	10
0.8 mm	0.098	0.122	0.117	0.123	0.106	0.116	0.087	0.075
1 mm		0.121	0.121	0.118	0.123	0.140	0.103	0.112
1.25 mm		0.128	0.132	0.127	0.102	0.098	0.103	0.095
1.75 mm		0.106	0.092	0.090	0.105	0.107	0.124	0.118
2.25 mm		0.121	0.101	0.069	0.092	0.082	0.089	0.086

Note: 1 MPa = 145 psi; 1 mm = 0.03937 in

Tab. D.7 – 8. Losses of mechanical properties

	Virgin Specimen	20% Sand	Loss (%)
Young's Modulus [MPa]	1319	1096	17
Stress [MPa]	10.40	8.52	18
Strain [mm/mm]	0.190	0.126	34

APPENDIX D.8: Durability Tests (Putty)

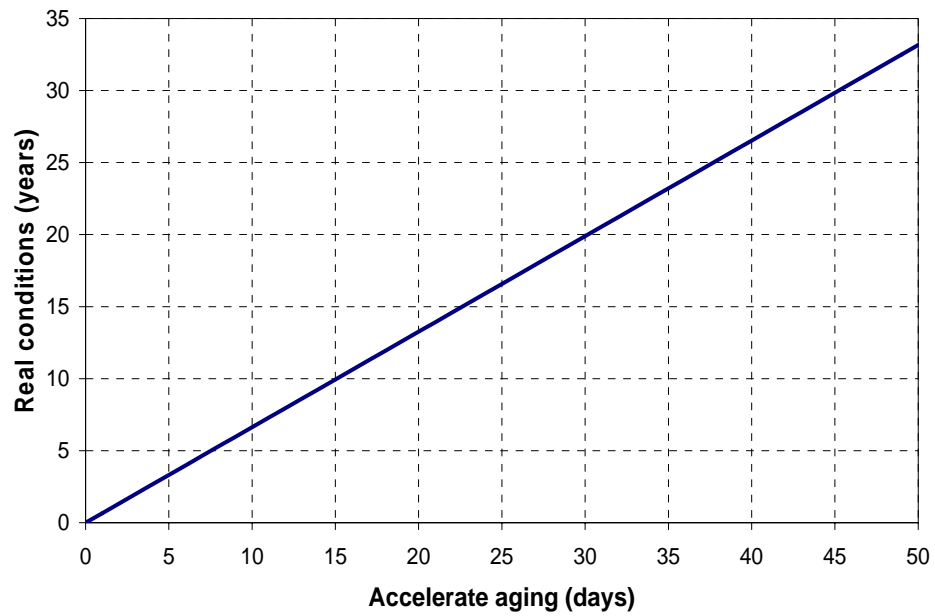


Fig D.8 – 1. Accelerated aging in alkaline solutions for $T = 60\text{ }^{\circ}\text{C}$ ($140\text{ }^{\circ}\text{F}$)

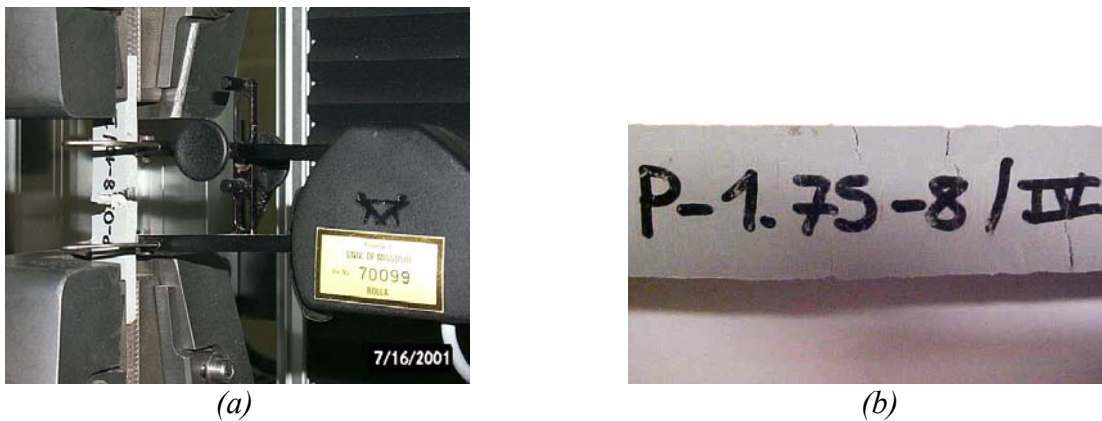


Fig. D.8 – 2. Failure of the specimens

Tab. D.8 – 1. Young's Modulus values [MPa]

Beads %								
Beads diameters	0	1	2	3	4	5	8	10
0.8 mm	687	561	552	581	587	547	687	581
1 mm		676	685	631	594	587	576	606
1.25 mm		569	596	554	698	658	616	685
1.75 mm		629	608	692	564	552	495	522
2.25 mm		656	658	641	621	601	565	502

Note: 1 MPa = 145 psi; 1 mm = 0.03937 in

Tab. D.8 – 2. Stress values [MPa]

Beads %								
Beads diameters	0	1	2	3	4	5	8	10
0.8 mm	4.497	4.742	4.492	4.663	4.655	4.337	4.113	4.058
1 mm		4.960	4.775	4.764	3.822	4.224	4.150	4.384
1.25 mm		3.731	3.835	4.150	4.303	4.442	4.415	3.571
1.75 mm		4.122	3.644	3.463	3.879	3.489	3.378	3.252
2.25 mm		3.307	3.152	2.901	3.408	3.066	3.313	2.672

Note: 1 MPa = 145 psi; 1 mm = 0.03937 in

Tab. D.8 – 3. Strain values [mm/mm]

Beads %								
Beads diameters	0	1	2	3	4	5	8	10
0.8 mm	0.098	0.122	0.117	0.123	0.106	0.116	0.087	0.075
1 mm		0.121	0.121	0.118	0.123	0.140	0.103	0.112
1.25 mm		0.128	0.132	0.127	0.102	0.098	0.103	0.095
1.75 mm		0.106	0.092	0.090	0.105	0.107	0.124	0.118
2.25 mm		0.121	0.101	0.069	0.092	0.082	0.089	0.086

Note: 1 MPa = 145 psi; 1 mm = 0.03937 in

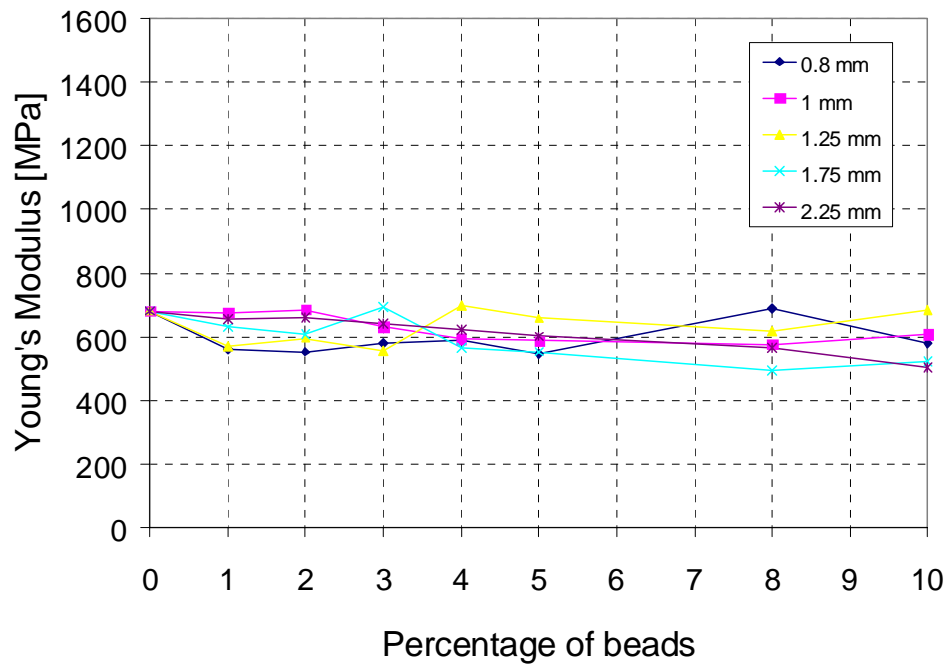


Fig. D.8 – 3. Comparison between Young's Modulus for specimens with and without beads

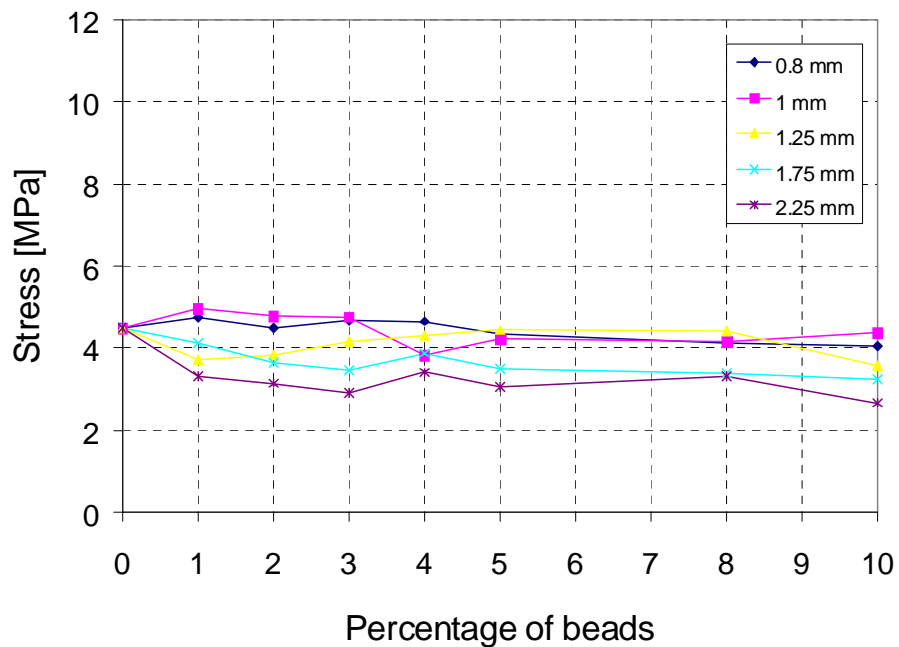


Fig. D.8 – 4. Comparison between stresses for specimens with and without beads

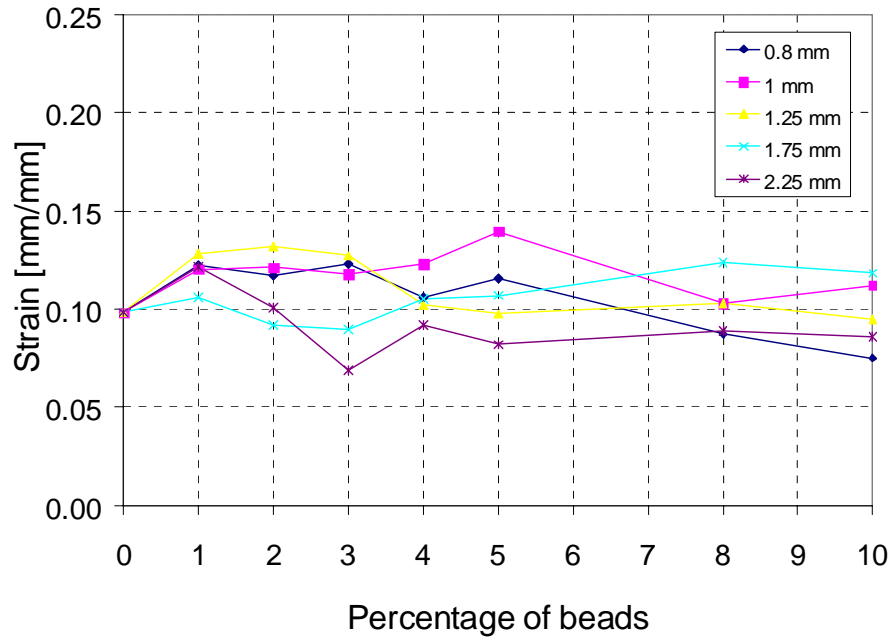


Fig. D.8 – 5. Comparison between strains for specimens with and without beads

Tab. D.8 – 4. Values for the specimens with the sand

	0%	5%	10%	15%	20%
Young's Modulus [MPa]	680.6	687.0	677.4	760.8	876.8
Stress [MPa]	4.497	3.786	3.584	3.631	3.433
Strain [mm/mm]	0.098	0.113	0.078	0.073	0.081

Note: 1 MPa = 145 psi; 1 mm = 0.03937 in

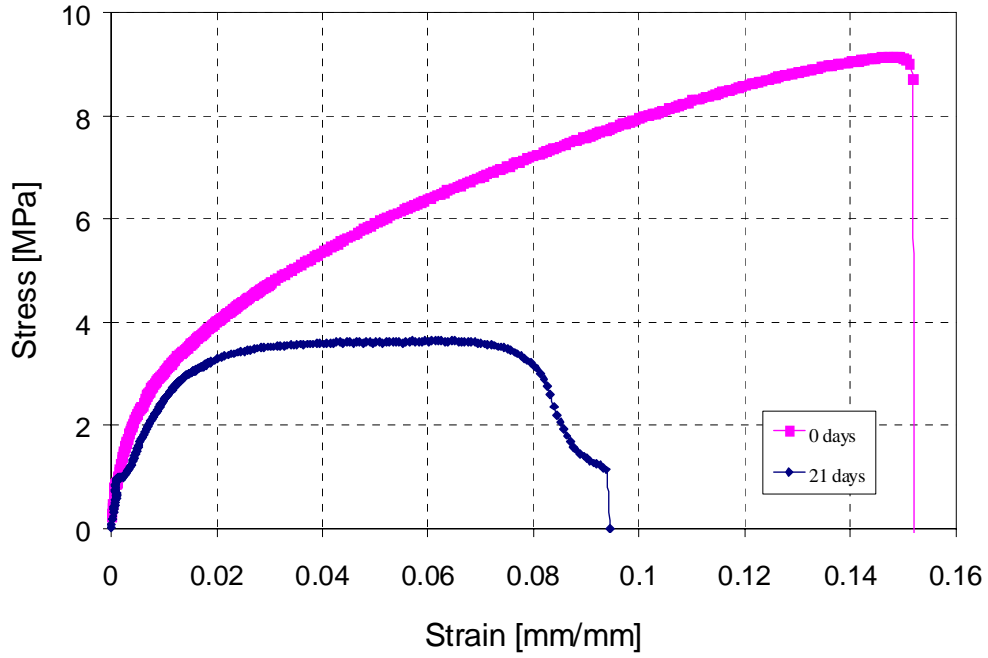


Fig. D.8 – 6. Comparison between the behavior of a specimen at 0 and 21 days

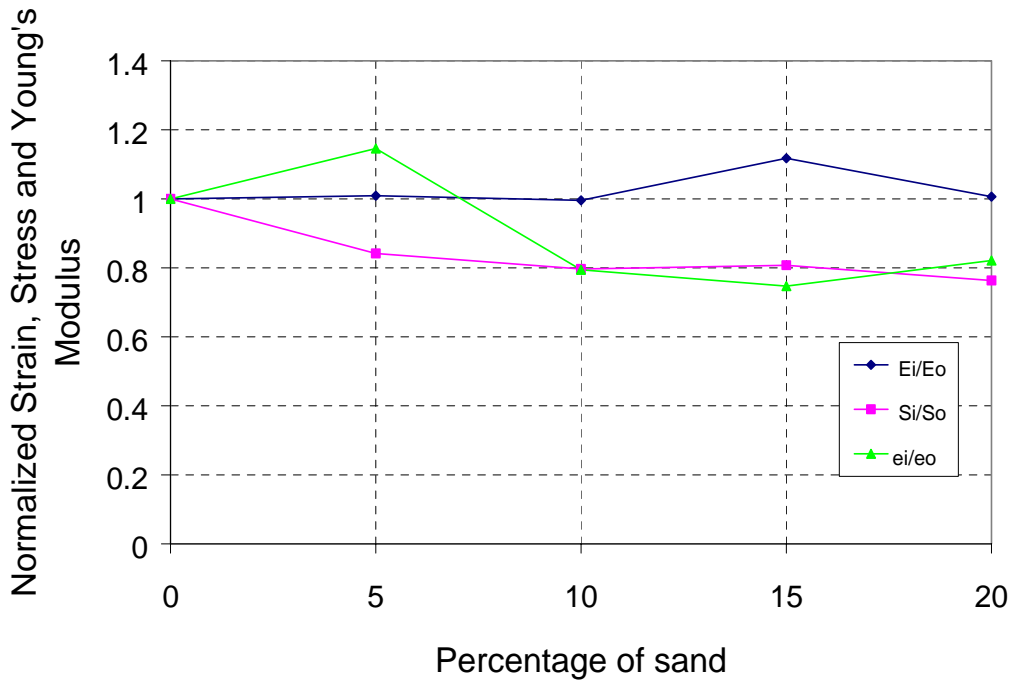


Fig. D.8 – 7. Young's modulus, stresses and strains for specimens with and without sand

Gravimetric Measurements

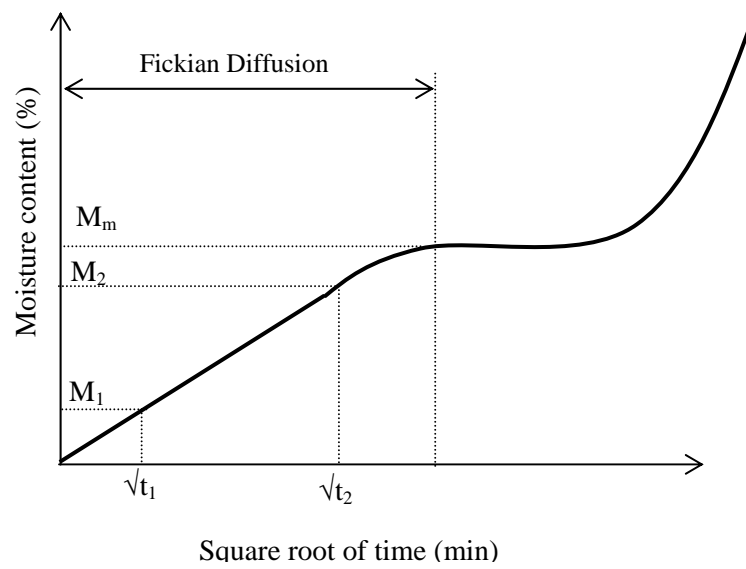


Fig. D.8 – 8. Typical absorption behavior of FRP composites



Fig. D.8 - 9. Precision scale



Fig. D.8 – 10. Alkaline bath

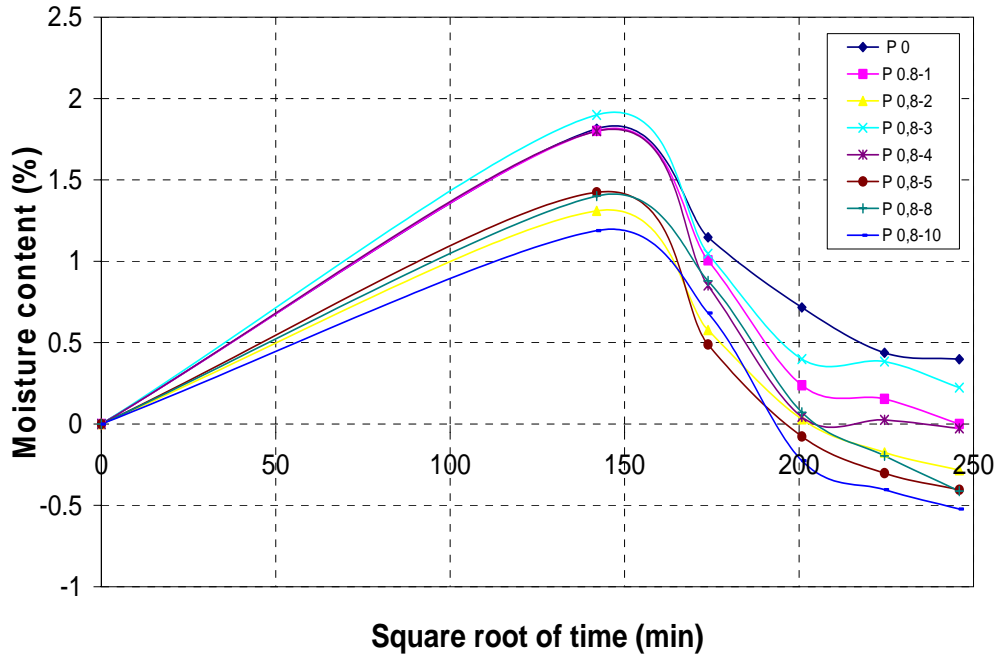


Fig. D.8 – 11. Absorption behavior of putty with beads of 0.8 mm

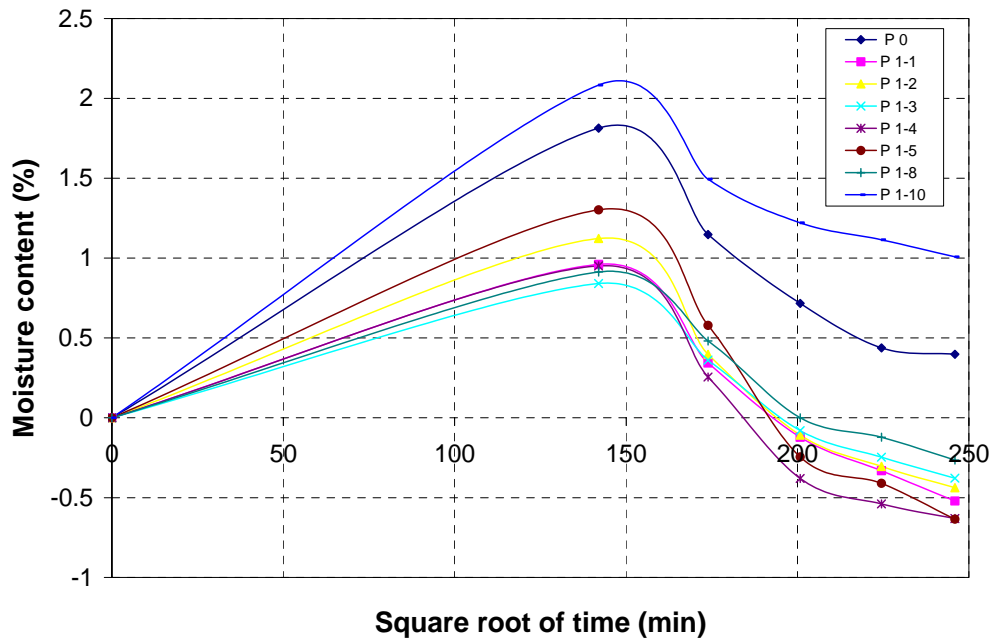


Fig. D.8 – 12. Absorption behavior of putty with beads of 1 mm

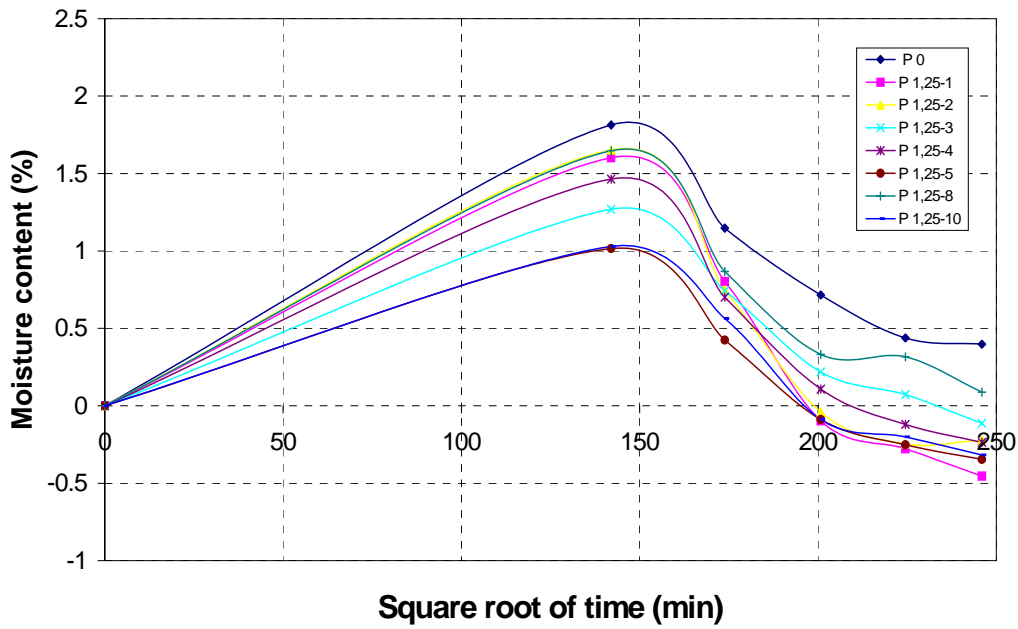


Fig. D.8 – 13. Absorption behavior of putty with beads of 1.25 mm

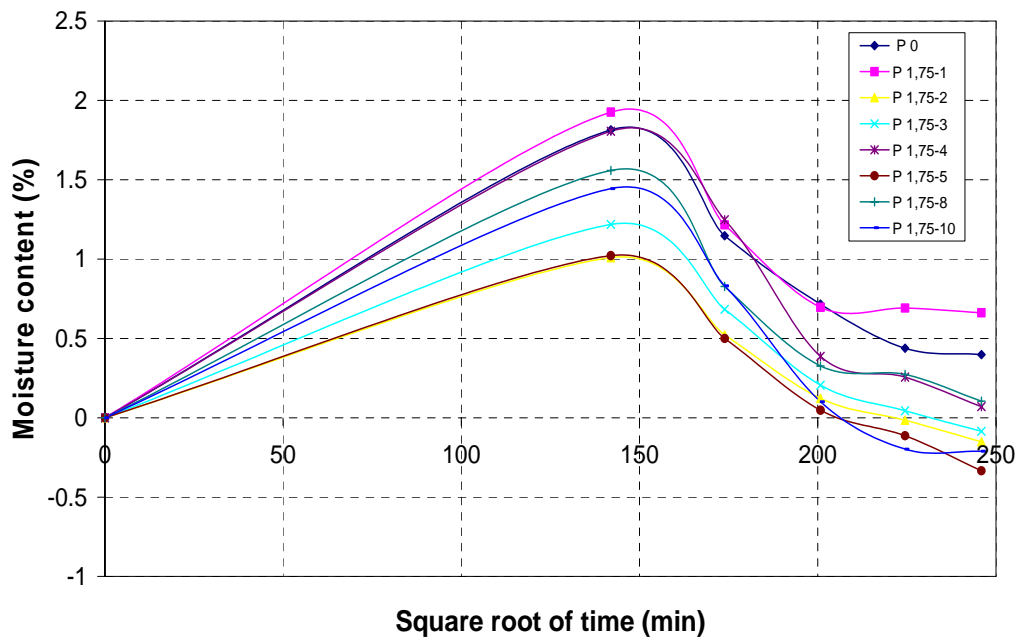


Fig. D.8 – 14. Absorption behavior of putty with beads of 1.75 mm

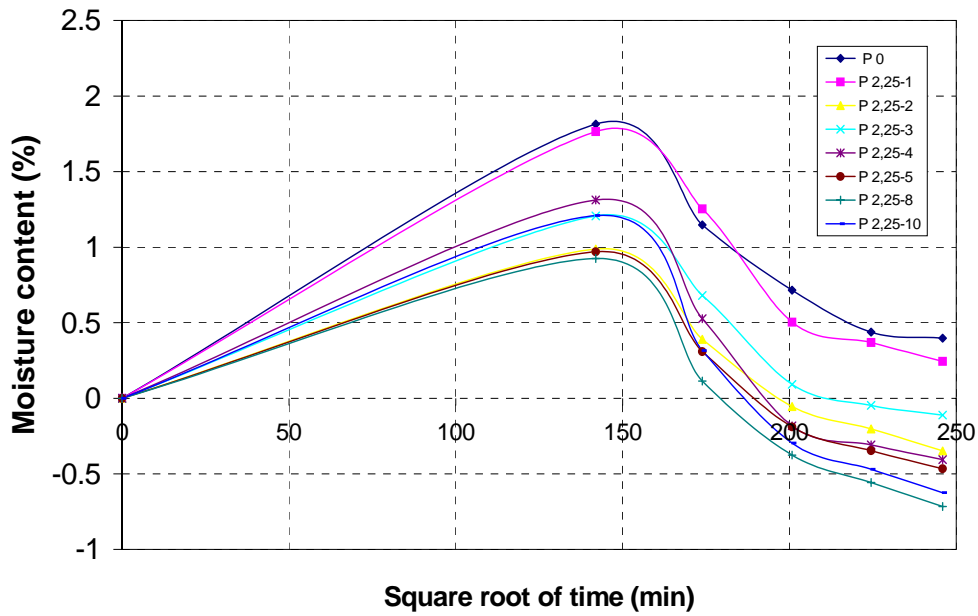


Fig. D.8 – 15. Absorption behavior of putty with beads of 2.25 mm

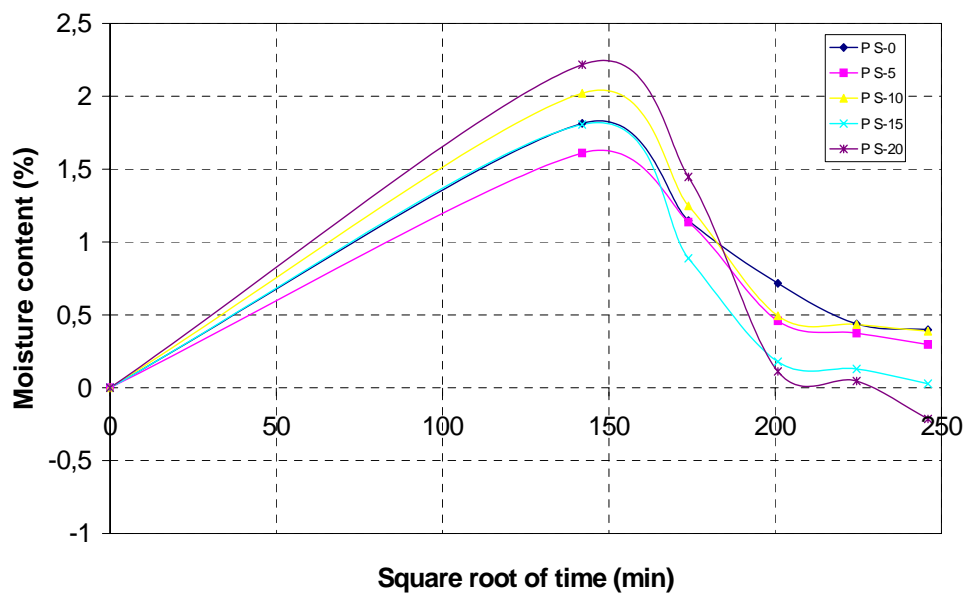


Fig. D.8 – 16. Absorption behavior of putty with sand

APPENDIX D.9: Test Specimens (Controlling the Putty)

Tab. D.9 - 1. Thickness of putty for each specimen

Specimens	Thickness of the putty [mm]
P-0-1	0
P-0-2	0
P-0-3	0
P-0.8-1	0.8
P-0.8-2	0.8
P-0.8-3	0.8
P-1.75-1	1.75
P-1.75-2	1.75
P-1.75-3	1.75

Note: 1 mm = 0.03937 in



(a)



(b)



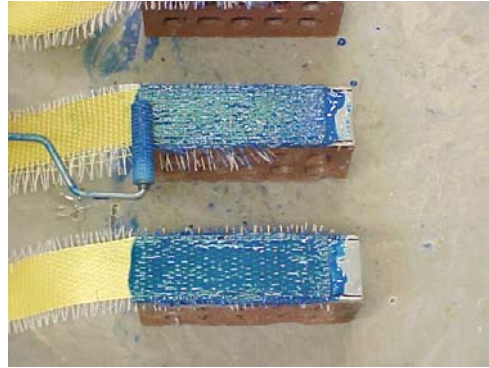
(c)



(d)



(e)



(f)

Fig. D.9 – 1. Preparation of the specimens

APPENDIX D.10: Test Setup (Controlling the Putty)

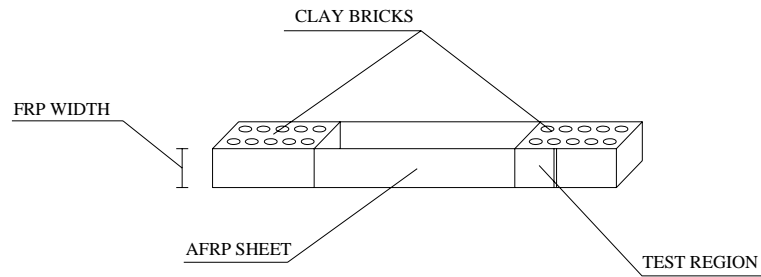
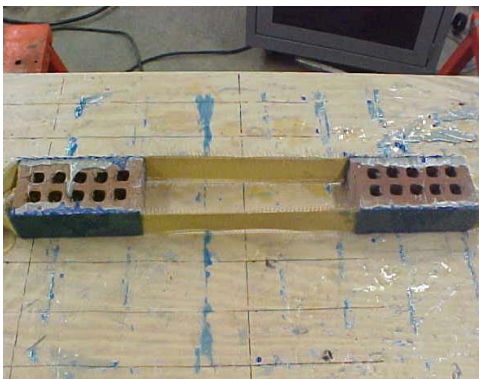


Fig. D.10 – 1. Scheme of the generic test specimens



(a)



(b)

Fig. D.10 – 2. Preparation of the setup

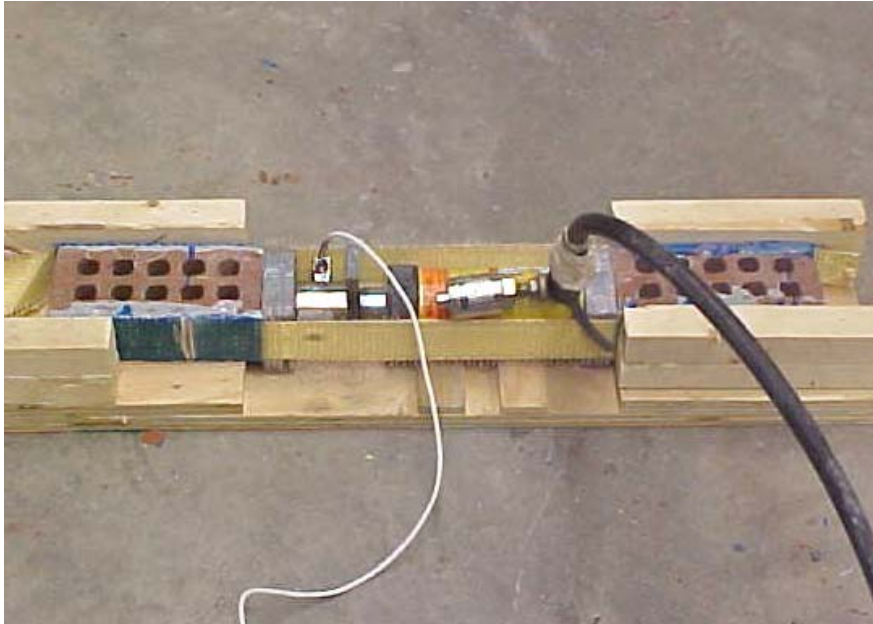


Fig. D.10 – 3. Generic test configuration

APPENDIX D.11: Test Results (Controlling the Putty)

Tab. D.11 – 1. Values for the specimens

Specimens	Load [kN]	Load Average [kN]
P-0-1	13,5	11.8
P-0-2	n.d.	
P-0-3	10,1	
P-0.8-1	12,7	11.7
P-0.8-2	12,3	
P-0.8-3	13,5	
P-1.75-1	12,5	12.8
P-1.75-2	11,9	
P-1.75-3	14,1	

Note: 1kN = 0.228 kip



(a)

(b)

Fig. D.11 – 1. Failure of the specimens

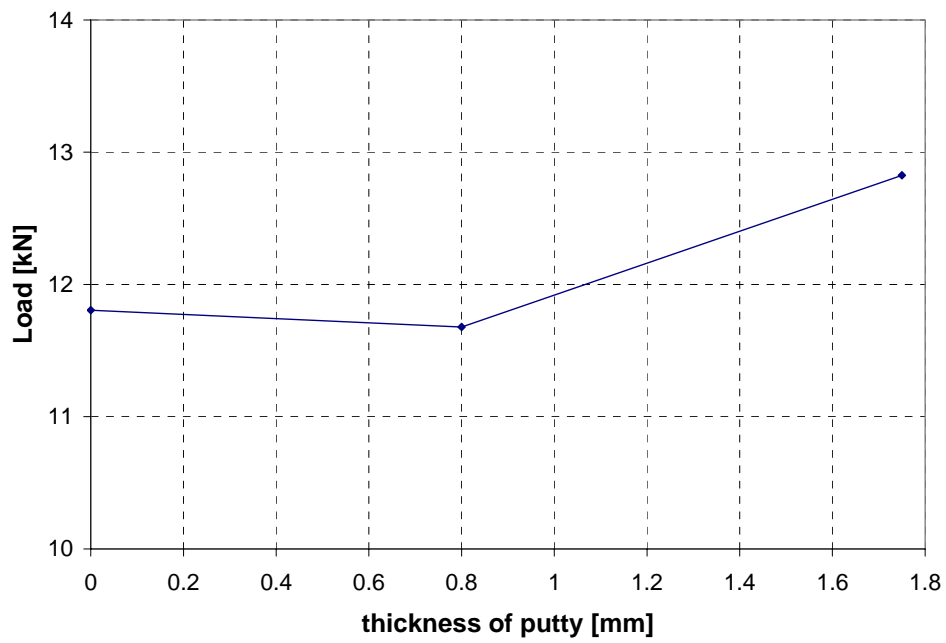


Fig. D.11 – 2. behavior of the load in function of the thickness of putty

BIBLIOGRAPHY

- American Concrete Institute (ACI), Committee 440 (2001). "Guide for the design and construction of concrete reinforced with FRP bars".
- American Concrete Institute (ACI), Committee 440 (2001). "Guide for the design and construction of externally bonded FRP system for strengthening concrete structures" (document under review).
- American Concrete Institute, Masonry Standard Joint Committee (1999). "Code, Specifications and Commentaries, ACI-530-99/ASCE 5-99/ TMS 402-99", American Concrete Institute, American Society of Civil Engineering, The Masonry Society, Detroit, New York and Boulder, 1999.
- Angel R., Abrams D.P., Shapiro D., Uzarski J. Webster M. (1994). "Behavior of reinforced concrete frames with masonry infills". Structural research series report No. 589, Department of Civil Engineering, University of Illinois at Urbana-Champaign, March 1994.
- ASTM D3039 (1987), American Society for Testing and Materials, "Tensile Properties of Advanced Composites Materials".
- ASTM C1019 (1993), American Society for Testing and Materials, "Test Method of Sampling and Testing Grout".
- ASTM E111 (1997), American Society for Testing and Materials, "Standard Test Method for Young's Modulus, Tangent Modulus, and Chord Modulus".
- ASTM C1314 (1998), American Society for Testing and Materials, "Standard Test Method for Constructing and Testing Masonry Prisms Used to Determine Compliance with Specified Compressive Strength of Masonry."
- ASTM C270 (1998), American Society for Testing and Materials, "Standard Specification of Mortar for Unit Masonry".
- ASTM E518 (2001), American Society for Testing and Materials, "Test Method E518-00a Standard Test Methods for Flexural Bond Strength of Masonry".
- ASTM 638 (2000), American Society for Testing and Materials, "Standard Test Method for Tensile Properties of Plastics".
- Baker L.R., Franken G.L. (1978). "Precracking behavior of laterally loaded brickwork panels with In-Plane restraints". Proceedings of the British Ceramic Society, No. 27, 1978.

- Bank, L.C., (1993) "Properties of FRP Reinforcements for Concrete: Fiber-Reinforced-Plastic (FRP) Reinforcement for Concrete Structures: Properties and Applications", A.C. Nanni, ed., Elsevier Science Publishers B.V., Amsterdam, 1993.
- Burgoyne, C.J., (1993) "Advanced Composites in Construction", lecture given at the Pennsylvania State University, 26 August 1993.
C.I.E.S. report – University of Missouri Rolla.
- Chajes, M.J., Finch W.W.Jr, Januszka T.F., and Thomson T.A. (1996). "Bond and force transfer of composite materials plates bonded to concrete", ACI Structural Journal, ACI, Vol. 93, No. 2.
- De Lorenzis L., A. Nanni (2000). "Strengthening of RC structures with near surface mounted rods", C.I.E.S. report – University of Missouri Rolla.
- De Lorenzis L., Miller B. and Nanni A. (2000). "Bond of FRP laminates to concrete", ACI Structures Journal, July 2000.
- Devalapura, R.K., Gauchel, J.V., Greenwood, M.E., Hankin, A., and Humphrey, T. (1997), "Long-Term Durability of GFRP Composites in Alkaline Environments", Proc. 3rd Non-Metallic (FRP) Reinforcement for Concrete Structures, International Symposium, Sapporo, Japan, October 14-16th 1997, Sapporo Japan, Vol.2.
- Dixon Troy O. (1994). "Behavior of Anchor/Tendon Systems for Prestressed FRP Construction", Pennsylvania State University thesis.
- Drysdale G. R., Hamid A. A., Baker R. L. (1999). "Masonry Structures – Behavior and design", The Masonry Society, Boulder, Colorado.
- Ehsani M.R. and Saadatmanesh H. (1996), "Repair and Strengthening of Earthquake-Damaged Concrete and Masonry Walls with Composite Fabrics", First International Conference on Composites in Infrastructure ICCI'96, Tucson, Arizona, January 1996.
- Erki, M.A. and S.H. Rizkalla, "Anchorage for FRP Reinforcement" Concrete International, ACI, June 1993b.
- Franke, L. and Overback, E., (1987), "Loss in strength and damage to glass fibers in alkaline solutions and cement extracts", Dur. Build. Mat., No.5, 1987.
- Gabrielsen B.L., Kaplan K., Wilton C. (1975). "A study of arching in non-reinforced masonry walls". SSI 748-1, Scientific Services, Inc., Redwood City, CA, 1975.

- Ganga Rao, H.V.S., and Vijay P.V., (1997), "Aging of Structural Composites Under Varying Environmental Conditions", Proc. 3rd Non-Metallic (FRP) Reinforcement for Concrete Structures, International Symposium, Sapporo, Japan, October 14-16th 1997, Sapporo Japan, Vol.2,
- Gerritse, A., and J. Werner, (1988). "ARAPREE: The Prestressing Element Composed of Resin Bonded Twaron® Fibres", Manufacturer's Report, Rijswijk, Netherlands.
- Gilstrap J.M., Dolan C.W. (1998). "Out-of-plane bending of FRP reinforced masonry walls", Composites science and technology, 1998.
- Hamilton H.R. III, Holberg A., Caspersen J., and Dolan C.W. (1999), "Strengthening Concrete Masonry with Fiber Reinforced Polymers", Fourth International Symposium on Fiber Reinforced Polymer (FRP) for Reinforced Concrete Structures, Baltimore, Maryland, November 1999.
- Hendry H.W. (1981), Structural Brickwork. The Macmillan Press Ltd.m London, 1981.
- Holte, L.E., C.W. Dolan, and R.J. Schmidt, (1993). "Epoxy Socketed Anchors for Non-Metallic Prestressing Tendons", ACI SP 138-26, Proceedings of the International Symposium on FRP Reinforcement for Concrete Structures, A.C. Nanni and C.W. Dolan, editors, Vancouver, BC, Canada, 28-31 March 1993.
- K. Roko, T.E. Boothby, C.F. Bakis (1999). "Failure modes of sheet bonded fiber reinforced to brick masonry", Fourth international symposium on fiber reinforced polymer for RC structures, 1999 (editing by: Charles W. Dolan, Sami H. Rizkalla, and Antonio Nanni).
- Laursen P.T., Seible F., Hegemier G.A., and Innamorato D., „Seismic Retrofit and Repair of Masonry Walls with Carbon Overlays,“ Non-Metallic (FRP) Reinforcement for Concrete Structures, edited by L. Taerwe, RILEM, 1995.
- Litherland, K.L., Oakley, D.R., and Proctor, B.A., (1981), "The Use of Accelerated Ageing Procedures to Predict the Long Term Strength of GRF Composites", *Cement and Concrete Research*, Vol. 11
- Maeda T., Asano Y., Sato Y., Ueda T., and Kakuta Y. (1997). "A study on bond mechanism of carbon fiber sheet", Non-metallic (FRP) reinforcement for concrete structures, Vol. 1, Japan Concrete Institute.
- MBrace composite strengthening system engineering design guidelines second edition (1998). Master Builders, Inc. and Structural Preservation Systems.

MDA Composites industries website. www.mdacomposites.org

Micelli F., Nanni A. (2001). "Mechanical Properties and Durability of FRP Rods". C.I.E.S. report, University of Missouri – Rolla.

Miller B. (1999). "Bond between carbon fiber reinforced polymer sheets and concrete", UMR thesis, 1999.

Morbin A. (2001), "Strengthening of Masonry Elements with FRP Composites", C.I.E.S. report, University of Missouri – Rolla.

Mukae, K., S. Kumagai, H. Nakai, and H. Asai, (1993). "Characteristics of Aramid FRP Rod," ACI SP 138-26, Proceedings of the International Symposium on FRP Reinforcement for Concrete Structures, A.C. Nanni and C.W. Dolan, editors, Vancouver, BC, Canada, 28-31 March 1993.

Nanni A. (1999). "Composites: coming on strong", Concrete construction, vol. 44, 1999.

Pei-Chang H., Nanni A. (1999). "Dapped-end strengthening of precast prestressed concrete double tee beams with FRP composites", C.I.E.S. Report – University of Missouri – Rolla.

Post-tensioning institute web site. www.post-tensioning.org.

Randy M., Nanni A., Watkins S., Barker M., Bootby T. (1999). "Strengthening of bridge G-270 with externally bonded CFRP", C.I.E.S. Report – University of Missouri – Rolla.

Sabnis G.M. (1976). "Interaction between masonry walls and frames in multistory structures". First Canadian Masonry Symposium, Calgary, Alberta, 1976.

Santoh, Norihiko, (1993). "CFCC (Carbon Fiber Composite Cable): Fiber-Reinforced-Plastic (FRP) Reinforcement for Concrete Structures: Properties and Applications", A.C. Nanni, ed., Elsevier Science Publishers B.V., Amsterdam, 1993.

Schwegler G., "Masonry Costruction Strengthened with Fiber Composites in Seismically Endangered Zones," Proceedings of the Tenth European Conference on Earthquake Engineering, Rotterdam, 1995.

Taghdi M., Bruneau M., Saatcioglu M. (2000). "Seisming retrofitting of low-rise masonry and concrete walls using steel strips". ASCE Journal of Structural Engineering, September 2000.

- Taljsten B. (1994). "Plate bonding. Strengthening of existing structures with epoxy bonded plates of steel or reinforced plastics", Doctoral thesis, Lulea University of technology, Sweden.
- Tamura, Tomio (1993). "FiBRA: Fiber-Reinforced-Plastic (FRP) Reinforcement for Concrete Structures: Properties and Applications", A.C. Nanni, ed., Elsevier Science Publishers B.V., Amsterdam, 1993.
- Tinazzi D., Nanni A. (2000). "Assessment of technologies of masonry retrofitting with FRP", C.I.E.S. Report – University of Missouri – Rolla.
- Tumialan G. (2001). "Strengthening of masonry structures with FRP composites", Doctoral thesis, University of Missouri – Rolla.
- Uomoto T., Nishimura T. (1999). "Deterioration of aramid, glass, and carbon fibers due to alkali, acid and water in different temperature", Fourth international symposium on fiber reinforced polymer for RC structures, 1999 (editing by: Charles W. Dolan, Sami H. Rizkalla, and Antonio Nanni).
- Van Gemert D., Vandewalle L. (2001). "Anchorage of externally bonded steel plates and CFRP laminates for strengthening of concrete elements", Doctoral thesis, Katholieke Universiteit Leuven (May 2001).
- Velazquez Dimas J.I, Ehsani M.R., and Saadatamtanesh H. (2000). "Out-of-plane behavior of brick masonry walls strengthened with fiber composites", ACI Structural Journal, May-June 2000.
- Velazquez Dimas J.I, Eshani M.R. (2000). "Modeling out-of-plane behavior of UR walls retrofitted with fiber composites", Journal of composites for construction, November 2000.
- Vijay, P.V., and Ganga Rao H.V.S., (1999), "Accelerated and Natural Weathering of Glass Fiber Reinforced Plastic Bars", Proc. FRPRCS-4, November 1-4th, 1999, Baltimore.

ACKNOWLEDGEMENTS

We would like to express our appreciations to all the CIES members for their support throughout our thesis program. It has been an honour and we are very proud to have worked with Dr. Antonio Nanni for his availability and extreme intelligence. We would also acknowledge Jaime Gustavo Tumialan, he has been not only a guide with all his advises, but also a friend with whom share good times. We would recognize also the support of Harold Martin from Rolla Technical Institute, Mr. Jason Cox, Jeff Thomas, Steve Gable, Nestore Galati, Sinaph Namboorimadathil, Danielle Stone, Antonio Morbin, Dr. J. Myers, Dr. P. Silva, Jeff Bradshaw and also Tong Li, Khaled El-Domiaty, Xianlin Shen, Anand Khataukar, Sharath Murthy, Xinbao Yang and Yumin Yang.

Special thanks to “the” Parretti, Jason, Nestore, Danielle, Paolo, Sinaph and Antonio for the beautiful moments spent together.

Thanks to the CIES staff, Mrs. Ravonda McGauley, Mrs. Gayle Spitzmiller, Mrs. Susan Tripp, and to all our colleagues.

A special thanks to the National Science Foundation Industry/University Cooperative Research Center, Repair of Buildings and Bridges with Composites at the University of Missouri-Rolla for providing the financial and material assistance for the completion of our research as visiting scholars.

We would like to express also our sincere gratitude to Prof. Sergio Lagomarsino from the University of Genoa - Italy, who gave us the opportunity to do this fantastic experience in the United States.

Marco, Olly e Ale

BIBLIOGRAPHY

- American Concrete Institute (ACI), Committee 440 (2001). "Guide for the design and construction of concrete reinforced with FRP bars".
- American Concrete Institute (ACI), Committee 440 (2001). "Guide for the design and construction of externally bonded FRP system for strengthening concrete structures" (document under review).
- American Concrete Institute, Masonry Standard Joint Committee (1999). "Code, Specifications and Commentaries, ACI-530-99/ASCE 5-99/ TMS 402-99", American Concrete Institute, American Society of Civil Engineering, The Masonry Society, Detroit, New York and Boulder, 1999.
- Angel R., Abrams D.P., Shapiro D., Uzarski J. Webster M. (1994). "Behavior of reinforced concrete frames with masonry infills". Structural research series report No. 589, Department of Civil Engineering, University of Illinois at Urbana-Champaign, March 1994.
- ASTM D3039 (1987), American Society for Testing and Materials, "Tensile Properties of Advanced Composites Materials".
- ASTM C1019 (1993), American Society for Testing and Materials, "Test Method of Sampling and Testing Grout".
- ASTM E111 (1997), American Society for Testing and Materials, "Standard Test Method for Young's Modulus, Tangent Modulus, and Chord Modulus".
- ASTM C1314 (1998), American Society for Testing and Materials, "Standard Test Method for Constructing and Testing Masonry Prisms Used to Determine Compliance with Specified Compressive Strength of Masonry."
- ASTM C270 (1998), American Society for Testing and Materials, "Standard Specification of Mortar for Unit Masonry".
- ASTM E518 (2001), American Society for Testing and Materials, "Test Method E518-00a Standard Test Methods for Flexural Bond Strength of Masonry".
- ASTM 638 (2000), American Society for Testing and Materials, "Standard Test Method for Tensile Properties of Plastics".
- Baker L.R., Franken G.L. (1978). "Precracking behavior of laterally loaded brickwork panels with In-Plane restraints". Proceedings of the British Ceramic Society, No. 27, 1978.

- Bank, L.C., (1993) "Properties of FRP Reinforcements for Concrete: Fiber-Reinforced-Plastic (FRP) Reinforcement for Concrete Structures: Properties and Applications", A.C. Nanni, ed., Elsevier Science Publishers B.V., Amsterdam, 1993.
- Burgoyne, C.J., (1993) "Advanced Composites in Construction", lecture given at the Pennsylvania State University, 26 August 1993.
C.I.E.S. report – University of Missouri Rolla.
- Chajes, M.J., Finch W.W.Jr, Januszka T.F., and Thomson T.A. (1996). "Bond and force transfer of composite materials plates bonded to concrete", ACI Structural Journal, ACI, Vol. 93, No. 2.
- De Lorenzis L., A. Nanni (2000). "Strengthening of RC structures with near surface mounted rods", C.I.E.S. report – University of Missouri Rolla.
- De Lorenzis L., Miller B. and Nanni A. (2000). "Bond of FRP laminates to concrete", ACI Structures Journal, July 2000.
- Devalapura, R.K., Gauchel, J.V., Greenwood, M.E., Hankin, A., and Humphrey, T. (1997), "Long-Term Durability of GFRP Composites in Alkaline Environments", Proc. 3rd Non-Metallic (FRP) Reinforcement for Concrete Structures, International Symposium, Sapporo, Japan, October 14-16th 1997, Sapporo Japan, Vol.2.
- Dixon Troy O. (1994). "Behavior of Anchor/Tendon Systems for Prestressed FRP Construction", Pennsylvania State University thesis.
- Drysdale G. R., Hamid A. A., Baker R. L. (1999). "Masonry Structures – Behavior and design", The Masonry Society, Boulder, Colorado.
- Ehsani M.R. and Saadatmanesh H. (1996), "Repair and Strengthening of Earthquake-Damaged Concrete and Masonry Walls with Composite Fabrics", First International Conference on Composites in Infrastructure ICCI'96, Tucson, Arizona, January 1996.
- Erki, M.A. and S.H. Rizkalla, "Anchorage for FRP Reinforcement" Concrete International, ACI, June 1993b.
- Franke, L. and Overback, E., (1987), "Loss in strength and damage to glass fibers in alkaline solutions and cement extracts", Dur. Build. Mat., No.5, 1987.
- Gabrielsen B.L., Kaplan K., Wilton C. (1975). "A study of arching in non-reinforced masonry walls". SSI 748-1, Scientific Services, Inc., Redwood City, CA, 1975.

- Ganga Rao, H.V.S., and, Vijay P.V., (1997), "Aging of Structural Composites Under Varying Environmental Conditions", Proc. 3rd Non-Metallic (FRP) Reinforcement for Concrete Structures, International Symposium, Sapporo, Japan, October 14-16th 1997, Sapporo Japan, Vol.2,
- Gerritse, A., and J. Werner, (1988). "ARAPREE: The Prestressing Element Composed of Resin Bonded Twaron® Fibres", Manufacturer's Report, Rijswijk, Netherlands.
- Gilstrap J.M., Dolan C.W. (1998). "Out-of-plane bending of FRP reinforced masonry walls", Composites science and technology, 1998.
- Hamilton H.R. III, Holberg A., Caspersen J., and Dolan C.W. (1999), "Strengthening Concrete Masonry with Fiber Reinforced Polymers", Fourth International Symposium on Fiber Reinforced Polymer (FRP) for Reinforced Concrete Structures, Baltimore, Maryland, November 1999.
- Hendry H.W. (1981), Structural Brickwork. The Macmillan Press Ltd.m London, 1981.
- Holte, L.E., C.W. Dolan, and R.J. Schmidt, (1993). "Epoxy Socketed Anchors for Non-Metallic Prestressing Tendons", ACI SP 138-26, Proceedings of the International Symposium on FRP Reinforcement for Concrete Structures, A.C. Nanni and C.W. Dolan, editors, Vancouver, BC, Canada, 28-31 March 1993.
- K. Roko, T.E. Boothby, C.F. Bakis (1999). "Failure modes of sheet bonded fiber reinforced to brick masonry", Fourth international symposium on fiber reinforced polymer for RC structures, 1999 (editing by: Charles W. Dolan, Sami H. Rizkalla, and Antonio Nanni).
- Laursen P.T., Seible F., Hegemier G.A., and Innamorato D., „Seismic Retrofit and Repair of Masonry Walls with Carbon Overlays,“ Non-Metallic (FRP) Reinforcement for Concrete Structures, edited by L. Taerwe, RILEM, 1995.
- Litherland, K.L., Oakley, D.R., and Proctor, B.A., (1981), "The Use of Accelerated Ageing Procedures to Predict the Long Term Strength of GRF Composites", *Cement and Concrete Research*, Vol. 11
- Maeda T., Asano Y., Sato Y., Ueda T., and Kakuta Y. (1997). "A study on bond mechanism of carbon fiber sheet", Non-metallic (FRP) reinforcement for concrete structures, Vol. 1, Japan Concrete Institute.
- MBrace composite strengthening system engineering design guidelines second edition (1998). Master Builders, Inc. and Structural Preservation Systems.

MDA Composites industries website. www.mdacomposites.org

Micelli F., Nanni A. (2001). "Mechanical Properties and Durability of FRP Rods". C.I.E.S. report, University of Missouri – Rolla.

Miller B. (1999). "Bond between carbon fiber reinforced polymer sheets and concrete", UMR thesis, 1999.

Morbin A. (2001), "Strengthening of Masonry Elements with FRP Composites", C.I.E.S. report, University of Missouri – Rolla.

Mukae, K., S. Kumagai, H. Nakai, and H. Asai, (1993). "Characteristics of Aramid FRP Rod," ACI SP 138-26, Proceedings of the International Symposium on FRP Reinforcement for Concrete Structures, A.C. Nanni and C.W. Dolan, editors, Vancouver, BC, Canada, 28-31 March 1993.

Nanni A. (1999). "Composites: coming on strong", Concrete construction, vol. 44, 1999.

Pei-Chang H., Nanni A. (1999). "Dapped-end strengthening of precast prestressed concrete double tee beams with FRP composites", C.I.E.S. Report – University of Missouri – Rolla.

Post-tensioning institute web site. www.post-tensioning.org.

Randy M., Nanni A., Watkins S., Barker M., Bootby T. (1999). "Strengthening of bridge G-270 with externally bonded CFRP", C.I.E.S. Report – University of Missouri – Rolla.

Sabnis G.M. (1976). "Interaction between masonry walls and frames in multistory structures". First Canadian Masonry Symposium, Calgary, Alberta, 1976.

Santoh, Norihiko, (1993). "CFCC (Carbon Fiber Composite Cable): Fiber-Reinforced-Plastic (FRP) Reinforcement for Concrete Structures: Properties and Applications", A.C. Nanni, ed., Elsevier Science Publishers B.V., Amsterdam, 1993.

Schwegler G., "Masonry Costruction Strengthened with Fiber Composites in Seismically Endangered Zones," Proceedings of the Tenth European Conference on Earthquake Engineering, Rotterdam, 1995.

- Taghdi M., Bruneau M., Saatcioglu M. (2000). "Seismic retrofitting of low-rise masonry and concrete walls using steel strips". ASCE Journal of Structural Engineering, September 2000.
- Taljusten B. (1994). "Plate bonding. Strengthening of existing structures with epoxy bonded plates of steel or reinforced plastics", Doctoral thesis, Lulea University of technology, Sweden.
- Tamura, Tomio (1993). "FiBRA: Fiber-Reinforced-Plastic (FRP) Reinforcement for Concrete Structures: Properties and Applications", A.C. Nanni, ed., Elsevier Science Publishers B.V., Amsterdam, 1993.
- Tinazzi D., Nanni A. (2000). "Assessment of technologies of masonry retrofitting with FRP", C.I.E.S. Report – University of Missouri – Rolla.
- Tumialan G. (2001). "Strengthening of masonry structures with FRP composites", Doctoral thesis, University of Missouri – Rolla.
- Uomoto T., Nishimura T. (1999). "Deterioration of aramid, glass, and carbon fibers due to alkali, acid and water in different temperature", Fourth international symposium on fiber reinforced polymer for RC structures, 1999 (editing by: Charles W. Dolan, Sami H. Rizkalla, and Antonio Nanni).
- Van Gemert D., Vandewalle L. (2001). "Anchorage of externally bonded steel plates and CFRP laminates for strengthening of concrete elements", Doctoral thesis, Katholieke Universiteit Leuven (May 2001).
- Velazquez Dimas J.I, Ehsani M.R., and Saadatmanesh H. (2000). "Out-of-plane behavior of brick masonry walls strengthened with fiber composites", ACI Structural Journal, May-June 2000.
- Velazquez Dimas J.I, Eshani M.R. (2000). "Modeling out-of-plane behavior of UR walls retrofitted with fiber composites", Journal of composites for construction, November 2000.
- Vijay, P.V., and Ganga Rao H.V.S., (1999), "Accelerated and Natural Weathering of Glass Fiber Reinforced Plastic Bars", Proc. FRPRCS-4, November 1-4th, 1999, Baltimore.